



Universitat Autònoma de Barcelona

Department of Chemistry

Faculty of Science

**Encapsulation of Stimuli-Responsive Molecules
for the Preparation of Photofunctional Materials**

Nuria Alexandra Vázquez Mera

PhD Thesis

PhD in Materials Science

2015

Supervisors:

Dr. Daniel Ruiz Molina

Dr. Jordi Hernando Campos

Dr. José Luis Bourdelande Fernández

ACKNOWLEDGMENTS

Primero de todo, me gustaría agradecer a mis supervisores: Dr. Daniel Ruiz Molina, Dr. Jordi Hernando Campos y Dr. José Luis Bourdelande Fernández. Sin vuestras ideas, apoyo y paciencia esta disertación no hubiera sido posible. Agradezco también el financiamiento recibido por el Ministerio de Educación, que me ha permitido dedicarme en exclusiva al desarrollo de mi investigación al concederme la beca FPU.

También debo agradecer al Servei d'Anàlisi Química (SAQ), al Servei de Ressonància Magnètica Nuclear (RMN) y al Servei de Microscòpia de la Universtat Autònoma de Barcelona; así como también a la Divisiò de Microscopia Electrònica y a los técnicos del Core Research Support Facilities del Institut Català de Nanociència i Nanotecnologia, por el soporte técnico y la ayuda prestada a lo largo de la tesis.

Gracias a los colegas de grupo presentes y pasados, y al resto de compañeros. El colaborar con vosotros siempre ha sido estimulante y divertido, os habéis convertido en mis amigos. Gracias también al resto de amigos por vuestro apoyo consciente o inconsciente.

Finalmente, me gustaría agradecer a mi familia por su apoyo y cariño, sin ellos no habría llegado hasta aquí. Estoy también muy agradecida a mi pareja y a su familia por su cariño todos estos años.

Gracias a todos por el apoyo en los momentos duros de la tesis.

RESUMEN

El color juega un papel importante en nuestra vida diaria y no solo desde un punto de vista estético. Existe un gran mercado centrado en las aplicaciones tecnológicas derivadas del color, el cual engloba desde sus usos clásicos en colorantes y pigmentos hasta monitores, LEDs, almacenamiento óptico de datos y optoelectrónica, entre otros. En particular, la comunidad de materiales inteligentes ha dedicado especial atención al desarrollo de sistemas capaces de presentar una variación de color reversible al aplicar estímulos externos y a los cambios derivados en otras propiedades físicas, lo que se denomina cromismo.

En esta tesis nos hemos interesados particularmente en colorantes orgánicos que exhiban propiedades fotocromicas y termocromicas, es decir, cambios de color inducidos por exposición a la luz o variaciones de temperatura. Estos compuestos poseen una gran variedad de aplicaciones potenciales; sin embargo no pueden ser aplicados directamente ya que en muchos casos sus propiedades crómicas características en disolución se ven modificadas, ralentizadas o inhibidas cuando son introducidos en materiales sólidos.

El objetivo de esta tesis es proponer y explorar una nueva metodología capaz de solventar estos inconvenientes y permitir la transferencia directa de las propiedades fotocromicas y termocromicas observadas en disolución al estado sólido. Básicamente, nuestra aproximación consiste en la encapsulación de compuestos foto- y termocromicos en el interior de cápsulas poliméricas con núcleos líquidos, capaces de preservar el comportamiento crómico característico en solución y ofrecer la posibilidad de introducir estos sistemas en matrices sólidas en las cuales el cambio del color se vería inhibido de ser incorporados de forma directa. Aplicando la aproximación propuesta, tres tipos diferentes de materiales fotoactivos han sido desarrollados a lo largo de esta tesis: (i) recubrimientos fotocromicos de respuesta rápida con fines fotoprotectores, (ii) materiales sólidos termocromicos basados en tautoméros de valencia, (iii) y sistemas sólidos basados en fluoróforos termosensibles capaces de emitir luz blanca sintonizable.

ABSTRACT

Colour plays an important role in our everyday life and not only from an aesthetic point of view. There is a big market centred in technological applications derived from chromic phenomena and colour science, encompassing from the classical commercial uses of dyes and pigments to visual displays, light emitting diodes, optical data storage and optoelectronics, among others. Particularly, the smart materials community has paid special attention to systems exhibiting a reversible colour change upon application of external stimuli and the variations that this induces in other physical properties- namely, chromism.

In this thesis we have been particularly interested in photochromic and thermochromic organic dyes whose colour-tunability is induced by light irradiation and heat, respectively. These compounds present a wide range of potential applications; however, their usage is not straightforward since in many cases the well-established chromic properties of these species in solution are modified, slowed down or prevented when applied in solid materials.

The aim of this thesis is to propose and explore a novel methodology to address this issue and allow the direct transfer of photo- and thermochromic properties from solution to the solid state. Basically, it consists in the encapsulation of the photo- and thermochromic compounds of interest inside liquid-filled polymeric capsules, which should preserve their solution-like chromic behaviour and offer the possibility to introduce these systems into any type of matrix that would restrain their colour tunability when directly incorporated. As proof of concepts of this strategy, three specific types of photoactive systems have been developed along this thesis: (i) fast-responsive photochromic coatings for photoprotective purposes, (ii) solid thermochromic materials made of valence tautomers, and (iii) white-light colour-tunable materials based on thermoresponsive fluorophores.

Table of Contents

TABLE OF CONTENTS

Chapter 1 *General Introduction*

1.1	Introduction.....	3
1.1.1	Why to encapsulate?	3
1.1.2	Encapsulation systems	4
1.2	Synthesis of polymeric capsules	5
1.2.1	Mechanical methods	6
1.2.2	Physico-chemical methods	8
1.2.3	Chemical methods	10
1.3	Polymeric capsule applications	12
1.3.1	Dye and pigment encapsulation	12
1.3.2	Encapsulation of active ingredients and controlled release	14
1.3.3	Other applications	16
1.4	Encapsulation of photo- and thermochromic compounds	18
1.5	References	21

Chapter 2 *Objectives*

2.1	Objectives.....	33
-----	-----------------	----

Chapter 3 *Fast-responsive Photochromic Capsules*

3.1	Introduction.....	37
3.1.1	Photochromism	37
3.1.2	Photochromic compounds for the preparation of photoprotective coatings....	39
3.1.3	Liquid-filled capsules as an alternative approach for fast-responsive photochromic materials.....	44
3.1.4	Objectives	47
3.2	Results and discussion.....	47
3.2.1	Preparation of photochromic liquid-filled microcapsules	47

3.2.1.1	Melamine-formaldehyde microcapsules	48
3.2.1.2	Toluene-filled polyamide microcapsules	51
3.2.2	Characterisation of photochromic liquid-filled microcapsules	55
3.2.3	Preparation and characterisation of miglyol-filled photochromic polyamide microcapsules	59
3.2.4	Photochromic thin films based on liquid-filled microcapsules	63
3.2.5	Photochromic liquid-filled nanocapsules for the preparation of transparent coatings	69
3.3	Conclusions.....	73
3.4	References.....	74

Chapter 4 *Valence Tautomeric Thermochromism*

4.1	Introduction.....	83
4.1.1	Valence tautomerism	83
4.1.2	State-of-the art of VT systems micro/nanostructuring	86
4.1.3	Encapsulation of metal complexes as an alternative approach to valence tautomerism in the solid state	87
4.1.4	Our VT complex of choice: [Co ^{III} (Cat-N-BQ)(Cat-N-SQ)].....	89
4.1.5	Objectives	92
4.2	Results and discussion.....	92
4.2.1	Encapsulation into polymeric solid particles	92
4.2.1.1	Optimization of the encapsulation conditions	93
4.2.1.2	Solid PMMA particles loaded with VT1	97
4.2.2	Liquid-filled polymeric capsules	100
4.2.2.1	Capsule synthesis	101
4.2.2.2	VT1@PU_tol valence tautomerism	106
4.2.2.3	Valence tautomerism of miglyol-filled capsules	110
4.3	Conclusions.....	115
4.4	References.....	116

Chapter 5 Colour-Tunable White-Light Emitting Capsules

5.1	Introduction.....	123
5.1.1	How to define light colour: CIE 1931 chromaticity diagram.....	123
5.1.2	White-light emitting materials	126
5.1.2.1	White-light emission from individual multicomponent materials	128
5.1.2.2	Colour tunability in white-light emitting materials	133
5.1.2.3	Micro- and nanostructured white-light emitting materials	134
5.1.3	Liquid-filled capsules for the design of white-light emitting and colour tunable materials.....	136
5.1.3.1	ZW5: a thermally-responsive fluorophore	137
5.1.4	Objectives	140
5.2	Results and discussion.....	141
5.2.1	Selection of the capsules nature.....	141
5.2.1.1	Capsules liquid interior	141
5.2.1.2	Capsules shell.....	145
5.2.2	Selection of dye relative concentration and encapsulation of the optimized solution: preparation of BPEA-ZW5@PU_DOTP capsules.....	149
5.2.3	Colour-tunable white-light emission from liquid-filled capsules	153
5.3	Conclusions.....	155
5.4	References.....	156

Chapter 6 General Conclusions

4.3	General conclusions	165
-----	---------------------------	-----

Chapter 7 Experimental Section

7.1	General procedures.....	169
7.1.1	Materials	169
7.1.2	Microscopy imaging techniques	169
7.1.3	Optical characterization	170

7.1.4	Other	171
7.2	Synthesis of liquid-filled polymeric capsules	172
7.2.1	Photochromic capsules	172
	Synthesis of toluene melamine-formaldehyde capsules (MF_tol)	172
	Synthesis of toluene polyamide capsules (PA_tol).....	173
	Synthesis of miglyol polyamide capsules (PA_mig).....	174
	Attempts to synthesise of polystyrene nanocapsules	174
7.2.2	Thermochromic capsules	175
	Attempts to synthesise of polyamide capsules.....	175
	Attempts to synthesise of liquid-filled capsules by solvent evaporation	176
	Synthesis of toluene polyurea capsules (PU_tol)	176
	Synthesis of miglyol polyurea capsules (PU_mig).....	177
7.2.3	White-light emitting capsules	177
	Synthesis of miglyol polyurea capsules (PU_DOTP)	177
7.3	Synthesis of solid polymeric particles.....	178
7.3.1	Photochromic solid particles.....	178
	Synthesis of photochromic polystyrene nanoparticles (PhI@PS Nps)	178
7.3.2	Thermochromic solid particles	179
	Attempts to synthesise VT1@PMMA particles by emulsion polymerization	179
	Synthesis of VT1@PMMA particles by solvent evaporation	179
	Synthesis of solid polyurea particles containing VT1 complex (VT1@PU).....	180
7.4	Preparation of polymeric films.....	181
7.4.1	Photochromic polymeric films.....	181
	Polymeric thin films loaded with free PhI	181
	Polystyrene films loaded with PhI@PA_mig capsules (PhI@PA_mig@PS)	181
	Preparation of test lens matrices loaded with PhI@PA_mig capsules (PhI@PA_mig@lens).....	181
7.4.2	Thermochromic polymeric films	182
	Polymeric thin films loaded with VT1	182
7.5	References.....	182

Chapter **1**

General Introduction

1.1 Introduction

Encapsulation is the process by which a substance or mixture of substances are entrapped within another substance. This term encompasses a large variety of materials including natural structures such as eggs, shellfishes, fruits, plant seeds, spores and cells, or manmade objects of our daily life like medicine capsules, electrical cables, sweets or sport balls (Figure 1.1).



Figure 1.1 Examples of daily life encapsulated products.

Concerning smaller scales (micro- or nano-), encapsulation was introduced in the market in the 1940s for the synthesis of vitamin preparations¹. Around fifteen years later, dye-containing microcapsules were produced for the manufacture of carbonless copying paper², although the inventors already foresaw its applicability to other substances such as perfumes or adhesives^{3,4}. Since then, the potential of encapsulation has attracted the attention of the scientific community resulting in the publication of a vast number of papers and patents⁵ and the establishment of encapsulation methodologies in many industrial sectors⁶⁻⁸.

1.1.1 Why to encapsulate?

Encapsulation offers several advantages some of which are listed below⁹⁻¹⁵:

- (i). the protection of sensitive substances from the external environment improving the stability and the resistance of the final product.
- (ii). the separation of incompatible components (e.g. reactive molecules in a mixture).
- (iii). the controlled and targeted release of the encapsulated material.
- (iv). to mask organoleptic properties like colour, taste or odour.
- (v). to combine the properties of different types of materials.

- (vi). to retain the characteristics of the encapsulated substances when dispersed into another material and improve their compatibility preventing agglomeration and allowing a uniform dispersion.
- (vii). to alter colloidal and surface properties or introduce new attributes such as stimuli-responsive features or other "smart" functionalities.
- (viii). to manipulate liquid and gasses as solid powdered materials.
- (ix). to facilitate manipulation, afford safe handling and prolonged storage.

This versatility allows obtaining a wide range of products depending on the nature of the substance enclosed, the material used for the encapsulation and the process applied.

1.1.2 Encapsulation systems

Encapsulation systems are composed of: (i) the substance encapsulated that generally carries the fundamental property of the system (payload); and (ii) the material that encloses the former and determines its behaviour. They can present different designs, among which films and particles made of porous, compact, gel-like, glassy or rubbery materials, with crystalline or amorphous structures, are the most common¹⁶⁻²¹. The substance encapsulated can be either dispersed within the matrix of the system or entrapped by a layer of the encapsulating material in a core-shell distribution. These features altogether will determine the properties of the system and its possible applications. For instance, the encapsulation of a perfume within a porous matrix would allow its slow release; on the contrary, to prevent the unintended delivery of a toxic compound, a robust and impermeable coating would be required.

Among the different systems reported in literature, spherical capsules are one of the most common. Capsules are defined as hollow particles composed of a solid shell surrounding a core-forming space capable to entrap, permanently or temporarily, different type of substances in order to form composite materials²². Although this term is frequently used as a more general concept, the presence of an outer layer is what differentiates capsules from other type of particles used for encapsulation. Figure 1.2 aims to illustrate this difference comparing the structure of a spherical solid particle with the core-shell distribution of spherical monocoreshell and multicore capsules.

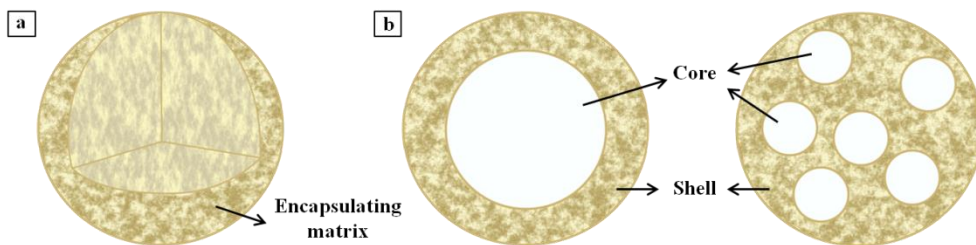


Figure 1.2 (a) Spherical solid particle. (b) Spherical moncore and multicore capsules and their core-shell structure.

The core of capsules can be solid, liquid or gaseous and contain dispersed and/or dissolved materials. On the other hand, the shell must be chemically compatible but non-reactive with the core material (in order to retain the attributes of the encapsulated substances) and provide the desired physical properties to the system (resistance, strength, flexibility, permeability, optical properties, etc)^{9,15}. Polymers and silica-based materials are often selected to form the outer-layer of the capsules due to their stability and robustness^{21,23}. Whereas the latter are mechanically stable, chemically and biology inert, and present high temperature resistance, the vast variety of polymers and techniques available to prepare polymeric structures allows to easily tune the properties of the capsule shells for a desired purpose. The work developed in the present doctoral thesis is based on polymeric capsules, in whose interior the photoactive stimuli-responsive molecules of interest will be confined. Therefore, the following section will describe the main methods developed for their synthesis.

1.2 Synthesis of polymeric capsules

Polymeric capsules can be synthesised through (i) mechanical, (ii) physical or (iii) chemical methods. The two first categories include those procedures that employ preformed polymers in their formulations, whereas chemical methods involve a polymerisation reaction.

1.2.1 Mechanical methods

Mechanical methods require specific equipment and are mostly employed for the production of encapsulating systems at the microscale. This category comprises spray drying, fluidised bed and pan coating, methods well established in industry, and spinning disc, co-extrusion and supercritical fluids techniques, which are mainly used on a laboratory scale.

Spray drying is mostly employed for the encapsulation of fragrances, oils and flavours^{22,23}. A schematic illustration of this method is shown in Figure 1.3(a). The substances to be encapsulated are homogenised into a concentrated solution of the encapsulating polymer. The resultant emulsion is atomised forming a spray of droplets that is subsequently introduced into a heated compartment where the solvent of the emulsion (generally water) is evaporated. As a consequence, the polymer solidifies yielding the formation of multicore capsules or solid particles depending on the formulations^{12,13}.

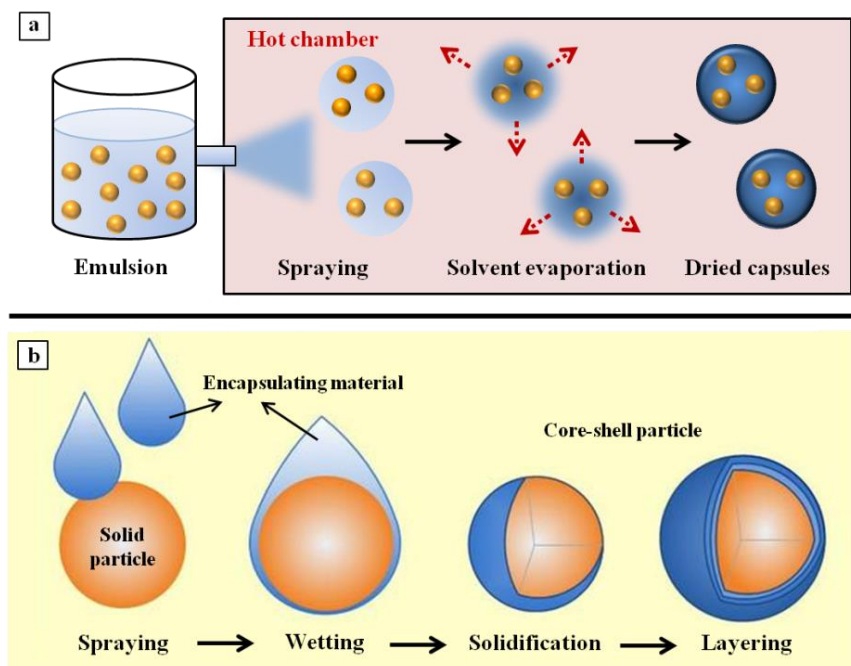


Figure 1.3 Schematic representation of (a) spray-drying and (b) fluidised bed coating process ((b) is adapted from reference 26).²⁶

On the other hand, **fluidised bed coating** is used for the encapsulation of solid or porous particles¹⁵. The basic steps of this procedure are illustrated in Figure 1.3(b). In this case, the

liquid coating material (a melt or dissolved polymer) is sprayed onto the surface of the core-forming particles, which are suspended in a jet of air. The small droplets of the liquid spread and coalesce, and after cooling or solvent evaporation the polymeric coating solidifies and adheres to the particle surface. The process is repeated until the capsule shell achieves the desired thickness. This method is extensively employed in pharmaceuticals and cosmetics^{11,24}.

Pan coating and **spinning disc** are also employed for the encapsulation of solid materials, although the former is used with relatively large particles^{9,12}. Similarly to fluidised bed coating, in pan coating method the encapsulating polymer is applied as a solution or as an atomised spray over the core particles in a rotating coating pan. Warm air removes the solvent and the polymer solidifies. In spinning disc method, microencapsulation is carried out by using a rotating disc^{15,25}. The solid particles to be encapsulated are dispersed in the polymeric coating liquid. The resulting suspension is poured into a rotating disc and due to its spinning action the core particles become coated with the polymeric material. The centrifugal force casts out the coated particles from the edge of the disc and the polymer is then solidified usually by cooling.

Extrusion and co-extrusion^{15,24} methods consist in pumping a fluid stream through a tube. By the influence of vibration, the stream breaks into droplets and core-shell particles are obtained after hardening the encapsulating polymer by chemical cross-linking, cooling or solvent evaporation. **Co-extrusion** is mainly used for the synthesis of liquid-filled capsules, and in this case a dual fluid stream of immiscible liquids is pumped through concentric tubes: the inner tube contains the liquid core and the outer tube the polymeric shell material.

Supercritical fluid methods are employed for the synthesis of micro- and nanocapsules^{25,27}. They are considered as clean processes due to the low amounts of residual organic solvents generated. The absence of water and the relatively mild conditions required (high temperatures are not needed) allow the encapsulation of sensitive materials, making these methodologies promising for the development of drug delivery systems^{25,28}. The basic concept of these methods is the mixture of the encapsulating polymer and the core material with a supercritical fluid (i.e. substances above its thermodynamic critical point of temperature and pressure, exhibiting simultaneously properties typical of liquids and gases). In a process similar to spray drying, the mixture is sprayed out, the pressure drops and, consequently, the polymer shell forms around the core material by different mechanisms depending on the specific method employed^{15,27}.

1.2.2 Physico-chemical methods

Physico-chemical methods rely on a physical process induced by changes in physico-chemical parameters of a dispersion (pH, temperature, solubility, etc) for the fabrication of the core-shell structure departing from a preformed polymer, sometimes in combination with a chemical reaction to enhance the shell resistance and stability (e.g. polymer cross-linking). Many of the methods encompassed in this category are based on a phase separation process. Basically, they consist in the precipitation of the encapsulating polymer around the capsule core forced by a reduction of polymer miscibility with the medium in which it has been dissolved.

Coacervation¹⁵ is a physical phenomenon characterised by the partial desolvation of a homogeneous polymer solution (generally, an aqueous solution²⁵) into a polymer-rich phase, the coacervate, and a polymer-poor phase, the coacervation medium, by the addition of a desolvation agent. This was the mechanism followed for the synthesis of the first polymeric capsules developed^{1,2}. When applied to an encapsulation process, the coacervate deposits around the core material which has been previously dispersed in the reaction medium, as shown in the schematic illustration of the process in Figure 1.4. For this to happen, the core material used must be compatible with the encapsulating polymer but insoluble in the coacervation medium.

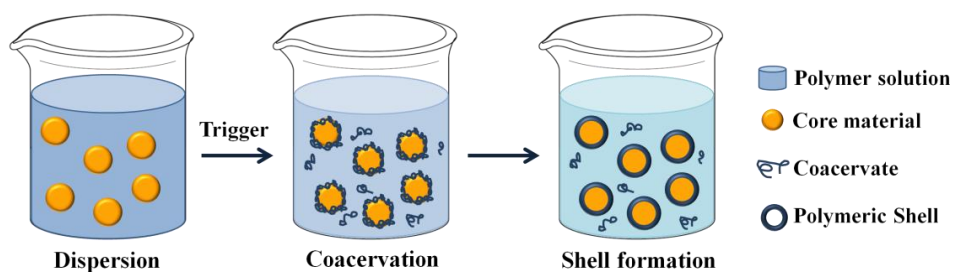


Figure 1.4 Schematic illustration of capsule formation by coacervation method.

This method is divided in two types according to the way in which the phase separation is carried out: in **simple coacervation**, the desolvation agent induces the simple precipitation of the coacervate around the core material, whereas **complex coacervation** involves the

complexation between two oppositely charged polymers. In any case, desolvation can be triggered by a variety of factors, such as temperature or pH changes, the addition of a salt (salting-in) or a non-solvent^{9,12}. In a final step, the capsules prepared are stabilised by further desolvation, cross-linking or thermal treatment.

Solvent evaporation and **solvent diffusion** methods can also be employed for the synthesis of liquid-filled capsules. Figure 1.5 displays the basic process of these methods. Although they also involve a phase separation process as in the coacervation method, in this case the immiscible encapsulating polymer and the core material are dissolved in a common solvent and already initially confined in the dispersed phase of the emulsion. This is generally an organic phase, which is emulsified in a second liquid (the continuous phase, mostly water) that is immiscible with both the core material and the shell polymer. Then, the solvent is removed from the dispersed solution and, as a result, the polymer deposits at the interface of the emulsion droplets, which act as templates, enclosing the core material²⁹. To obtain capsules instead of solid spheres at the end of the process, the polymer and the core material must possess quite different polarities. In the **solvent evaporation** method, the polymer-core solution is prepared using a volatile solvent in order to induce polymer precipitation as it evaporates^{23,30}. On the other hand, in the **solvent diffusion** method capsules are formed by forcing the diffusion of the solvent out from the dispersed phase by a variety of methods, such as: (i) spontaneous emulsification, (ii) dilution of saturated emulsions; (iii) salting-out and (iv) the addition of a third liquid miscible with the continuous phase and the diffusing solvent^{29,31,32}.

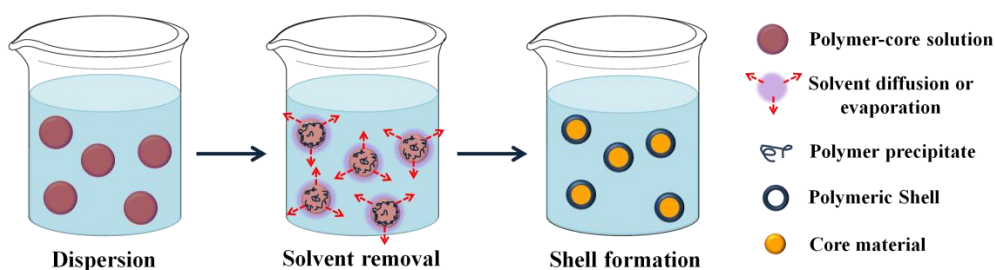


Figure 1.5 Schematic illustration of capsule formation by solvent removal (i.e. solvent evaporation or solvent diffusion methods).

Another important encapsulation method is **layer-by-layer deposition** (L-b-L)^{17,33}. The general procedure of this method is depicted in Figure 1.4, where polyelectrolyte multilayers are deposited around a charged spherical template by sequential immersion in positively and

negatively charged polyelectrolyte solutions. If the template (generally, colloidal particles) is removed, a cavity is formed inside the polyelectrolyte shell. These hollow capsules can be loaded with a substance of interest by permeation through the shell, which is held together due to the strong electrostatic forces that exist between each component layer. Recently, the synthesis of liquid-filled capsules through L-b-L deposition in oil-in-water emulsions has been reported. In this case, the emulsion droplets act simultaneously as template and capsule core^{23,34}.

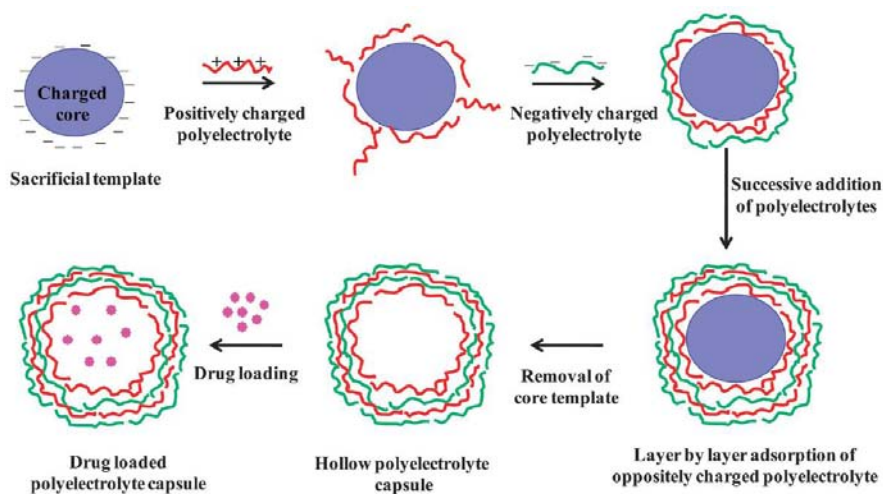


Figure 1.6 Schematic representation of colloid-templated polyelectrolyte hollow capsules prepared by layer-by-layer deposition³⁵.

1.2.3 Chemical methods

Polymeric capsules can also be obtained by means of polymerisation reactions²³ in dispersed systems. The resulting polymer must be insoluble in both the continuous phase and the core material such that, as the reaction proceeds, the polymer shell is formed around the dispersed phase, enclosing capsule core. The existing polymerisation mechanisms that lead to core-shell structures can be classified into two main groups depending on how the reactive monomers are distributed in the initial dispersion: interfacial polymerisation and in-situ polymerisation. These two methods are schematically represented in Figure 1.7.

In **interfacial polymerisation**¹⁰, two complementary monomers dissolved in different phases of the system react as they diffuse to the interface of the droplets of the dispersed solution. Frequently used lyophilic monomers are polyacid chlorides and polyisocyanates. They are dissolved within the core material and polymerise with polyamines or polyalcohols added to the aqueous continuous phase to form polyamide^{36,37}, polyurea^{38,39} or polyurethane^{40,41} shells. A variation of this methodology is **interfacial cross-linking**^{42,43}, which is often used to prepare polymeric capsules based on proteins and polysaccharides. In this case capsule shell forms by the reaction of a water-soluble polymer with a cross-linker contained in the dispersed organic phase, once they get in contact at the interface.

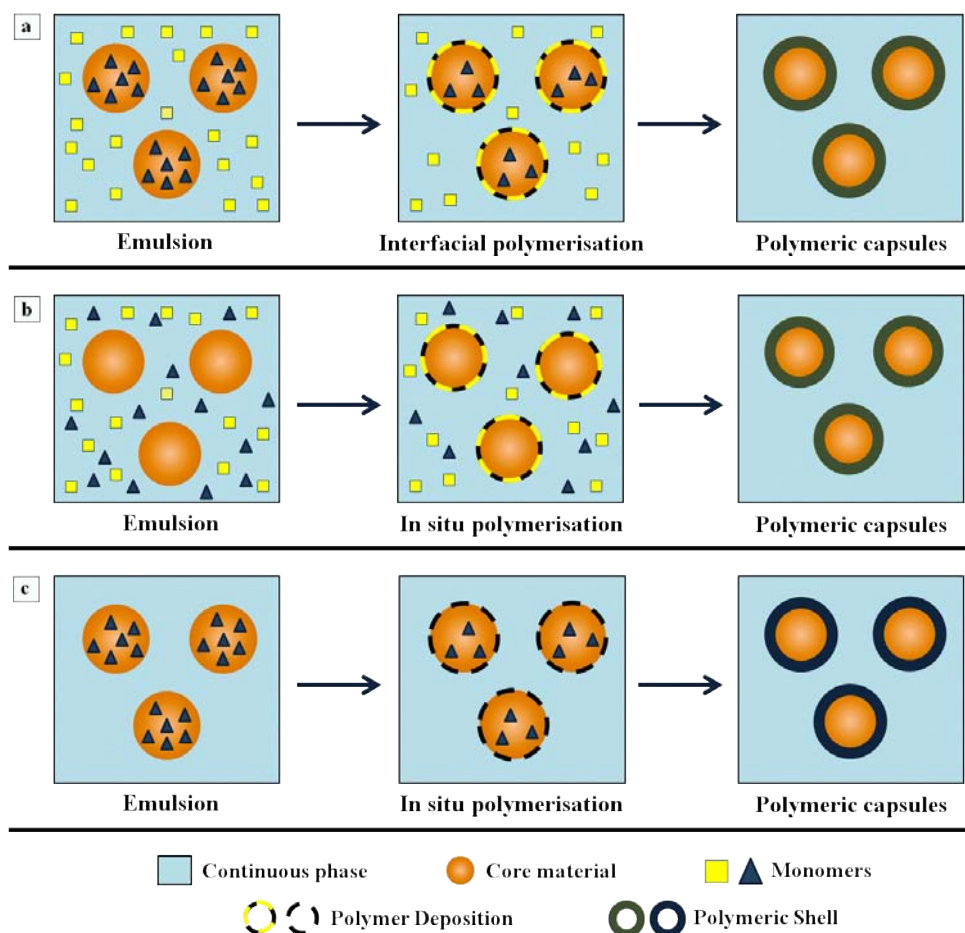


Figure 1.7 Schematic representation of (a) interfacial polymerisation, (b) in situ polymerisation carried out in the aqueous phase, and (c) in situ polymerisation carried out in the dispersed phase.

On the contrary, if **in situ polymerisation**¹² is employed, all the monomers required are located in the same phase, either in the continuous (typically, aqueous) or in the dispersed phases (typically, organic). The capsule shell forms as the polymeric chains grow and deposit at the interface of the dispersed system. Many water-immiscible liquids have been encapsulated in oil-in-water emulsions through this method. Different reactions mechanism have been used depending on the phase in which the polymerisation takes place. One of the most common is melamine-formaldehyde or urea-formaldehyde polycondensation reactions in the continuous aqueous phase⁴⁴⁻⁴⁶. Free-radical polymerisation or anionic polymerisation carried out in the oil-dispersed phase have also been reported for the synthesis of polyalkylcyanoacrylate and polystyrene capsules, among others^{29,47}. In these cases, the polymerisation initiators (e.g. radical initiator, water) are dissolved in the continuous aqueous phase, thus forcing polymer formation to start at the interface of the droplets of the organic dispersed phase.

1.3 Polymeric capsule applications

The variety of monomers and techniques available for the synthesis of polymeric capsules, allows adapting capsule properties to the requirements of specific applications. This flexibility has enabled the encapsulation of very different types of materials (from dyes to cells) and the development of a large number of encapsulation products, some of which are already commercially exploited.

1.3.1 Dye and pigment encapsulation

The manufacture of carbonless copy paper based on microencapsulated dyes was one of the first applications of polymeric capsules. This technology, patented in 1955 by National Cash Register Corporation, consists of a paper coating composed of oil-filled microcapsules containing printing dyes². The procedure reported for the synthesis of these capsules was a complex coacervation of colloidal materials, mainly gelatine and gum arabic^{2,48}.

Carbonless copy paper is still in use today and although many changes have been introduced in the original procedure, the basic concept remains the same⁴⁹. The pressure applied locally

during printing or writing on a sheet containing these coatings induces capsule rupture and, as a consequence, the dye precursor dissolved in the liquid core is transferred to an underlying sensitised sheet containing the colour developer. When in contact, the dye precursor and the colour developer react to form a distinctive colour, producing an instant replica of the information inscribed. Moreover, the encapsulation prevents dye leakage from random cracks produced in the coating film due to folding on rough handling, and the impermeability of the shell protects the dye from the surrounding media improving the resistance of the material to heat, moisture and other harmful influences.

Nowadays, pigment encapsulation is frequently employed in ink and paint industries⁵⁰. Pigment particles are enclosed by polymeric shells to prevent their agglomeration, protect them from environmental aggressions and enhance colour durability and storage stability^{51,52}. Moreover, these polymeric coatings also allow the use of organic pigments (insoluble in water) in water-based formulations.

Another successful application of microencapsulation is the electronic ink used in paper-like displays, which is based on the encapsulation of an electrophoretic dispersion in a dielectric fluid of highly light-scattering charged pigment particles of different colours⁵³⁻⁵⁵. The pigment-containing capsules are mostly prepared by urea-formaldehyde in situ polymerisation^{10,54,56,57}, although other methodologies have also been applied^{58,59}. Figure 1.8(a) depicts the operation of a two-particle system of black and white pigments with opposite charges, which is applied in black-and-white paper-like displays. The microcapsules are placed between a pair of electrodes and under the influence of the electric field the encapsulated pigment particles are forced to migrate towards the electrode possessing opposite polarity. Therefore, depending on their charge, pigments move inside the capsule (thanks to their liquid interior) towards or away from the viewer forming a white or black area on the upper surface of the display which corresponds to a pixel (an animated illustration can be watched in E Ink webpage: <http://www.eink.com/technology.html>⁶⁰). In this way images can be electrically written or erased repeatedly, as shown in Figure 1.8(b).

Electrophoretic image displays were first developed in the 1960s, however, the industrialisation of this technology was restrained because of serious problems with reliability and lifetime resulting from pigment particle clustering, agglomeration, and lateral migration^{10,53,54,59}. It was not until the introduction of the microcapsules that this technology succeeded. Encapsulation did not only solve lifetime issues (pigment dispersions are

enclosed in discrete compartments and particles cannot move or agglomerate on a scale larger than the capsule size), but also permitted the easy and simple manufacture of electronic displays by means of printing. Nowadays, the electronic ink is applied in a large variety of displays but especially in many of the e-books on the market (Kindle, Kobo, Nook, etc⁶¹).

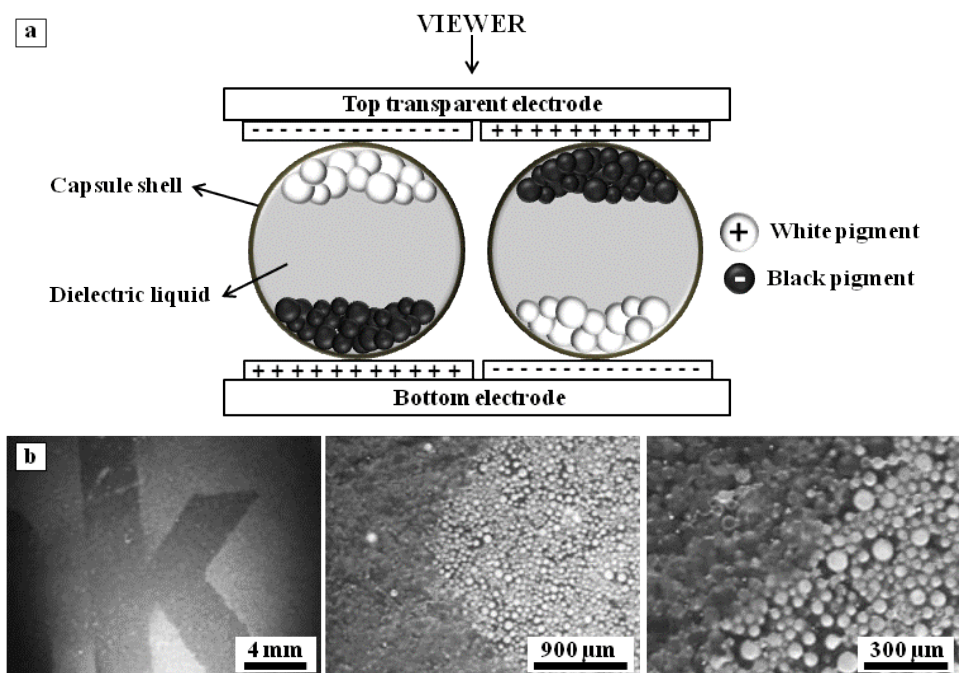


Figure 1.8 (a) Schematic illustration of the operation of an electronic ink based on a two-particle system formed by black and white pigments with opposite charges. (b) Series of photomicrographs at different magnifications in which the letter 'k' has been electronically written with electronic ink. Zoom-in into the ink allows discriminating the black- and white-coloured microcapsules that give rise to image contrast. Adapted from reference 54.

1.3.2 Encapsulation of active ingredients and controlled release

Polymeric capsules have been intensively explored for the encapsulation of active ingredients in many industrial sectors. Capsules do not only offer protection of the active components upon degradation and improve their stability during processing and in the final products, but also allow their sustained or controlled release by properly selecting the

characteristics of the polymeric shell in order to force the delivery of the capsule cargo in a selected location at desired rate.

In **pharmaceutics** area this research is focused on the development of delivery carriers for safe and efficient administration of drugs¹¹. Low aqueous solubility, reduction of drug efficiency (due to partial degradation before reaching the target site), and accumulation in undesired organs or tissues are some of the problems associated with pharmaceuticals³⁵. In this regard, drug encapsulation affords enhanced solubility, protection against enzymatic degradation and offers the possibility of targeted and localised cargo release by means of surface functionalisation of the capsule shells^{33,62}. These might reduce the drug dose required and the overall concentration of the drug in the body, diminishing adverse side effects and immune system responses. In order to attain such controlled release, many stimuli-responsive capsules have been reported^{63–66}, in which the integrity or permeability of the shell is modified by changes in environmental conditions (temperature, pH, reducing media, etc)^{67–72} or after the application of an external trigger (light or electric and magnetic fields)^{62,73}. As an example, Figure 1.9 schematically shows one the approaches followed, consisting in the incorporation of plasmonic metal nanoparticles in the polymeric shell. Upon irradiation, these nanoparticles absorb light and liberate heat, leading to a local increase of temperature which induces the rupture of the shell or an increase in polymer permeability and, as a consequence, the release of the drug incorporated.

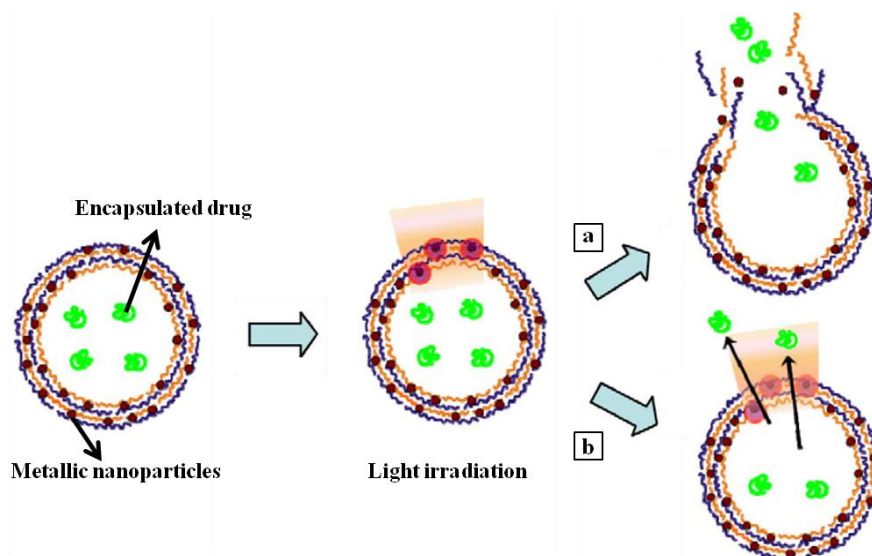


Figure 1.9 Schematic representation of drug release by laser interaction with plasmonic metal nanoparticles incorporated in the capsule shell. Adapted from reference 73.

In **food industry**, encapsulation has been employed to enhance product quality and stability. Flavour and aroma are two of the most important features of food products; however, manufacturing and storage processes, packaging materials and interactions with other ingredients often cause modifications in the overall taste and odour of the final products²⁴. On the other hand, there is a trend towards the development of "functional food" in which certain additives (polyphenols, vitamins, minerals, essential oils, antioxidants, nutraceuticals, etc) are incorporated for prevention of diseases or to improve food nutritional values^{11,32}. However, simply adding ingredients to food products can compromise their taste, colour, texture or aroma making them less appealing. Sometimes, their degradation can also induce the loss of their activity or the generation of hazardous products by oxidation reactions. Hence, food encapsulation in polymeric capsules aims to protect flavour and aromas from degradation or loss^{24,74}, mask the unpleasant effects of some additives^{70,76}, improve the effectiveness of active ingredients and their bioavailability^{13,14,77} or simplify manufacturing processes by converting liquids to solid powders^{11,13,14}.

The same idea is also applied in **cosmetics**, personal care products or fabrics^{8,78,79}, where encapsulation in core-shell particles is used for the entrapment of fragrances and perfumes, to increase the durability of the scent, or as carriers for the topical application of active ingredients⁸⁰⁻⁸². With this aim, polymeric capsules have been incorporated in creams, shampoos, deodorants, insect repellents, laundry products or household detergents.

Polymeric capsules have also been employed for **pest control** purposes in the area of crop protection^{5,11}. Pesticides, insect pheromones or microbial agents^{45,83-86} have been encapsulated in order to increase durability and attain a slow and sustained release. With the same objective, polymeric capsules containing biocide compounds are employed in the design of antifouling paints^{87,88}. In both cases, encapsulation reduces the number of applications and dosage, decreasing environmental issues, and affording a safer handling due to isolation during the coating process.

1.3.3 Other applications

Phase-change materials (PCMs) are substances capable of storing and releasing large amounts of heat when undergoing a phase transition⁸⁹. As the heat is supplied, the material

changes its phase from solid to liquid at constant temperature until it completely converts into liquid. Similarly, the material changes from liquid to solid until it solidifies completely realising heat. In bulk, PCMs are not easy to handle and can be highly corrosive and toxic. Their isolation within polymeric capsules solves these problems facilitating their manipulation and reducing their reactivity with the surrounding materials^{39,90–92}. In addition, capsules afford large heat transfer areas improving their efficiency, and prevent liquid leakage since polymeric shells can bear the large volume changes that occur during phase transition. Encapsulated PCMs are employed in refrigeration, air conditioning, and solar heating systems; in fabrics for dynamic heat regulation, thermal protection or as flame retardants; and in building construction to improve thermal comfort and reduce energy consumption^{46,89}.

Research on **self-healing materials** has also led to the incorporation of capsules in their formulations^{93,94}. Upon damage, these materials release a healing agent in order to restore their initial properties without the need for detection or any type of manual intervention. Polymeric capsules act as healant containers and they can also enclose corrosion inhibitors or warning dyes^{95,96}. They are especially used in self-healing polymeric coatings which are employed to prevent material corrosion. Figure 1.10(a) depicts their general operation.

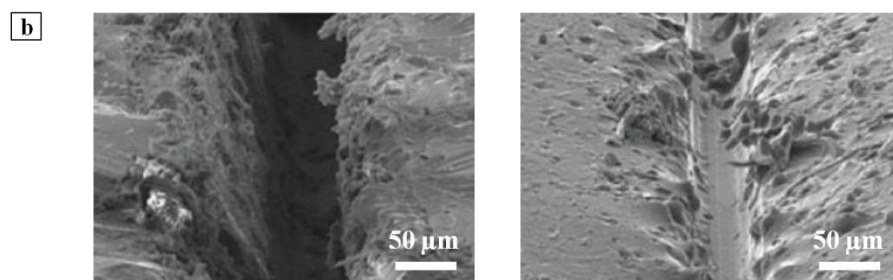
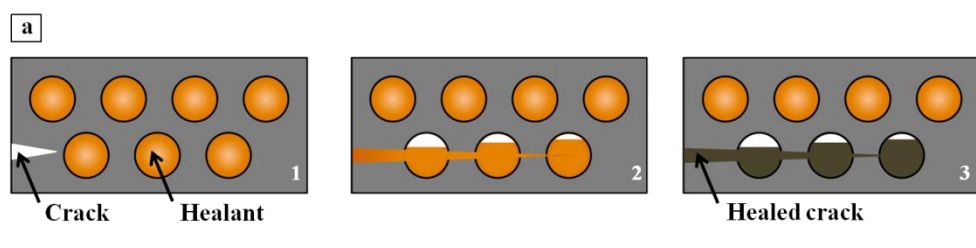


Figure 1.10 (a) Schematic representation of the operation of self-healing materials. (b) SEM images comparing the recovering capacity of two coatings in the absence (left) and the presence (right) of the microencapsulated healing agent, showing the healing potential of the latter (adapted from reference 97).

As cracks propagate in a material, microcapsules rupture and release healing agents that flow through the fracture plane and seal the crack by polymerisation, or solvent- or plasticiser-assisted welding, thus preventing further propagation and restoring the original mechanical properties of the system⁹⁷⁻⁹⁹. The recovery capacity of these materials is demonstrated in the SEM images of Figure 1.10(b) that show the behaviour of two coatings after being damaged: only the one on the right, which contains the microencapsulated healing agent, is repaired.

The wide variety of applications and the multiple purposes for which they are employed, demonstrates the ability of polymeric capsules to enclose materials of different nature. In our case we are interested on encapsulating solutions of stimuli-responsive molecules for the preparation of photofunctional materials.

1.4 Encapsulation of photo- and thermochromic compounds

Colour plays an important role in our everyday live and not only from an aesthetic point of view. There is a big market centred in technological applications derived from chromic phenomena and colour science, encompassing from the classical commercial uses of dyes and pigments to visual displays, light emitting diodes, optical data storage, digital printing, optoelectronics, solar energy conversion, biomedical probes or sensors, among others¹⁰⁰. Particularly, the smart materials community has paid special attention to systems exhibiting a reversible colour change and the variations that this induces in other physical properties. This phenomenon is called chromism, of which there are different types depending on the stimulus that induces the colour change¹⁰¹. Commercially the most important are photochromism, thermochromism, electrochromism and ionochromism induced by light irradiation, heat, oxidation or reduction processes, and the addition of salts, respectively.

In this thesis we have been particularly interested in photochromic and thermochromic organic dyes, whose colour-tunability can be employed in a wide range of applications. However, their usage is not straightforward since in many cases the well-established chromic properties of these species in solution are modified, slowed down or prevented when applied in solid materials¹⁰²⁻¹⁰⁵. Actually, this is often one of the major bottlenecks in the incorporation of photo- and thermochromic molecular compounds into truly functional

devices, as will be discussed in detail in Chapters 3-5 dealing with particular applications of these types of dyes. The aim of this thesis is to propose and explore a novel methodology to address this issue and allow direct transfer of photo- and thermochromic properties from solution to the solid state.

Figure 1.11 shows a schematic diagram of the fundamentals of our approach. Basically, it consists in the encapsulation of the photo- and thermochromic compounds of interest inside liquid-filled polymeric capsules, which should preserve their solution-like chromic behaviour and offer the possibility to introduce these systems into any type of matrix that would restrain their colour tunability when directly incorporated. In our strategy, the shell of the capsules would isolate the chromic molecules from the obstructing surrounding media in which they must be dispersed, while the core must be selected in order to maximise their chromic properties.

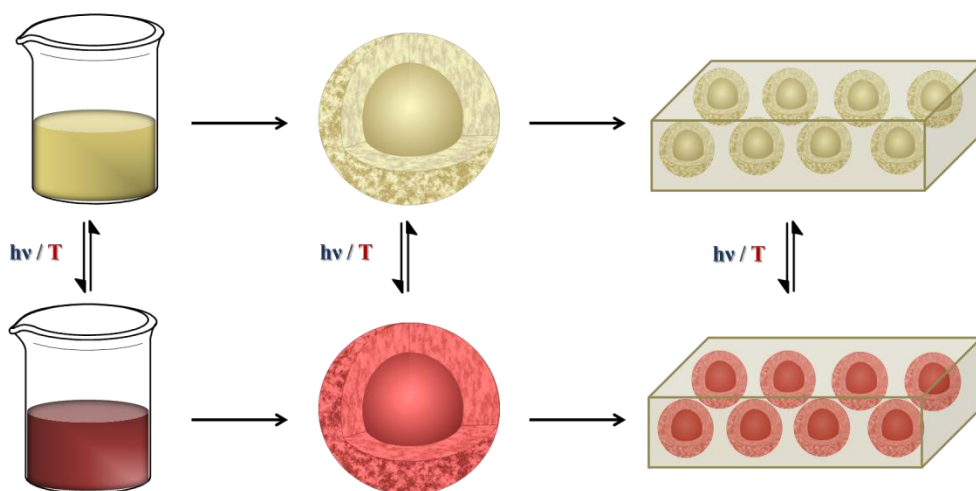


Figure 1.11 Schematic representation of the strategy proposed in the present doctoral thesis: encapsulation of photoactive solutions inside polymeric capsules and their subsequent incorporation into solid matrices in order to attain solid materials with the desired chromic behaviour.

Some examples of encapsulation of photo- and thermochromic compounds can already be found in the literature and even in industrial applications. Thus, a similar approach to that proposed herein has already been applied for the development of thermochromic inks based on thermochromic liquid crystals, which selectively reflect specific wavelengths of light according to the structure that they exhibit at each temperature^{106,107}. In these materials, molecules are oriented in a preferred direction that varies periodically along their structure,

thus defining the colour perceived. Temperature changes produce thermal expansions that vary the layer spacing and consequently, modify the colour reflected by the system progressively. Generally, these materials are applied as printing inks composed of polymeric capsules containing the thermochromic liquid crystals, which are suspended on a binder that forms a coating when deposited on a substrate^{106,107}. The capsules shell encloses the liquid crystal and avoids its contamination by other components present in the coating formulation.

Similarly, the most widely used industrial thermochromic pigments are based on the encapsulation of dye/developer/solvent organic mixtures^{108,109}. These systems are composed of (i) a leuco dye presenting two distinct forms, one of which is colourless, that interconvert through pH variations (i.e. a ionochromic dye); (ii) the colour developer that is a proton donor; and (iii) a low-melting, non-volatile solvent that controls the transition temperature at which the colour change takes place¹⁰⁶. The changes in the solvent state (solid or melted) with temperature modify the interactions between the dye and the colour developer, shifting the equilibrium towards the coloured or the colourless form of the dye. Again, the capsules enclose the thermochromic mixture acting as pigment containers in inks formulations and imparting the colour to the final coating.

On the other hand, the encapsulation of photochromic systems inside liquid-filled polymeric capsules is not very common. Actually, the few existing examples by the time we started this work are based on viscous polymeric or resinous particles loaded with photochromic dyes and coated with cross-linked polymers or inorganic oxides^{110,111}. These capsules are then dispersed in another matrix whose photochromic response is determined by the interactions of the capsule core material with the dye molecules.

It must be noted that all these precedents share a common bottom line: to use liquid-filled capsules as mere containers or vehicles of the stimuli-responsive species, thus simply ensuring incorporation to the final device, transfer between two different materials and/or contact between different active species. Instead, our strategy is intended to go a step beyond by exploiting the liquid interior of the capsules to tune and optimise the chromic response of the dyes of interest and preserve this behaviour regardless of the final solid surrounding matrix required for a given application. In this way, we aim to minimise detrimental effects of rigid solid environments on the molecular processes involved in photo- and thermochromic interconversion and enable direct transfer of solution-like chromic behaviour into any type of desired functional material. As proof of concepts of this

strategy, three specific types of photoactive systems have been developed along this thesis by encapsulating photo- or thermochromic dyes: photochromic coatings for photoprotective purposes (Chapter 3), solid thermochromic materials made of valence tautomeric complexes (Chapter 4), and white-light colour-tunable materials based on thermoresponsive fluorophores (Chapter 5).

1.5 References

1. Taylor, H. F. Vitamin preparation and method of making same. US2183053 A (1939).
2. Green, B. K. Pressure sensitive record material. US2712507 A (1955).
3. Green, B. K. Oil-containing microscopic capsules and method of making them. US2800458 A (1957).
4. Green, B. K. & Schleicher, L. Oil-containing microscopic capsules and method of making them. US2800457 A (1957).
5. Vemmer, M. & Patel, A. V. Review of encapsulation methods suitable for microbial biological control agents. *Biol. Control* **67**, 380–389 (2013).
6. Frost & Sullivan. European Microencapsulation Technologies. (2002). at <<http://www.frost.com/sublib/display-report.do?id=B059-01-00-00-00>>
7. Boh, B. Microcapsules deliver. *Chem. Ind.* (2008). at <<http://www.soci.org/Chemistry-and-Industry/CnI-Data/2008/2/Microcapsules-deliver>>
8. Martins, I. M., Barreiro, M. F., Coelho, M. & Rodrigues, A. E. Microencapsulation of essential oils with biodegradable polymeric carriers for cosmetic applications. *Chem. Eng. J.* **245**, 191–200 (2014).
9. Sampath Kumar, K. P., Tejbe, S., Shameem Banu, A. S., Naga Lakshmi, P. & Bhowmik, D. Microencapsulation Technology. *Indian J. Res. Pharm. Biotechnol.* **1**, 324–328 (2013).
10. Guo, H., Zhao, X. & Wang, J. Synthesis of functional microcapsules containing suspensions responsive to electric fields. *J. Colloid Interface Sci.* **284**, 646–651 (2005).

11. Dubey, R., Shami, T. C. & Bhasker Rao, K. U. Microencapsulation technology and applications. *Def. Sci. J.* **59**, 82–95 (2009).
12. Jyothi, N. V. N. *et al.* Microencapsulation techniques, factors influencing encapsulation efficiency. *J. Microencapsul.* **27**, 187–197 (2010).
13. Fang, Z. & Bhandari, B. Encapsulation of polyphenols - A review. *Trends Food Sci. Technol.* **21**, 510–523 (2010).
14. Nedovic, V., Kalusevic, A., Manojlovic, V., Levic, S. & Bugarski, B. An overview of encapsulation technologies for food applications. *Procedia Food Sci.* **1**, 1806–1815 (2011).
15. Ghosh, S. K. & Ed: Ghosh, S. K. *Functional coatings and microencapsulation: a general perspective. (in Functional coatings: by polymer microencapsulation).* (Wiley-VCH, 2006).
16. Shim, T. S., Kim, S. H. & Yang, S. M. Elaborate design strategies toward novel microcarriers for controlled encapsulation and release. *Part. Part. Syst. Charact.* **30**, 9–45 (2013).
17. Fu, G.-D., Li, G. L., Neoh, K. G. & Kang, E. T. Hollow polymeric nanostructures- Synthesis, morphology and function. *Prog. Polym. Sci.* **36**, 127–167 (2011).
18. Huxford, R. C., Della Rocca, J. & Lin, W. Metal-organic frameworks as potential drug carriers. *Curr. Opin. Chem. Biol.* **14**, 262–268 (2010).
19. Raboin, L., Matheron, M., Biteau, J., Gacoin, T. & Boilot, J.-P. Photochromism of spirooxazines in mesoporous organosilica films. *J. Mater. Chem.* **18**, 3242–3248 (2008).
20. Kim, S., Seo, J., Jung, H. K., Kim, J.-J. & Park, S. Y. White luminescence from polymer thin films containing excited-state intramolecular proton-transfer dyes. *Adv. Mater.* **17**, 2077–2082 (2005).
21. Ciriminna, R., Sciortino, M., Alonzo, G., De Schrijver, A. & Pagliaro, M. From molecules to systems: Sol-gel microencapsulation in silica-based materials. *Chem. Rev.* **111**, 765–789 (2011).
22. Vert, M. *et al.* Terminology for biorelated polymers and applications (IUPAC Recommendations 2012). *Pure Appl. Chem.* **84**, 377–410 (2012).
23. Lensen, D., Vriezema, D. M. & van Hest, J. C. M. Polymeric microcapsules for synthetic applications. *Macromol. Biosci.* **8**, 991–1005 (2008).
24. Madene, A., Jacquot, M., Scher, J. & Desobry, S. Flavour encapsulation and controlled release - a review. *Int. J. Food Sci. Technol.* **41**, 1–21 (2006).

25. Gouin, S. Microencapsulation: Industrial appraisal of existing technologies and trends. *Trends Food Sci. Technol.* **15**, 330–347 (2004).
26. Fluidized Bed Processes - Neuhaus Neotec. at <http://www.neuhaus-neotec.de/partikel_ws/en/wirbelschicht/coating/>
27. Reverchon, E. & Adami, R. Nanomaterials and supercritical fluids. *J. Supercrit. Fluids* **37**, 1–22 (2006).
28. Boury, F., Tewes, F., Benoit, J.-P. & Ed: Benita, S. *Biodegradable microspheres: advances in production technology.* (in *Microencapsulation. Methods and industrial applications*). (Taylor & Francis, 2005).
29. Vauthier, C. & Bouchemal, K. Methods for the preparation and manufacture of polymeric nanoparticles. *Pharm. Res.* **26**, 1025–1058 (2009).
30. Zhao, Y., Fickert, J., Landfester, K. & Crespy, D. Encapsulation of self-healing agents in polymer nanocapsules. *Small* **8**, 2954–2958 (2012).
31. Pinto Reis, C., Neufeld, R. J., Ribeiro, A. J. & Veiga, F. Nanoencapsulation I. Methods for preparation of drug-loaded polymeric nanoparticles. *Nanomedicine NBM* **2**, 8–21 (2006).
32. Ezhilarasi, P. N., Karthik, P., Chhanwal, N. & Anandharamakrishnan, C. Nanoencapsulation techniques for food bioactive components: a review. *Food Bioprocess Technol.* **6**, 628–647 (2013).
33. Del Mercato, L. L. *et al.* LbL multilayer capsules: recent progress and future outlook for their use in life sciences. *Nanoscale* **2**, 458–467 (2010).
34. Grigoriev, D. O., Bukreeva, T., Möhwald, H. & Shchukin, D. G. New method for fabrication of loaded micro- and nanocontainers: Emulsion encapsulation by polyelectrolyte layer-by-layer deposition on the liquid core. *Langmuir* **24**, 999–1004 (2008).
35. Verma, G. & Hassan, P. a. Self assembled materials: design strategies and drug delivery perspectives. *Phys. Chem. Chem. Phys.* **15**, 17016–17028 (2013).
36. Zhang, M., Ni, P. & Yan, N. Effect of operation variables and monomers on the properties of polyamide microcapsules. *J. Microencapsul.* **12**, 425–435 (1995).
37. Pastine, S. J., Okawa, D., Zettl, A. & Fréchet, J. M. J. Chemicals on demand with phototriggerable microcapsules. *J. Am. Chem. Soc.* **131**, 13586–13587 (2009).
38. Jacquemond, M., Jeckelmann, N., Ouali, L. & Haefliger, O. P. Perfume-containing polyurea microcapsules with undetectable levels of free isocyanates. *J. Appl. Polym. Sci.* **114**, 3074–3080 (2009).

39. Zhang, H. & Wang, X. Synthesis and properties of microencapsulated n-octadecane with polyurea shells containing different soft segments for heat energy storage and thermal regulation. *Sol. Energy Mater. Sol. Cells* **93**, 1366–1376 (2009).
40. Frere, Y., Danicher, L. & Gramain, P. Preparation of polyurethane microcapsules by interfacial polycondensation. *Eur. Polym. J.* **34**, 193–199 (1998).
41. Jinglei, Y., Keller, M. W., Moore, J. S., White, S. R. & Sottos, N. R. Microencapsulation of isocyanates for self-healing polymers. *Macromolecules* **41**, 9650–9655 (2008).
42. Pariot, N., Edwards-Lévy, F., Andry, M. C. & Lévy, M. C. Cross-linked beta-cyclodextrin microcapsules: preparation and properties. *Int. J. Pharm.* **211**, 19–27 (2000).
43. Chu, T. X. *et al.* Comparison between measurements of elasticity and free amino group content of ovalbumin microcapsule membranes: Discrimination of the cross-linking degree. *J. Colloid Interface Sci.* **355**, 81–88 (2011).
44. Hong, K. & Park, S. Melamine resin microcapsules containing fragrant oil: synthesis and characterization. *Mater. Chem. Phys.* **58**, 128–131 (1999).
45. Rochmadi, Prasetya, A. & Hasokowati, W. Mechanism of microencapsulation with urea-formaldehyde polymer. *Am. J. Appl. Sci.* **7**, 739–745 (2010).
46. Zhao, C. Y. & Zhang, G. H. Review on microencapsulated phase change materials (MEPCMs): Fabrication, characterization and applications. *Renew. Sustain. Energy Rev.* **15**, 3813–3832 (2011).
47. Luo, Y. & Zhou, X. Nanoencapsulation of a hydrophobic compound by a miniemulsion polymerization process. *J. Polym. Sci. Part A Polym. Chem.* **42**, 2145–2154 (2004).
48. Green, B. K. & Schleicher, L. Pressure responsive record materials. US2730457 A (1956).
49. White, M. A. The chemistry behind carbonless copy paper. *J. Chem. Educ.* **75**, 1119–1120 (1998).
50. Hakeim, O. A., Fan, Q. & Kim, Y. K. Encapsulation of pigment red 122 into UV-curable resins via a mini-emulsion technique. *Pigment Resin Technol.* **39**, 3–8 (2010).
51. Fu, S., Zhang, K., Zhhang, M. & Tian, L. Encapsulated phthalocyanine blue pigment with polymerisable dispersant for inkjet printing inks. *Pigment Resin Technol.* **41**, 3–8 (2012).

52. Lelu, S., Novat, C., Graillat, C., Guyot, A. & Bourgeat-Lami, E. Encapsulation of an organic phthalocyanine blue pigment into polystyrene latex particles using a miniemulsion polymerization process. *Polym. Int.* **52**, 542–547 (2003).
53. Bai, P. F. *et al.* Review of paper-like display technologies. *Prog. Electromagn. Res.* **147**, 95–116 (2014).
54. Comiskey, B., Albert, J. D., Yoshizawa, H. & Jacobson, J. An electrophoretic ink for all-printed reflective electronic displays. *Nature* **394**, 253–255 (1998).
55. Kim, C. A. *et al.* Microcapsules as an electronic ink to fabricate color electrophoretic displays. *Synth. Met.* **151**, 181–185 (2005).
56. Qiao, R., Zhang, X. L., Qiu, R. & Kang, Y. S. Synthesis of functional microcapsules by in situ polymerization for electrophoretic image display elements. *Colloids Surfaces A Physicochem. Eng. Asp.* **313-314**, 347–350 (2008).
57. Wang, J. P., Zhao, X. P., Guo, H. L. & Zheng, Q. Preparation and response behavior of blue electronic ink microcapsules. *Opt. Mater.* **30**, 1268–1272 (2008).
58. ALBERT, J. D. *et al.* Electronic displays and materials. EP1010036 B1 (2004).
59. Inoue, S., Kawai, H., Kanbe, S., Saeki, T. & Shimoda, T. High-resolution microencapsulated electrophoretic display (EPD) driven by poly-Si TFTs with four-level grayscale. *IEEE Trans. Electron Devices* **49**, 1532–1539 (2002).
60. E Ink electrophoretic technology. at <<http://www.eink.com/technology.html>>
61. E Ink eReaders. at <http://www.eink.com/customer_showcase_eReaders.html>
62. Amstad, E. & Reimhult, E. Nanoparticle actuated hollow drug delivery vehicles. *Nanomedicine* **7**, 145–164 (2012).
63. Esser-Kahn, A. P., Odom, S. A., Sottos, N. R., White, S. R. & Moore, J. S. Triggered release from polymer capsules. *Macromolecules* **44**, 5539–5553 (2011).
64. Skorb, E. V. & Möhwald, H. Dynamic interfaces for responsive encapsulation systems. *Adv. Mater.* **25**, 5029–5043 (2013).
65. Ngwuluka, N. Application of in situ polymerization for design and development of oral drug delivery systems. *AAPS PharmSciTech* **11**, 1603–1611 (2010).
66. Antipov, A. A. & Sukhorukov, G. B. Polyelectrolyte multilayer capsules as vehicles with tunable permeability. *Adv. Colloid Interface Sci.* **111**, 49–61 (2004).

-
67. De Geest, B. G., McShane, M. J., Demeester, J., De Smedt, S. C. & Hennink, W. E. Microcapsules ejecting nanosized species into the environment. *J. Am. Chem. Soc.* **130**, 14480–14482 (2008).
68. Cheng, C. J., Chu, L. Y., Ren, P. W., Zhang, J. & Hu, L. Preparation of monodisperse thermo-sensitive poly(N-isopropylacrylamide) hollow microcapsules. *J. Colloid Interface Sci.* **313**, 383–388 (2007).
69. Broaders, K. E., Pastine, S. J., Grandhe, S. & Fréchet, J. M. J. Acid-degradable solid-walled microcapsules for pH-responsive burst-release drug delivery. *Chem. Commun.* **47**, 665–667 (2011).
70. Yang, X., Han, X. & Zhu, Y. (PAH/PSS)₅ microcapsules templated on silica core: Encapsulation of anticancer drug DOX and controlled release study. *Colloids Surfaces A Physicochem. Eng. Asp.* **264**, 49–54 (2005).
71. Watnasirichaikul, S., Davies, N. M., Rades, T. & Tucker, I. G. Preparation of biodegradable insulin nanocapsules from biocompatible microemulsions. *Pharm. Res.* **17**, 684–689 (2000).
72. Kim, E. *et al.* Facile, template-free synthesis of stimuli-responsive polymer nanocapsules for targeted drug delivery. *Angew. Chem. Int. Ed.* **49**, 4405–4408 (2010).
73. Bédard, M. F., De Geest, B. G., Skirtach, A. G., Möhwald, H. & Sukhorukov, G. B. Polymeric microcapsules with light responsive properties for encapsulation and release. *Adv. Colloid Interface Sci.* **158**, 2–14 (2010).
74. Kim, Y. D. & Morr, C. V. Microencapsulation properties of gum arabic and several food proteins: Liquid spray-dried orange oil emulsion particles. *J. Agric. Food Chem.* **44**, 1314–1320 (1996).
75. Comunian, T. A., Abbaspourad, A., Favaro-Trindade, C. S. & Weitz, D. A. Fabrication of solid lipid microcapsules containing ascorbic acid using a microfluidic technique. *Food Chem.* **152**, 271–275 (2014).
76. Wang, J. C., Chen, S. H. & Xu, Z. C. Synthesis and properties research on the nanocapsulated capsaicin by simple coacervation method. *J. Dispers. Sci. Technol.* **29**, 687–695 (2008).
77. Barras, A. *et al.* Formulation and characterization of polyphenol-loaded lipid nanocapsules. *Int. J. Pharm.* **379**, 270–277 (2009).
78. Ammala, A. Biodegradable polymers as encapsulation materials for cosmetics and personal care markets. *Int. J. Cosmet. Sci.* **35**, 113–124 (2013).
79. Mercadé-Prieto, R. *et al.* Determination of the shell permeability of microcapsules with a core of oil-based active ingredient. *J. Microencapsul.* **29**, 463–474 (2012).

80. Lertsutthiwong, P. & Rojsitthisak, P. Chitosan-alginate nanocapsules for encapsulation of turmeric oil. *Pharmazie* **66**, 911–915 (2011).
81. Xiao, Z., Liu, W., Zhu, G., Zhou, R. & Niu, Y. Production and characterization of multinuclear microcapsules encapsulating lavender oil by complex coacervation. *Flavour Fragr. J.* **29**, 166–172 (2014).
82. Cheng, S. Y. *et al.* Cosmetic textiles with biological benefits: Gelatin microcapsules containing Vitamin C. *Int. J. Mol. Med.* **26**, 411–419 (2009).
83. Yang, C.-C. & Pan, I.-H. Preparation of pesticide microcapsule. US5576008 A (1996).
84. Mihou, A. P., Michaelakis, A., Krokos, F. D., Mazomenos, B. E. & Couladouros, E. A. Prolonged slow release of (Z)-11-hexadecenyl acetate employing polyurea microcapsules. *J. Appl. Entomol.* **131**, 128–133 (2007).
85. Chen, Z., Fang, Y. & Zhang, Z. Synthesis and assessment of attractiveness and mating disruption efficacy of sex pheromone microcapsules for the diamondback moth, *Plutella xylostella* (L.). *Chinese Sci. Bull.* **52**, 1365–1371 (2007).
86. Patel, A. V., Jakobs-Schönwandt, D., Rose, T. & Klaus-Dieter, V. Fermentation and microencapsulation of the nematophagous fungus *Hirsutella rhossiliensis* in a novel type of hollow beads. *Appl. Microbiol. Biotechnol.* **89**, 1751–1760 (2011).
87. Hart, R. L., Virgallito, D. R. & Work, D. E. Microencapsulation of biocides and antifouling agents. US7938897 B2 (2011).
88. Wolfgang, O., Mechtel, M. & Kaesler, K.-H. Antifouling paint. US6365066 B1 (2002).
89. Tyagi, V. V., Kaushik, S. C., Tyagi, S. K. & Akiyama, T. Development of phase change materials based microencapsulated technology for buildings: A review. *Renew. Sustain. Energy Rev.* **15**, 1373–1391 (2011).
90. Hawlader, M. N. A., Uddin, M. S. & Zhu, H. J. Encapsulated phase change materials for thermal energy storage: Experiments and simulation. *Int. J. Energy Res.* **26**, 159–171 (2002).
91. Su, J. F., Wang, L. X. & Ren, L. Preparation and characterization of double-MF shell microPCMs used in building materials. *J. Appl. Polym. Sci.* **97**, 1755–1762 (2005).
92. Jamekhorshid, A., Sadrameli, S. M. & Farid, M. A review of microencapsulation methods of phase change materials (PCMs) as a thermal energy storage (TES) medium. *Renew. Sustain. Energy Rev.* **31**, 531–542 (2014).

-
93. Samadzadeh, M., Boura, S. H., Peikari, M., Kasiriha, S. M. & Ashrafi, A. A review on self-healing coatings based on micro/nanocapsules. *Prog. Org. Coatings* **68**, 159–164 (2010).
 94. Shchukin, D. G. Container-based multifunctional self-healing polymer coatings. *Polym. Chem.* **4**, 4871–4877 (2013).
 95. Zheludkevich, M. L., Tedim, J. & Ferreira, M. G. S. ‘Smart’ coatings for active corrosion protection based on multi-functional micro and nanocontainers. *Electrochim. Acta* **82**, 314–323 (2012).
 96. Di Credico, B., Griffini, G., Levi, M. & Turri, S. Microencapsulation of a UV-responsive photochromic dye by means of novel uv-screening polyurea-based shells for smart coating applications. *ACS Appl. Mater. Interfaces* **5**, 6628–6634 (2013).
 97. Caruso, M. M., Blaiszik, B. J., White, S. R., Sottos, N. R. & Moore, J. S. Full recovery of fracture toughness using a nontoxic solvent-based self-healing system. *Adv. Funct. Mater.* **18**, 1898–1904 (2008).
 98. Nesterova, T., Dam-Johansen, K., Pedersen, L. T. & Kiil, S. Microcapsule-based self-healing anticorrosive coatings: Capsule size, coating formulation, and exposure testing. *Prog. Org. Coatings* **75**, 309–318 (2012).
 99. Cho, S. H., White, S. R. & Braun, P. V. Self-healing polymer coatings. *Adv. Mater.* **21**, 645–649 (2009).
 100. Bamfield, P. & Hutchings, M. G. *Chromic phenomena: technological applications of colour chemistry*. (RSC Publishing, 2010).
 101. Bouas-Laurent, H. & Dürr, H. Organic photochromism. *Pure Appl. Chem.* **73**, 639–665 (2001).
 102. Nigel Corns, S., Partington, S. M. & Towns, A. D. Industrial organic photochromic dyes. *Color. Technol.* **125**, 249–261 (2009).
 103. Ercole, F., Davis, T. P. & Evans, R. A. Photo-responsive systems and biomaterials: photochromic polymers, light-triggered self-assembly, surface modification, fluorescence modulation and beyond. *Polym. Chem.* **1**, 37–54 (2010).
 104. Caneschi, A., Cornia, A. & Dei, A. Valence tautomerism in a cobalt complex of a schiff base diquinone ligand. *Inorg. Chem.* **37**, 3419–3421 (1998).
 105. Cador, O. *et al.* Temperature-induced solid-state valence tautomeric interconversion in two cobalt-schiff base diquinone complexes. *Inorg. Chem.* **42**, 6432–6440 (2003).
 106. White, M. A. & LeBlanc, M. Thermochromism in commercial products. *J. Chem. Educ.* **76**, 1201–1205 (1999).

107. Sage, I. Thermochromic liquid crystals. *Liq. Cryst.* **38**, 1551–1561 (2011).
108. Seeboth, A., Löttsch, D., Ruhmann, R. & Muehling, O. Thermochromic polymers-Function by design. *Chem. Rev.* **114**, 3037–3068 (2014).
109. Christie, M. R. & Ed: Gulrajani, M. L. *Chromic materials for technical textile applications. (in Advances in the dyeing and finishing of technical textiles)*. (Elsevier, 2013).
110. Bernardus, T. N. M. *et al.* Photochromic optical element. WO2003001555 A1 (2003).
111. Chu, N. Y. C., Hovey, R. J., Snitzer, E. & Uhlmann, D. R. Stabilized photochromic materials. US4367170 A (1983).

Chapter 2

Objectives

2.1 Objectives

As already mentioned, photochromic and thermochromic materials are of great interest in the area of smart materials due to the variety of areas in which they can be employed, ranging from pure aesthetics to high-tech applications such as light emitting diodes, optical data storage or optoelectronics. However, the lack of a universal methodology capable to transfer the well-established chromic properties of these systems in solution to the solid state prevent their integration into real functional devices. Hence, the global aim of the present thesis was *to obtain solid materials with solution-like behaviour capable to retain the enhanced chromic properties observed in solution by the encapsulation of photochromic and thermochromic compounds inside liquid-filled polymeric capsules*. To demonstrate the feasibility of the approach proposed, the following objectives were pursued:

(i) To attain *fast-responsive photochromic materials* through the encapsulation of photochromic solutions into liquid-filled capsules and their subsequent incorporation in polymeric rigid matrices. The resulting systems should display optimal properties for the preparation of functional photoprotective coatings, a type of material whose performance is often limited by the detrimental effects derived from the direct dispersion of the active photochromic compounds of choice within the corresponding solid supporting matrices. The studies conducted on this topic are described in Chapter 3.

(ii) To develop a general methodology capable to produce *robust thermochromic solid structures based on valence tautomeric metal complexes*, which are excellent spin transition candidates for the preparation of molecular memories and room-temperature spintronic devices. Encapsulation of these compounds into liquid-filled capsules should not only enable preserving their solution-like valence tautomeric properties in the solid state, but also affording a *simple way of tuning their thermochromic behaviour* on demand. The results obtained in this part of the thesis are shown in Chapter 4.

(iii) To produce microstructured *solid materials presenting white-light emission at room temperature* as well as *thermally-induced colour tunability* for application in the area of display devices. As described in Chapter 5, this was attempted through the encapsulation of different thermochromic fluorescent dyes inside liquid-filled capsules.

Chapter 3

Fast-responsive Photochromic Capsules

3.1 Introduction

3.1.1 Photochromism

Photochromism is a light-induced chemical process in which a compound reversibly interconverts between two states with different absorption spectra. In other words, it consists in a reversible colour change upon irradiation with light (Figure 3.1). Photochromism was first described in 1867 by Fritzsche, who reported the bleaching of an orange solution of tetracene with daylight and subsequent colour regeneration in the dark. However, it was not until 1950s that Hirshberg introduced the term photochromism to refer to this phenomenon^{1,2}.

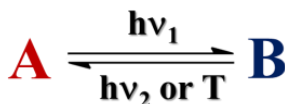


Figure 3.1 Photochromism as the reversible transformation between two forms of a chemical system displaying different colours, which must be photoinduced at least in one direction.

Reversibility is an important characteristic of photochromism. While the transformation from the initial, thermodynamically stable form (A) to the photoinduced state (B) always occurs upon light absorption, the B→A back reaction can instead take place either thermally or photochemically, thus giving rise to two different classes of photochromism: T-type (thermally reversible type) and P-type (photochemically reversible type) photochromism, respectively^{1,3}. In the first case, the initial colour is regained once illumination is removed and it accounts for most photochromic systems described to date. In P-type compounds, B is thermally stable and A is only recovered by irradiation with light of different frequency. Well-known examples of both types of photochromic dyes are shown in Figure 3.2: the T-type spirooxazine-merocyanine system and a P-type dithienylethene compound. In both cases, the absorption spectrum of their initial states shifts to longer wavelengths upon light absorption (the so called positive photochromic behaviour³) and, indeed, they undergo a colourless-to-coloured transformation. This situation is often encountered for most photochromic dyes, while negative photochromism (i.e. interconversion from an initial coloured state to a photoinduced colourless form) or positive photochromism between differently coloured species are less common⁴.

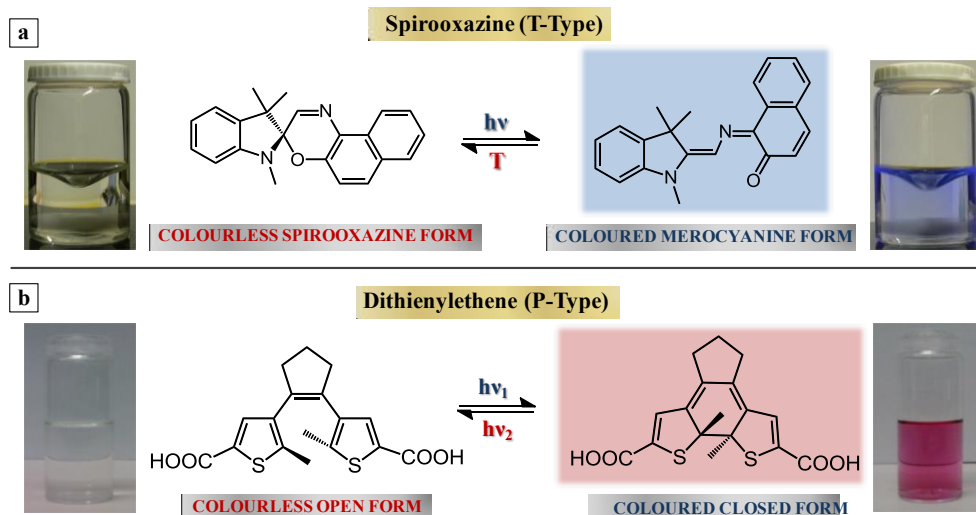


Figure 3.2 Structure and photochromism of two different types of photochromic dyes: **(a)** a T-type spirooxazine compound suffering the light-induced heterolytic photocleavage of its C-O spiro-bond to yield a blue-coloured merocyanine state; **(b)** a P-type dithienylethene derivative capable to undergo photoinduced interconversion between its open and closed forms.

Although different types of chemical transformations can account for the reversible interconversion of photochromic dyes, they mostly consist in unimolecular isomerisation reactions, such as the cyclisation/ring-opening processes undergone by the spirooxazine-merocyanine and dithienylethene compounds shown in Figure 3.2. For these and other cases, photochromic transformations involve the rearrangement of the bonding between atoms and/or the modification of the geometry and the electronic distribution of molecular systems. Therefore, light-induced colour changes in these compounds are usually accompanied by variations in other chemical and physical properties such as redox potentials, refractive indices, solubility, viscosity, surface wettability, conductivity or dielectric constants^{3,4}. This enables the use of photochromic systems for the preparation of a variety of light-responsive functional materials, including data storage devices, logic operators, security printing or sensors^{5,6}. Among them, the manufacturing of photoprotective coatings that darken when exposed to sunlight and reverse back to colourless in low light situations (e.g. indoors) is the main current industrial application of photochromism^{5,7} and it has been the subject of study of the first part of this thesis.

3.1.2 Photochromic compounds for the preparation of photoprotective coatings

Colour-changing ophthalmic lenses capable to self-regulate the transmittance of sunlight are the major commercial application of photochromic dyes nowadays and their development has greatly stimulated research in this area⁵. At the beginning, most advances relied on the use of inorganic materials such as metal oxides and halides or transition metal compounds due to their better photostability and fatigue resistance⁴. Particularly, silver halide crystals have been extensively applied in photochromic lenses since the first spectacles marketed in 1966^{5,7}. Unfortunately, the use of these compounds presents two main drawbacks: (i) they have a limited colour range, and (ii) they are not suitable for encapsulation within organic matrices and films^{4,8}.

Consequently, as plastic lenses surpassed their glass counterparts in commercial importance, lens manufacturers required photochromic systems compatible with polymeric organic matrices. This fuelled research into organic photochromic dyes, which has led to the development of a large variety of compounds and a wide colour range of photochromic responses. For application in the ophthalmic industry as well as in other types of photoprotective coatings (e.g. smart windows, agricultural films or optical elements in the automotive sector), these organic photochromic compounds must obey a number of conditions. On the one hand, they should photoconvert from a colourless to a coloured state (i.e. positive photochromism), revert back thermally to the initial situation in absence of irradiation (i.e. T-type photochromism), and present fast colour darkening and fading kinetics⁵. In addition, they should also display good photo- and thermal stability, fatigue resistance, and dispersability within the final organic matrices of interest.

Although a number of T-type organic photochromes have been developed to fulfil these requirements in solution, their properties dramatically deteriorate upon loading into the final solid materials required for functional applications. Commonly, the main issue has to do with the effect of the surrounding matrix on the photochromic kinetics (the so-called matrix effect), which is critically influenced by a variety of factors, such as matrix rigidity, free volume, polarity and hydrophobicity⁹⁻¹¹, and dye-matrix intermolecular interactions and miscibility^{12,13}. Overall, this results in a significant decrease in the interconversion rates of the photochromic system upon dispersion or covalent attachment to supporting matrices,

which makes achieving high switching speeds in solid materials still remain a challenge. Of particular importance is the effect on the thermal discolouration process of these compounds, which is largely slowed down with respect to solution owing to the steric restrictions imposed by the surrounding matrix to the molecular motions typically involved in the interconversion between the two states of the photochromes^{5,14,15}. This critically affects their performance or even prevents the application of the final photochromic materials.

Different strategies have been suggested to overcome this obstacle and obtain high fading rates in solid matrices for T-type organic photochromes. Some of them rely on enhancing the intrinsic switching speeds of the dyes. This can be accomplished by either chemically modifying well-known photochromic systems^{16–21} (i.e. varying their structure or the electronic nature of their substituents) or by synthesizing new compounds that show little sensitivity to matrix effects^{22,23}. A very nice example of the latter approach are the bridged imidazole dimers reported by Abe et al., which interconvert via a single bond cleavage/formation process with minimal geometrical variations between the two states of the photochrome (Figure 3.3)²³. As such, their interconversion rates are hardly affected by the nature of the surrounding matrix and they display fast colouration and fading speeds upon dispersion in solid materials. Unfortunately, this and other related strategies are hard to be generalized and they prevent the use of readily available commercial photochromes.

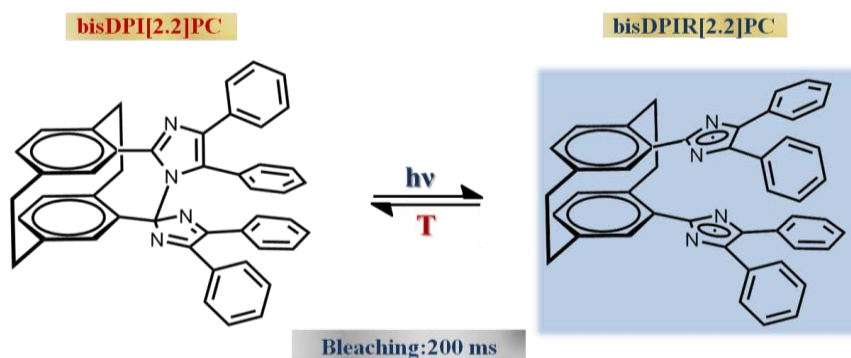


Figure 3.3 Photochromic interconversion of a colourless paracyclophane-bridged bis(diphenyl)imidazole dimer (bisDPI[2.2]PC), which undergoes a photoinduced homolytic bond cleavage to yield the coloured biradical bisDPIR[2.2]PC. This species rapidly reverts thermally to the initial compound regardless of the surrounding medium. Adapted from reference 22.

Other approaches focus on minimising the steric restrictions imparted by the matrix on the supported photochromic molecules. For instance, organic and hybrid materials with fast fading rates have been obtained using polymers with low glass transition temperatures (T_g)^{24–27}. The flexibility provided by these soft matrices favours dye molecular motion and, therefore, photochromic switching rates. The use of plasticizers to decrease polymer T_g and, consequently, accelerate the thermal bleaching has also been reported^{2,15,28}. Unfortunately, high hardness and abrasion resistance are required for many practical applications and, in this regard, the use of soft polymers compromises the mechanical properties of the resulting material. To overcome this drawback, the development of composite photochromic organic-inorganic coatings (Nanomer[®]) has been proposed, which combine a low- T_g hybrid photochromic polymer with embedded ceramic nanoparticles (SiO_2) to improve the hardness of the system without affecting dye switching⁸.

Another approach to reduce matrix effects on photochromic switching rates without detrimentally varying the mechanical properties of the final material consists in the inclusion of the dyes of interest within nanometer-sized local flexible domains into the rigid host matrices.

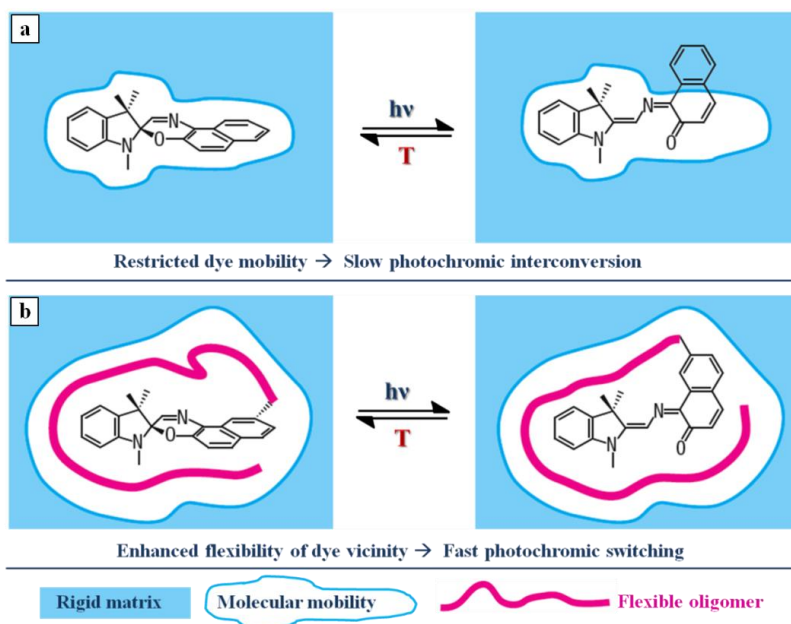


Figure 3.4 Schematic representation of the mobility restrictions imposed by matrix rigidity to a T-type spirooxazine-merocyanine photochrome (**a**), and the mobility enhancement introduced by dye conjugation to a flexible, low- T_g oligomer (**b**). Adapted from reference 29.

This methodology, which has been mainly developed by Evans and co-workers, is based on the covalent binding of photochromic compounds to low- T_g oligomers that spontaneously coil around the dyes^{29,30}. As depicted in Figure 3.4, these oligomers isolate the photochromic compounds from the rigid, high- T_g surroundings and provide a soft favourable environment for the photochromic interconversion. In addition, since short chain oligomers are needed to accomplish this effect, changes in the mechanical properties of the final host matrix are highly minimised. This strategy has been proven to be applicable to a large number of photochromic compounds and matrices^{29,31–41}; however, it requires previous chemical functionalization of the photochromes. In addition, oligomer/matrix compatibility should be carefully addressed since phase separation can ultimately occur if high concentrations of photochromes are required^{38–41}.

Alternatively, microporous, mesoporous and mesostructured inorganic and hybrid materials have also been used for the development of fast-responsive and robust photochromic matrices^{4,27,42,43}. As shown in Figure 3.5, these systems accommodate photochromic compounds inside cavities and pores, thus facilitating molecular mobility. However, to attain fast fading kinetics through this approach requires proper adjustment of dye interactions with the functional groups of the matrix walls as well as of dye loadings and cavity/pore volumes. Otherwise, opposite results to those initially intended may be obtained. For instance, the presence of acid groups (e.g. silanol groups) exposed on the pore walls stabilises the photoinduced merocyanine form of spirooxazine photochromes and, consequently, slow down the colour fading rate of the system⁴⁴.

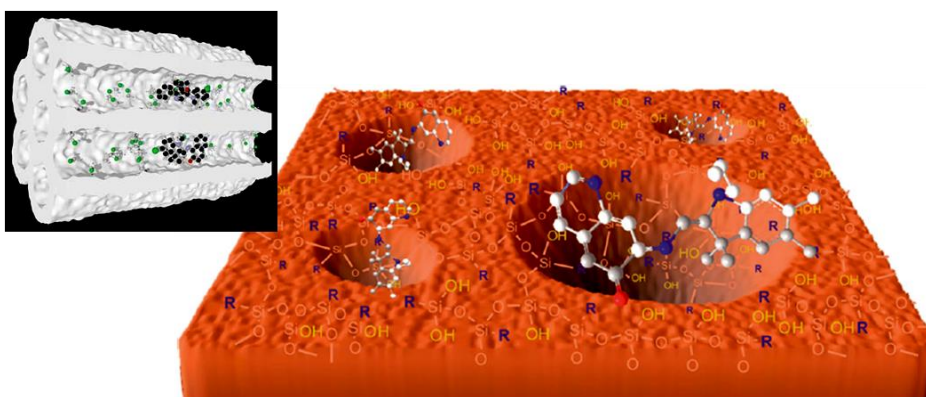


Figure 3.5 Schematic representation of dye distribution inside mesoporous and mesostructured matrices and their interaction with wall functional groups, which might enhance or slow down the photochromic interconversion processes. Adapted from references 4 and 44.

To prevent this situation, superficial basic functional groups⁴⁵ or less polar organic groups^{46,47} are required and, if mesostructured hybrid materials are to be used, dyes should be located within the hydrophobic and flexible organic parts of the composites^{27,48,49}. On the other hand, while large pores and cavities enhance dye loadings, excessive dye content might result in reduced free volume and/or dye aggregation and, as such, increased steric hindrance and slower switching speeds⁴⁵. Besides, the occurrence of other detrimental effects derived from the use of porous matrices cannot be overlooked, such as the loss of photochromic activity in time due to dye migration out of the material and/or photodegradation processes related to freely diffusing water and oxygen molecules⁵⁰⁻⁵².

Finally, fast photochromic coatings have also been obtained introducing dye-loaded micro-/nanostructures with rapid colouration-decolouration responses inside rigid matrices. In this methodology, the colour fading rate of the final material is determined by the dye bleaching kinetics inside the encapsulating media and no effect from the surrounding matrix is observed. With this aim, photochromic compounds have been entrapped within the voids of dendrimers and hyperbranched polymers^{53,54}, in the cavities of mesostructured silicate particles⁴⁹ and inside particles with a soft solid core made of low- T_g polymers⁵⁴ or resins⁵⁵ and subsequently coated with high- T_g cross-linked polymers or inorganic-oxide shells. Similarly, a fast photochromic material with high mechanical strength was recently obtained by dispersing a photochromic organogel in a rigid polymer⁵⁶ (Figure 3.6). However, poor photostability and chemical resistance was observed for the resulting composite, since both the dye and the liquid phase of the gel were removed after treatment with organic solvents.

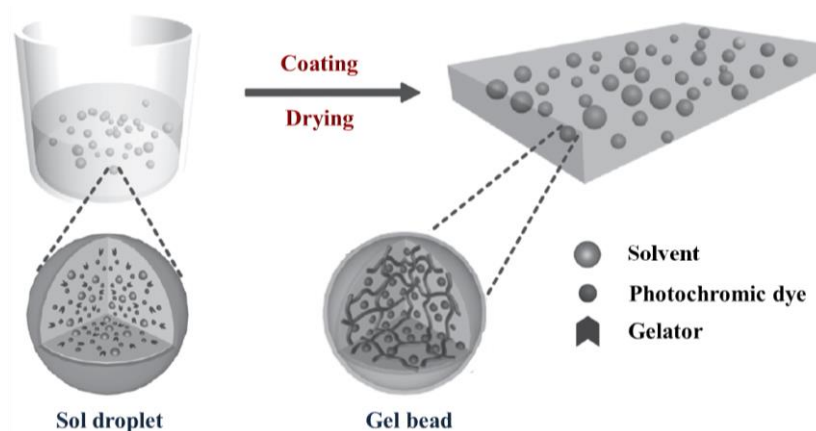


Figure 3.6 Schematic illustration of the fabrication of a photochromic film based on an organogel dispersion in a high- T_g polymer matrix. Adapted from reference 55.

To summarise, most of the approaches described so far to attain fast photochromic responses pursue the modification of the local environment around the dyes to favour conformational motion and, thus, rapid molecular interconversion within solid rigid matrices. For such strategies, the best scenario would be to surround the photochromic compounds of interest by a liquid micro-/nanoenvironment, since the fastest bleaching rates are exhibited in solution where the dyes experience greater molecular mobilities. Based on this design concept, we have developed in this thesis a novel methodology for the preparation of solid photochromic materials with fast switching behaviour.

3.1.3 Liquid-filled capsules as an alternative approach for fast-responsive photochromic materials

Aiming at the production of optimized photochromic coatings for ophthalmic lenses and other functional systems, it would be largely desirable to develop a methodology to attain high colour switching rates that (i) allows the use of commercially available photochromes without requiring synthetic modifications, (ii) preserves the photochromic behaviour observed in solution, and (iii) does not compromise the mechanical properties of the resulting material. In view of this, a new strategy has been proposed and explored in this work that relies on the following aspects:

(i) The encapsulation of the photochromic systems of interest within the interior of liquid-filled solid-shell hollow capsules. Capsules must therefore be prepared composed of a liquid solution of photochromes coated with a robust transparent shell (Figure 3.7a). The latter should maintain capsule integrity, protect the photochromic dyes, allow the excitation radiation to reach the inner core and afford the colour change perception. Since the liquid core would contain a photochromic solution and the encapsulation is not expected to interfere in the photochromic interconversion, the same colour switching rates exhibited in solution should be observed within the capsules and, as such, a solid material with fast photochromic response could be obtained.

(ii) The dispersion of the core-shell photochromic capsules into the final desired rigid matrices, such as polymeric thin films. This process should take place without compromising the morphology of the capsules, whose liquid interior must not be leaked.

Therefore, it requires their shell to be chemically, mechanically and/or thermally resistant to the processing conditions of the target materials. If so, the fast, solution-like photochromic switching of the capsules will be directly transferred to the rigid surrounding matrix without significantly altering its mechanical properties. In addition, this methodology should allow tackle other severe problems encountered when directly dispersing photochromic molecules within solid matrices such as poor loadings, dye aggregation, phase separation and migration.

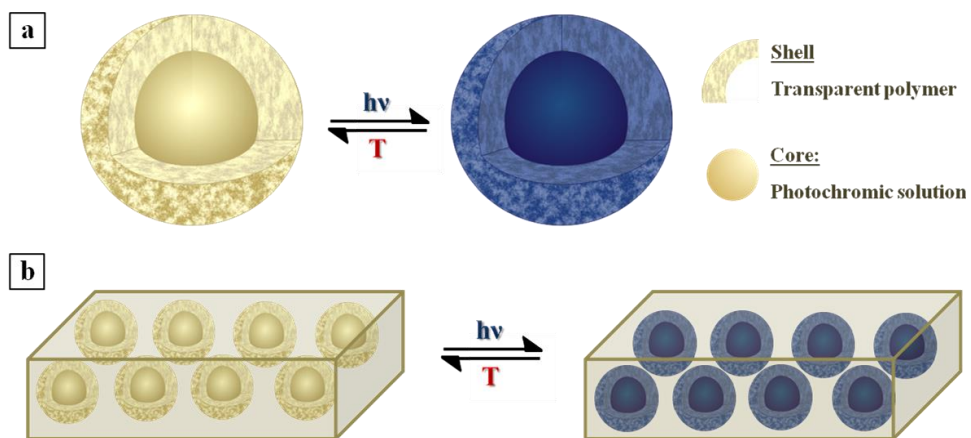


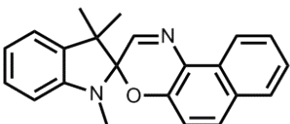
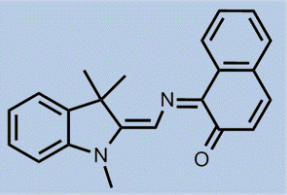
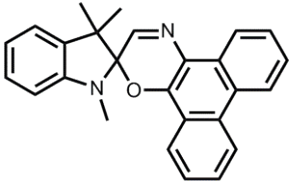
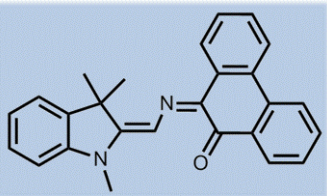
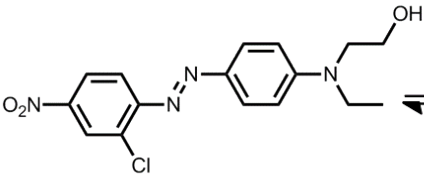
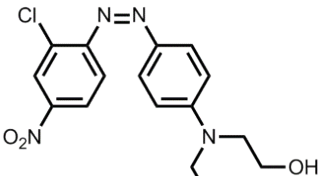
Figure 3.7 Schematic representation of: (a) photochromic liquid-filled solid-shell hollow capsules; (b) fast-responsive photochromic films obtained by dispersing the core-shell capsules into the rigid matrices of interest.

In order to demonstrate the feasibility of this approach, three commercial T-type photochromic dyes were used in this work: 1,3-dihydro-1,3,3-trimethylspiro[2*H*-indole-2,3'-[3*H*]naphth[2,1-*b*](1,4)oxazine] or Photorome I (**PhI**), 1,3-dihydro-1,3,3-trimethylspiro[2*H*-indole-2,3'-[3*H*]phenanthr[9,10-*b*](1,4)oxazine] or Photorome III (**PhIII**), and 2-[4-(2-chloro-4-nitrophenylazo)-*N*-ethylphenylamino]ethanol or Disperse Red 13 (**DR13**). Table 3.1 gathers the structure, isomerisation states and optical properties of these three dyes.

PhI and **PhIII** are two similar photochromes switching between an initial transparent spirooxazine state ($\lambda_{\text{abs, PhI}} = 322 \text{ nm}$; $\lambda_{\text{abs, PhIII}} = 359 \text{ nm}$ in toluene) and a photoinduced blue-coloured merocyanine state ($\lambda_{\text{abs, PhI}} = 593 \text{ nm}$; $\lambda_{\text{abs, PhIII}} = 583 \text{ nm}$ in toluene). As shown in Table 3.1, their photochromic interconversion involves the cleavage of the C-O spiro-bond upon exposure to UV light and a 90° rotation of one half of the molecule around the C-C bond^{3,14}. Consequently, the conformation of these dyes should change from orthogonal to planar during the isomerisation process in order to give rise to the open, coloured

merocyanine structure. Such large conformational motion required for interconversion explains why **PhI** is often selected to investigate the matrix effect on photochromic activity, as we did in this work^{12,24,27}. For the same reason, we were also interested in employing **PhIII**, since its spirooxazine-merocyanine isomerisation implies the movement of a bulkier group, thus making this molecule even more sensitive to steric restrictions. On the other hand, **DR13** is an azobenzene derivative that interconverts between the planar *trans* ($\lambda_{\text{abs}} = 491 \text{ nm}$) and the bent *cis* configurations of its azoaromatic unit. For this dye the *trans-cis* interconversion is not visualized as a colour variation, because the absorption spectra of both isomers largely overlap and the lifetime of the *cis* state is on the sub-second time scale⁵⁷. However, it undergoes important geometry and size changes upon photoisomerisation¹⁴, which also makes this dye useful for studying the encapsulation effect on photochromism.

Table 3.1 Structure, isomerisation states and absorption wavelengths in toluene of **PhI**, **PhIII** and **DR13**. The absorption spectrum of *cis*-**DR13** was not determined due to its short lifetime and the overlap with the absorption spectrum of the *trans* state.

PHOTOCHROME	ISOMERIZATION STATES	
PhI	 $\lambda_{\text{abs}}: 322 \text{ nm}$	 $\lambda_{\text{abs}}: 593 \text{ nm}$
PhIII	 $\lambda_{\text{abs}}: 359 \text{ nm}$	 $\lambda_{\text{abs}}: 583 \text{ nm}$
DR13	 $\lambda_{\text{abs}}: 491 \text{ nm}$	 $\lambda_{\text{abs}}: _$

3.1.4 Objectives

The aim of the work described along this chapter is to attain *fast-responsive photochromic materials through the encapsulation of photochromic solutions into liquid-filled capsules*. To achieve this objective, the following studies were conducted: (i) entrapment of the photochromic solutions of interest into polymeric solid-shell hollow microcapsules as proof-of-concept materials of our approach; (ii) characterisation of their photochromic response and comparison with that obtained for the same dyes in free solutions; (iii) preparation and characterisation of rigid polymeric thin films loaded with photochromic microcapsules to demonstrate the viability of the full process of transferring solution-like behaviour into final functional materials; (iv) exploration of the capacity of our methodology to be brought down to the nanometre scale and allow the preparation of photochromic nanocapsules, which would ultimately be required for the preparation of highly transparent light-responsive coatings for real applications.

3.2 Results and discussion

3.2.1 Preparation of photochromic liquid-filled microcapsules

The encapsulation of photochromic solutions is the basic principle of the approach that we proposed in this work. Therefore, it is important to properly select the type of capsules and the nature of their outer shell to achieve the desired behaviour. Among the large variety of hollow micro- and nanoparticles developed in the last years for the encapsulation of materials^{58,59}, we decided to work with cross-linked polymeric capsules in search of shell impermeability and stability. In situ and interfacial polymerizations in oil-in-water emulsions were the processes selected for the synthesis of the cross-linked polymeric capsules since these methodologies are relatively simple, easy to scale, applicable to typical oil-soluble organic photochromes and allow the direct loading of the capsule core, avoiding diffusion processes that could risk the tightness of the shell or reduce capsule payloads. In particular, melamine-formaldehyde and polyamide were the polymers tested as capsules shell since they have already been employed for the encapsulation of a diversity of

substances^{60–63}. The results obtained with each of these polymers are described separately in the following sections.

3.2.1.1 Melamine-formaldehyde microcapsules

In our first attempt to synthesise photochromic polymer microcapsules, we tried to entrap **PhI** toluene solutions inside melamine-formaldehyde polymeric shells (**MF_tol**). The procedure followed, adapted from the literature^{64–66}, is schematically described in Figure 3.8. Basically, photochromic toluene solutions were emulsified in an aqueous phase containing an emulsion stabilizer using magnetic stirring or a mechanical stirrer. Subsequently, an aqueous mixture of melamine and formaldehyde monomers was added to the emulsion, and after adjusting the pH between 4 and 5 and increasing the temperature at around 338 K, both monomers started to polymerise around the droplets of the organic solvent phase.

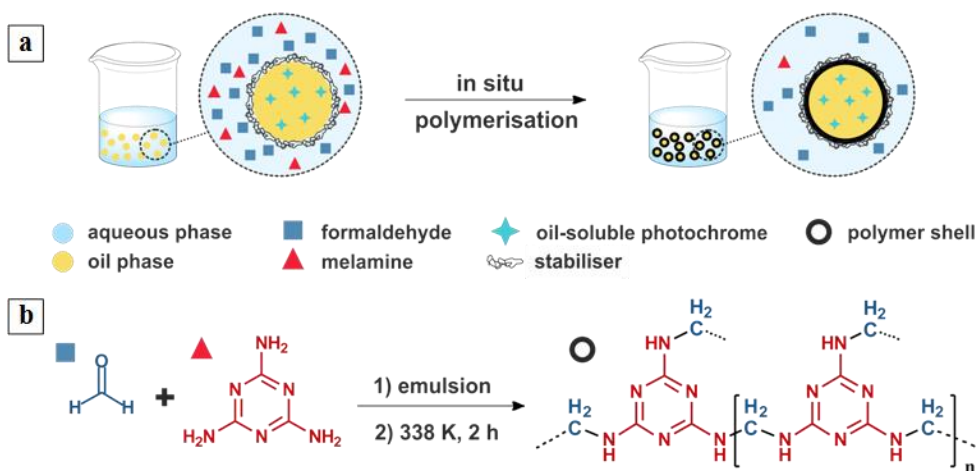


Figure 3.8 (a) Schematic illustration of the in situ polymerization process followed to prepare photochromic **MF_tol** capsules. (b) Polymerization reaction between melamine and formaldehyde to give rise to the cross-linked **MF_tol** shell.

Capsule formation was clearly observed by direct inspection of the final emulsion through optical microscopy. The sizes obtained varied from millimetres to a few micra depending on the stirring rate, although all the samples presented remarkable polydispersion. As expected,

PhI@MF_tol capsules changed from colourless to intense blue when irradiated at the appropriate wavelengths, and returned to the initial colourless state only after the irradiation was suppressed. However, two different fading rates were distinguished by in situ monitoring by optical microscopy, as shown in Figure 3.9. Within the capsules, fast decolouration was observed, which was completed in less than 10 s. Instead, the blue colour of the unstructured polymer surrounding the capsules was found to remain for several minutes, proving that only the encapsulated photochromic solutions could attain fast fading kinetics, as originally planned.

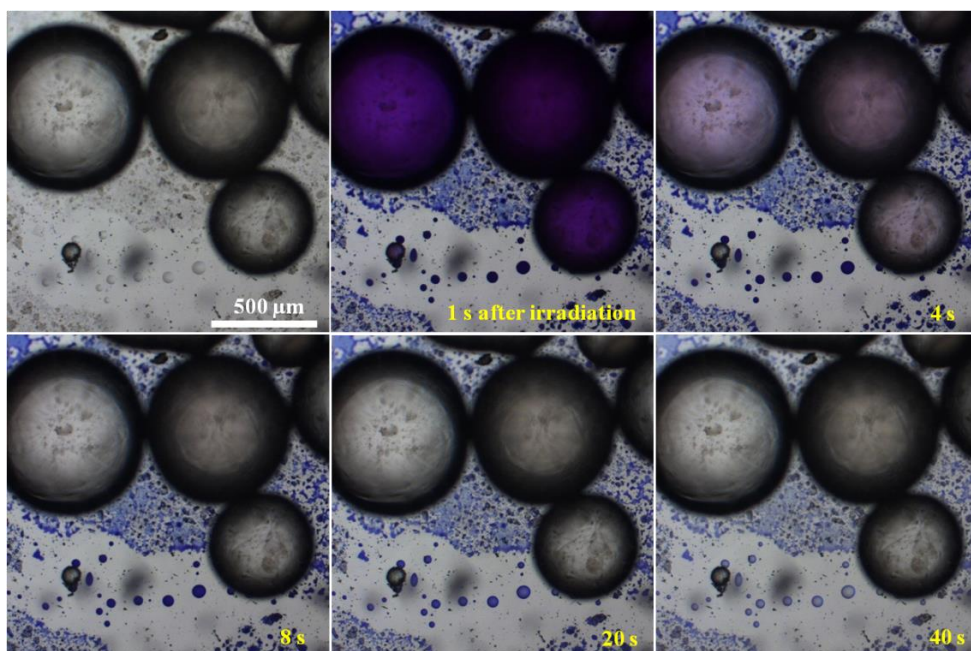


Figure 3.9 Optical micrographs of the photochromism displayed by **PhI@MF_tol** capsules directly deposited onto a microscope slide from the aqueous suspension of the reaction mixture. The first image corresponds to the initial situation prior to irradiation with UV light. The following were measured after stopping UV irradiation and monitoring colour bleaching in time.

The **MF_tol** capsules obtained were stable when dispersed in an aqueous medium but, as shown in Figure 3.10(a-c), they broke and collapsed once we tried to isolate them from the mother liquor and the solvent was removed. Although this demonstrated the obtaining of the desired hollow morphology, it prevented capsule separation and purification for further processing of the material. In addition, two different phases were distinguishable inside the capsule cores in some cases, which evidenced the presence of water into their hollow

interior. This was clearly observed when irradiating **PhI@MF_tol** capsules with UV light, since only the toluene phase containing the photochromic molecules changed its colour upon irradiation (Figure 3.10(d-e)), note that **PhI** is insoluble in water and when crystallized it loses its photochromic behaviour).

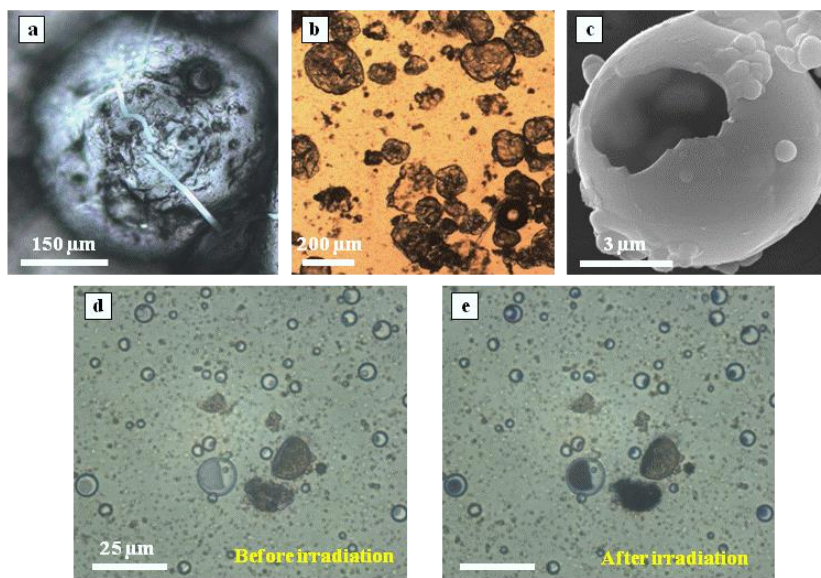


Figure 3.10 (a-c) Optical micrographs (a-b) and SEM image (c) of broken and collapsed capsules after solvent removal, showing the fractures formed on the polymeric shell and the capsule hollow morphology. (d-e) Optical micrographs of **PhI@MF_tol** capsules containing two phases in their core, as clearly revealed by irradiation with UV light.

To tackle these two issues and improve shell resistance, we modified several synthesis parameters such as the nature of the emulsion stabilizer, the ratio of reactants and/or the addition order. However, we could not obtain robust dried capsules in any case. In some of the reactions performed, we observed the presence of small stable capsules but no toluene was detected in their interior and they were always accompanied by a large amount of collapsed capsules and solid nanoparticles. Transmission electron microscopy images (TEM) of these samples revealed the existence of porosity within the melamine-formaldehyde polymer, which might be responsible for the permeability and fragility of the shell and, as a consequence, for poor capsule resistance (Figure 3.11(a-c)). On the other hand, we also obtained macroporous particles using Tween[®] 20 as surfactant that, although not useful for our approach, could be of interest for other applications (Figure 3.11(d-f)).

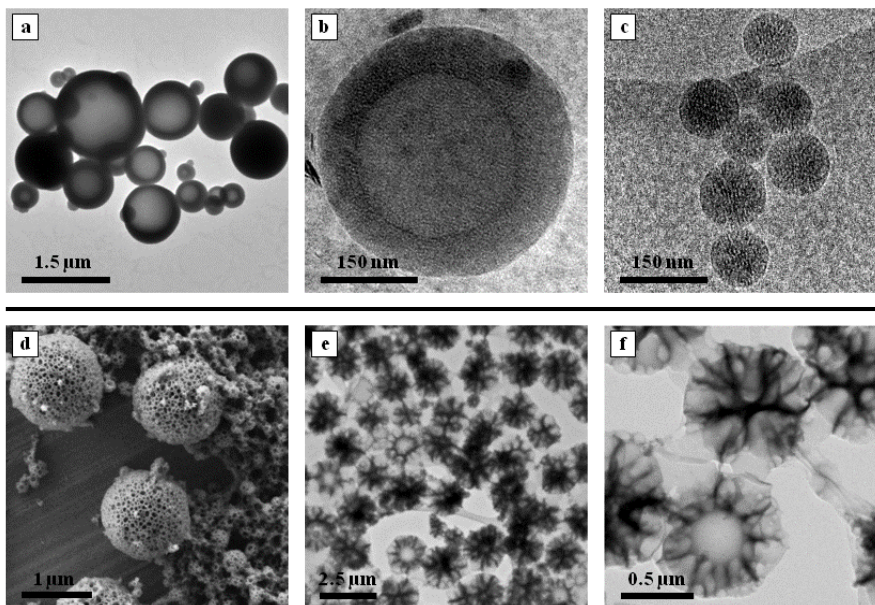


Figure 3.11 (a-c) TEM images of the mixtures of hollow capsules and solid nanoparticles obtained, which seem to present porous in their melamine-formaldehyde polymer shells. (d-f) SEM and TEM images of macroporous particles obtained through the same methodology using Tween[®] 20 as surfactant.

Even though we could not obtain stable liquid-filled capsules with melamine-formaldehyde shells, this first attempt demonstrated how the encapsulation of photochromic solutions enhanced the colour fading rates, thus allowing us to qualitatively prove the basic concept of our approach. Encouraged by this result, we then explored the preparation of robust photochromic capsules using a similar methodology but a different polymeric shell structure.

3.2.1.2 Toluene-filled polyamide microcapsules

In a second step, we attempted the preparation of polyamide capsules (PA) filled with photochromic solutions by interfacial polymerisation of a diacyl chloride (terephthaloyl chloride) with a triamine (diethylenetriamine, DETA)⁶¹. A schematic representation of the process followed is presented in Figure 3.12(a). In this case, monomers were dissolved separately in the different phases of the emulsion. Thus, terephthaloyl chloride was first dissolved in toluene together with the photochrome of interest, which was subsequently

emulsified in the water phase containing the emulsion stabilizer. Then, a DETA aqueous solution was added to the mixture and once both monomers made contact at the interface between the toluene droplets and the aqueous phase, polymerisation started and cross-linked polyamide shells were formed around the droplets enclosing the photochromic solution (Figure 3.12(b)).

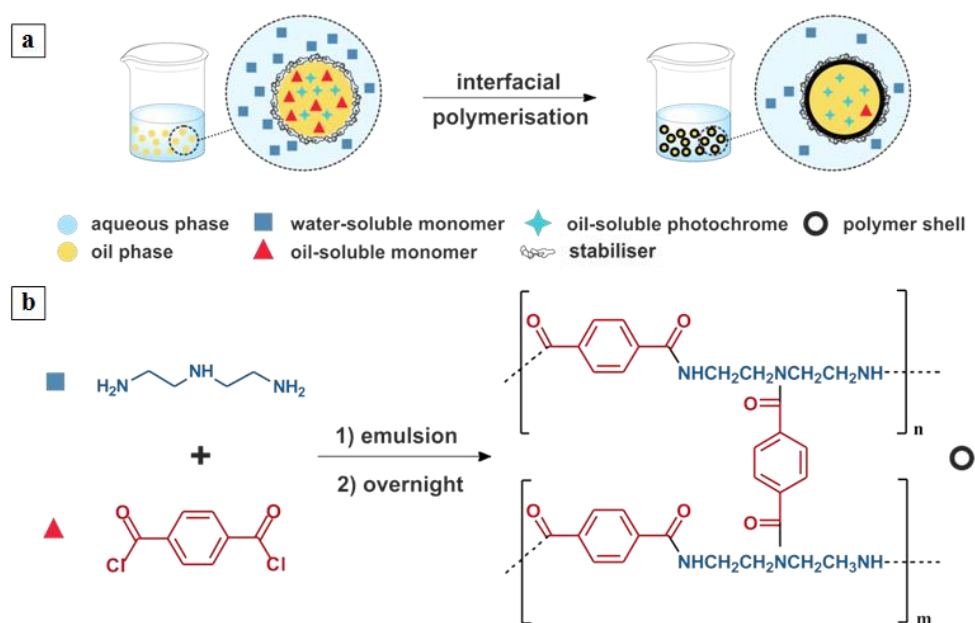


Figure 3.12 (a) Schematic representation of the interfacial polymerisation procedure used to prepare photochromic PA capsules. (b) Polycondensation reaction between tetrachloro-1,4-benzenedicarbonyl chloride and DETA to yield the target cross-linked polyamide shell.

This time the capsules prepared (**PA_tol**) were stable enough to be collected as a dried powder upon filtration, which prompted us to encapsulate all the reference photochromes selected in this work. The colour of the resulting materials depended on the loaded photochromes: yellowish white colour for **PhI** (**PhI@PA_tol**) and **PhIII** (**PhIII@PA_tol**), red for **DR13** (**DR13@PA_tol**), and white for photochrome-free capsules. Figure 3.13(a-c) shows the morphology of the capsules obtained with dimensions ranging from tens to hundreds of micrometers (diameter \sim 50-200 μm). SEM images of physically crushed capsules revealed their hollow interior and allowed us to determine capsule shell thicknesses, which were found to range from 100 to 850 nm and strongly depend on capsule size (Figure 3.13(d-f)). In contrast with the grainy aspect of the shell inner wall, capsule surface were observed to be quite smooth by electron microscopy.

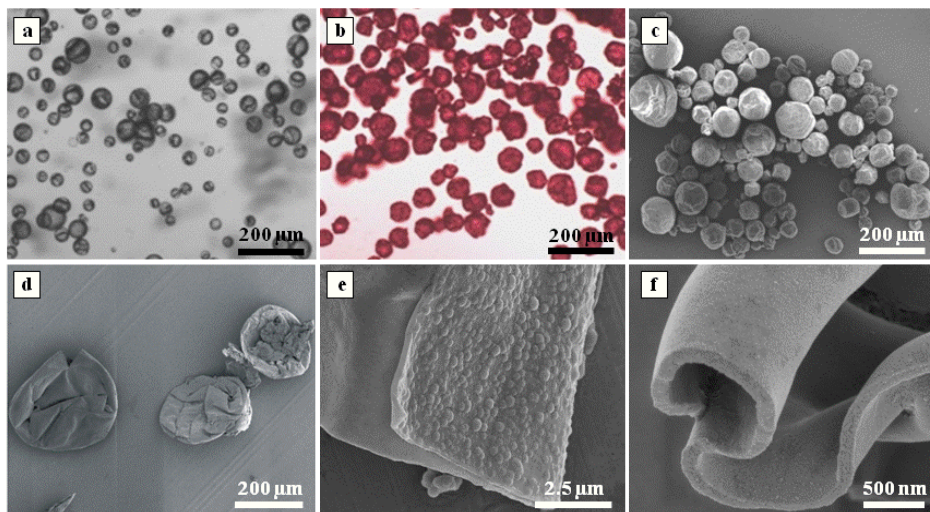


Figure 3.13 (a-b) Optical images of white **PA_tol** capsules and red-coloured **DR13@PA_tol** capsules. (c) SEM image of **PA_tol** capsules. (d-f) SEM images of physically crushed **PhI@PA_tol** capsules showing their hollow interior and shell morphology and thickness.

To demonstrate the presence of liquid solvent inside **PA** capsules, we performed different experiments. First, we investigated capsule behaviour upon redispersion in solvents of different densities (Figure 3.14(a)). Clearly, photochrome-loaded **PA_tol** capsules remained in the liquid-air interface when dispersed in a solvent of higher density than toluene (i.e. water, $\rho_{\text{toluene}} = 0.8669 \text{ g mL}^{-1}$); in contrast, they moved to the bottom of the flask upon dispersion in a solvent of lower density than toluene (i.e. hexane, $\rho = 0.6548 \text{ g mL}^{-1}$).

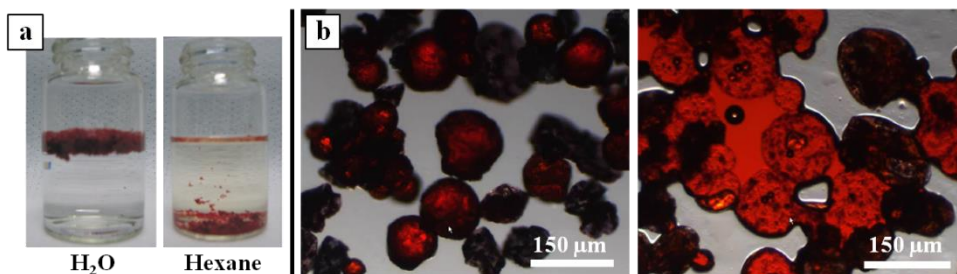


Figure 3.14 (a) Photographs of **DR13@PA_tol** capsules dispersed in water and hexane. (b) Optical microscopy images of **DR13@PA_tol** capsules before and after being physically crushed.

Capsule liquid core was further demonstrated by mechanically crushing the capsules. The ejection of their liquid interior could be observed in situ by optical microscopy, as shown in Figure 3.14(b). Subsequent elimination of the liquid released by evaporation in vacuo or filtration allowed determining the liquid content of the capsules, which accounted for around 85 wt%. From UV-vis absorption measurements of the liquid content ejected, we could also measure photochrome loadings (defined as g of photochrome per g of capsules): 2.3% for **PhI@PA_tol**, 2.6% for **PhIII@PA_tol** and 0.5% for **DR13@PA_tol**.

Finally, the ^1H NMR spectrum of **PA_tol** capsules in CDCl_3 was also acquired to confirm the presence of solvent within their hollow core. The plot on Figure 3.15 compares the spectra recorded for intact and broken capsules with that of toluene. A controlled amount of dimethylformamide (DMF) was added to the NMR tube as a reference (signals at 7.96 (m), 2.97 (s) and 2.88 (s) ppm). Because toluene is less dense than CDCl_3 , most of the intact capsules laid at the liquid-air interface of the NMR tube and above the volume probed in the experiment; consequently, a very small toluene signal was measured. Conversely, broken capsules delivered their liquid content to the CDCl_3 solution, thus accounting for the intense toluene signal detected in this case.

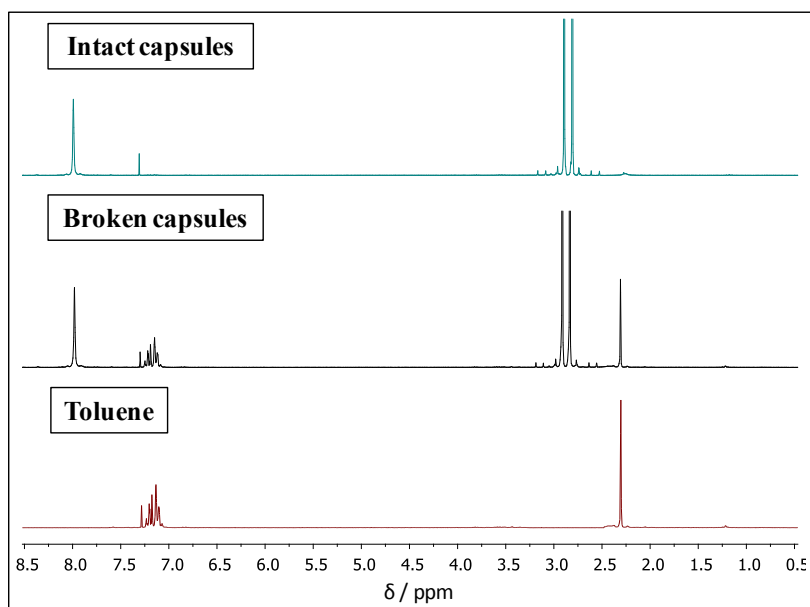


Figure 3.15 ^1H NMR spectra in CDCl_3 of intact and broken **PA_tol** capsules and free toluene. For both capsule samples, a controlled amount of DMF was added as a reference (signals at 7.96 (m), 2.97 (s) and 2.88 (s) ppm).

3.2.2 Characterisation of photochromic liquid-filled microcapsules

Once successfully prepared photochrome-loaded toluene-filled polyamide microcapsules, their photochromic activity was evaluated. First preliminary experiments demonstrated that **PhI@PA_tol** and **PhIII@PA_tol** capsules readily turned blue upon irradiation with UV light (Figure 3.16) and, as previously observed for melamine-formaldehyde capsules, this colouration faded within seconds. In order to quantitatively determine the thermal colour switching rates of these materials and of **DR13@PA_tol**, kinetic measurements were carried out by monitoring the time dependence of their UV-vis absorption spectra after reaching the photostationary state (i.e. the equilibrium under irradiation that leads to a constant value of the absorbance, and corresponds to the maximum colouration which can be reached for **PhI@PA_tol** and **PhIII@PA_tol**).

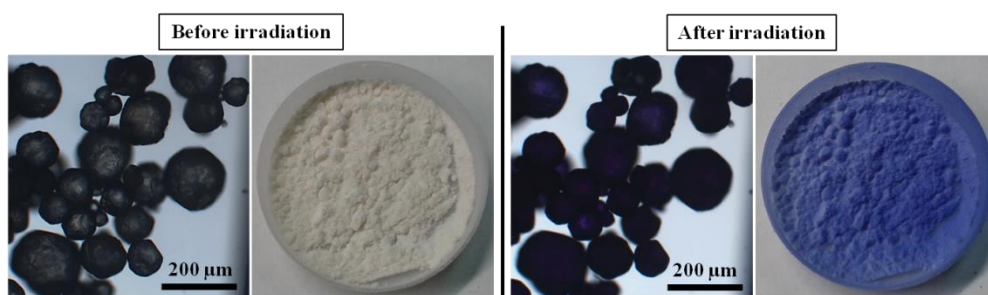


Figure 3.16 Pictures and optical micrographs of **PhI@PA_tol** capsules before and after irradiation.

In the case of **PhI**- and **PhIII**-loaded samples, this implied measuring the time decay of the absorption of the coloured photoinduced merocyanine state in the dark and at room temperature. For comparison purposes, we did not only analyse the kinetics of **PhI@PA_tol** and **PhIII@PA_tol** capsules in air, but also of the free photochromes in toluene solutions and of the capsule samples after being physically crushed and allowed the solvent to partially evaporate. The results obtained are shown in Figure 3.17.

The colour decay curves obtained for **PhI@PA_tol** and **PhIII@PA_tol** could be fitted with a monoexponential function due to the homogenous liquid environment where the photoisomerisable molecules lay^{14,29} (**PhI@PA_tol**: $k = 0.22 \text{ s}^{-1}$; **PhIII@PA_tol**: $k = 0.10 \text{ s}^{-1}$). In addition, very fast thermal decolouration rates were retrieved which

reasonably resembled those measured when directly dissolving the photoactive molecules in toluene (**PhI** in toluene: $k = 0.27 \text{ s}^{-1}$; **PhIII** in toluene: $k = 0.13 \text{ s}^{-1}$).

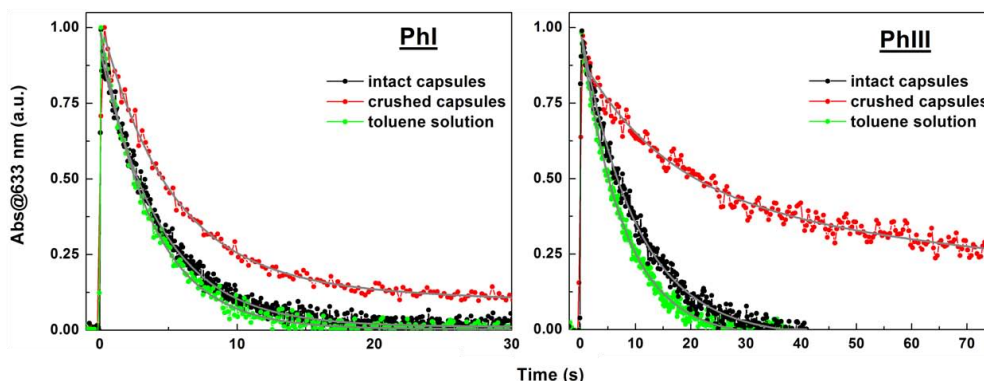


Figure 3.17 Absorption variation with time of the coloured merocyanine state of **PhI** and **PhIII** molecules inside intact and crushed **PA** capsules, and in free toluene solution. Samples were excited at 355 nm until the photostationary state was reached, and thermal decolouration kinetics were then recorded at 633 nm in the dark and at room temperature. The grey lines correspond to the mono- or biexponential fits of the experimental data.

These results demonstrate that the encapsulation within **PA_tol** particles does not significantly slow down the thermal isomerisation kinetics of **PhI** and **PhIII**, as pursued in a our novel approach to obtain fast-responsive photochromic materials. The small differences observed between the time-dependent absorption signals of the capsules and the free photochromes could be ascribed to the effect of molecular diffusion, which should make the kinetic profiles registered for **PhI** and **PhIII** in toluene faster than the actual ones due to motion of irradiated (and non-irradiated) molecules out of (and into) the probed volume during the timescale of the experiment.

In any case, a dramatic change in photochromic response was observed when toluene was removed from the capsule interior. Thus, physical crushing of the particles and evaporation of the solvent resulted in non-monoexponential decolouration kinetics and a remarkable reduction of the photochromic thermal switching speeds, most probably due to photochrome crystallization (crushed **PhI@PA_tol**: $k_1 = 0.19 \text{ s}^{-1}$, $A_1 = 0.88$, $k_2 = 0.019 \text{ s}^{-1}$, $A_2 = 0.11$; crushed **PhIII@PA_tol**: $k_1 = 0.07 \text{ s}^{-1}$, $A_1 = 0.52$, $k_2 = 0.007 \text{ s}^{-1}$, $A_2 = 0.48$). This allowed the fast decolouration rates measured for intact capsules to be ascribed to their liquid interior, which prevented the loaded photochromic molecules to suffer from matrix effects.

In the case of the **DR13** thermal back-isomerisation process, we monitored the recovery of the thermally-stable *trans*-**DR13** state upon spontaneous *cis* \rightarrow *trans* interconversion in the dark after light irradiation. Figure 3.18 plots the results obtained for **DR13@PA_tol** capsules in air compared to those measured for **DR13** directly dissolved in toluene, whose absorption time profile was measured at 490 nm. Since the extinction coefficient of the *trans* state of the photochrome at this wavelength is larger than for the *cis* state, a negative signal was observed upon irradiation ($t = 0$) that decayed in the dark as the initial concentration of *trans*-**DR13** was progressively recovered. As previously observed for **PhI@PA_tol** and **PhIII@PA_tol**, **DR13@PA_tol** experimental data could be fitted with a monoexponential function, thus indicating that the photoisomerisable molecules lie in a homogenous liquid environment (**DR13@PA_tol**: $k = 0.84 \text{ s}^{-1}$). More importantly, encapsulation allowed the rapid thermal *cis* \rightarrow *trans* isomerisation observed for **DR13** in solution to be preserved (**DR13@PA_tol**: $k = 1.2 \text{ s}^{-1}$) with small differences probably arising from diffusion effects.

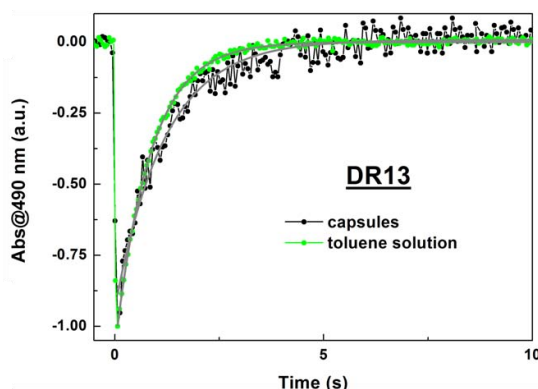


Figure 3.18 Absorption variation with time of the photostationary state of irradiated **DR13@PA_tol** capsules and **DR13** in toluene. Samples were irradiated at 532 nm and thermal *cis* \rightarrow *trans* isomerisation kinetics were recorded at 490 nm in the dark and at room temperature. Grey lines correspond to the monoexponential fits of the experimental data.

To summarise, the results exposed above demonstrate that the rapid colour fading kinetics observed in solution can be preserved through the encapsulation of photochromic molecules inside liquid-filled capsules, independently of the selected photochrome or the nature of the photochromic process followed. Since this fast-responsive behaviour ultimately depends on the preservation of the liquid interior of the capsules, our attention then focused on investigating the impermeability of the polymeric shell.

As previously described in the literature⁶¹, **PA_tol** capsules were found to retain their liquid core when standing in air or in water suspension for several days. However, a significant loss of mass was observed for larger periods of time (~ 30% of liquid leakage after 4 months in air) suggesting slow evaporation of their toluene interior. SEM images revealed how capsules lost their shape with time as porous appeared on the shell surface, and the formation of crystals due to solvent evaporation (Figure 3.19(a)). In addition, capsules collapsed and delivered its content when redispersed in organic solvents (hexane, chloroform and acetone), which would prevent their further processing (Figure 3.19(b)). In view of this, the synthesis of more stable liquid-filled photochromic PA capsules was pursued, for which we considered replacing the toluene core with a higher boiling point organic solvent.

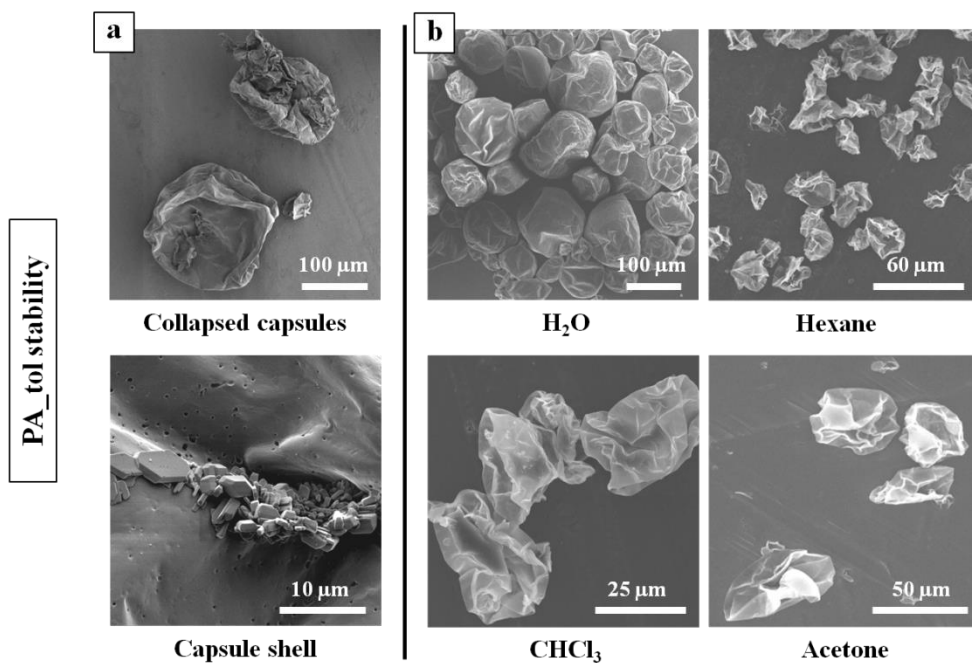


Figure 3.19 (a) SEM images of collapsed **PA_tol** capsules and their shell surface after standing four months in air. (b) SEM images of **PA_tol** capsules after incubation for one day in different media.

3.2.3 Preparation and characterisation of miglyol-filled photochromic polyamide microcapsules

After screening different high boiling point organic solvents, we decided to use Miglyol[®] 812 (miglyol) as the oil phase to prepare robust photochromic liquid-filled capsules. Miglyol is a commercial oil commonly employed in cosmetics and food industry composed by a mixture of decanoyl and octanoyl glycerides distilled from coconut oil⁶⁰.

PA capsules filled with photochromic miglyol solutions were synthesised following a similar procedure to that described for **PA_tol** (see Figure 3.12), but using miglyol as the oil phase (**PA_mig**). Capsules ranging from 10 to 200 μm in diameter were obtained, with similar shell thicknesses as those measured for toluene-filled capsules (Figure 3.20(a-b)). They were collected as a dried powder after filtration and their hollow structure was confirmed by SEM images of broken capsules, which also showed the formation of smooth outer surfaces and the roughness of the inner wall of the shell (Figure 3.20(c-e)). Separation of the oil ejected upon capsule crushing allowed the liquid content of **PA_mig** to be estimated, determining similar values to those calculated for **PA_tol** capsules (~ 85 wt%).

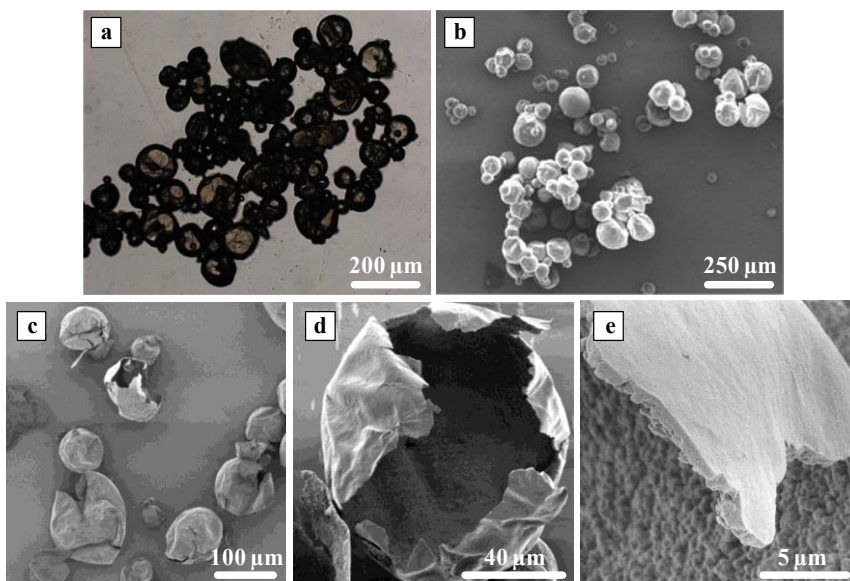


Figure 3.20 (a) Optical microscopy (b) and SEM image of **PA_mig** capsules containing a miglyol solution of **PhI** (**PhI@PA_mig**). (c-e) SEM images of physically crushed **PhI@PA_mig** capsules showing their hollow interior and shell morphology and thickness.

Analysis of this liquid by UV-Vis spectroscopy for **PhI@PA_mig** capsules revealed that photochrome loadings between 1.2% and 3% could be obtained depending on the photochrome concentration in the initial miglyol solution.

As previously done for **PA_tol**, the presence of solvent within the isolated **PA_mig** capsules was confirmed by redispersion in solvents of different densities, physical crushing and ^1H NMR spectroscopy.

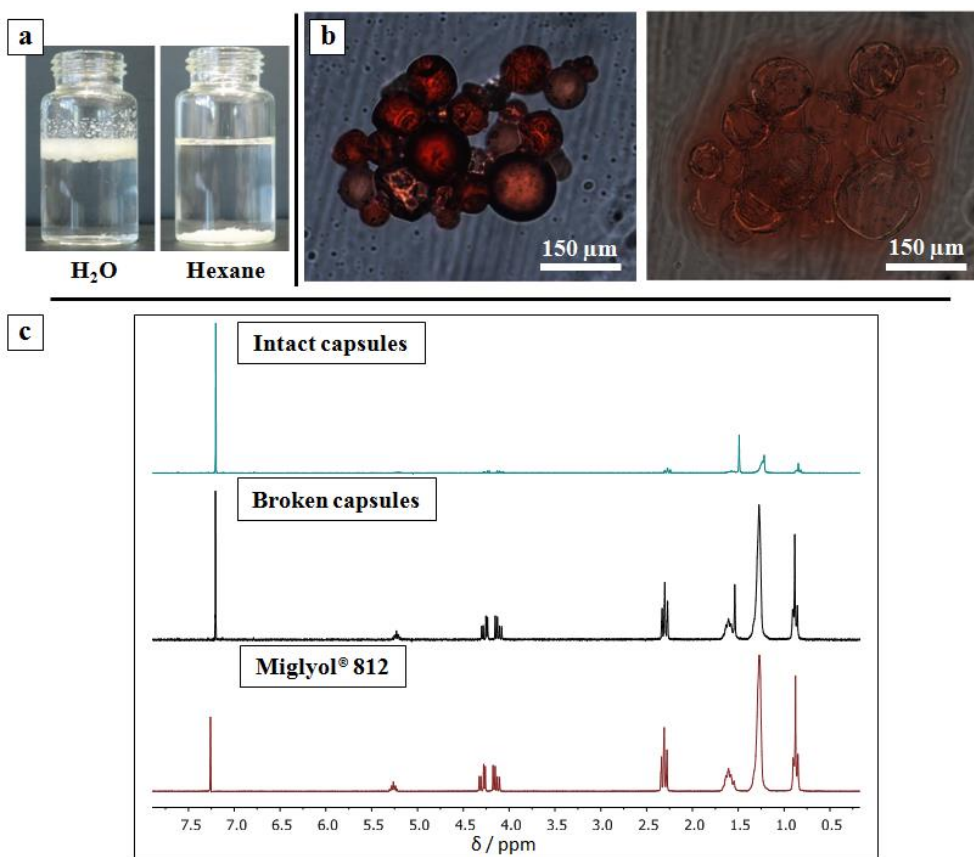


Figure 3.21 (a) Photographs of **PhI@PA_mig** capsules dispersed in water and hexane. (b) Optical microscopy images of **DR13@PA_mig** capsules before and after being physically crushed. (c) ^1H NMR spectra in CDCl_3 of intact and broken **PA_mig** capsules and of miglyol (the CHCl_3 signal at 7.26 ppm was used as a reference in this case).

Thus, as expected, **PA_mig** capsules moved to the liquid-air interface in water, and to the bottom of the flask when redispersed in hexane ($\rho_{\text{miglyol}} = 0.9438 \text{ g mL}^{-1}$, Figure 3.21(a)). In addition, when mechanically crushing capsules containing **DR13** miglyol solutions

(**DR13@PA_mig**), ejection of the red-coloured liquid interior could be observed in real time by optical microscopy (Figure 3.21(b)). Finally, comparing the ^1H NMR spectra of intact and broken capsules with that of miglyol, we could also confirm the presence of solvent inside capsules core since when the broken capsules delivered their liquid content to the CDCl_3 solution, an intense miglyol signal was detected (Figure 3.21(c)).

Subsequently, the stability of **PA_mig** capsules when standing in air or redispersed in a variety of organic solvents was carefully checked. In agreement with the low volatility of miglyol, evaporation of the liquid interior of the capsules was not observed after four months and no losses of mass were determined for the powder sample during this period. More importantly, **PA_mig** capsules preserved their morphology after standing for 24 hours in either chloroform or hexane, being partially damaged only when treated with acetone, as demonstrated by the SEM images in Figure 3.22. These observations demonstrate the enhancement of capsule stability when miglyol is used as the solvent in the liquid interior.

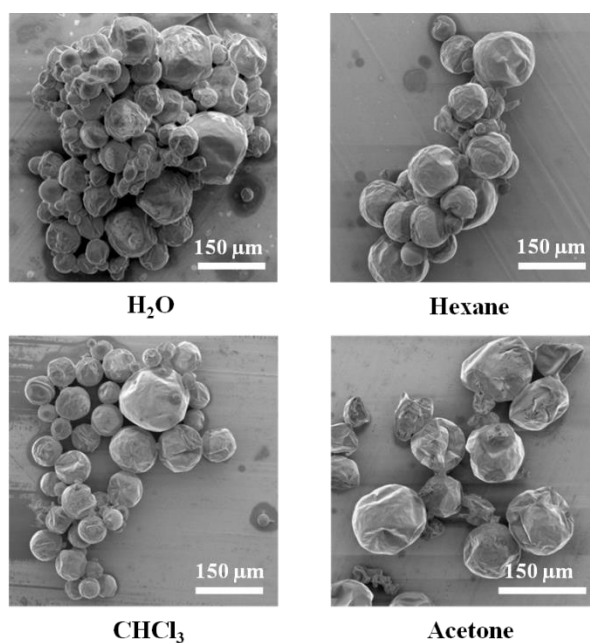


Figure 3.22 SEM images of **PA_mig** capsules after incubation for one day in different media.

On account of their superior stability, the photochromism inside **PA_mig** capsules was then investigated, for which we mainly focused on **PhI**-loaded materials as a reference system. Thus, we measured the thermal colour fading kinetics of **PhI@PA_mig** capsules upon photoinduced spirooxazine \rightarrow merocyanine isomerisation.

Figure 3.23 shows the decays registered for **PhI@PA_mig** in air compared to those measured for free **PhI** molecules in miglyol solution and for **PhI@PA_tol** capsules. As expected due to capsule liquid interior, the kinetic profile measured for **PhI@PA_mig** was clearly monoexponential ($k = 0.31 \text{ s}^{-1}$) and very similar to that in solution ($k = 0.46 \text{ s}^{-1}$). The slightly faster decay registered for the latter might arise from diffusion effects in solution measurements, as previously discussed. On the other hand, the higher viscosity of miglyol ($\sim 30 \text{ mPa}\cdot\text{s}$) with respect to toluene ($0.59 \text{ mPa}\cdot\text{s}$) did not slow down the colour fading rate of **PhI@PA_mig** with respect to **PhI@PA_tol** ($k = 0.22 \text{ s}^{-1}$) since very similar values were found.

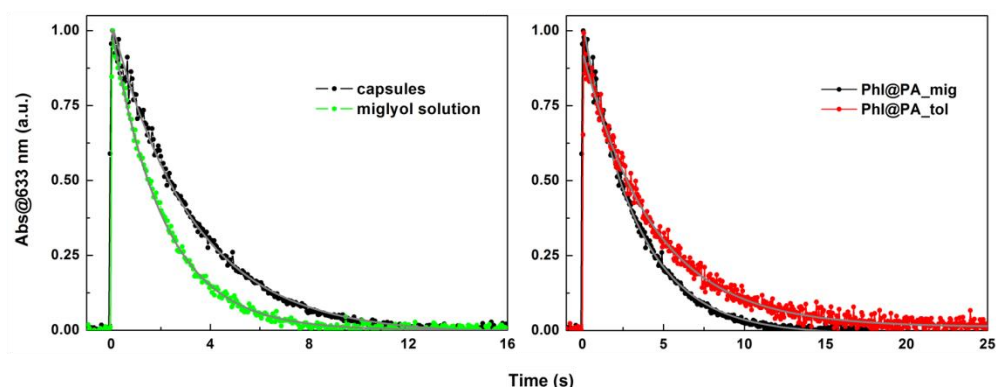


Figure 3.23 Absorption variation with time of photoinduced **PhI** merocyanine molecules in miglyol solution and inside polyamide capsules filled with miglyol or toluene. Samples were excited at 355 nm until the photostationary state was reached, and thermal decolouration kinetics were then recorded at 633 nm in the dark and at room temperature. The grey lines correspond to the monoexponential fits of the experimental data.

Considering these results, it can be concluded that the use of miglyol as liquid core allowed us to obtain fast-responsive photochromic capsules with enhanced stability. We expected these capsules to retain their behaviour when introduced inside rigid polymers, thus ultimately enabling the preparation of functional photoprotective coatings with optimised properties.

3.2.4 Photochromic thin films based on liquid-filled microcapsules

To demonstrate the viability of our approach for the preparation of solid materials with fast photochromic response, we introduced **PhI@PA_mig** capsules inside different polymer matrices and compared their colour fading rates to those measured when the photochrome molecules were directly dispersed within the polymer network.

In particular, polyamide capsules containing miglyol solutions of **PhI** were loaded inside polystyrene thin films (**PhI@PA_mig@PS**) and test lens matrices of cross-linked poly(ethylene glycol) dimethacrylate and bisphenol A ethoxylate diacrylate (**PhI@PA_mig@lens**). The first was prepared dispersing **PhI@PA_mig** in a PS solution of a volatile solvent. The resulting suspension was dropcasted onto a clean glass-slide, and the **PhI@PA_mig@PS** film was formed upon the evaporation of the solvent. On the other hand, **PhI@PA_mig@lens** matrices were prepared dispersing the capsules in the monomer solution previously to the addition of the polymerization initiator. Photographs of the polymeric films obtained are shown in Figure 3.24. The capsule content of these films was 6 wt% (i.e. 0.08 wt% in **PhI**), and because of the size of the loaded particles (higher than 1 μm), they presented very limited transparency. Interestingly, SEM images of **PhI@PA_mig@PS** revealed the presence of intact capsules on the lateral edges of the films, which confirmed the robustness of the **PA_mig** capsules when processed.

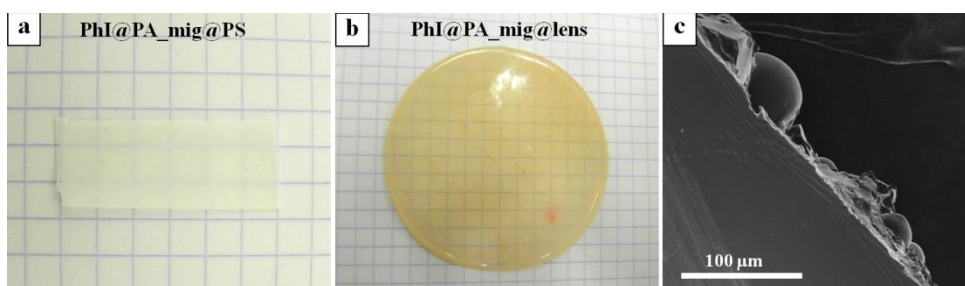


Figure 3.24 (a-b) Photographs of a **PhI@PA_mig@PS** film (thickness of $\sim 200 \mu\text{m}$) and a **PhI@PA_mig@lens** matrix (thickness of $\sim 0.85 \text{ mm}$). (c) SEM image of the lateral edge of a **PhI@PA_mig@PS** film.

To compare the photochromic activity of these films with capsule-free polymeric materials, two other types of samples were developed. First, we prepared transparent thin films (thickness of $\sim 200 \mu\text{m}$) of polymers commonly used in the coating industry bearing 5 wt% content in directly dispersed photochromic molecules: **PhI**-loaded polystyrene (**PhI@PS**,

$T_g = 368$ K), poly(methyl methacrylate) (**PhI@PMMA**, $T_g = 378$ K) and poly(bisphenol A carbonate) (**PhI@PC**, $T_g = 423$ K) films. All of them were prepared by casting appropriate solutions of **PhI** and the polymer of interest in organic solvents.

Second, solid polystyrene nanoparticles with embedded **PhI** molecules (**PhI@PS Nps**) were synthesised aiming to investigate the effect of micro-/nanostructuration on the photochromic properties. These particles were prepared by emulsifier-free emulsion copolymerization of styrene and sodium styrenesulfonate^{67,68}, which proceeded in the presence of **PhI** in the oil phase and, consequently, resulted in the entrapment of the photochrome molecules between the growing polymer chains. In this way, a monodisperse sample of photochromic solid beads of spherical shape and nanometer scale dimensions (~ 190 nm in diameter) was obtained, as shown in Figure 3.25(b) (**PhI@PS_Nps**). The **PhI** loadings achieved were estimated to be $\sim 1\%$ by UV-visible absorption spectroscopy after dissolving the particles formed in chloroform.

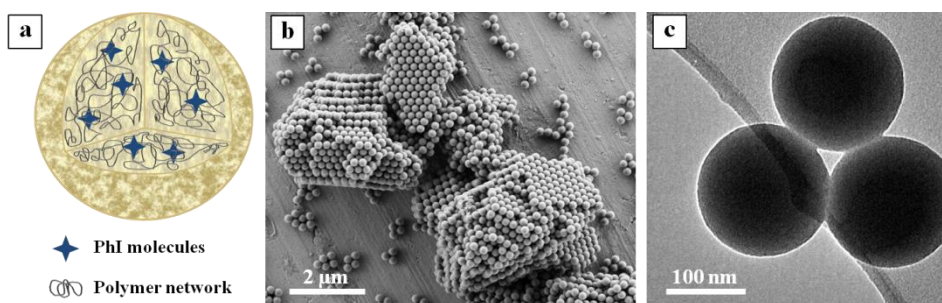


Figure 3.25 (a) Schematic illustration of dye-loaded solid particles where the photochromic molecules were dispersed within the polymer network. (b-c) SEM and TEM images of the resulting **PhI@PS Nps** are also shown.

All the prepared materials were then subjected to photochromic studies intended to determine their thermal colour bleaching rates in the dark after irradiation. The resulting absorption decay curves are depicted in Figure 3.26 and they were characterised by fitting mono- or multiexponential functions and calculating their $t_{1/2}$ and the $t_{3/4}$ values, which are defined as the times required for the initial absorption of the coloured state of the photochromic system to be reduced by half and three quarters, respectively. All the kinetic parameters obtained are gathered in Table 3.2, where the best results reported so far using other approaches to prevent matrix effects on photochrome performance are also shown for comparison purposes: the incorporation of **PhI** within mesoporous¹⁰ (**PhI@sol-gel**),

mesostructured⁴⁸ (**PhI@meso film**) and low- T_g polymeric materials²⁴ (**PhI@PDMS**), as well as **PhI** covalent tethering to soft oligomers²⁹ (**PhI-PDMS@film**).

As can be observed in Figure 3.26 and Table 3.2, **PhI@PA_mig@PS** thin films and **PhI@PA_mig@lens** matrices presented fast and monoexponential decolouration traces ($k = 0.33 \text{ s}^{-1}$ and $k = 0.32 \text{ s}^{-1}$, respectively) that fairly reproduce those measured for free mygliol solutions of **PhI** and **PhI@PA_mig** capsules. These results therefore prove that photochromic molecules protected in the interior of the liquid-filled capsules preserve the rapid fading observed in solution when introduced in rigid matrices.

In contrast, very slow decolouration rates were measured upon direct dispersion of **PhI** molecules within rigid polymers (**PhI@PS**, **PhI@PMMA**, **PhI@PC** and **PhI@PS Nps**). The absorption decays recorded for these materials had to be fitted with triexponential functions, indicating that **PhI** molecules lay in a heterogeneous distribution of sites, with different rigidities and free volumes rather than in a homogenous solution-like environment^{14,29}. Noticeably, structuration of the photochromic material in spherical particles had no effect on the thermal colour fading kinetics since very similar results were obtained for PS thin films and solid nanoparticles.

The improvement on fading speeds introduced by dye encapsulation is clearly illustrated by $t_{1/2}$ and $t_{3/4}$ values, which are about one order of magnitude smaller for the capsule-containing materials than for polymer thin films and solid particles. In addition, this rapid decolouration response matches the best results reported in literature, thus demonstrating the validity of our approach for the preparation of fast photochromic solid materials.

To better expose the results obtained, we recorded a video comparing in real time the colour fading of **PhI@PA_mig** capsules, both free and loaded into a PS thin film and a test lens matrix, with those of **PhI** molecules in miglyol solution, PMMA thin films and PS nanoparticles. In all cases, a region of the sample was irradiated with a laser beam at 355 nm until reaching the photostationary state and once the irradiation ceased, the decolouration process of the blue-coloured area was monitored in time. Figure 3.27 depicts some representative snapshots of this video illustrating how capsules-containing materials display fast, solution-like photochromic response, the ultimate objective of this part of the thesis.

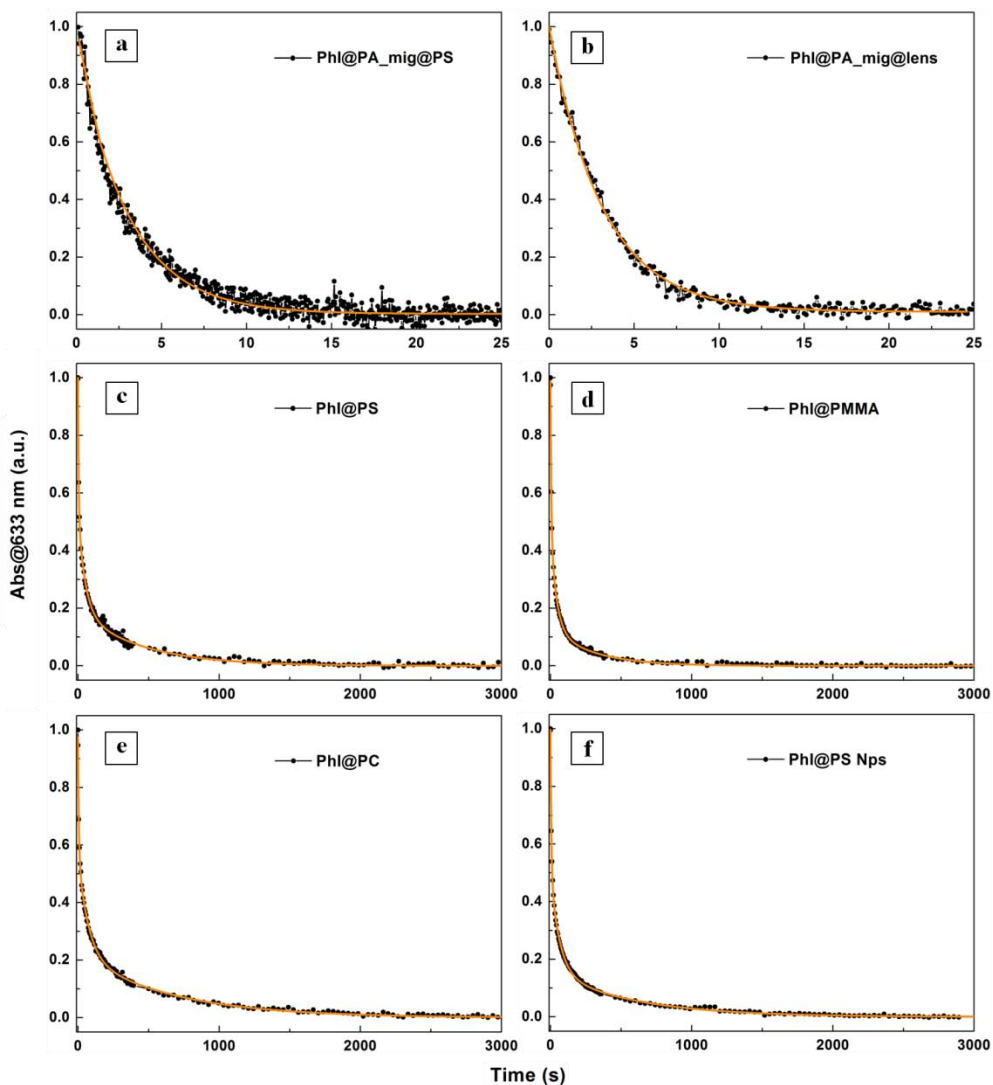


Figure 3.26 Time dependence of the absorption spectra of: (i) **PhI@PA_mig** capsules loaded into polystyrene thin films (a) and test lens matrices (b); (ii) **PhI** molecules directly dispersed within polystyrene (c), poly(methyl methacrylate) (d) and poly(bisphenol A carbonate) (e) thin films; and (iii) **PhI** molecules entrapped into solid polystyrene nanoparticles (f). Samples were excited to the photostationary state at 355 nm and thermal decoloration kinetics were recorded at 633 nm in the dark and at room temperature. The orange lines correspond to the monoexponential or triexponential fits of the experimental data.

Table 3.2 Kinetic parameters of the thermal decolouration process of **PhI** molecules embedded in different solid materials.

	k_1 (s ⁻¹)	A_1	k_2 (s ⁻¹)	A_2	k_3 (s ⁻¹)	A_3	$t_{1/2}$ (s)	$t_{3/4}$ (s)
PhI in toluene	0.27	–	–	–	–	–	2.5	5.2
PhI @PA_tol (intact)	0.22	–	–	–	–	–	3.3	6.6
PhI@PA_tol (crushed)	0.19	0.88	0.019	0.11	–	–	4.6	10.1
PhI in miglyol	0.46	–	–	–	–	–	1.5	2.9
PhI@PA_mig	0.31	–	–	–	–	–	2.2	4.4
PhI@PA_mig@PS film	0.33	–	–	–	–	–	2.0	4.0
PhI@PA_mig@lens matrix	0.32	–	–	–	–	–	2.2	4.4
PhI@PS film	0.22	0.47	$2.0 \cdot 10^{-2}$	0.35	$2.2 \cdot 10^{-3}$	0.18	12.5	68.4
PhI@PMMA film	0.20	0.51	$2.5 \cdot 10^{-2}$	0.36	$3.3 \cdot 10^{-3}$	0.13	9.6	37.1
PhI@PC film	0.18	0.41	$1.4 \cdot 10^{-2}$	0.37	$1.5 \cdot 10^{-3}$	0.22	21.9	121.2
PhI@PS Nps	0.18	0.49	$1.6 \cdot 10^{-2}$	0.35	$1.7 \cdot 10^{-3}$	0.16	13.6	69.0
PhI@sol-gel¹⁰	0.20	–	–	–	–	–	3.5*	6.9*
PhI@meso film⁴⁸	0.20	–	–	–	–	–	3.5*	6.9*
PhI@PDMS²⁴	0.22	–	–	–	–	–	3.1	6.2
PhI-PDMS@film²⁹	0.26	0.91	$7.4 \cdot 10^{-3}$	0.061	–	–	3	7

PhI@sol-gel: PhI molecules dispersed in sol-gel matrices prepared by copolymerization of methyl-diethoxysilane and triethoxysilane¹⁰. PhI@meso film: PhI molecules embedded in mesostructured films based on a poly(ethylene oxide)-poly(propylene oxide) copolymer⁴⁸. PhI@PDMS: PhI molecules bound to a poly(dimethylsiloxane) (PDMS) network²⁴. PhI-PDMS@film: PhI molecules covalently attached to PDMS soft oligomers and subsequently embedded in rigid polymer films²⁹ ($T_g = 393$ K).

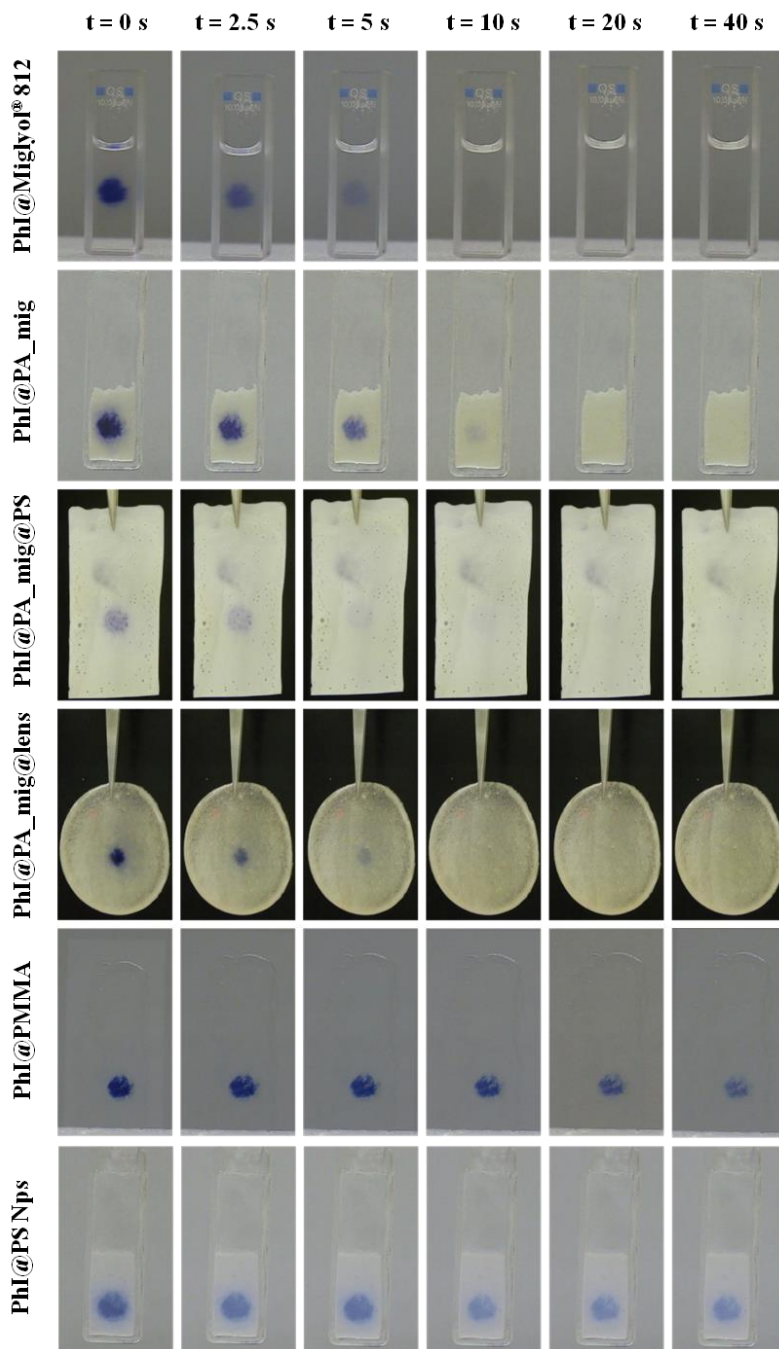


Figure 3.27 Representative images comparing the colour fading kinetics of **PhI** in miglyol solution (**PhI@Miglyol® 812**), **PhI@PA_mig** capsules, **PhI@PA_mig** capsules embedded into a PS thin film, **PhI@PA_mig** capsules embedded into a test lens matrix, **PhI** molecules directly dispersed in a PMMA thin film and **PhI** molecules entrapped into solid polystyrene nanoparticles.

3.2.5 Photochromic liquid-filled nanocapsules for the preparation of transparent coatings

Although the preparation of liquid-filled microcapsules allowed successful demonstration of the viability of our approach to fabricate fast-responsive solid photochromic materials, their use still poses an important drawback for many practical applications: they strongly scatter visible light owing to their microscale dimensions and, as such, the resulting capsule-loaded materials are opaque or just poorly translucent (e.g. see Figure 3.24). To overcome this obstacle, the size of the capsules should be brought down to the nanometer domain, that is to say, to dimensions much smaller than the wavelength of visible light where only Tyndall scattering effects play a role^{69,70}. Since transparency is strongly required for some of the most relevant applications of photochromic materials (i.e. ophthalmic lenses), a last effort was done in this part of the thesis to explore the feasibility of preparing liquid-filled nanocapsules.

A number of different strategies have been described in the literature for the synthesis of liquid-filled nanocapsules, most of which rely on high energy methods requiring high speed homogenizers for the preparation of nanoemulsions (e.g. ultrasonicators)^{71,72}. Since this sort of equipment was not available in our laboratories at the time of this work, a different type of methodology was explored. In particular, our attention focused on the process developed by Xia's group, based on the transformation of solid polymeric nanoparticles into hollow capsules with a big hole in their shell that can be subsequently filled with the solution of interest and finally closed⁷³⁻⁷⁵.

Figure 3.28(a) shows a schematic illustration of the first part of this process, in which opened capsules were prepared from solid polystyrene beads. With this aim, PS Nps synthesized by emulsifier-free emulsion copolymerization of styrene and sodium styrenesulfonate^{73,76} were suspended in water and swollen by adding controlled amounts of toluene, which diffused into the polymer network due to its immiscibility with water. Subsequently, the swollen particles were quickly frozen by pouring the aqueous suspension inside liquid nitrogen, which caused the shrinkage of the particle volume and the formation of a temperature gradient due to PS poor thermal conductivity. As a result, toluene started to solidify at the particle surface ($T_m = 178$ K) inducing both solvent molecules and polymer chains to migrate towards the outer side of the particles, thus creating an internal void at the

centre. The frozen dispersion was slowly warmed up under vacuum, and as toluene evaporated a big hole appeared on the particles surface. During the evaporation process, temperature was maintained below 273 K to retain the ice matrix that prevents the deformation of the hollow structure.

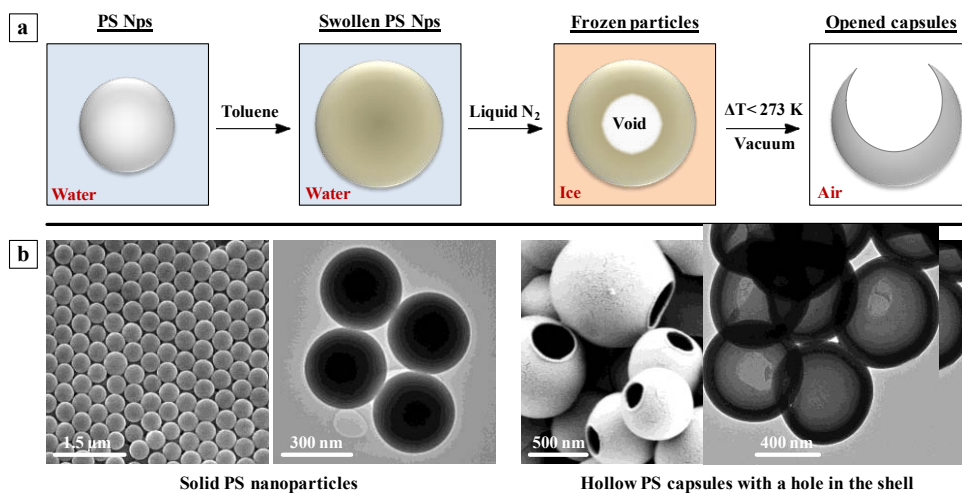


Figure 3.28 (a) Schematic representation of the methodology followed^{73–75} for the synthesis of opened hollow polymeric capsules. (b) SEM and TEM images of the initial solid polystyrene nanoparticles used in the process and the capsules obtained showing their hollow interior and the hole in the surface.

Figure 3.28(b) shows SEM and TEM images of the initial PS beads and the final opened capsules obtained upon applying this methodology. Although capsules of diameters smaller than 100 nm would be required to minimise visible light scattering, in a first step we decided to work with larger polystyrene nanoparticles (diameter = 357 ± 21 nm) in order to test the viability of the process and facilitate capsule characterisation. As observed in Figure 3.28(b), these particles could be successfully converted into the desired hollow capsules with a hole in their shell. However, it must be noted that they became significantly bigger than the initial nanoparticles (diameter = 728 ± 208 nm) and presented higher polydispersity. Since it was reported that the size of the opened capsules depends on the dimensions of the initial particles⁷³, to attain the desired size at the end of the procedure would require the use of initial solid beads smaller than 50 nm in diameter.

In their pioneering work, Xia et al. also demonstrated that by heating opened capsules slightly above the glass transition temperature of their constituting polymer or by adding a good solvent into the suspension, polymer chains within the shell should migrate and seal

the capsule hole without destroying their hollow structure^{74,75}. Thus, we should be capable to load the opened capsules prepared with photochromic solutions if this closing treatment was performed while the capsules were dispersed in a liquid containing the light-responsive molecules of interest dissolved (Figure 3.29(a)). It was in this step of the process where we found the main limitation of the approach, since most of the solvents that show good dye solubility also dissolved the polymeric capsules, thus leading to undesired solid particles and unstructured material. In addition, time was also found to be a critical parameter of the closing procedure since, if excessive, capsules closed completely and lost their hollow structure.

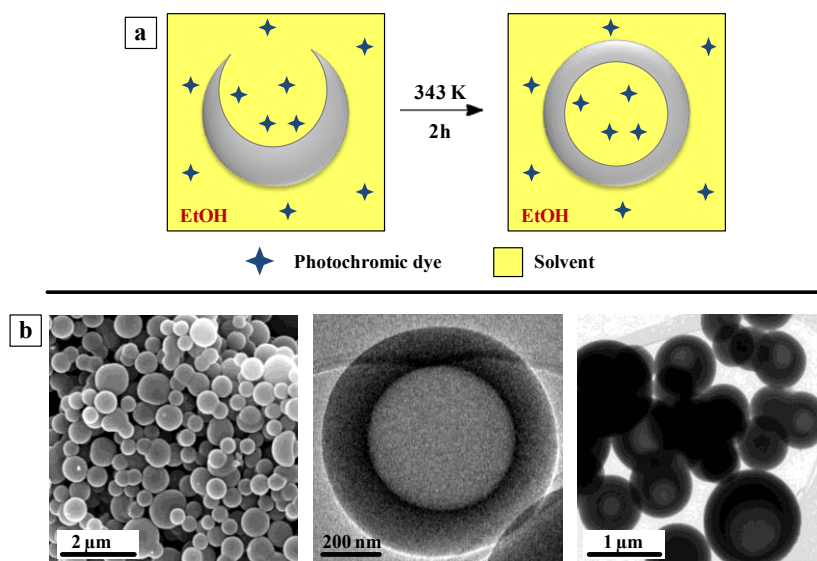


Figure 3.29 (a) Schematic representation of the closing treatment applied to opened PS particles to prepare photochrome-loaded liquid-filled nanocapsules. (b) SEM and TEM images of the resulting closed capsules. While no differences were observed between them by SEM, TEM measurements allowed revealing the coexistence of both hollow capsules and solid particles after the closing treatment.

After exploring different conditions to close PS opened capsules, the best results were obtained by heating the capsule dispersion during 2 hours at 343 K in an ethanol solution containing **PhI** as a reference photochrome. This process enabled us to seal the surface holes while maintaining the hollow structure of the capsules, although the concomitant formation of a significant amount of solid particles could not be prevented (Figure 3.29(b)). Attempts to circumvent this problem by reducing the reaction time led to the presence of opened capsules in the final sample, while assays performed using other solvents (toluene and hexane, among others) gave rise to worse results.

The best of the nanocapsules sample obtained after the thermal closing treatment was subjected to photochromic experiments. Unfortunately, poor colouration and slow fading rates resembling those obtained for **PhI** molecules directly dispersed in rigid polymeric matrices were observed. This fact was attributed to the evaporation of ethanol from the capsule core due to its relatively high volatility, which could be demonstrated by analysing the content of the capsules using ¹H NMR and headspace gas chromatography. In none of these measurements ethanol signals could be detected, which meant that the slow photochromic responses registered had to arise from **PhI** molecules crystallised onto the inner wall of capsules shell and/or dispersed into polystyrene shells and solid particles. To overcome this problem, we tried to replace ethanol by high boiling point solvents such as miglyol or hexadecane during the closing process, but this led to polymer shell melting during the treatment. In view of this, we decided at this point to abandon the preparation of liquid-filled photochromic nanocapsules following Xia's group methodology.

At the time this unsuccessful results were obtained, a patent application was filed by us describing our novel strategy towards fast-responsive photochromic solid materials⁷⁷. Since then much effort has been devoted in our group to the development of alternative methodologies for the preparation of liquid-filled photochromic nanocapsules, which has been carried out in joint collaboration with the spin off company Futurechromes S.L.. Personally I have not been directly involved in this work and, actually, my research activity immediately turned to the application of the liquid-filled capsule approach to the preparation of light-responsive systems other than photochromic materials (see Chapters 4 and 5). In spite of this, some of the most advanced results obtained by our group in the development of liquid-filled photochromic nanocapsules are shown in Figure 3.30, which clearly demonstrate the potential of the methodology explored during my thesis.

They consist in the preparation of polymer films loaded with nanocapsules filled with **PhI** solutions in a high boiling point solvent. As observed in the figure, fast thermal colour fading rates are obtained for the film without compromising the high transparency of the material ($T > 90\%$). According to this and other similar results, potential applications of the encapsulation strategy pioneered in this dissertation could be developed in the near future in the field of photoprotective coatings. For this, however, work is still to be done in the improvement of the synthesis and properties of the materials based on liquid-filled photochromic capsules.

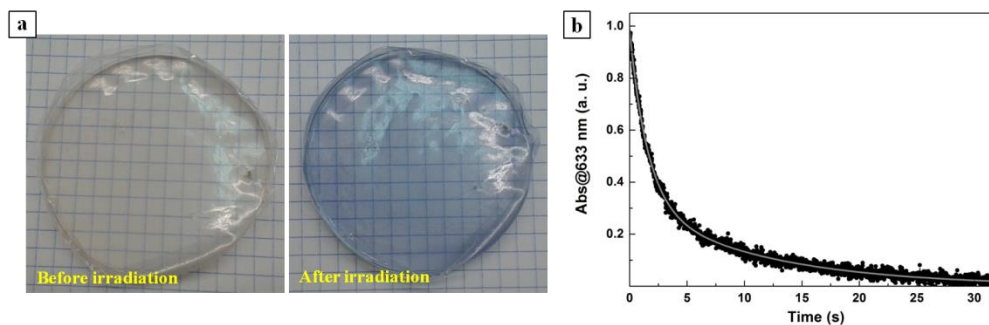


Figure 3.30 (a) Pictures of the nanocapsule-containing films prepared before and after light irradiation. (b) Absorption variation with time of the light-induced **PhI** merocyanine state inside the nanocapsule-loaded films. Samples were excited at 355 nm until the photostationary state was reached, and thermal decolouration kinetics were recorded at 633 nm in the dark and at room temperature. The grey lines correspond to the exponential fits of the experimental data.

3.3 Conclusions

In this part of the thesis we have explored the development of a simple and universal methodology for the preparation of fast-responsive photochromic materials based on the encapsulation of the photoactive molecules within liquid-core capsules. The main results and conclusions obtained in this work are summarised below.

(i) We have demonstrated the synthesis of photochromic polymeric capsules by interfacial polymerization in oil in water emulsions, capable to reproduce the photochromic properties observed in solution for the systems encapsulated. This way, we have attained solution-like colour fading kinetics in a solid material, which are about one order of magnitude faster than those measured upon direct dispersion of the photosensitive molecules into rigid polymer thin films and solid particles.

(ii) By properly selecting the nature of the liquid core, we have successfully prepared photochromic capsules displaying high stability both in time and upon redispersion in a variety of solvents without compromising their photochromic performance, which facilitates their manipulation and integration in future devices.

(iii) In this regard, we have proved the fabrication of fast photochromic materials consisting of capsule-containing polymer films and test lens matrices with relatively high

photochromic loadings (up to 0.1%). We have also demonstrated that the rapid decolouration rates of these materials matches the best results reported so far using other approaches. Importantly, in our case the fast responsive behaviour is attained independently of the nature of the photochromic compound or the encapsulating matrix used, while it does not require any further chemical modification of these substances. Although these materials are rather opaque, they could already be of used as fast responsive agricultural films, awnings and elements for optical data processing devices.

(iv) In order to attain the high transparency levels required for some applications such as ophthalmic lenses, we have tried to avoid light scattering reducing the size of the liquid-filled capsules prepared. Even though the procedure followed in the present doctoral thesis for this aim failed to attain fast photochromic liquid-filled nanocapsules; our group have demonstrated the preparation of highly transparent polymeric coatings with fast photochromic responses based on the encapsulation of the photoactive compounds in polymeric nanocapsules.

Although future work is still needed for the development and characterization of high quality capsule-containing photochromic films, the results reported herein demonstrated the potential of this methodology for the fabrication of fast-responsive photochromic materials.

3.4 References

1. Bouas-Laurent, H. & Dürr, H. Organic photochromism. *Pure Appl. Chem.* **73**, 639–665 (2001).
2. Dürr, H. & Bouas-Laurent, H. *Photochromism: Molecules and Systems*. (Elsevier, 2003).
3. Crano, J. C., Guglielmetti, R. J. & Robert, J. *Organic Photochromic and Thermochromic Compounds*. (Springer US, 2002).
4. Pardo, R., Zayat, M. & Levy, D. Photochromic organic-inorganic hybrid materials. *Chem. Soc. Rev.* **40**, 672–687 (2011).
5. Nigel Corns, S., Partington, S. M. & Towns, A. D. Industrial organic photochromic dyes. *Color. Technol.* **125**, 249–261 (2009).

6. Berkovic, G., Krongauz, V. & Weiss, V. Spiropyrans and Spirooxazines for Memories and Switches. *Chem. Rev.* **100**, 1741–1754 (2000).
7. Crano, J. C., Flood, T., Knowles, D., Kumar, A. & Van Gemert, B. Photochromic compounds: Chemistry and application in ophthalmic lenses. *Pure Appl. Chem.* **68**, 1395–1398 (1996).
8. Mennig, M., Fries, K., Lindenstruth, M. & Schmidt, H. Development of fast switching photochromic coatings on transparent plastics and glass. *Thin Solid Films* **351**, 230–234 (1999).
9. Lebeau, B. & Innocenzi, P. Hybrid materials for optics and photonics. *Chem. Soc. Rev.* **40**, 886–906 (2011).
10. Schaudel, B., Guermeur, C., Sanchez, C., Nakatani, K. J. & Delaire, J. A. Spirooxazine-and spiropyran-doped hybrid organic–inorganic matrices with very fast photochromic responses. *J. Mater. Chem.* **7**, 61–65 (1997).
11. Biteau, J. & Boilot, J. Photochromism of Spirooxazine-Doped Gels. *J. Phys. Chem.* **3654**, 9024–9031 (1996).
12. Zelichenok, A. *et al.* Steric effects in photochromic polysiloxanes with spirooxazine side groups. *Macromolecules* **25**, 3179–3183 (1992).
13. Goldburt, E., Shvartsman, F., Krongauz, V. & Fishman, S. Intramolecular interactions in photochromic spiropyran-merocyanine polymers. *Macromolecules* **17**, 1225–1230 (1984).
14. Ercole, F., Davis, T. P. & Evans, R. A. Photo-responsive systems and biomaterials: photochromic polymers, light-triggered self-assembly, surface modification, fluorescence modulation and beyond. *Polym. Chem.* **1**, 37–54 (2010).
15. Ishii, N. & Abe, J. Fast photochromism in polymer matrix with plasticizer and real-time dynamic holographic properties. *Appl. Phys. Lett.* **102**, 163301 (2013).
16. Zou, Q., Li, X., Zhou, J., Bai, K. & Ågren, H. Synthesis and photochromism of a spirooxazine derivative featuring a carbazole moiety: Fast thermal bleaching and excellent fatigue resistance. *Dyes and Pigments* **107**, 174–181 (2014).
17. Han, S. & Chen, Y. Modification of a photochromic 3-aryl-3-(α -naphthalene)-3H-naphtho[2,1-b]pyran system with a fast fading speed in solution and in a rigid polymer matrix. *J. Mater. Chem.* **21**, 4961–4965 (2011).
18. Han, S. & Chen, Y. Rapid fading of 3H-naphtho[2,1-b]pyrans with protonation of N,N-disubstituted group. *J. Mater. Chem.* **21**, 12402–12406 (2011).

19. Melo, S. De & Coelho, P. J. Preventing the formation of the long-lived colored transoid-trans Photoisomer in photochromic benzopyrans. *Org. Lett.* **13**, 4040–4043 (2011).
20. Tomasulo, M., Sortino, S., White, A. J. P., Chimiche, S. & Doria, A. Fast and stable photochromic oxazines. *J. Org. Chem.* **70**, 8180–8189 (2005).
21. Coelho, P. J., Silva, C. J. R., Sousa, C. & Moreira, S. D. F. C. Fast and fully reversible photochromic performance of hybrid sol–gel films doped with a fused-naphthopyran. *J. Mater. Chem. C* **1**, 5387–5394 (2013).
22. Kimoto, A., Tokita, A., Horino, T., Oshima, T. & Abe, J. Fast photochromic polymers carrying [2.2]paracyclophane-bridged imidazole dimer. *Macromolecules* **43**, 3764–3769 (2010).
23. Kishimoto, Y. & Abe, J. A fast photochromic molecule that colors only under UV light. *J. Am. Chem. Soc.* **131**, 4227–4229 (2009).
24. Gushiken, T., Saito, M., Ubukata, T. & Yokoyama, Y. Fast decoloration of spironaphthooxazine bound to a poly(dimethylsiloxane) network. *Photochem. Photobiol. Sci.* **9**, 162–171 (2010).
25. Photochromic, N., Organic, H., Built, I. M. & Blocks, W. N. New Photochromic Hybrid Organic–Inorganic Materials Built from Well-Defined Nano-Building Blocks. *Adv. Mater.* **14**, 1496–1499 (2010).
26. Li, D., Zhang, M., Wang, G. & Xing, S. Toward modulation of the naphthopyran photochromism: a miniemulsion copolymerization strategy. *New J. Chem.* **38**, 2348–2353 (2014).
27. Raboin, L., Matheron, M., Biteau, J., Gacoin, T. & Boilot, J.-P. Photochromism of spirooxazines in mesoporous organosilica films. *J. Mater. Chem.* **18**, 3242–3248 (2008).
28. Chen, D. & Morawetz, H. Photoisomerization and fluorescence of chromophores built into the backbones of flexible polymer chains. *Macromolecules* **9**, 463–468 (1976).
29. Evans, R. a *et al.* The generic enhancement of photochromic dye switching speeds in a rigid polymer matrix. *Nat. Mater.* **4**, 249–253 (2005).
30. Ichimura, K. Photochromic materials: a molecular cushion for isomerization. *Nat. Mater.* **4**, 193–194 (2005).
31. Ercole, F., Malic, N., Davis, T. P. & Evans, R. a. Optimizing the photochromic performance of naphthopyrans in a rigid host matrix using poly(dimethylsiloxane) conjugation. *J. Mater. Chem.* **19**, 5612–5623 (2009).

32. Ercole, F., Malic, N., Harrisson, S., Davis, T. P. & Evans, R. A. Photochromic polymer conjugates: the importance of macromolecular architecture in controlling switching speed within a polymer matrix. *Macromolecules* **43**, 249–261 (2010).
33. Malic, N., Campbell, J. A. & Evans, R. A. Superior photochromic performance of naphthopyrans in a rigid host matrix using polymer conjugation: fast, dark, and tunable. *Macromolecules* **41**, 1206–1214 (2008).
34. Malic, N., Dagley, I. J. & Evans, R. A. Preparation and photochromic performance characteristics of polyester-naphthopyran conjugates in a rigid host matrix. *Dyes and Pigments* **97**, 162–167 (2013).
35. Malic, N. & Evans, R. A. The use of poly(alkylene oxide)s to achieve fast and controlled photochromic switching in rigid matrices. *J. Polym. Sci. Part A Polym. Chem.* **50**, 1434–1444 (2012).
36. Such, G. K., Evans, R. A. & Davis, T. P. Rapid photochromic switching in a rigid polymer matrix using living radical polymerization. *Macromolecules* **39**, 1391–1396 (2006).
37. Guo, K. & Chen, Y. A strategy for the design of photochromic naphthopyrans with large optical density at photosteady state and fast fading speed at ambient temperature in the dark. *J. Mater. Chem.* **20**, 4193–4197 (2010).
38. Malic, N. *et al.* Controlling molecular mobility in polymer matrices: synchronizing switching speeds of multiple photochromic dyes. *Macromolecules* **43**, 8488–8501 (2010).
39. Such, G. K. *et al.* The use of block copolymers to systematically modify photochromic behavior. *Macromolecules* **39**, 9562–9570 (2006).
40. Sriprom, W., Néel, M., Gabbutt, C. D., Heron, B. M. & Perrier, S. Tuning the color switching of naphthopyrans via the control of polymeric architectures. *J. Mater. Chem.* **17**, 1885–1893 (2007).
41. Sriprom, W., Neto, C. & Perrier, S. Rapid photochromic nanopatterns from block copolymers. *Soft Matter* **6**, 909–914 (2010).
42. Zhang, F. *et al.* Microwave-assisted crystallization inclusion of spiropyran molecules in indium trimesate films with antidromic reversible photochromism. *J. Mater. Chem.* **22**, 25019–25026 (2012).
43. Gilbert, A. *et al.* ‘Ship-in-a-bottle’ synthesis and photochromism of spiropyran encapsulated within zeolite Y supercages. *Tetrahedron* **56**, 6951–6956 (2000).
44. Raboin, L., Matheron, M., Biteau, J., Gacoin, T. & Boilot, J.-P. Photochromism of spirooxazines in mesoporous organosilica films. *J. Mater. Chem.* **18**, 3242–3248 (2008).

45. Mühlstein, L. a., Sauer, J. & Bein, T. Tuning the thermal relaxation of a photochromic dye in functionalized mesoporous silica. *Adv. Funct. Mater.* **19**, 2027–2037 (2009).
46. Zayat, M., Pardo, R. & Levy, D. The role of organic groups in ormosil matrices in the photochromism of naphthopyrans in sol-gel thin films. *J. Mater. Chem.* **13**, 2899–2903 (2003).
47. Pardo, R., Zayat, M. & Levy, D. Thin film photochromic materials: Effect of the sol-gel ormosil matrix on the photochromic properties of naphthopyrans. *Comptes Rendus Chim.* **13**, 212–226 (2010).
48. Wirnsberger, G., Scott, B. J., Chmelka, B. F. & Stucky, G. D. Fast response photochromic mesostructures. *Adv. Mater.* **12**, 1450–1454 (2000).
49. Andersson, N., Alberius, P., Örtengren, J., Lindgren, M. & Bergström, L. Photochromic mesostructured silica pigments dispersed in latex films. *J. Mater. Chem.* **15**, 3507–3513 (2005).
50. Dubois, K. D., Liu, C. & Li, G. Involvement of surface-adsorbed water in photochromism of spiropyran molecules deposited on NaY zeolite. *Chem. Phys. Lett.* **598**, 53–57 (2014).
51. Mennig, M., Fries, K. & Schmidt, H. Photochromic organic-inorganic hybrid nanocomposite hard coatings with tailored fast switching properties. *MRS Proceedings* **576**, 409–414 (1999).
52. Hou, L., Schmidt, H., Hoffmann, B. & Mennig, M. Enhancement of the photochromic performance of spirooxazine in sol-gel derived organic-inorganic hybrid matrices by additives. *J. Sol-Gel Sci. Technol.* **8**, 927–929 (1997).
53. Arykwan, A., Prihantoro, A. & Shihui, X. Encapsulated photochromic dyes. US12/746,761 (2008).
54. Bernardus, T. N. M. *et al.* Photochromic optical element. WO2003001555 A1 (2003).
55. Chu, N. Y. C., Hovey, R. J., Snitzer, E. & Uhlmann, D. R. Stabilized photochromic materials. US4367170 A (1983).
56. Long, S., Bi, S., Liao, Y., Xue, Z. & Xie, X. Concurrent solution-like decoloration rate and high mechanical strength from polymer-dispersed photochromic organogel. *Macromol. Rapid Commun.* **35**, 741–746 (2014).
57. Poprawa-Smoluch, M. *et al.* Photoisomerization of disperse red 1 studied with transient absorption spectroscopy and quantum chemical calculations. *J. Phys. Chem. A* **110**, 11926–11937 (2006).

58. Peyratout, C. S. & Dähne, L. Tailor-made polyelectrolyte microcapsules: from multilayers to smart containers. *Angew. Chem. Int. Ed.* **43**, 3762–3783 (2004).
59. Meier, W. Polymer nanocapsules. *Chem. Soc. Rev.* **29**, 295–303 (2000).
60. Broaders, K. E., Pastine, S. J., Grandhe, S. & Fréchet, J. M. J. Acid-degradable solid-walled microcapsules for pH-responsive burst-release drug delivery. *Chem. Commun.* **47**, 665–667 (2011).
61. Pastine, S. J., Okawa, D., Zettl, A. & Fréchet, J. M. J. Chemicals on demand with phototriggerable microcapsules. *J. Am. Chem. Soc.* **131**, 13586–13587 (2009).
62. Zhang, H. & Wang, X. Fabrication and performances of microencapsulated phase change materials based on n-octadecane core and resorcinol-modified melamine-formaldehyde shell. *Colloids Surfaces A Physicochem. Eng. Asp.* **332**, 129–138 (2009).
63. Sun, G. & Zhang, Z. Mechanical properties of melamine-formaldehyde microcapsules. *J. Microencapsul.* **18**, 593–602 (2001).
64. Misawa, H., Kitamura, N. & Masuhara, H. Laser manipulation and ablation of a single microcapsule in water. *J. Am. Chem. Soc.* **113**, 7859–7863 (1991).
65. Hong, K. & Park, S. Melamine resin microcapsules containing fragrant oil: synthesis and characterization. *Mater. Chem. Phys.* **58**, 128–131 (1999).
66. Zhang, X. X., Fan, Y. F., Tao, X. M. & Yick, K. L. Fabrication and properties of microcapsules and nanocapsules containing n-octadecane. *Mater. Chem. Phys.* **88**, 300–307 (2004).
67. Zeng, F. *et al.* Preparation of highly charged, monodisperse nanospheres. *Macromol. Chem. Phys.* **203**, 673–677 (2002).
68. Qiu, D., Cosgrove, T. & Howe, A. M. Narrowly distributed surfactant-free polystyrene latex with a water-soluble comonomer. *Macromol. Chem. Phys.* **206**, 2233–2238 (2005).
69. Bohren, C. F. & Huffman, D. R. *Absorption and Scattering of Light by Small Particles*. (WILEY-VCH, 2008).
70. Cox, A. J., DeWeerd, A. J. & Linden, J. An experiment to measure Mie and Rayleigh total scattering cross sections. *Am. J. Phys.* **70**, 620–625 (2002).
71. Solans, C., Izquierdo, P., Nolla, J., Azemar, N. & Garcia-Celma, M. J. Nano-emulsions. *Curr. Opin. Colloid Interface Sci.* **10**, 102–110 (2005).

72. Lamers, P. H. *et al.* Methods for producing photosensitive microparticles. US08563213 B2 (2013).
73. Im, S. H., Jeong, U. & Xia, Y. Polymer hollow particles with controllable holes in their surfaces. *Nat. Mater.* **4**, 671–675 (2005).
74. Jeong, U., Im, S. H., Camargo, P. H. C., Kim, J. H. & Xia, Y. Microscale fish bowls: a new class of latex particles with hollow interiors and engineered porous structures in their surfaces. *Langmuir* **23**, 10968–10975 (2007).
75. Bai, M.-Y. *et al.* A facile and general method for the encapsulation of different types of imaging contrast agents within micrometer-sized polymer beads. *Adv. Funct. Mater.* **22**, 764–770 (2012).
76. Kim, J. H., Chainey, M., Elaasser, M. S. & Vanderhoff, J. W. Emulsifier-free emulsion copolymerization of styrene and sodium styrene sulfonate. *J. Polym. Sci. Part A-Polymer Chem.* **30**, 171–183 (1992).
77. Hernando Campos, J., Roscini, C., Vázquez-Mera, N. & Ruiz-Molina, D. Coating with photochromic properties, method for producing said coating and use thereof applicable to optical articles and glazed surfaces. WO2013132123 A1 (2013).

Chapter 4

Valence Tautomeric Thermochromism

4.1 Introduction

4.1.1 Valence tautomerism

Valence tautomeric (VT) complexes combine transition metal ions and non-innocent electroactive ligands with at least two nearly-degenerated electronic states with different structural, optical and magnetic properties^{1,2}. These electronic isomers, or valence tautomers, interconvert through a reversible intramolecular electron transfer between the metal ion and the redox-active ligand promoted by different external stimuli^{1,3,4}. For instance, irradiation with the appropriate wavelength can force VT interconversion heading to photoinduced valence tautomerism⁵. Pressure can also be applied to shift the tautomeric equilibrium considering the different molecular size of the two isomers⁶. However, among the possible external perturbations that promote VT transitions, the most widespread is temperature.

The vast majority of thermally-responsive VT complexes reported on literature are based on quinone or quinone-type ligands⁷; however, other redox active ligands have also been found to induce valence tautomerism when coordinated to the appropriate transition metal ion (e.g. schiff-base or phenoxyl radicals, among others)^{1,2,8}. Regarding metal centres, cobalt complexes are by far the most well studied VT systems, mainly due to the characteristic spin transition that accompanies the electron transfer in these compounds.

One of the first descriptions of valence tautomerism was the cobalt *bis*(quinone) complex [Co^{III}(3,5-DTBCat)(3,5-DTBSQ)(bpy)], where bpy stands for the counter ligand 2,2'-bipyridine and (3,5-DTBCat)²⁻ and (3,5-DTBSQ)⁻ refer to the catecholate and radical semiquinonate forms of 3,5-di-*tert*-butyl-*o*-quinone, respectively⁹. This complex presents a thermally induced electron transfer accompanied by a cobalt-based spin transition (Figure 4.1). Upon heating, an electron is transferred from the catecholate moiety to the low spin (*ls*) cobalt(III) centre, leading to an electronic isomer with a high spin (*hs*) cobalt(II) ion coordinated to two semiquinonate ligands. Since each tautomeric isomer exhibits a different electronic distribution, the optical and magnetic properties of the complex vary with temperature as the VT transition takes place. On the one hand, the magnetic susceptibility of the system changes owing to the spin transition induced; on the other, thermochromic behaviour is observed due to the colour changes caused by tautomer interconversion, as illustrated by the photographs of Figure 4.1. This is not only important for their relevance as

potential candidates for the fabrication of sensors or molecular electronic devices, but also because such changes represent the best way to monitor tautomer interconversion by techniques such as variable temperature magnetisation or absorption spectroscopy.

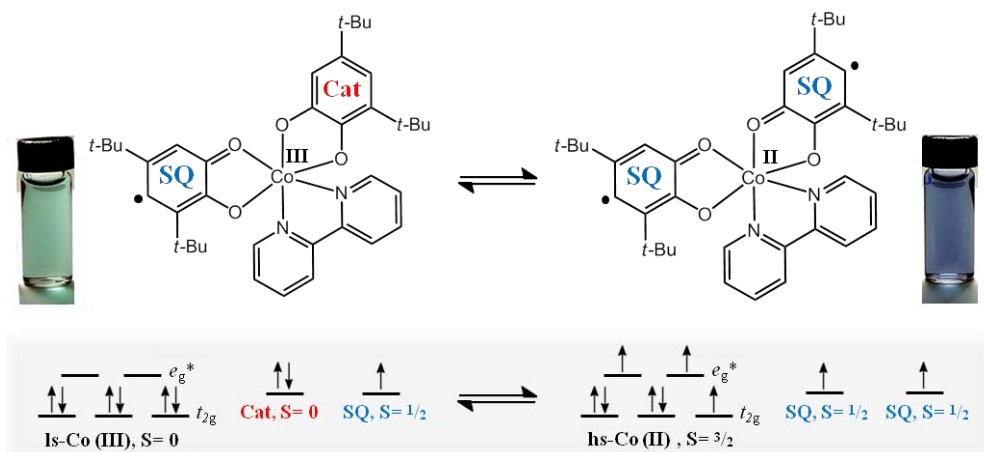


Figure 4.1 Schematic representation of the VT equilibrium of complex $[\text{Co}^{\text{III}}(3,5\text{-DTBCat})(3,5\text{-DTBSQ})(\text{bpy})]$ and the molecular orbitals involved in the electron transfer process. The vials show the colour changes induced by the VT interconversion in this compound.

Since this pioneering work, the number of VT compounds reported has been considerably increasing over time. It has been proven that metal and ligand characteristics^{1,2,10}, steric hindrance^{11,12}, donor/acceptor abilities of the counter ligand^{4,5} and/or the volume and coulombic interactions of the counterion¹³ strongly affect the electronic distribution and, therefore, the isomer interconversion.

Despite these findings, achieving full control over VT behaviour independently of the environment in which the system is placed remains one of the main challenges for VT scientific community. Thermally-induced valence tautomerism most characteristic parameter is the critical temperature, T_c , defined as the temperature at which the two tautomeric forms are present in 1:1 ratio (i.e. being above or below this value will shift VT equilibrium towards one of the two isomers). T_c deviations or even the suppression of the interconversion are common phenomena observed in different VT materials when moving from amorphous to crystalline phases or introducing the compound in different solid and liquid matrices¹⁴. Indeed, whereas most of the VT complexes reported exhibit thermally induced interconversion in solution, the number of examples displaying valence tautomerism in the solid state is rather limited. These changes have been attributed to the

subtle modifications of the crystal-phonon interactions produced when varying molecules environment. Intercalation of solvent molecules within the crystalline network has also been proven to influence T_c values, as it affects vibrational relaxation and imparts "softness" to the lattice helping to accomplish the dimensional changes involved in VT transitions.

The reason for such phonon dependence is that valence tautomerism is an entropy-driven process, as will be explained next^{3,5,15}. Figure 4.2 represents the energy curves of two cobalt valence tautomers plotted as a function of the nuclear coordinate. Thermal population of tautomeric states is dictated by the change in Gibbs free energy between both isomers, which can be decomposed in the corresponding enthalpic and entropic contributions ($\Delta G = \Delta H - T\Delta S$). Since the *hs*-Co(II) form presents higher spin state degeneracy and, as a result of its longer metal-to-ligand bond length, larger density of vibrational states, the entropy variation for the formation of this state is positive ($\Delta S = S_{hs-Co(II)} - S_{ls-Co(III)} > 0$). At low temperatures, $T\Delta S$ term is negligible compared to enthalpy changes ($\Delta H = H_{hs-Co(II)} - H_{ls-Co(III)} > 0$), and only the *ls*-Co(III) state is populated. On warming, the entropy factor will increase its contribution, favouring the population of the *hs*-Co(II) state up to the critical temperature (T_c), where both terms will have the same value ($\Delta H = T\Delta S$; $\Delta G = 0$). A further increase in the temperature will change the sign of ΔG and the *hs*-Co(II) state would become the most stable form. Taking this into account, VT transitions can be expected when the value of ΔH is positive but small enough to be overcome by the entropy term upon increasing the temperature. In addition, ΔS variations induced by crystalline packing modifications or matrix effects will affect the electron transfer equilibrium constants and, therefore, T_c ^{4,10}.

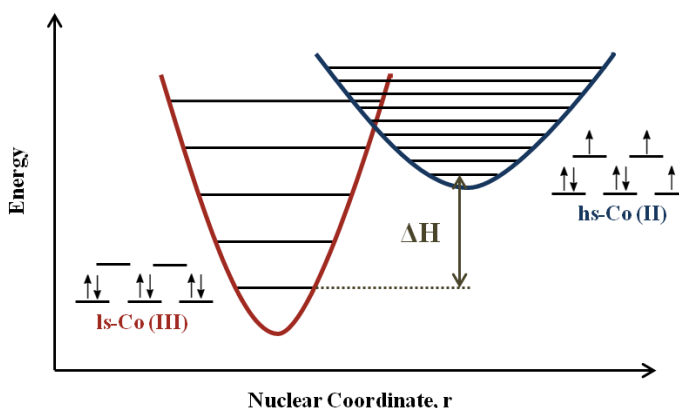


Figure 4.2 Potential energy curves of cobalt valence tautomers plotted as a function of the nuclear coordinate.

VT systems are expected to be used in the development of molecular electronics and spintronics; however, even though great improvements have been made in this regard, VT-based functional devices working at room temperature in the micro/nanoscale and robust enough to be handled and integrated without compromising their functionality have not been realized yet. Accordingly, there is a need for the development of proper methodologies capable to preserve VT behaviour and properties when moving from well characterised solutions to functional solid matrices via scalable, low cost, robust and easily transferable processes. This is perhaps one of the greatest requirements for the employment of valence tautomerism in high added-value applications.

4.1.2 State-of-the art of VT systems micro/nanostructuration

To achieve robust VT-based devices that could be easily handled and integrated in solid materials, one of the most promising approaches so far explored is the structuration of VT materials as micro-/nanoparticles. In spite of this, only a few works devoted to this topic had been reported up to now. The first was described by Schultz's group and consists in the functionalisation of 2 nm gold nanoparticles using [Co^{III}(3,5-DTBCat)(3,5-DTBSQ)] VT units bearing a 1-mercapto-6-(4'-methyl)bipyridine linker¹⁶. In this way VT molecular units could be grafted to the metal nanoparticle surface, thus allowing the tautomer interconversion behaviour to be reproduced in the solid state and on the nanoscale. Nevertheless, a T_c decrease from 389 K to 318 K was observed with respect to liquid solutions and ascribed to surface confinement effects.

Amorphous spherical nanoparticles with diameters ranging from 76 to 204 nm and based on a [Co^{III}(bix)(3,5-DTBCat)(3,5-DTBSQ)] coordination polymer were alternatively reported by our group¹⁷. In this case a flexible ditopic counter ligand (1,4-bis(imidazol-1-ylmethyl)benzene, bix) was used to enable the formation of the target polymer, whose structure is shown in **Figure 4.3** together with that of the resulting nanoparticles. The variable-temperature magnetisation measurements performed on the said nanoparticles revealed a gradual and incomplete thermally induced VT transition (**Figure 4.3(b)**). In a following work the same types of particles were exploited for the encapsulation of a fluorescent dye through coordination and mechanical entrapment and VT behaviour was used to report on their internal structure¹⁸.

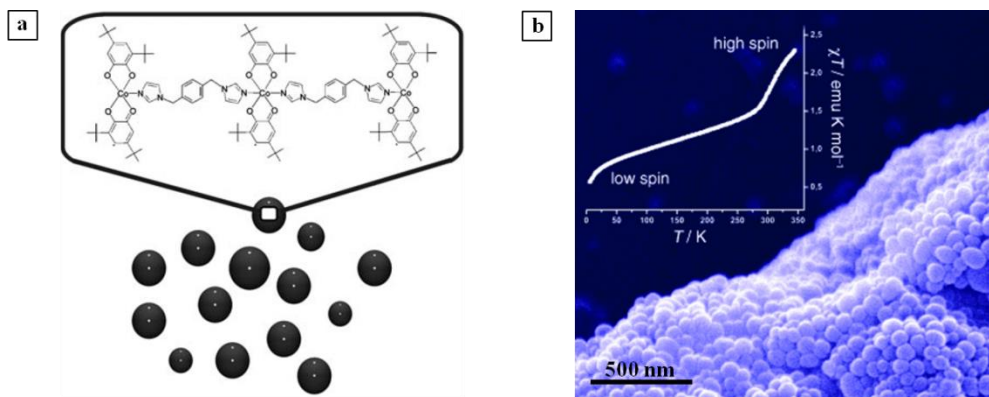


Figure 4.3 (a) Structure of the coordination polymer used to obtain VT nanoparticles. (b) SEM image of these nanoparticles and the temperature dependence of their magnetic susceptibility.¹⁷

4.1.3 Encapsulation of metal complexes as an alternative approach to valence tautomerism in the solid state

Although valence tautomerism in the solid state could be successfully observed in the micro/nanostructured materials described above^{16–18}, the approaches applied were rather specific in terms of the metal complex and/or surrounding matrix used and they could hardly be expanded to other compounds and media. In addition, the original VT properties of the same complexes in solution could not be perfectly reproduced, and significant variations in T_c and/or tautomerisation efficiency were measured. To overcome these limitations, in this part of the thesis we pursued the development of a universal methodology for the structuration of VT systems that enabled direct transfer of solution-like VT properties to the solid state. With this aim, herein we proposed the encapsulation of VT compounds in different polymeric particles, a strategy that should not require complicated synthetic methodologies and could in principle be applied to several families of VT complexes. To our knowledge, no previous examples of VT encapsulation using similar methods had been reported by the start of this thesis work.

Two different encapsulation approaches have been explored to prepare structured VT solid materials, which are schematically shown in Figure 4.4:

(i) *The direct dispersion of the VT molecules within solid polymeric particles* (Figure 4.4(a)). In this case, a non negligible effect of the surrounding polymer matrix was expected on the VT behaviour of the encapsulated complexes. However, given the almost unlimited number of available polymers that can be used to prepare such particles, careful screening of the nature of the polymer matrix should allow fair reproduction, or even fine tuning, of the VT properties in solution.

(ii) *The encapsulation of VT compounds inside liquid-filled microcapsules* (Figure 4.4(b)). As demonstrated in Chapter 3 for photochromic molecules, the presence of liquid inside the capsules should ensure the preparation of solid materials with solution-like responses and optimised VT behaviour, which could then be loaded into any final functional matrix of interest. In addition, it should afford the possibility to tailor the VT properties of the final system by just changing the nature of the solvent used in the encapsulation process. Finally, this strategy should also enable overcoming other typical problems encountered when directly dispersing VT molecules within solid matrices, such as phase segregation or migration.

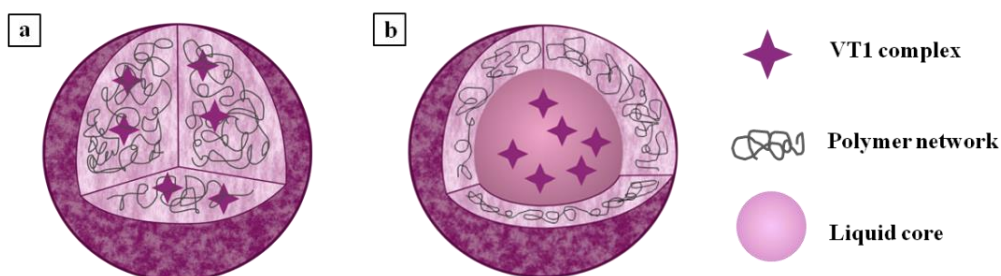


Figure 4.4 Schematic representation of the two approaches followed in this chapter to obtain structured VT solid materials: **(a)** encapsulation within solid polymeric particles; **(b)** encapsulation inside liquid-filled polymeric capsules.

To evaluate the potential of these two strategies to attain solution-like valence tautomerism in the solid state, a cobalt-based VT complex was taken as benchmark system, which is described in detail in the next section.

4.1.4 Our VT complex of choice: $[\text{Co}^{\text{III}}(\text{Cat-N-BQ})(\text{Cat-N-SQ})]$

The VT compound selected as model case for the encapsulation studies was $[\text{Co}^{\text{III}}(\text{Cat-N-BQ})(\text{Cat-N-SQ})]$ (**VT1**). In this complex the cobalt ion is coordinated to the O,N,O'-tridentate Schiff base ligand 3,5-di-*tert*-butyl-1,2-quinone-1-(2-hydroxy-3,5-di-*tert*-butylphenyl)imine, where $(\text{Cat-N-BQ})^-$ and $(\text{Cat-N-SQ})^{\bullet 2-}$ denote its monoanionic and radical dianionic forms, respectively (Figure 4.5). This compound is a dark-purple highly coloured crystalline solid due to biquinone ligands intense absorption.

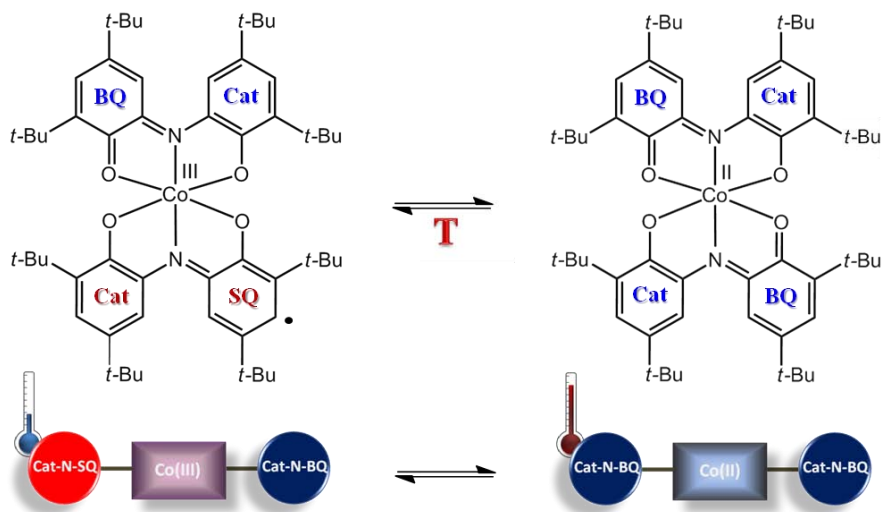


Figure 4.5 Structure of complex **VT1** and schematic representation of the equilibrium associated to its valence tautomerism ($[\text{Co}^{\text{III}}(\text{Cat-N-BQ})(\text{Cat-N-SQ})] \leftrightarrow [\text{Co}^{\text{II}}(\text{Cat-N-BQ})_2]$).

This system was chosen because, in addition to its high chemical stability and resistance to atmospheric oxygen, it exhibits remarkable differences between its VT behaviour in solution and in the solid state, thus representing an excellent challenge for the planned studies. Although first reported in 1988, evidences of its VT properties were not described until ten years later by Caneschi and coworkers^{19,20}. Figure 4.5 depicts the tautomerisation equilibrium undergone by **VT1**. The predominant form of this complex at low temperature is the low spin tautomer (*ls*-Co(III), $S = 1/2$). As the temperature is increased, the $(\text{Cat-N-SQ})^{\bullet 2-}$ ligand transfers one electron to the Co(III) ion, evolving to $(\text{Cat-N-BQ})^-$ and forcing the interconversion to the high spin tautomer (*hs*-Co(II), $S = 3/2$). The other ligand remains temperature-invariant and does not participate in the VT transition. Note that this thermally

induced electron transfer is also accompanied by the cobalt-characteristic spin transition already mentioned for complex $[\text{Co}^{\text{III}}(3,5\text{-DTBCat})(3,5\text{-DTBSQ})(\text{bpy})]$.

The temperature dependence of the spectroscopic and magnetic properties of **VT1** in solution have been previously described^{14,19–21} and shown to reveal the characteristic features of the VT equilibrium. Figure 4.6 displays the colour variations and the changes in the absorption spectra observed for a toluene solution of **VT1** upon increasing temperature. The spectra colour gradient stands for temperature variation, blue and red colours used for the coldest and the hottest measurements, respectively. This code of colours will be maintained along the chapter. The absorption bands attributed to the low spin isomer, with maxima at 388, 436, 530, 720 (shoulder), 801, 896 and 1030 nm, dominate the spectra at low temperatures (< 300 K). As the high spin tautomer is favoured upon heating, the intensity of *ls*-Co(III) absorption bands decreases while new bands appear between 600 and 800 nm with a maximum around 796 nm. The presence of three isosbestic points at 427, 570 and 878 nm also corroborates the existence of a thermally induced interconversion between the two electronic isomers.

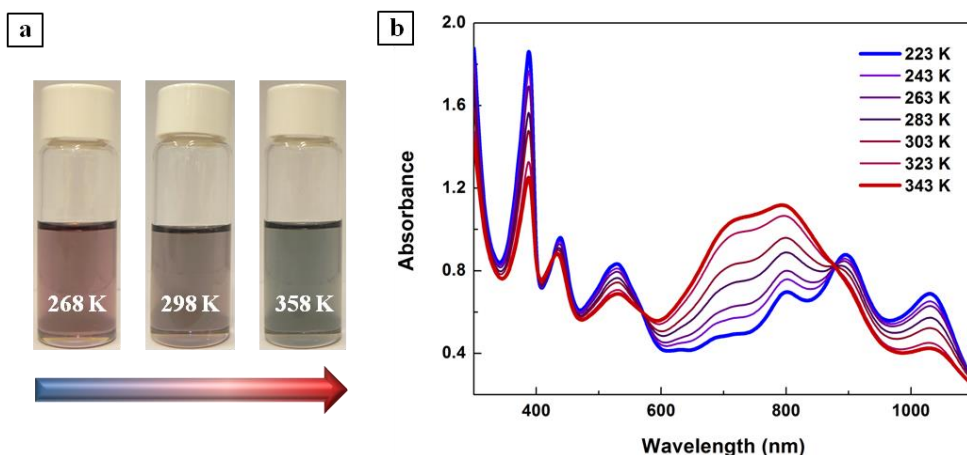


Figure 4.6 Temperature-induced variations of the absorption properties of a toluene solution of complex **VT1**. (a) Photographs of the solution colour at three different temperatures. (b) Corresponding electronic absorption spectra acquired between 203 K and 343 K.

It has also been demonstrated that VT equilibrium can be tuned by variation of the solvent nature^{14,20}. Figure 4.7 shows the marked changes occurring in the absorption spectra of complex **VT1** for a number of solvents and the differences observed in the temperature dependence of the effective magnetic moment of this compound. While toluene, methanol

and acetone solutions exhibit VT transitions between 220 and 360 K, T_c is shifted towards lower temperatures in chloroform and a more gradual, but incomplete transition is then observed. In any case, the tautomeric equilibrium is dominated by the high spin isomer at room temperature in all these solvents. More remarkable are the divergences observed for acetonitrile solution, in which the low-spin isomer is predominant at least up to 340 K, indicating that the VT behaviour of the complex is either suppressed in this solvent or the corresponding T_c value shifted to much higher temperatures.

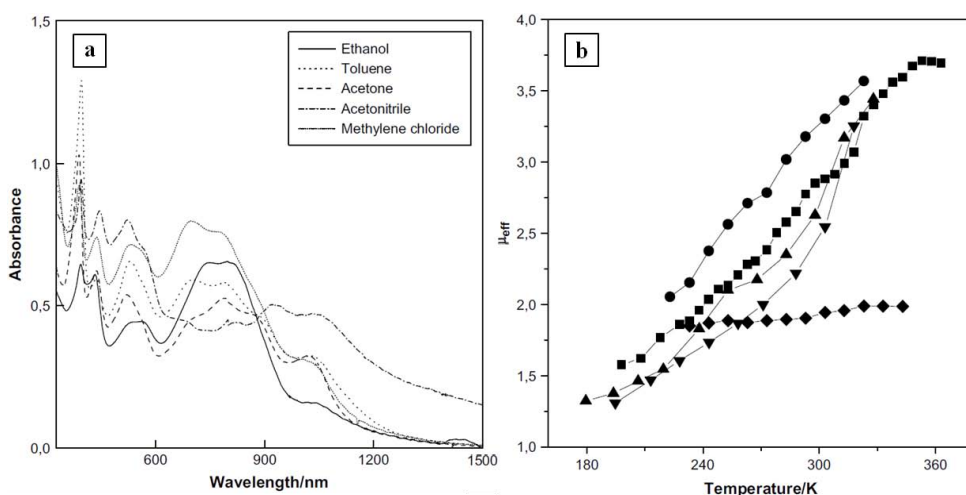


Figure 4.7 (a) Electronic absorption spectra of [Co^{III}(Cat-N-BQ)(Cat-N-SQ)] complex in ethanol, toluene, acetone, acetonitrile and methylene chloride at room temperature. (b) Temperature dependence of its effective magnetic moment (μ_{eff}) in chloroform (●), toluene (■), acetone (▼), methanol (▲) and acetonitrile (◆).¹⁴

On the other hand, variable-temperature magnetisation measurements performed in the solid state concluded that no valence tautomerism takes place before reaching 370 K²². Although VT1 decomposes before complete interconversion, its T_c in the solid state was estimated to be around 597 K (300 K higher than the value found for the toluene solution). This behaviour is reproducible along a whole series of crystals obtained from different solvents, since in all the cases crystallisation leads to the same crystalline phase independently of the solvent used¹⁴.

4.1.5 Objectives

The purpose of the work performed in this chapter is the *encapsulation of complex VT1 inside polymeric particles in order to develop a universal methodology capable to produce robust structures presenting solution-like valence tautomerism in the solid state*. This methodology should also afford an easy way of tuning T_c values and, therefore, the thermal response of the system at will. To achieve these objectives, the following studies were carried out in the framework of the two strategies explored: (a) *encapsulation within polymeric solid matrices*: (i) selection of the optimal polymer and conditions to obtain solution-like VT behaviour, (ii) preparation of the corresponding nanoparticles, and (iii) study of their VT properties; (b) *confinement into liquid-filled capsules*: (i) synthesis of the capsules loaded with VT1, (ii) characterisation of their thermochromic properties, and (iii) fine tuning of their thermal response by solvent replacement.

4.2 Results and discussion

4.2.1 Encapsulation into polymeric solid particles

Our first attempts to obtain VT solid micro/nanostructures consisted in the encapsulation of VT1 molecules within solid polymeric particles simply by physical entrapment during their formation process. Ideally, the VT complex should maintain its thermochromic properties when properly dispersed inside the polymer network. However, possible steric hindrance effects imparted by the surrounding matrix, undesired VT1-polymer interactions, and/or aggregation and phase segregation processes resulting from poor complex-polymer miscibility could dramatically affect the thermal response of the system and even prevent its VT interconversion. Therefore, before conducting any structuration study, we first investigated the bulk behaviour of different polymer thin films containing VT1 for the selection of the appropriate conditions to attain solution-like valence tautomerism in the final nanoparticles.

4.2.1.1 Optimisation of the encapsulation conditions

The effect of the polymer nature on **VT1** tautomeric interconversion was analysed using thin films made out of three different polymers: PVAc (poly(vinyl acetate), $M_w \sim 100,000$), PC ($M_w \sim 64000$), and PMMA ($M_w \sim 350000$). For each polymer, three different concentrations of the cobalt complex were tested (2, 4 and 8 wt%), thus giving rise to distinct **VT1@PVAc**, **VT1@PC** and **VT1@PMMA** samples. This work was performed in collaboration with the Master student Sérgio António Pires Mendes (from the Technical University of Lisbon) during his Erasmus placement at the Nanosfun group. In a typical experiment, dichloromethane solutions containing 15 wt% of polymer and the corresponding concentrations of the thermochromic complex were deposited by drop casting onto glass slides. After solvent evaporation, thin films oscillating between 5 and 20 microns in width were obtained (Figure 4.8(d)).

Initially, optical microscopy was used to detect any possible phase segregation resulting in the formation of crystals or any other kind of inhomogeneities in the polymer thin films. Figure 4.8 shows the optical micrographs of the different sample tested, acquired with 270° polarised light. No crystals or phase segregation were detected for the PC and PMMA thin films doped with 2 wt% of **VT1**, indicating a good dispersion of the complex within these polymeric matrices. This was confirmed by X-ray diffraction (XRD) experiments, where no crystalline patterns could be observed for any of these samples. Upon increasing the content of the thermochromic compound up to 4 wt%, however, crystalline seeds of complex **VT1** started to appear, which resulted in the formation of several crystals (particularly notable in PC films) once the concentration was further augmented to 8 wt%. Phase segregation and crystallisation was much more favoured for PVAc thin films, since **VT1** crystals were formed even at the lowest concentration employed (2 wt%). Divergences between PVAc and **VT1** hydrophilic/hydrophobic balance are most likely at the origin of this behaviour.

According to these results and the well-known detrimental effects of complex crystallisation^{14,22}, we then applied variable-temperature UV-Vis spectroscopy to investigate the valence tautomerism of crystal-free polymer thin films: 2 wt% **VT1@PMMA**, and 2 wt% **VT1@PC**. For comparison purposes, the behaviour of 4 wt% **VT1@PC** was also analysed, in order to directly evaluate the effect of complex crystallisation within polymer thin films.

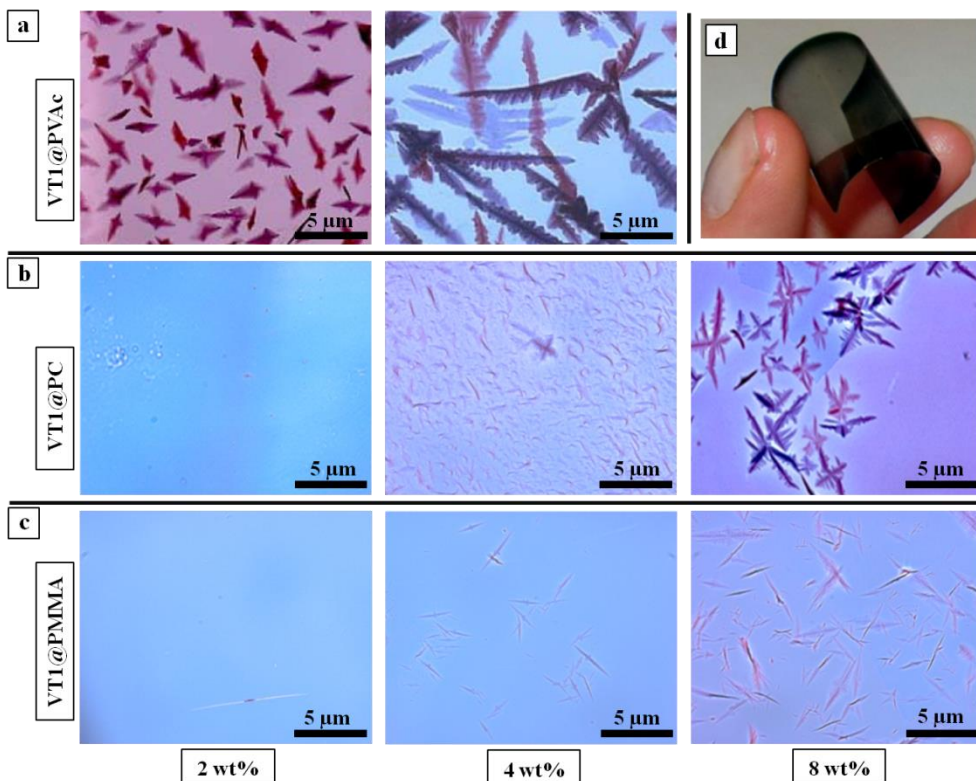


Figure 4.8 Optical micrographs of polymeric thin films containing complex **VT1**, obtained with 270° polarised light: **(a)** PVAc films at 2 and 4 wt%; **(b)** PC films at 2, 4 and 8 wt%; and **(c)** PMMA films at 2, 4 and 8 wt%. **(d)** Image of the 2 wt% **VT1@PMMA** thin film after detachment from the supporting glass slide.

As seen in Figure 4.9(a), the absorption bands of the *hs*-Co(II) isomer dominated the spectra of 4 wt% **VT1@PC** along the whole temperature range studied. This result differs from those found for bulk crystals of **VT1**, in which the *ls*-Co(III) isomer was favoured for the same range of temperatures^{23,24}. The specific effects leading to the stabilisation of the *hs*-Co(II) isomer in polymer-dispersed **VT1** microcrystals remain unclear to us and are outside the scope of this thesis work. In any case, it is clear that **VT1** crystallisation within the polymer matrix also induces the loss of the VT interconversion (at least in the temperature range measured) and, consequently, less concentrated thin films are needed to reproduce the solution-like behaviour.

In the case of crystal-free 2 wt% **VT1@PC** sample (Figure 4.9(b)), *ls*-Co(III) isomer bands dominated the film absorption spectrum at all the temperatures measured, and only small thermal changes with no clear isosbestic points were detected. From this we concluded that

not only the concentration of the VT complex (i.e. aggregation and crystallisation) influenced its valence tautomerism behaviour, but also the nature of the polymeric matrix. In the case of PC, proper dispersion of VT1 molecules within the polymer film resulted in strong stabilisation of the low spin isomer of the complex and, as such, lack of electronic interconversion within the temperature range scanned.

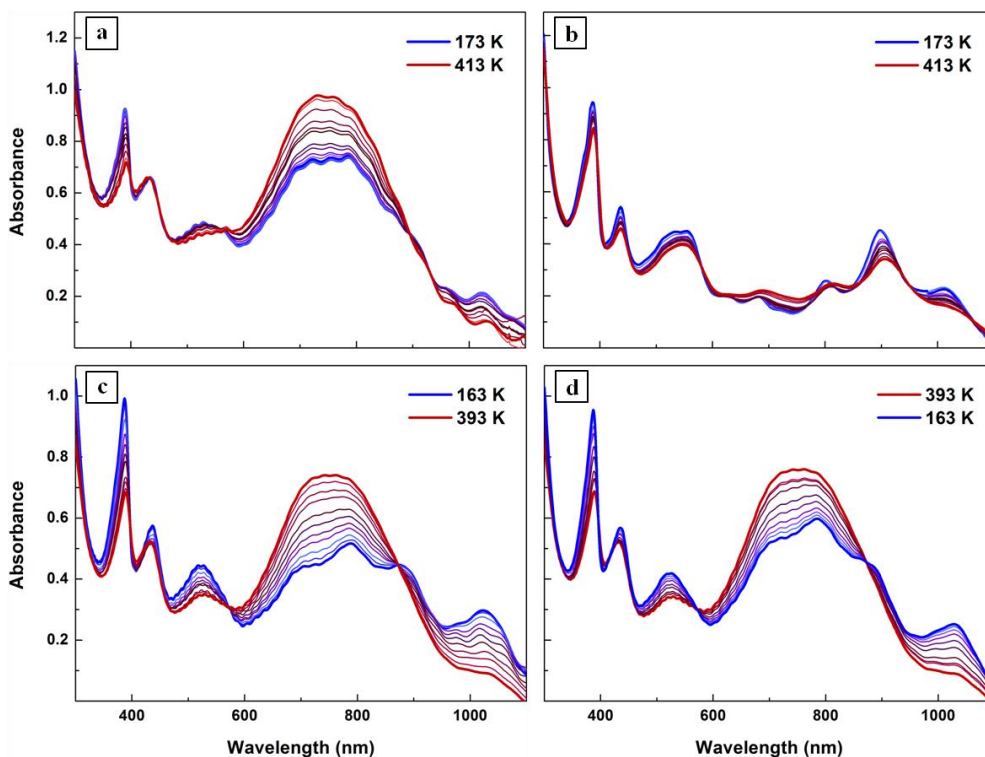


Figure 4.9 (a-b) Temperature dependence of the absorption spectra of PC films doped with (a) 4 wt% and (b) 2 wt% of VT1, between 173 and 413 K. (c-d) Temperature dependence of the absorption spectra of a PMMA film loaded with 2 wt% of VT1 and acquired upon (c) heating and (d) cooling between 163 and 393 K. Measurements were recorded by increments of 20 K.

On the contrary, satisfactory results were obtained for the 2 wt%-PMMA thin film, for which a similar thermochromic behaviour to that measured in toluene solution could be clearly observed (Figure 4.9(c)). At the lowest temperature (163 K), mostly the *ls*-Co(III) isomer bands of the complex could be distinguished; however, as temperature increased, the bands associated to the *hs*-Co(II) isomer became more intense and eventually dominated the spectra. Nevertheless, it must be noted that the VT interconversion in this case started around 120 K below the temperature observed for toluene, thus reassuring the influence of

the surrounding media on the T_c of these systems. On the other hand, it is worth to mention that the variable-temperature UV-Vis behaviour of this thin film was not fully reversible upon cooling and a larger contribution of the *hs*-Co(II) isomer spectral features was observed when returning to 163 K (Figure 4.9(d)). This was tentatively attributed to **VT1** partial crystallisation, which was favoured by the onset of polymer chain mobility at the highest experimental temperatures. To shed light on this fact, the thin film was heated up just above the PMMA glass transition temperature ($T_g = 403$ K) and allowed to slowly cool down to room temperature (1 K min^{-1} or less). Optical microscopy performed on the resulting sample revealed the formation of crystals within the polymeric matrix (Figure 4.10(d)), confirming that crystallisation was responsible for the stabilisation of the high-spin tautomer at low temperatures, as previously described for the 4 wt% **VT1@PC** thin films. On the contrary, when the sample was fast cooled after reaching 405 K, no crystallisation was observed, the **VT1** molecules remained well dispersed and, consequently, the switching behaviour turned out to be fully reversible.

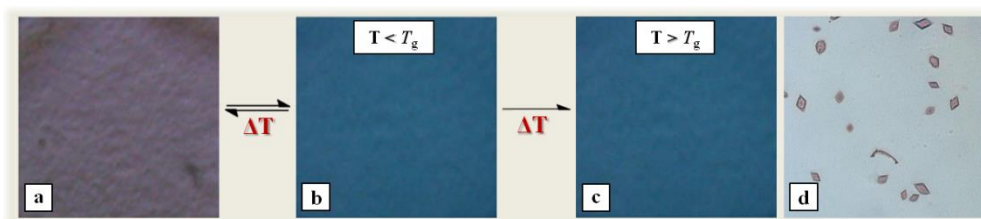


Figure 4.10 Photographs of the 2 wt% PMMA film (a) at room temperature, (b) heated at 393 K (i.e. slightly below its T_g) and (c) heated at 405 K (i.e. slightly above its T_g). (d) Optical micrograph of the film after heating at 405 K and slowly recovering the room temperature.

To summarise the behaviour of the 2 wt% **VT1@PMMA** thin film, Figure 4.10 shows the colour variation of this sample with temperature, although the real colours observed by naked eye slightly differed from those displayed in the photographs due to optical restrictions of the microscope camera used. In any case, the **VT1**-loaded polymeric film clearly showed the desired thermochromic behaviour, the magenta-like colour found at room temperature (a) changing to cyan in a reversible manner if heated below T_g (b), and irreversibly (c) when heated above T_g and slowly cooled down as a result of the formation of complex crystals (d).

In view of all these results, we concluded that in order to assure **VT1** valence tautomerism into polymeric matrices it is essential to (i) avoid phase segregation of the complex and the

consequent formation of crystals/aggregates, (ii) consider polymer nature since it clearly influences the VT interconversion process, and (iii) avert heating near the polymer T_g unless irreversible interconversion is desired (e.g. for permanent information storage systems). Among the different polymer matrices and compositions explored in this work, only the use of PMMA and complex concentrations below 2 wt% enabled these requirements to be fulfilled. Consequently, these were the conditions applied for the preparation of VT solid nanoparticles, although it led to T_c values significantly lower than those found for **VT1** in most organic solvents.

4.2.1.2 Solid PMMA particles loaded with VT1

In a first attempt to synthesise VT PMMA-based particles, we carried out methyl methacrylate (MMA) emulsifier-free emulsion polymerisation following a methodology described in literature²⁵. With this aim, the VT complex was added to MMA monomer and the mixture was emulsified in an aqueous solution containing the reaction initiator. We expected **VT1** to get trapped in between polymer chains as the reaction proceeded to yield PMMA particles, similarly to what we observed in the synthesis of solid PS NPs in section 3.2.4. The SEM and TEM images of Figure 4.11 show the spherical shape and the solid structure of the particles obtained, which presented an average size of 131 nm. Note that when acquiring the pictures, particles partially melted due to electron beam heating effects²⁶⁻²⁸, thus adhering to each other and reducing their size in approximately 9%. This behaviour was observed for all the PMMA particles prepared. Despite obtaining well defined nanoparticles through this methodology, the tautomer loading efficiency achieved was quite low since, as the reaction proceeded, the complex molecules precipitated out of the monomer droplets resulting on a suspension of white polymer nanoparticles instead of brown-magenta coloured.

To improve the encapsulation efficiency, the solvent evaporation method²⁹ was tested using preformed PMMA polymer. A schematic representation of this method is shown in Figure 4.12. In a typical procedure, a volatile organic phase containing dissolved PMMA and 2 wt% of VT complex was emulsified in an aqueous phase. Once the solvent was removed by evaporation, the polymer precipitated into spherical particles trapping the thermochromic compound inside the polymer network.

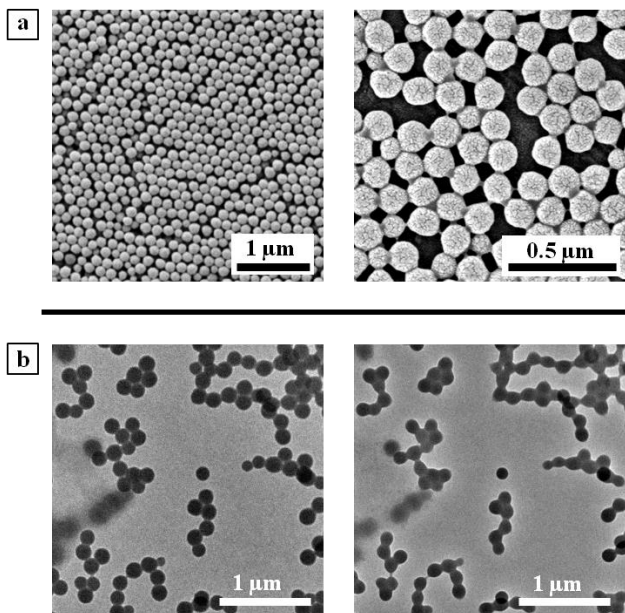


Figure 4.11 (a) SEM and (b) TEM images of PMMA solid particles obtained by soap-free emulsion polymerisation (131 ± 13 nm). The TEM images display the effect of the electron beam on particle morphology.

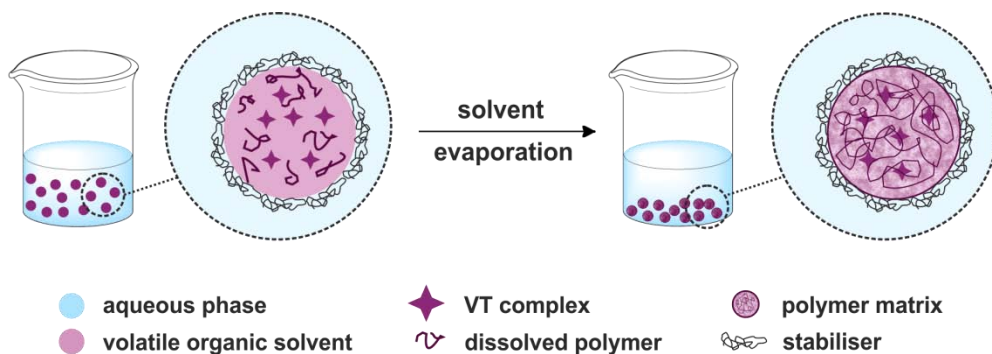


Figure 4.12 Schematic representation of the solvent evaporation method applied for obtaining solid PMMA particles loaded with VT1.

Dense spherical particles with smooth surfaces were obtained (**VT1@PMMA**), whose diameter varied from a few millimetres to hundreds of nanometres in size depending on experimental conditions (stirring rate, evaporation temperature or the organic solvent/aqueous phase ratio, see section 6.3.2). Figure 4.13 gathers images of three different samples prepared varying in size. Their solid structure was confirmed by STEM and the strong colour that the particles exhibited (Figure 4.13(a)) evidenced the enhancement in **VT1** encapsulation efficiency. Efficiencies of approximately 93% and **VT1** payloads of

1.9% were obtained, as determined by UV-Vis absorption measurements after dissolving the particles in toluene.

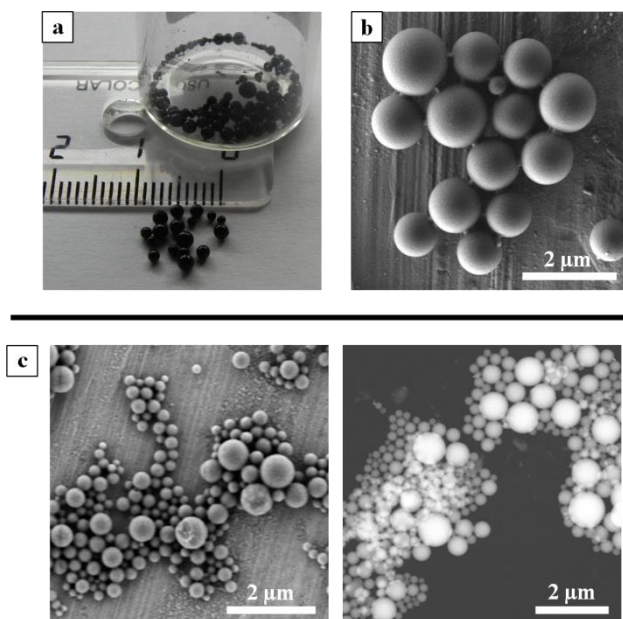


Figure 4.13 (a) Picture of millimetre-sized dark VT1@PMMA particles. (b) SEM image of VT1@PMMA particles with an average size of 526 ± 311 nm. (c) STEM (scanning transmission electron microscopy) images corresponding to the smallest VT1@PMMA particles obtained with an average size of 337 ± 135 nm.

Unfortunately, particle opacity and the lack of the proper spectrophotometric equipment at the time of this work prevented us from quantitatively studying the variable-temperature spectroscopic behaviour of these samples. In practice, we could only tentatively follow their thermochromic interconversion by recording particle colour variations with an optical microscope. Figure 4.14(a) shows the significant change in colour monitored in this way when heating the particles from 300 K to 373 K. Again, owing to the optical limitations of the microscope camera, the actual colours of the particles differed from those in the photographs. Nevertheless, this colour change demonstrated the occurrence of valence tautomerism for the solid VT1@PMMA samples prepared.

To reinforce this qualitative result, we also measured the variable-temperature magnetisation of the particles under an external applied magnetic field of 1 T ($\chi_{M,T}$ vs. T, Figure 4.14(b)). At low temperatures, the observed $\chi_{M,T}$ value ($0.4 \text{ emu K mol}^{-1}$) was in agreement with the presence of one unpaired electron, as expected for the low-spin isomer of VT1. This value remained approximately constant up to 300 K, whereupon the magnetic moment gradually

increased towards $0.8 \text{ emu K mol}^{-1}$, a value associated with partial interconversion to the high-spin isomer at the highest temperature assayed. Such temperature-induced changes confirmed the presence of the VT switchable behaviour within the solid particles, proving the feasibility of this approach.

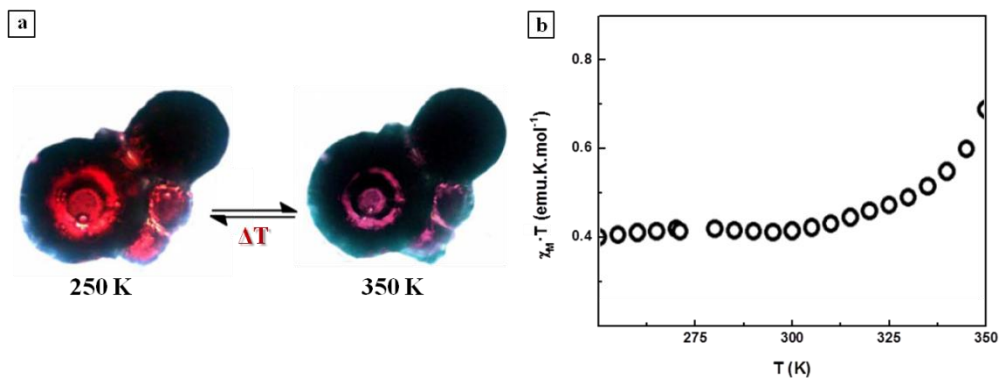


Figure 4.14 (a) Optical micrographs of **VT1@PMMA** particles colour change upon temperature variation from 300 to 373 K. (b) Temperature dependence of particle magnetization ($\chi_M \cdot T$) under an external applied magnetic field of 1 T measured between 250 and 350 K.

The results described in this section demonstrate that the encapsulation of VT complexes within organic polymeric particles might be a successful approach for the synthesis of VT micro/nanostructures. However, this methodology turns out to be restricted to a specific range of concentrations, polymers and temperatures, which may limit its use in future devices and require of a thorough screening of these conditions for any new type of metal complex considered in order to attain the desired VT properties. For this reason, as a follow-up study to this work, we aimed to develop **VT1**-loaded liquid-filled capsules as a better way to accomplish solution-like VT behaviour in solid structured materials.

4.2.2 Liquid-filled polymeric capsules

The second of the approaches explored in this part of the thesis consisted in the encapsulation of **VT1** solutions inside polymeric capsules composed of a liquid core and a polymeric shell that entraps and isolates it from capsule surrounding medium. As previously demonstrated in Chapter 3 for photochromic compounds, this should allow the thermochromic behaviour of **VT1** in liquid solution to be preserved in the solid state.

4.2.2.1 Capsule synthesis

First attempts to fabricate liquid-filled polymeric capsules containing complex **VT1** were done adopting the same methodology described in the previous chapter for the synthesis of polyamide capsules, which consisted in the interfacial polycondensation of terephthaloyl chloride and diethylenetriamine (DETA) in an emulsified system (see section 3.2.1.2). In this case, both the VT compound and terephthaloyl chloride had to be initially dissolved in the dispersed oil phase. Unfortunately, this method failed to yield the desired microcapsules due to **VT1** decomposition. This was perceived as a change in the colour of the solution and was confirmed by the consequent modification of its UV-Vis spectrum .

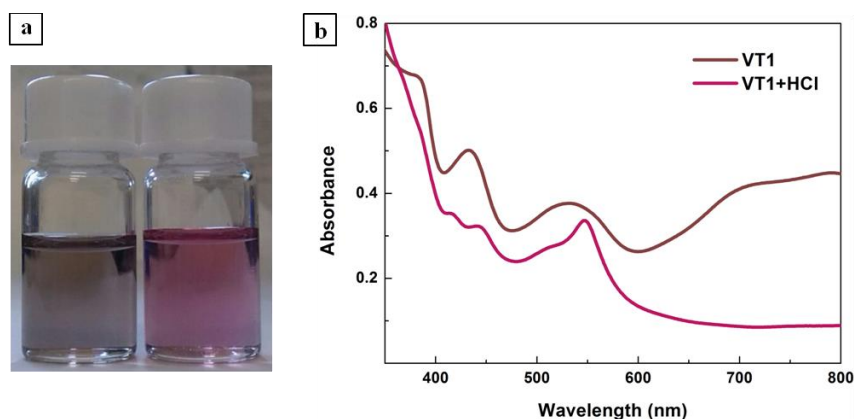


Figure 4.15 (a) Images and (b) absorption spectra of a **VT1** in toluene solution before and after the addition of hydrochloric acid.

This fact was attributed to the formation of hydrochloric acid upon acyl chloride condensation reaction and hydrolysis during the interfacial polymerisation process, which then induced **VT1** degradation. This process was verified by direct addition of aqueous HCl to a **VT1** solution in toluene, which resulted in a similar change in colour as that observed during the preparation of the liquid-filled capsules. Figure 4.15 shows the colour changes observed in this experiment, which clearly demonstrate decomposition of the metal complex. Replacement of the terephthaloyl chloride originally used in the reaction by other acyl chlorides did not prevent **VT1** degradation, thus reinforcing our assumption.

Alternatively, we tried to synthesise liquid-filled capsules by solvent evaporation methodologies similar to those used in the previous section³⁰. A schematic representation of this method is depicted in Figure 4.16.

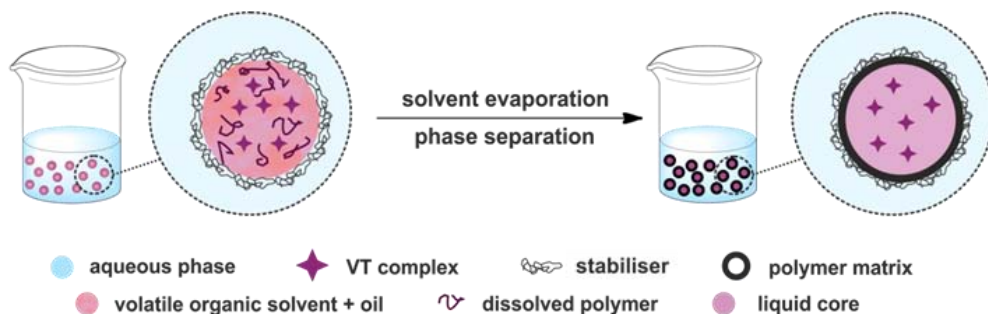


Figure 4.16 Schematic representation of the solvent evaporation method applied for the synthesis of liquid-filled polymeric capsules.

As previously done for the synthesis of solid PMMA particles, the polymer selected and the complex **VT1** had to be dissolved in a volatile organic phase. However, in this case, the solution also contained certain amounts of oil, concretely, hexadecane or miglyol. The mixture was emulsified in an aqueous phase and, as the volatile solvent evaporated, we expected an internal phase separation to occur that should lead to polymer precipitation at the interface of the oil droplets and formation of a closed shell around the internal **VT1** solution.

Representative SEM images of the microstructures obtained via this experimental procedure are shown in Figure 4.17. They presented porous, spherical, half-spherical, cup, oval or coin-like morphologies depending on the polymer (PMMA or PS), the oil (hexadecane or miglyol) or the organic solvent (chloroform or dichloromethane) employed as well as the oil/polymer ratio, the type and amount of emulsifier or the emulsification rate used (see section 7.2.2). Optical and electron microscopy images of these structures revealed that most of these particles were solid and, even though some of them possessed core-shell architectures, no liquid ejection was detected upon physical crushing. However, no phase segregation of the organic oil from the aqueous continuous phase was observed after the end of the reaction and the subsequent separation of the solid particles from the resulting colloidal dispersion. Therefore, hexadecane and miglyol most likely got trapped inside the polymer network of the particles formed during solvent evaporation, acting as polymer plasticizers³¹.

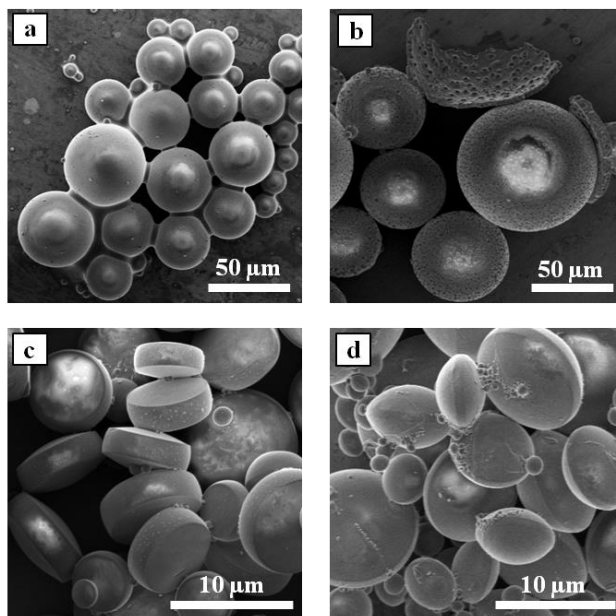


Figure 4.17 SEM images of the different **PMMA** microstructures obtained through the solvent evaporation method upon scanning different reaction parameters: (a) spherical, (b) porous core-shell, (c) coin-like and (d) oval morphologies.

In view of these results, we decided to reconsider the use of interfacial polymerisation for the preparation of **VT1**-loaded liquid-filled capsules. In particular, we focused our attention on the synthesis of polymeric shells via this strategy whose formation would not generate by-products leading to metal complex degradation. With this in mind, we were capable to successfully prepare polyurea (PU)³² capsules filled with toluene solutions of **VT1**. The interfacial polymerisation methodology applied and a tentative structure of the cross-linked polymeric shell formed are schematically represented in Figure 4.18. Briefly, an oil phase comprising a toluene solution of **VT1** ($5.6 \cdot 10^{-4}$ M) and the biuret triisocyanate Desmodur[®] N 100 was emulsified in an aqueous phase in which the emulsion stabiliser (PVA) and the water-soluble monomer (DETA) had been previously dissolved. Once monomers made contact at the interface between the oil droplets and the aqueous phase, and the temperature was increased up to 333 K, polymerisation started creating a polyurea shell around the droplets and trapping the toluene thermochromic solution inside.

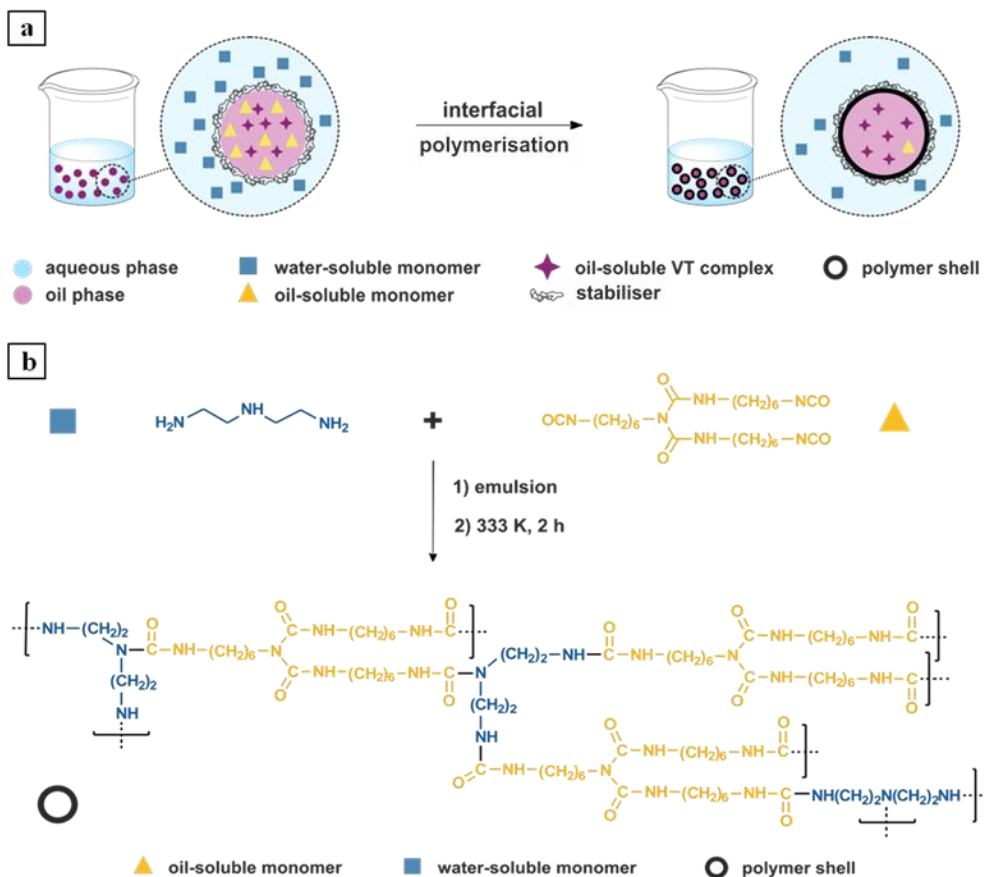


Figure 4.18 (a) Schematic representation of the interfacial polymerisation in oil-in-water emulsions procedure used for the synthesis of polyurea capsules. (b) Tentative structure of the polymerisation product formed by reaction of DETA and Desmodur[®] N 100.

When the reaction finished and the stirring was stopped, a creaming process took place and the capsules obtained (**VT1@PU_tol**) moved towards the liquid-air interface forming a dark brownish layer over the water surface (Figure 4.19(a)). This phenomenon, which was also observed for liquid-filled polyamide capsules in Chapter 3, is a first evidence of the presence of **VT1**-oil phase inside the capsules prepared, since they must possess a density lower than water ($\rho_{\text{toluene}} = 0.8669 \text{ g mL}^{-1}$). Subsequently, the mother liquor was removed (using centrifugation if needed), and the capsules were finally washed with abundant water and lyophilised.

SEM images of the resulting microcapsules are shown in Figure 4.19(b) and (c). Overall, they presented sphere-like morphologies with average diameters ranging from 17 to 63 μm

depending on reaction parameters. In general, higher stirring rates and lower reaction temperatures resulted in smaller capsules. A closer look to the SEM images revealed that **VT1@PU_tol** capsules exhibited indentations on their surface, which were ascribed either to the pressure imparted by neighbouring capsules or to partial loss of the inner solvent. On the other hand, images of crushed capsules (Figure 4.19(d)) allowed proving their hollow interior and the smoothness of both the inner and outer surfaces of their shell, whose thickness varied between 100 and 850 nm according to the capsule size.

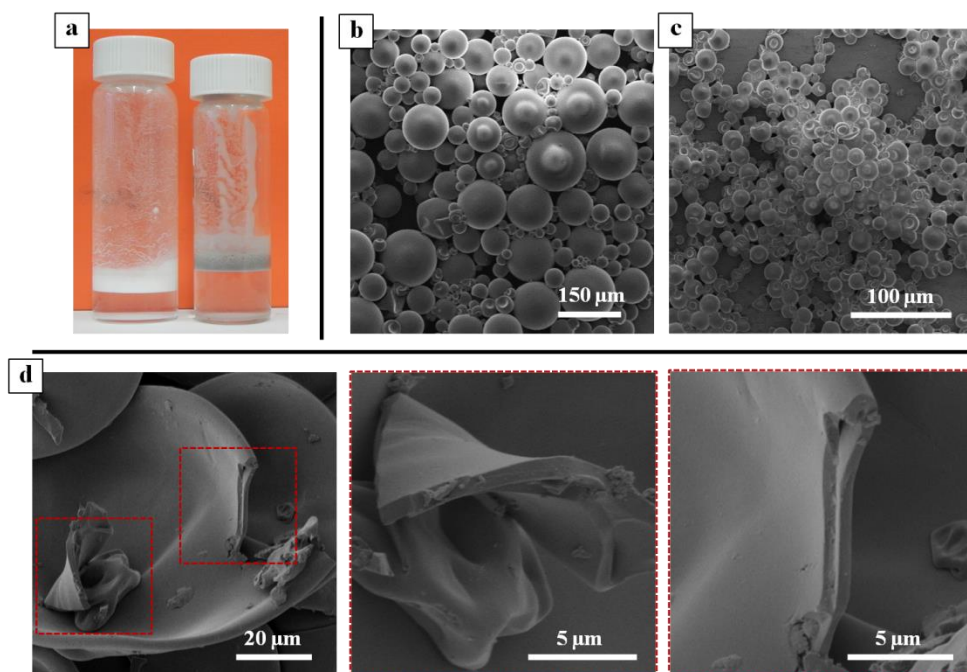


Figure 4.19 (a) Images of the creaming process observed when complex-free **PUtol** (left, white layer) and **VT1@PU_tol** capsules (right, brown layer) were dispersed in water. (b-c) SEM images of **VT1@PU_tol** capsules with (b) $63 \pm 26 \mu\text{m}$ average diameter and (c) $17 \pm 3 \mu\text{m}$ average diameter. (d) SEM images of **VT1@PU_tol** crushed capsules displaying broken shells and their hollow interior.

In addition to the creaming process, the presence of solvent into the capsule core was also confirmed by liquid ejection after mechanically crushing the capsules. The images on Figure 4.20 show how solvent droplets could be clearly seen around the smashed capsules when monitoring this process *in situ* by optical microscopy. From the liquid liberated by the broken capsules, we estimated their liquid content to account for 81 wt% of capsule total mass. Encapsulation efficiencies of approximately 88% and **VT1** payloads of 0.04% were also determined by means of UV-Vis absorption measurements of the ejected liquid.

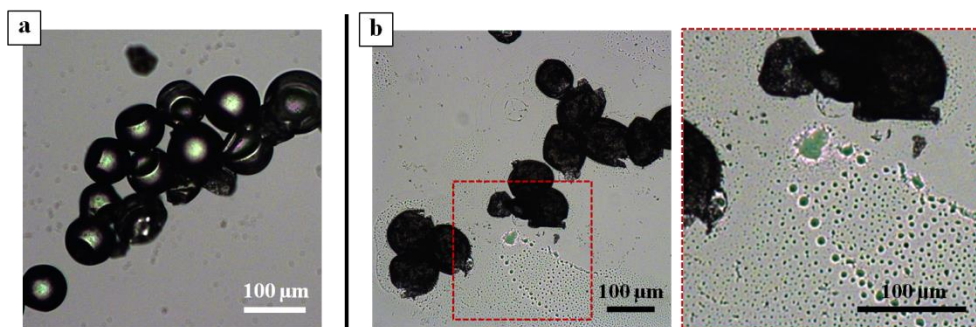


Figure 4.20 Optical images of PU_tol capsules before (a) and after (b) mechanical crushing. The broken PU shells lie flat onto the substrate surrounded by the ejected toluene droplets.

4.2.2.2 VT1@PU_tol valence tautomerism

The valence tautomerism of the VT1-loaded capsules obtained was studied in the solid state by diffuse reflectance spectroscopy using a UV-visible spectrophotometer equipped with an integrating sphere. Because of the limited spectral response of this equipment, spectra were only recorded between 400 and 800 nm. Reflectance data (R_∞) was acquired relative to a reference sample composed of analogous complex-free capsules ($R_\infty = 100\%$), and the values obtained were transformed to the corresponding Kubelka-Munk (K-M) function^{33–36} ($F(R_\infty)$) using equation 4.1:

$$F(R_\infty) = \frac{K}{S} = \frac{(1 - R_\infty)^2}{2R_\infty} \quad (4.1)$$

In this equation, K and S correspond to the K-M function absorption and scattering coefficients, respectively, and the reflectance values R_∞ are assumed to be measured for a thick enough solid sample as to ensure that no light penetrates through it. Although the K-M model simplifies the analysis of the interaction between excitation light and the surface layer of a material, it gives a good estimate of the absorption spectrum of an opaque solid sample.

The temperature dependence of the diffuse reflectance absorption spectra obtained for two different batches of VT1-loaded polyurea capsules with varying size are compared with the spectra of VT1 in toluene solution in Figure 4.21. The same figure also shows two pictures illustrating the colour change of VT1@PU_tol capsules (from brown to grey) upon heating.

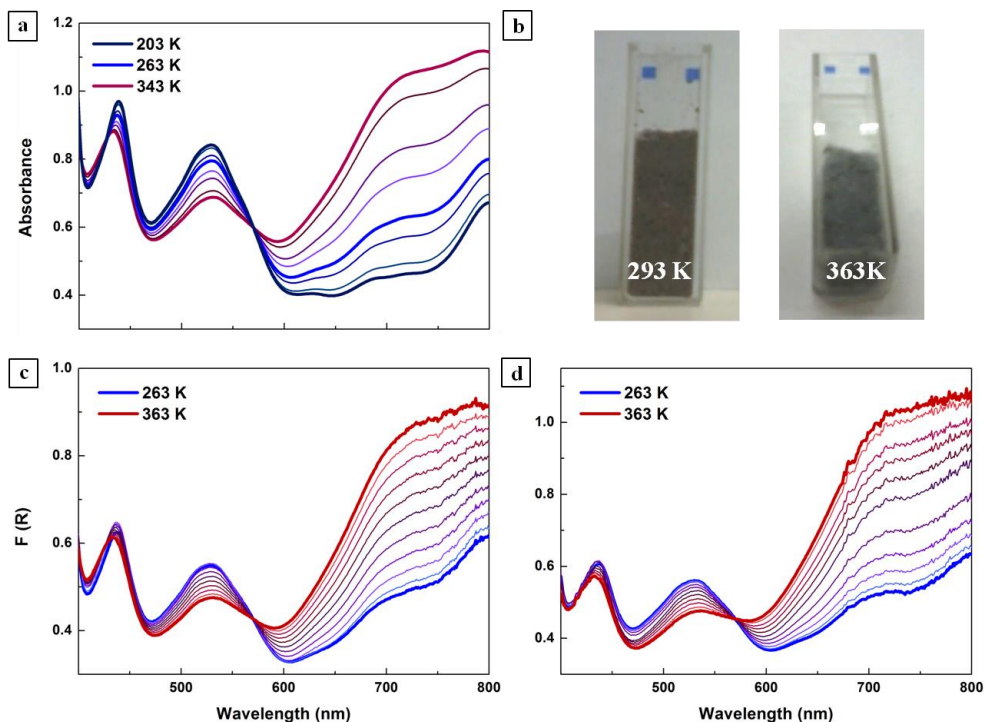


Figure 4.21 (a) Variable-temperature UV-Vis absorption spectra of a **VT1** toluene solution ($5.7 \cdot 10^{-4}$ M) measured at intervals of 20 K from 203 K to 343 K. (b) Photographs of **VT1@PU_tol** capsules at 293 K and 363 K displaying the colour change observed due to the VT interconversion of complex **VT1**. (c-d) Temperature dependence of the diffuse reflectance absorption spectra registered for two different-sized **VT1@PU_tol** capsule batches: (c) average diameter: 62 ± 26 μm and (b) average diameter: 17 ± 3 μm . Measurements were acquired from 263 to 363 K by increments of 10 K. Note that all the spectra corresponding to a given temperature are represented with the same colour.

Interestingly, both free and encapsulated toluene solutions of **VT1** molecules gave rise to the same spectral bands and variable-temperature dependence. Thus, while the absorption spectrum at 263 K of the **VT1@PU_tol** samples was dominated by the features arising from the *ls*-Co(III) isomer of the complex (i.e. absorption maxima at 436, 530, 720 and 800 nm), a decrease in the intensity of these bands and a concomitant increase of those corresponding to the *hs*-Co(II) isomer between 600 and 800 nm were observed when rising the temperature. Moreover, the two isosbestic points found in bulk toluene solutions within the 400-800 nm range were also fairly reproduced by the capsule samples, thereby confirming the occurrence of the spin transition process of the complex in their interior. On the basis of these results, two main conclusions could be drawn: (i) encapsulation within polyurea capsules does not only allow preserving valence tautomerism, but also to accurately

replicate the solution-like VT properties (i.e. colour and T_c); (ii) this behaviour is independent of the capsule size, since no significant differences were observed between the variable temperature F(R) functions registered for the two different families of capsules investigated. Actually, the slight variations found between them were most likely due to sample thermal equilibration differences.

To fully endorse the liquid-filled nature of the capsules as the responsible for its solution-like VT properties, we also analysed the optical behavior of **VT1@PU_tol** capsules after mechanical crushing and toluene evaporation. A SEM image of the resulting capsules and the corresponding variable-temperature F(R) functions are shown in Figure 4.22.

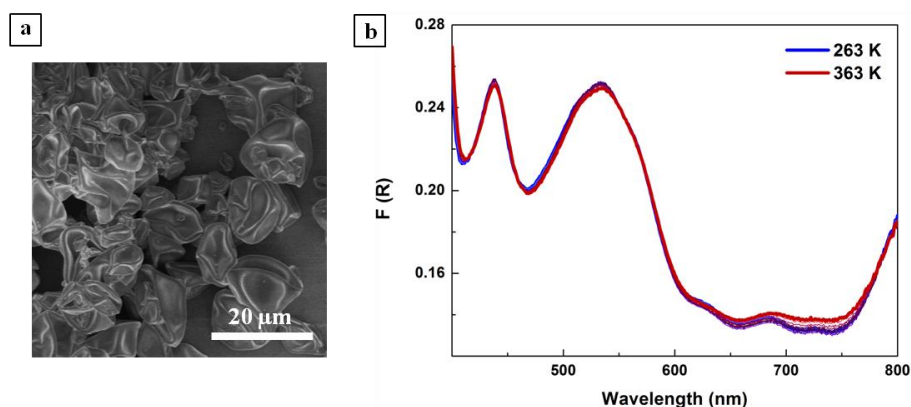


Figure 4.22 (a) SEM picture of **VT1@PU_tol** capsules after mechanical crushing and toluene evaporation. (b) Temperature dependence of the diffuse reflectance absorption spectra determined for **VT1@PU_tol** capsules after solvent removal. Measurements were acquired from 263 to 363 K by increments of 10 K.

After solvent removal, no significant temperature dependence of the diffuse reflectance absorption spectra was observed and the *ls*-Co(III) isomer of **VT1** was observed to dominate over the whole temperature range studied. Only small thermal variations were detected and they were tentatively attributed to the small fraction of non-crushed capsules that still retained their liquid core. Partial crystallization of **VT1** upon solvent evaporation should account for this result, though diffusion of the complex into the polyurea matrix could also account for the lack of VT activity.

To further corroborate the liquid dependence of the capsule properties, **VT1**-loaded solid polyurea particles (**VT1@PU**) were also synthesised employing a similar methodology to that adopted for the fabrication of the polyurea liquid-filled capsules. A schematic

illustration of the method followed is depicted in Figure 4.23(a). In this case, the toluene content was reduced to its minimum extent, using just the amount required for mixing the triisocyanate monomer and the thermochromic compound. As the polymerisation proceeded, the oil phase (consisting mainly in Desmodur[®] N 100) was consumed and, as a result, the VT1 molecules got entrapped into the polymeric matrix, similarly to what occurred in the synthesis of solid PMMA particles (VT1@PMMA described in section 4.2.1.2).

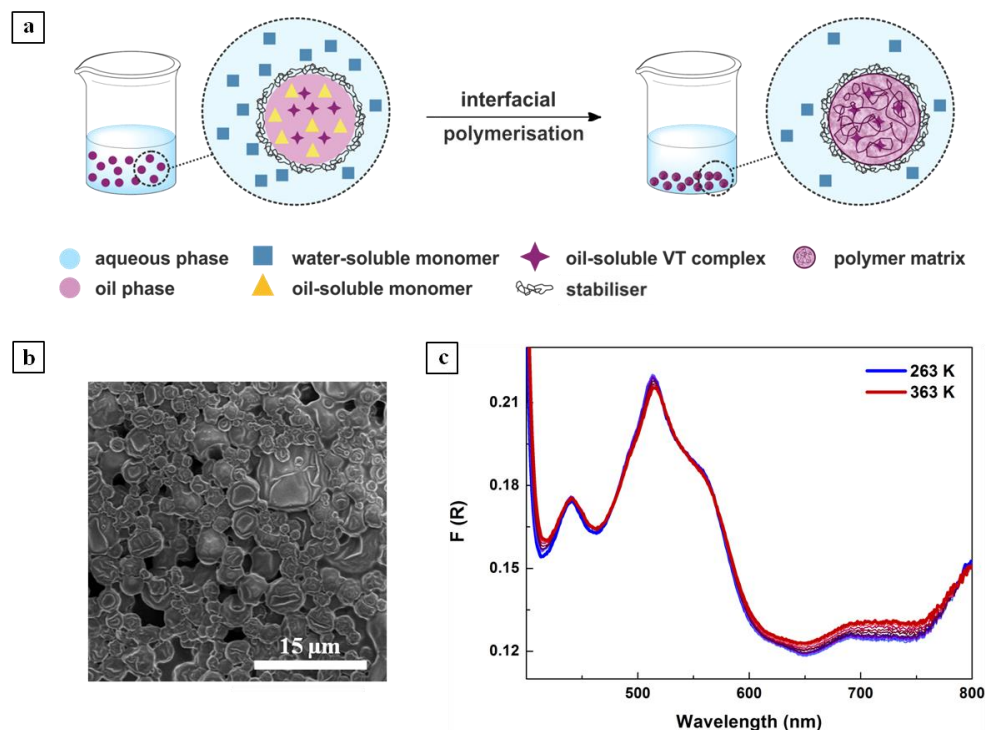


Figure 4.23 (a) Schematic representation of the interfacial polymerisation procedure applied for the synthesis of VT1-loaded solid polyurea capsules. (b) SEM image of VT1@PU solid particles. (c) Temperature dependence of the diffuse reflectance absorption spectra determined for VT1@PU solid particles. Measurements were acquired from 263 to 363 K by increments of 10 K.

Figure 4.23(b) and (c) show a SEM image of the resulting particles and the temperature dependence of their diffuse reflectance absorption. Even though they lacked the characteristic well-defined spherical shape of liquid-filled capsules and presented many indentations and wrinkles at their surface, these particles served as good models to study the behaviour of complex VT1 when directly embedded within a polyurea matrix. Interestingly, no significant thermal dependence was observed in the spectra acquired for this sample, which mainly corresponded to that of the *Is*-Co(III) isomer for all the temperatures

investigated. This shows that direct dispersion of **VT1** into a PU matrix also negatively affects the valence tautomerism of this complex.

Overall, these results demonstrated that the encapsulation of **VT1** inside liquid-filled capsules is an ideal approach to transfer the VT behaviour observed in solution to the solid state. Unfortunately, the **VT1@PU_tol** capsules prepared were found to be poorly stable. Thus, most of them deflated and lost their liquid interior five months and half after their synthesis. In addition, a large fraction of the capsules collapsed after performing absorption measurements at high temperatures, which prevented us to attempt successive heating-cooling cycles to prove the reversibility of their VT properties.

4.2.2.3 Valence tautomerism of miglyol-filled capsules

On a later stage of this work, capsules filled with miglyol solutions of **VT1** were also synthesised and studied. The reason for this was two-fold: (i) to increase capsule thermal stability, in a similar fashion to what had been done for photochromic capsules in Chapter 3; (ii) to modulate their VT properties with respect to those of **VT1@PU_tol**, since solvent replacement might induce a significant change on the T_c of the loaded complex molecules. To investigate this effect, we first registered the temperature dependence of the absorption spectrum of miglyol solutions of **VT1**. As can be seen in Figure 4.24(a), the spectrum is dominated at high temperatures by an intense and broad band at 797 nm characteristic of the *hs*-Co(II) isomer. As the temperature was decreased, the intensity of such band diminished, whereas that of the bands corresponding to the *ls*-Co(III) isomer at 533, 439 and 391 nm started to increase. However, such changes were observed to be less pronounced than in toluene solution and, in fact, the miglyol absorption spectrum at 263 K was found to be equivalent to the one acquired at 323 K in toluene. Therefore, although **VT1** tautomerisation also takes place in miglyol solution, its T_c value is shifted approximately 60 K towards lower temperatures than in toluene and, consequently, the electronic absorption spectrum of **VT1** in those two solvents exhibit remarkable differences at the same temperature (Figure 4.24(b)). As a consequence, this suggests that the T_c of the thermochemic liquid-filled capsules introduced in this work could be tuned in a simple and a rational manner by just varying the nature of the confined solvent.

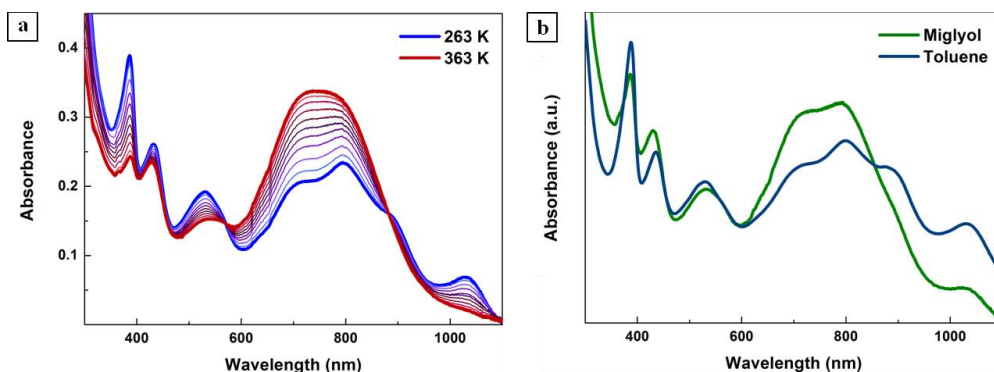


Figure 4.24 (a) Temperature dependence of the absorption spectrum of VT1 in miglyol solution from 203 to 343 K. Measurements were done by increments of 10 K. (b) Comparison of VT1 toluene and miglyol absorption spectra at 303 K.

Aiming to demonstrate this additional advantage of our strategy to prepare solid materials with solution-like VT behaviour, polyurea capsules comprising miglyol solutions of complex VT1 (VT1@PU_mig) were prepared by interfacial polymerisation in oil-in-water emulsions. A similar procedure to that applied for the synthesis of toluene-filled capsules was followed, although in this case a different triisocyanate monomer (Desmodur® N 3300, Figure 4.25) and emulsifier (sodium dodecyl sulphate, SDS) were used in order to enhance capsule morphology and reduce polydispersion.

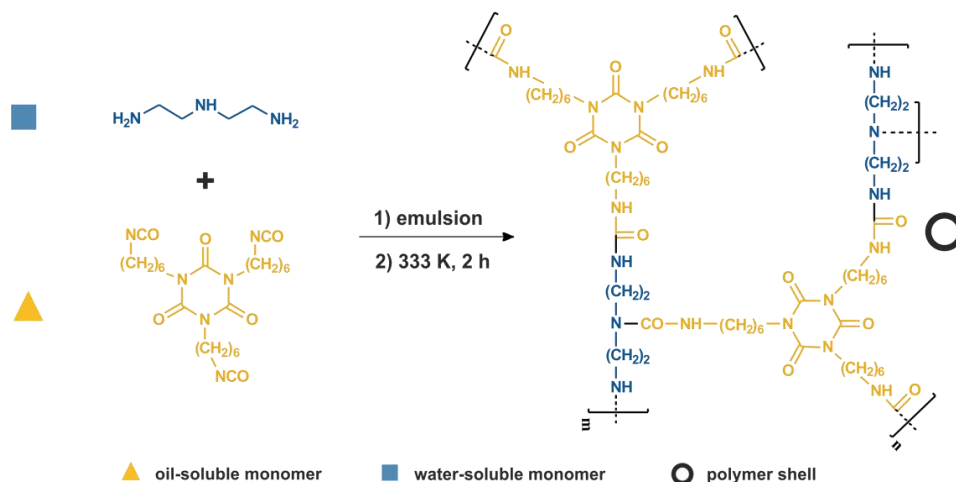


Figure 4.25 Polymerisation reaction between DETA and Desmodur® N 3300 conducting to the formation of VT1@PU_mig capsules.

A miglyol phase was then prepared containing the VT compound of interest ($4.6 \cdot 10^{-5}$ M) and Desmodur® N 3300, which was subsequently emulsified in an aqueous phase where DETA and SDS had been previously dissolved. Once both monomers made contact at the interface between the oil and aqueous phases, and the temperature was increased up to 333 K, polymerisation started forming a cross-linked polyurea shell around the **VT1**-containing miglyol droplets. Figure 4.25 shows a tentative structure for the polymerisation product obtained in this case. Once the reaction finished and stirring was stopped, a creaming process was again observed, which evidenced the presence of an oil phase inside the capsule interior ($\rho_{\text{miglyol}} = 0.9438 \text{ g mL}^{-1}$, Figure 4.25(a)). Then, the mother liquor was removed upon centrifugation and the capsules were washed and lyophilised. Because of the low solubility of **VT1** in miglyol, smaller amounts of the VT complex could be encapsulated in this case and, therefore, the colour of the isolated capsules was more faded than for **VT1@PU_tol**. In particular, they looked slightly greyish instead of strongly brown/grey coloured.

SEM images of the resulting microcapsules are shown in Figure 4.26(d-f). Average diameters ranging between 66 and 3 μm were obtained by increasing the emulsification rate from 1600 to 20000 rpm. All the capsules were spherically shaped, although the largest ones were less defined, presented higher polydispersity and possessed many indentations and wrinkles. Noticeably, they retained their structure and mass at least one year after their synthesis, which proved the enhancement of capsule stability by replacing toluene with a high boiling point solvent as miglyol.

SEM images of crushed capsules demonstrated their core-shell structure (Figure 4.26(g)). Capsule shell presented smooth outer surfaces in contrast with the high roughness of their inner part. Although the latter prevented proper measurement of the shell thickness, it was estimated to be around 340 nm independently of the capsule size. Once again, capsule liquid core was demonstrated by liquid ejection after capsule crushing, as shown in the optical images of Figure 4.26(b-c) where solvent droplets were observed to surround the smashed capsules. From the liquid liberated from the broken capsules, we estimated that the liquid content represented approximately about 90 wt% of capsule total mass; however, due to the low concentration of the initial **VT1** solution in miglyol (10-fold lower than for toluene-filled capsules), we could only get a rough estimate of the encapsulation efficiencies (ca. 90%) and **VT1** payloads (ca. 0.004%).

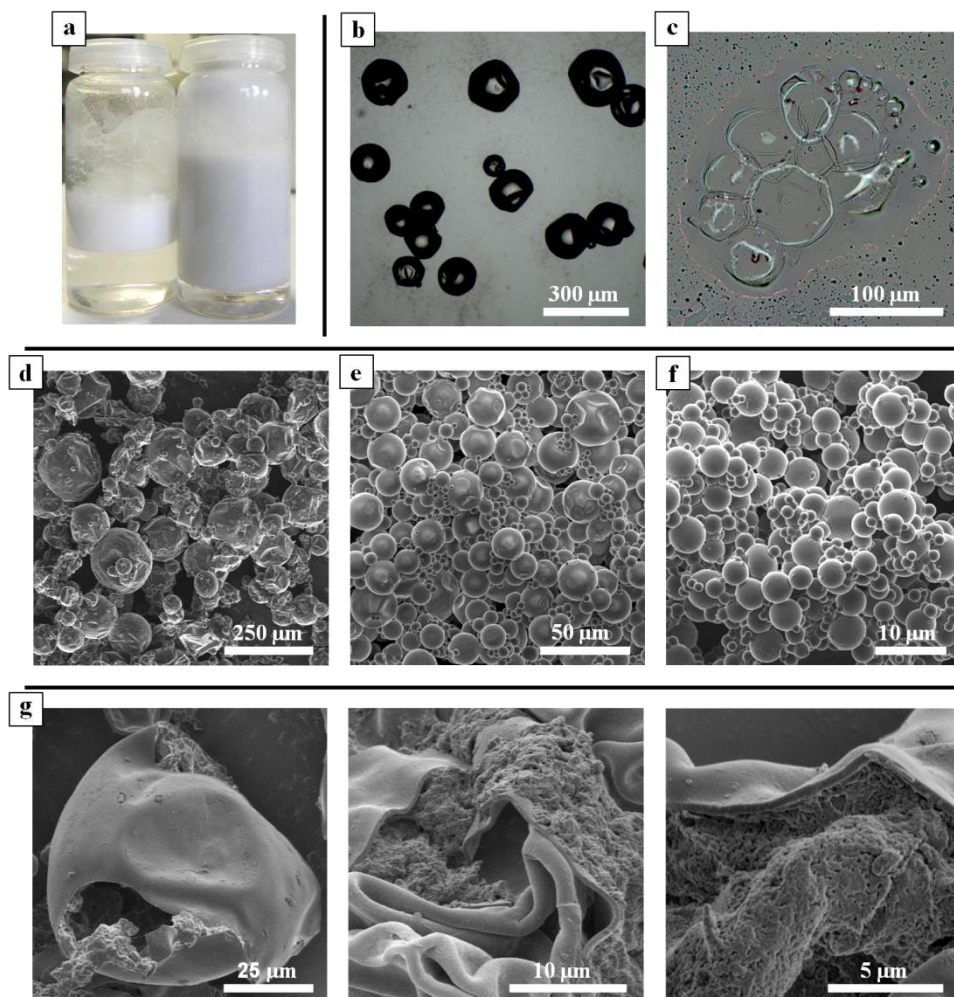


Figure 4.26 (a) Images of the creaming process observed when complex-free **PU_mig** (left, white layer) and **VT1@PU_mig** capsules (right, greyish layer) were dispersed in water. (b-c) Optical microscopy images of **PU_mig** capsules before (b) and after (c) mechanical crushing. (d-f) SEM images of **VT1@PU_mig** capsules with (d) $66 \pm 50 \mu\text{m}$ average diameter, (e) $12 \pm 7 \mu\text{m}$ average diameter and (f) $3 \pm 1 \mu\text{m}$ average diameter. (g) SEM images of **VT1@PU_mig** crushed capsules displaying broken shells and the core-shell structure.

The thermochromic behaviour of **VT1@PU_mig** was studied for the three capsule sizes prepared. As can be seen in Figure 4.27, the temperature dependence of the diffuse reflectance absorption spectra obtained fairly reproduced the VT behaviour of **VT1** in miglyol solution. Small spectral variations were however observed, which became more noticeable as capsule size was reduced. Thus, the band centered around 500 nm was found to be narrower and blue-shifted with respect to free **VT1** solutions, and the shoulder at 720 nm observed at low temperatures became more evident. Deviations of the assumptions made

for deriving the $F(R)$ function could stay at the origin of such divergences (e.g. the measured surface might not have been as planar as considered by the K-M model), together with the low complex concentration within the capsules resulting in tiny and noisy absorption signals. In any case, we could clearly distinguish the characteristic spectral changes caused by the occurrence of **VT1** valence tautomerism upon heating: the intensity of the two first bands of the spectra decreased, while a more intense and broader band appeared between 600 and 800 nm, as also observed for bulk miglyol solutions.

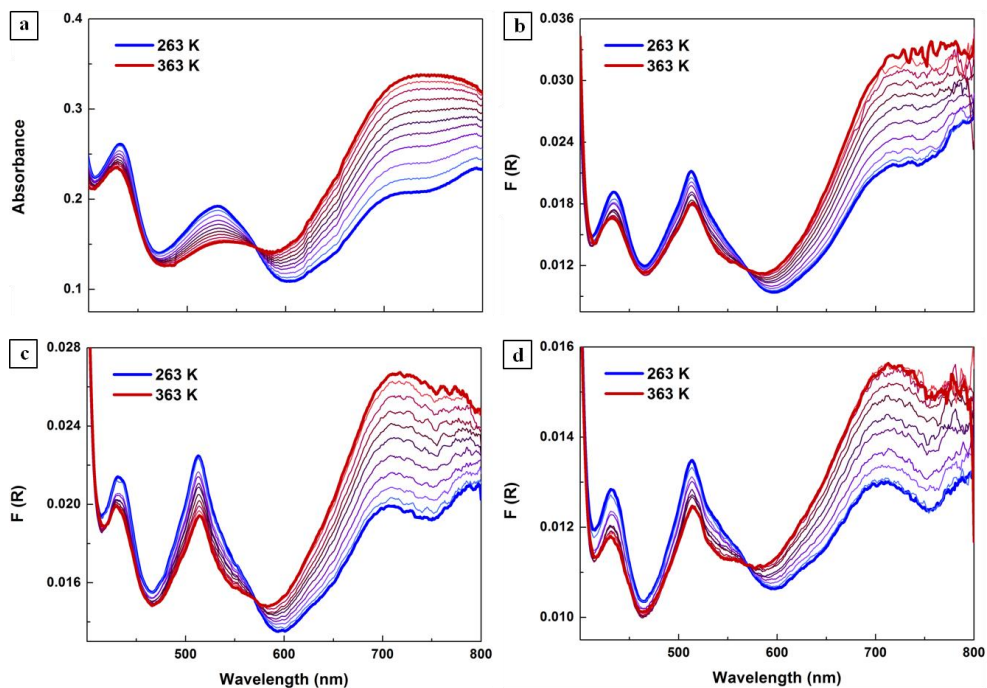


Figure 4.27 (a) Temperature dependence of the absorption spectrum of **VT1** in miglyol solution. (b-d) Temperature dependence of the diffuse reflectance absorption spectra obtained for three differently sized **VT1@PU_mig** capsule batches: (b) $66 \pm 50 \mu\text{m}$ average diameter, (c) $12 \pm 7 \mu\text{m}$ average diameter and (d) $3 \pm 1 \mu\text{m}$ average diameter. Measurements were acquired from 263 to 363 K by increments of 10 K.

The improvement of capsule thermal resistance thanks to miglyol encapsulation allowed measuring the optical response of **VT1@PU_mig** for successive cooling-heating cycles and, as such, the reversibility of the VT behaviour of the complex inside the capsules. The graph in Figure 4.28 shows how the value of the $F(R)$ function at 700 nm varied between the highest and lowest temperatures scanned through five of such cycles. Clearly, reproducible diffuse reflectance signals were obtained in time, thereby confirming the reversibility of the

VT properties of **VT1@PU_mig** capsules, the robustness of their thermal response and the overall good performance of the novel microstructured solid materials reported herein.

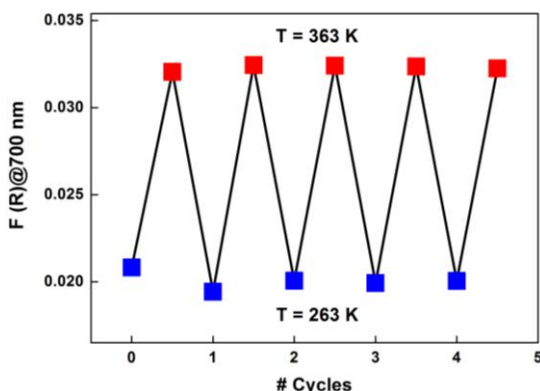


Figure 4.28 Variation of the F(R) function values at 700 nm for successive cooling-heating cycles performed on **VT1@PU_mig** capsules between 263 and 363 K.

4.3 Conclusions

The objective of the work developed along this chapter was the encapsulation of complex **VT1** inside polymeric particles in order to develop a universal methodology capable to produce robust structures presenting solution-like valence tautomerism in the solid state. For this purpose, two different approaches were explored, which relied on the encapsulation of the VT complex of choice into solid or liquid-filled polymeric particles. The main conclusions drawn from the studies conducted for each one of these methodologies are shown below:

Encapsulation into solid particles:

(i) We demonstrated the influence of the nature of the polymer (PMMA, PC and PVAc) and of the concentration of dispersed **VT1** complex molecules in the VT behaviour of different thin films. In particular, we found out that direct introduction of **VT1** into PC and PVAc matrices as well as aggregation and crystallisation within these and other polymeric networks inhibit the VT interconversion of the metal complex. In addition, we determined that 2 wt%-PMMA was the only formulation capable to retain the valence tautomeric **VT1** properties observed in solution. However, heating the resulting samples above the glass

transition temperature of PMMA induced VT1 crystallization, thus establishing a highest thermal threshold of application of the resulting material.

(ii) We successfully encapsulated VT1 complex molecules within the matrix of solid PMMA particles and at the concentration of interest (~2 wt%) by solvent evaporation. The particles obtained exhibited thermochromic valence tautomerism, although with a significant difference in T_c with respect to standard organic solutions. This demonstrated that the encapsulation of VT molecules into adequate polymeric capsules at appropriate concentrations is a feasible methodology to achieve VT behaviour in the solid state. However, this methodology turned out to be restricted to a specific range of concentrations, polymers and temperatures, thus limiting its use for the fabrication of future VT-based devices.

Encapsulation into liquid-filled capsules:

(iii) We managed to synthesise polyurea capsules filled with VT1 toluene and miglyol solutions by interfacial polymerisation. These capsules were not only demonstrated to be capable of nicely reproducing the valence tautomerism observed in solution, but also to fully retain the reversibility of the VT interconversion upon successive cooling-heating cycles. In addition, the T_c of the capsules developed could be fine tuned just by simply modifying the solvent confined into their core, thus evidencing the versatility of this approach. In combination with the lack of synthetic modification of the complex of choice and the simplicity of the encapsulation methods required, this makes the liquid-filled capsule strategy introduced in this work an ideal methodology for direct transferring valence tautomeric behaviour from solution to the solid state.

4.4 References

1. Evangelio, E. & Ruiz-Molina, D. Valence tautomerism: new challenges for electroactive ligands. *Eur. J. Inorg. Chem.* 2957–2971 (2005).
2. Tezgerevska, T., Alley, K. G. & Boskovic, C. Valence tautomerism in metal complexes: Stimulated and reversible intramolecular electron transfer between metal centers and organic ligands. *Coord. Chem. Rev.* **268**, 23–40 (2014).

3. Sato, O., Tao, J. & Zhang, Y.-Z. Control of magnetic properties through external stimuli. *Angew. Chem. Int. Ed.* **46**, 2152–2187 (2007).
4. Boskovic, C. & Ed: Halcrow, M. A. *Valence tautomeric transitions in cobalt-dioxolene complexes (in Spin-crossover materials: properties and applications)*. (John Wiley & Sons Ltd, 2013).
5. Adams, D. M. & Hendrickson, D. N. Pulsed laser photolysis and thermodynamics studies of intramolecular electron transfer in valence tautomeric cobalt o-quinone complexes. *J. Am. Chem. Soc.* **118**, 11515–11528 (1996).
6. Roux, C. *et al.* Pressure-induced valence tautomerism in cobalt o-quinone complexes: An X-ray absorption study of the low-spin [CoIII(3,5-DTBSQ)(3,5-DTBCat)(phen)] to high-spin [CoII (3,5-DTBSQ)2(phen)] Interconversion. *Inorg. Chem.* **35**, 2846–2852 (1996).
7. Pierpont, C. G. Studies on charge distribution and valence tautomerism in transition metal complexes of catecholate and semiquinonate ligands. *Coord. Chem. Rev.* **216-217**, 99–125 (2001).
8. Dei, A., Gatteschi, D., Sangregorio, C. & Sorace, L. Quinonoid metal complexes: toward molecular switches. *Acc. Chem. Res.* **37**, 827–835 (2004).
9. Buchanan, R. M. & Pierpont, C. G. Tautomeric catecholate-semiquinone interconversion via metal-ligand electron transfer. Structural, spectral, and magnetic properties of (3,5-Di-tert-butylcatecholato)-3,5-di-tert-butylsemiquinone(bipyridyl)cobalt(III), a complex containing mixed-valence. *J. Am. Chem. Soc.* **102**, 4951–4957 (1980).
10. Evangelio, E. & Ruiz-Molina, D. Valence tautomerism: More actors than just electroactive ligands and metal ions. *C. R. Chim.* **11**, 1137–1154 (2008).
11. Beni, A., Dei, A., Laschi, S., Rizzitano, M. & Sorace, L. Tuning the charge distribution and photoswitchable properties of cobalt-dioxolene complexes by using molecular techniques. *Chem. Eur. J.* **14**, 1804–1813 (2008).
12. Dei, A. & Sorace, L. Cobalt-dioxolene redox isomers: Potential spintronic devices. *Appl. Magn. Reson.* **38**, 139–153 (2010).
13. Caneschi, A. *et al.* Pressure- and temperature-induced valence tautomeric interconversion in a o-dioxolene adduct of a cobalt-tetraazamacrocyclic complex. *Chem. Eur. J.* **7**, 3926–3930 (2001).
14. Evangelio, E. *et al.* Solvent effects on valence tautomerism: A comparison between the interconversion in solution and solid state. *Solid State Sci.* **11**, 793–800 (2009).

15. Adam, D. M., Dei, A., Rheingold, A. L. & Hendrickson, D. N. Bistability in the $[\text{Co}^{\text{II}}(\text{semiquininate})_2]$ to $[\text{Co}^{\text{III}}(\text{catecholate})(\text{semiquinonate})]$ valence-tautomeric conversion. *J. Am. Chem. Soc.* **115**, 8221–8229 (1993).
16. Bin-Salamon, S. *et al.* Supramolecular control of valence-tautomeric equilibrium on nanometer-scale gold clusters. *J. Am. Chem. Soc.* **127**, 5328–5329 (2005).
17. Imaz, I. *et al.* Valence-tautomeric metal-organic nanoparticles. *Angew. Chem. Int. Ed.* **47**, 1857–1860 (2008).
18. Amorín-Ferré, L. *et al.* Encapsulation and release mechanisms in coordination polymer nanoparticles. *Chem. Eur. J.* **19**, 17508–17516 (2013).
19. Larsen, S. K. & Pierpont, C. G. Cobalt and manganese complexes of a schiff-base biquinone radical ligand. *J. Am. Chem. Soc.* **110**, 1827–1832 (1988).
20. Caneschi, A., Cornia, A. & Dei, A. Valence tautomerism in a cobalt complex of a schiff base diquinone ligand. *Inorg. Chem.* **37**, 3419–3421 (1998).
21. Evangelio, E. *et al.* Coexistence of two thermally induced intramolecular electron transfer processes in a series of metal complexes $[\text{M}(\text{Cat-N-BQ})(\text{Cat-N-SQ})]/[\text{M}(\text{Cat-N-BQ})_2]$ ($\text{M} = \text{Co}, \text{Fe}, \text{and Ni}$) bearing non-innocent catechol-based ligands: a combined experimental and theoretical. *Chem. Eur. J.* **16**, 6666–6677 (2010).
22. Cadour, O. *et al.* Temperature-induced solid-state valence tautomeric interconversion in two cobalt-schiff base diquinone complexes. *Inorg. Chem.* **42**, 6432–6440 (2003).
23. Evangelio, E. *et al.* Solvent effects on valence tautomerism: A comparison between the interconversion in solution and solid state. *Solid State Sci.* **11**, 793–800 (2009).
24. Cadour, O. *et al.* Temperature-induced solid-state valence tautomeric interconversion in two cobalt-schiff base diquinone complexes. *Inorg. Chem.* **42**, 6432–6440 (2003).
25. Wang, X., Xu, S. & Xu, W. Luminescent properties of dye-PMMA composite nanospheres. *Phys. Chem. Chem. Phys.* **13**, 1560–1567 (2011).
26. Ge, X., Wang, M., Ji, X., Ge, X. & Liu, H. Effects of concentration of nonionic surfactant and molecular weight of polymers on the morphology of anisotropic polystyrene/poly(methyl methacrylate) composite particles prepared by solvent evaporation method. *Colloid Polym. Sci.* **287**, 819–827 (2009).
27. Ziegler, A., Landfester, K. & Musyanovych, A. Synthesis of phosphonate-functionalized polystyrene and poly(methyl methacrylate) particles and their kinetic behavior in miniemulsion polymerization. *Colloid Polym. Sci.* **287**, 1261–1271 (2009).

28. Egerton, R. F., Li, P. & Malac, M. Radiation damage in the TEM and SEM. *Micron* **35**, 399–409 (2004).
29. Feczko, T., Varga, O., Kovács, M., Vidóczy, T. & Voncina, B. Preparation and characterization of photochromic poly(methyl methacrylate) and ethyl cellulose nanocapsules containing a spirooxazine dye. *J. Photochem. Photobiol. A* **222**, 293–298 (2011).
30. Zhao, Y., Fickert, J., Landfester, K. & Crespy, D. Encapsulation of self-healing agents in polymer nanocapsules. *Small* **8**, 2954–2958 (2012).
31. Nordstierna, L., Abdalla, A. A., Nordin, M. & Nydén, M. Comparison of release behaviour from microcapsules and microspheres. *Prog. Org. Coatings* **69**, 49–51 (2010).
32. Chao, H. Microencapsulated adhesive. US6375872 B1 (2002).
33. Džimbeg-Malčić, V., Barbarić-mikočević, Ž. & Itrić, . u bleka-Munk theory in describing optical properties of paper (I). *Tech. Gaz.* **18**, 117–124 (2011).
34. Torrent, J., Barrón, V., Ed: Ulery, A. L. & Drees, L. R. *Diffuse reflectance spectroscopy. (in Methods of soil nalysis: Mineralogical methods)*. (Soil Science Society of America, 2008).
35. Dahm, D. J. & Dahm, K. D. *Interpreting Diffuse Reflectance and Transmittance: A Theoretical Introduction to Absorption Spectroscopy of Scattering Materials*. (IM Publications, 2007).
36. Lang, K. *et al.* Layered double hydroxides with intercalated porphyrins as photofunctional materials: Subtle structural changes modify singlet oxygen production. *Chem. Mater.* **19**, 3822–3829 (2007).

Chapter 5

Colour-Tunable White-Light Emitting Capsules

5.1 Introduction

Artificial white lighting has been the subject of intensive research in the past decades¹⁻⁶. Since the 20% of the total global energy consumption accounts for lighting and its worldwide demand is increasing, light sources providing energy savings and environmental benefits are needed for many applications^{1,2}. The most active fields of research in this area are visual display technology and solid state lighting, where organic white-light emitting materials are receiving considerable attention due to their potential advantages over their inorganic counterparts^{3,4}: lower toxicity, density and cost, flexibility, larger transparency, easier fine-tuning, and simpler processability based on thin film deposition techniques and printing technologies. These relevant properties are attracting the interest of not only scientific but also industrial communities. Thus, since organic light emitting technologies such as OLEDs started to be commercialised several years ago^{2,3,5}, the industrial demand on the development of organic white-light emitting systems has considerably increased⁶ as the present performances and costs of these materials are still far from the market requirements.

However, research on emissive materials for lightning has not only being focused on white light production, and systems exhibiting tunability in their emission spectra have also generated considerable interest. On the lighting market colour variations can be used to define brands or modify environments or moods^{1,7}. For example, warm countries prefer “cooler” (bluish) light, while colder countries are more prone to the use of “warmer” (yellowish) light. In addition, multicolour fluorescent systems have also been studied for applications in biological imaging, labelling or sensors⁸⁻¹¹. Therefore, the development of materials displaying both white-light emission and colour tunability is interesting for a broad range of applications.

5.1.1 How to define light colour: CIE 1931 chromaticity diagram

Human colour vision is biologically designed to distinguish any set of colours when illuminated with visible light. In practice, two different properties are normally used to define the colour of light as perceived by the standard observer: luminance, which describes the brightness of a colour, and chromaticity, which refers to colour quality in terms of dominant wavelength (hue) and purity (saturation). To characterize colour perception,

different parameters have been developed such as the correlated colour temperature (CCT) and the CIE chromaticity coordinates^{1,3}. Among them, the CIE 1931 chromaticity diagram is the most commonly used tool to specify how the human eye sees the light of a given spectrum, and it shows all the possible chromaticities visible to an average person (i.e. the gamut of human vision). As such, it will be the system of choice to determine the quality of the white light (or the light of any other colour) generated by the materials developed in this work.

The CIE 1931 colour space (CIE XYZ colour space)¹²⁻¹⁴ is a mathematical model established by the "International Commission on Illumination" (Commission internationale de l'éclairage, CIE)¹⁵, which translates physically produced colours into human visual response with the aim of objectively describing colour sensation.

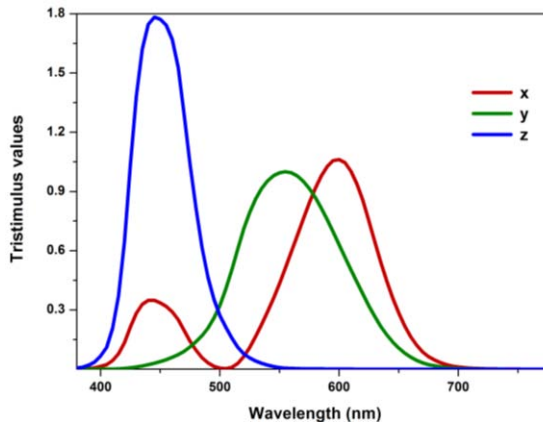


Figure 5.1 Representation of the colour matching functions \bar{x} , \bar{y} and \bar{z} . Three colour matching functions, \bar{x} , \bar{y} and \bar{z} , define this space (Figure 5.1). They are the numerical description of an average human's chromatic response and correspond to the amount of XYZ primary colours (related to R, G and B primaries) needed to represent the colour of monochromatic light. From these matching functions and the spectrum of any given light ($F(\lambda)$), the tristimulus values X, Y and Z can be determined using equations 5.1 which uniquely and precisely specify the perceived colour. In these equations, k is a normalizing constant.

$$X = k \int_{\lambda} F(\lambda) \bar{x}(\lambda) d\lambda ; Y = k \int_{\lambda} F(\lambda) \bar{y}(\lambda) d\lambda ; Z = k \int_{\lambda} F(\lambda) \bar{z}(\lambda) d\lambda \quad (5.1)$$

Therefore, the tristimulus values can be considered as the amount of the XYZ primary colours that constitute a certain light of spectral distribution $F(\lambda)$.

The CIE XYZ colour space was deliberately defined so that Y is a measure of the luminance of light, while the XZ plane shows all the possible chromaticities for a certain Y value. Based on that, the chromaticity of any colour can be described using the two chromaticity coordinates x and y, which are obtained as follows:

$$x = \frac{X}{X+Y+Z}; y = \frac{Y}{X+Y+Z} \quad ()$$

Plotting x against y for any colour visible for an average person, the CIE 1931 chromaticity diagram is obtained, whose curved edge (the so-called spectral locus) represents all visible monochromatic lights (Figure 5.2). Therefore, this diagram can be used to represent the chromaticity perceived for a given light source and, as a result, evaluate the quality of white-light emission.

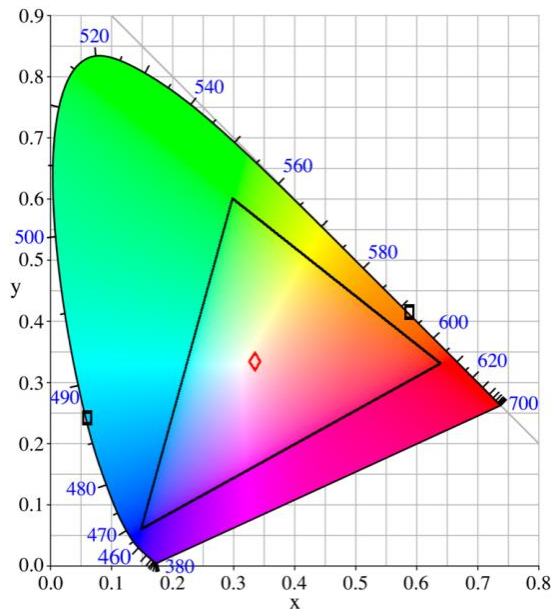


Figure 5.2 CIE 1931 chromaticity diagram. The symbols in the diagram correspond to the chromaticity coordinates of pure white light ($x = 0.333, y = 0.333$) and of two monochromatic lights (487 nm: $x = 0.059, y = 0.235$; 592 nm: $x = 0.587, y = 0.413$)¹⁶ with which white light can be obtained. The triangle inside the diagram denotes the standard RGB (sRGB) colour space generally used nowadays in monitors and printers, which is generated by combination of red ($x = 0.640, y = 0.330$), green ($x = 0.300, y = 0.600$) and blue ($x = 0.150, y = 0.060$) colours. Note that the printed colours of the image are defined on the basis of this RGB system. As a consequence, any colour outside of the sRGB gamut may not be properly represented.

In particular, pure white colour corresponds to the coordinates $x = 0.333$ and $y = 0.333$, although there is a region of the diagram around this point that could be considered as white

light¹⁷. In addition, the CIE 1931 chromaticity diagram allows predicting the chromaticity of light resulting from the mixture of two or three different colours. Thus, all the chromaticity coordinates that can be produced by combining three distinct colours are found inside the triangle that they form into the chromaticity diagram. Similarly, the chromaticity coordinates that can be generated by mixing two different colours lie on the straight line defined by the coordinates of these two colours. For instance, this means that by properly combining monochromatic light of 487 and 592 nm, pure white colour can be obtained.

5.1.2 White-light emitting materials

As anticipated in the previous section and shown in Figure 5.2, white light can be obtained following the additive colour mixing principle by concurrent emission of the three primary (red, green and blue) or two complementary colours (e.g. cyan and red) from distinct compounds. However, simultaneous light production from different emitting centres requires good control over the energy transfer processes that could take place among them^{3,4,6}, since they modify the luminescence intensity ratio that would arise from the independent activity of these sites. For instance, a complete transfer from the highest energy emitters (blue) to the lowest ones (orange/red) will result in selective emission from the latter and no mixed colour luminescence will be observed. Hence, to design white-light emitting materials is not only important to accurately select the emitting components and their relative amounts, but also to properly engineer their interactions.

Many different types of organic white-light emitting materials have been designed based on this concept^{3,6}. They can be classified by two main strategies: (i) the combination of two or more emitters of different colours on a single material with broad emission, and (ii) their confinement into well-separated, independently emitting stacked layers.

The latter approach is normally used in electroluminescent systems, mostly in WOLEDs^{2,3} (white organic light-emitting diodes). These devices present a multilayer structure generally created through vacuum deposition. Each of the emissive layers in the device is composed of a non-emitting host material doped with a fluorescent or phosphorescent emitter, so that it produces a defined colour different from the others (Figure 5.3). In addition, these layers are physically separated from one another to prevent layer mixing, exciton migration or any

energy transfer process, thus ensuring their independent behaviour. White light is then produced when all of them emit simultaneously with the appropriate intensity ratio in the multilayer architecture. Therefore, control over layer thickness and dopant concentration is required to achieve pure white-light emission, and in many cases the final mixed colour obtained is also observed to be voltage dependent. The main drawback of this strategy is the complex manufacturing of the multilayer structure,² which can be partially solved by the use of more easily processable polymeric hosts^{3,4}.

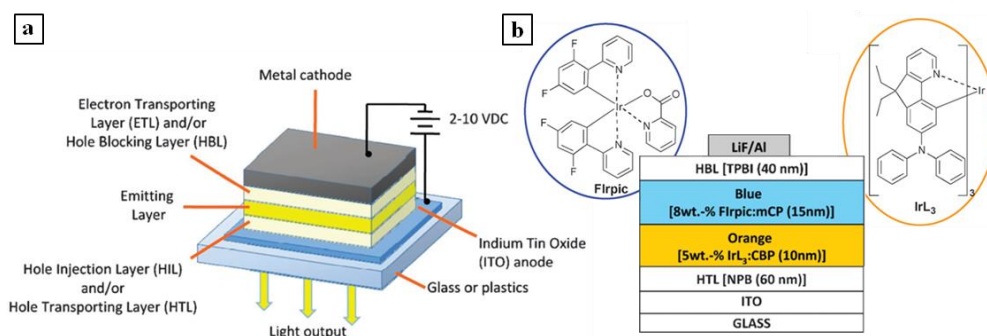


Figure 5.3 (a) OLED schematic drawing and (b) an example of the architecture of a WOLED with two different emissive layers; adapted from references 3 and 18. **TPBI**: hole blocking layer, 2,2',2''-(benzene-1,3,5-triyl)-tris-(1-phenyl-1*H*-benzimidazole). **Firpic**: blue emitter, iridium(III) [bis(4,6-difluorophenyl)-pyridinato-*N,C*^{2'}]picolate. **mCP**: non-emissive host, 1,3-bis(9-carbazolyl)benzene. **IrL₃**: orange emitter, iridium(III) complex with ligand (9,9-diethyl-7-pyridinylfluoren-2-yl)-diphenylamine. **CBP**: non-emissive host, 4,4'-*N,N'*-dicarbazolebiphenyl. **NPB**: hole transporting layer, 4,4'-bis[*N*-(1-naphthyl)-*N*-phenylamino]biphenyl.

Alternatively, electroluminescent devices are also being developed comprising a single, multidoped emissive layer where the host material accommodates more than one chromophore (and/or acts as the blue emitter). In these systems, however, the management of the energy transfer processes between the different nearby luminescent components is critical as it will define the colour eventually emitted. Actually, this is one of the main issues in the design of single materials displaying white luminescence, the strategy chosen in this work for the preparation of colour-tunable white-light emitting systems.

5.1.2.1 White-light emission from individual multicomponent materials

As already commented, white light can be obtained by properly combining the luminescence arising from different emitting sites embedded into a single material. This can be directly achieved by dispersing distinct molecular compounds with adequate emission spectra into the desired supporting matrices, which can range from simple liquid solutions to more complex hosts such as gels, mesoporous solids or micro- and nanoparticles^{3,6}. For instance, Nandi and coworkers¹⁹ produced a melamine-based white-light emitting hydrogel combining three different emitting units: 6,7-dimethoxy-2,4[1*H*,3*H*]-quinazolin-2(1*H*)-one (**Q**), blue emitter; riboflavin (**R**), green emitter and rodhamine B (**RhB**), orange emitter (Figure 5.4). Melamine binds to **Q** and **R** by hydrogen-bonding forming a co-assembled hydrogel to which **RhB** is incorporated. At the appropriate gel composition, a partial energy transfer from **Q** to **R**, **Q** to **RhB** and **R** to **RhB**, produces a broad emission spectra compose of three emission peaks corresponding to each of the emitting centres, that results in white-light emission upon 360 nm excitation (CIE coordinates: $x = 0.31$, $y = 0.36$).

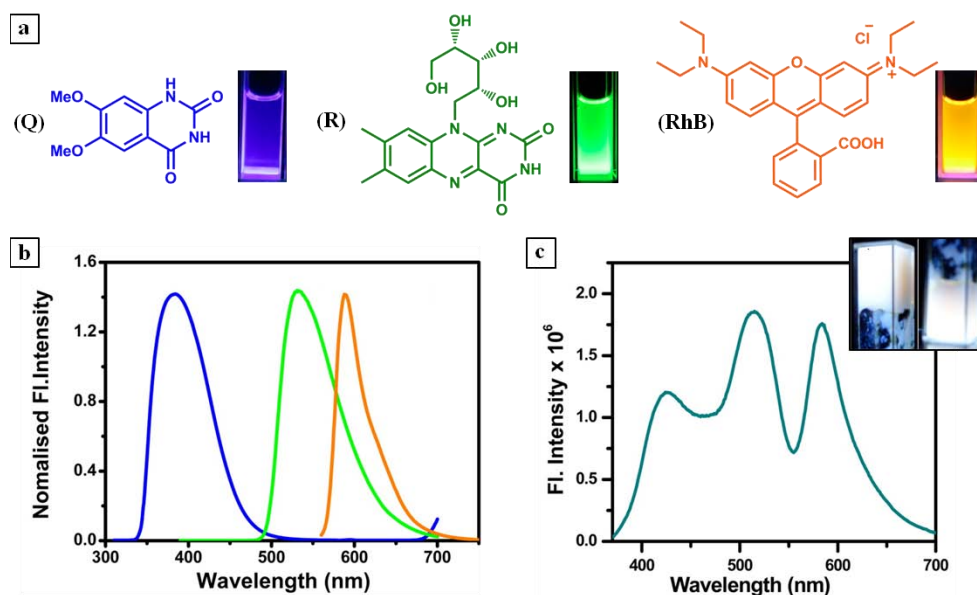


Figure 5.4 (a) Molecular structure of 6,7-dimethoxy-2,4[1*H*,3*H*]-quinazolin-2(1*H*)-one (**Q**), riboflavin (**R**) and rodhamine B (**RhB**); together with photographs of the fluorescent emission of the respective solutions under UV light irradiation (365 nm). (b) Normalized Fluorescence Spectra of **Q** (blue), **R** (green), and **RhB** (orange) in aqueous solution. (c) Photograph and fluorescence spectra of the white-light emitting hydrogel, formed at **Q**:**R**:**RhB** 100:0.5:0.02 molar ratio, upon excitation at 365 nm and 360 nm, respectively. Adapted from reference 19.

Alternatively, all the required emitting sites could be prepared from a single molecular component, a very appealing situation since it should allow reducing costs, simplifying

fabrication processes and enhancing colour stability by avoiding the differential aging of distinct emitters. Different strategies are exploited to achieve this objective. On the one hand, white light can be produced by the combined emission of monomeric species and excited-state aggregates (excimers, exciplexes or electromers) of a single compound.^{3,6} This is the case of the example given in Figure 5.5(a), in which the simultaneous emission of monomeric and excited oligomeric units of compound **D1c** (consisting of two push-pull moieties separated by a polymethylene chain) in solid state, produces a broad band covering a wide domain in the visible range that results in the generation of white light (CIE coordinates: $x = 0.34$, $y = 0.36$)²⁰.

On the other hand, compounds displaying different isomeric or protonation states with complementary luminescence spectra can be used to generate white light.^{3,6} For instance, Liu et al. recently reported white photo- and electroluminescent films for the fabrication of WOLEDs, based on the controlled acidification of two quinazoline derivatives (Figure 5.5(b))²¹. In both compounds, an incomplete energy transfer from the neutral (blue-emissive) to the protonated (orange-emissive) form at certain concentrations of acid, allows the concurrent emission of both species and, consequently, the production of white light (best CIE coordinates reported: $x = 0.33$, $y = 0.34$).

Finally, white-light emission can be produced by individual molecular compounds comprising different covalently-linked luminescent units.^{3,6} Figure 5.5(c) depicts the structure of one of these systems, a bimetallic assembly containing two complementary chromophoric moieties, obtained by the formation of an adduct between a red-emissive Eu(III) complex and a blue-emissive Ir(III) complex²². Upon irradiation with monochromatic light at 400 nm, where only the iridium moiety absorbs, the assembly exhibits almost white-light emission (CIE coordinates: $x = 0.28$, $y = 0.30$) owing to a partial energy transfer that allows the combined emission of the distinct emissive moieties.

Regardless of the number and nature of the components selected, to accomplish white-light emission from individual materials generally requires precise control of the energy transfer processes between the different emitting sites, which eventually govern the colour arisen from the system, as observed in some of the examples described above. These processes may be radiative (inner filter effect) or not (Dexter and Förster energy transfer), can take place on virtually any spatial scale (from macro- to nanoscale) and are concentration and/or distance dependent^{23,24}.

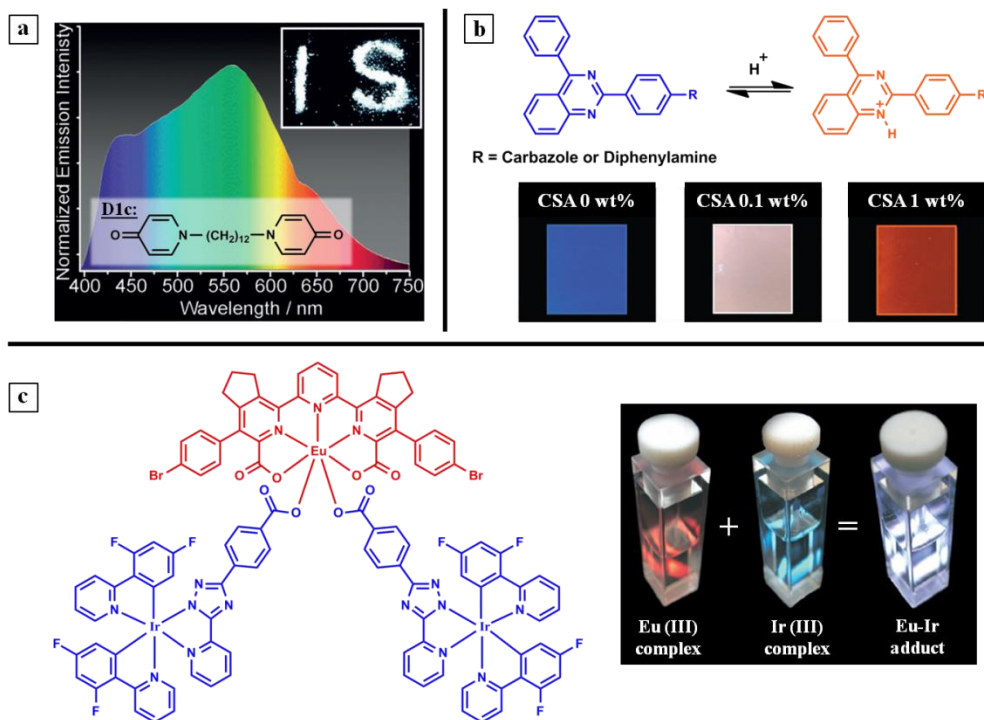


Figure 5.5 (a) Photograph and solid state photoluminescent spectrum of compound **D1c** containing two 4-pyridone units separated by a polymethylene chain, which displays white-light emission in solid state under excitation at 365 nm by combination of monomeric (short wavelengths emission) and excimeric (long wavelengths emission) emitting species. Adapted from reference 20. (b) Schematic representation of the acid-base balance of two donor-acceptor dyes consisting of a quinazoline derivative linked to a carbazole or a diphenylamine moiety via an aromatic tether (**Qz-Cbz** and **Qz-DPA**). Upon acidification, their emission spectrum bathochromically shifts from blue to orange allowing the preparation of mixed films (i.e. containing both, the neutral and the protonated form of each compound) for WOLED fabrication. The photographs show the photoluminescent of **Qz-Cbz** thin films prepared with different concentrations of camphorsulfonic acid (**CSA**). Adapted from reference 21. (c) Structure of a bimetallic assembly obtained by the formation of an adduct between a red-emissive **Eu(III)** complex and a blue-emissive **Ir(III)** complex. Upon irradiation at 400 nm, this system exhibits almost white-light emission due to a partial energy transfer between the different emissive moieties. The photograph displays the colour emitted by the uncoordinated complexes and the said **Eu-Ir** adduct. Adapted from reference 22.

In all the cases, energy transfer leads to the enhancement of the luminescence intensity of the red-shifted emitters of the system (*acceptors*) at the expense of the emission from the dyes with the highest excitation energy (*donors*), and it is almost unavoidable for any set of emitters chosen due to the occurrence of spectral overlaps^{3,25}. In view of this, Förster and/or Dexter energy transfer processes are very often exploited for the development of white-light emitting materials by mixing donor-acceptor pairs of blue and red emitters^{3,6}. Unfortunately,

this imposes several restrictions during the preparation of these systems. First, it requires very short (on the nanometer scale) and controlled separations between the different emitting sites in the materials, since the rates of non-radiative energy transfer dramatically depend on distance. To overcome this obstacle and bring the distinct dyes into close proximity, different strategies are followed, such as the attachment to well-defined biological scaffolds (e.g. DNA²⁶ and peptides²⁷), self-assembly processes^{28,29}, or surrounding the acceptor moieties by a donor host matrix (e.g. in organogels³⁰⁻³² or polymer films³³). Second, the complexity and heterogeneity of the final system and even the occurrence of undesired energy transfer processes make nearly impossible to predict precisely the colour obtained for each mixture prepared at certain experimental conditions. As a result, thoroughly screening through repetitive and time-consuming experiments is required to find the optimal settings (emitters ratio, distances and concentrations) that lead to the targeted white-light emission²⁵.

A very limited number of alternatives exist to white-light emitting materials based on energy transfer processes³⁴⁻³⁶. Among them, the use of ESIPT dyes has been recently suggested as a powerful strategy³⁰⁻³². In these compounds an excited-state intramolecular proton transfer process (ESIPT) such as the enol-keto intramolecular phototautomerisation shown in Figure 5.7(a), takes place upon excitation, producing a very large Stokes shift between the absorption and emission spectra²⁵. As a result, different UV-absorbing ESIPT dyes can be selected whose emission covers the whole visible range, which allows preventing the spectral overlap between donor emission and acceptor absorbance and frustrating energy transfer between neighbouring emitters. This enables the different units in the materials to emit independently even though they are located close to each other and, therefore, prepare white-light emitting systems in solution and in the solid phase displaying no detrimental effects due to energy transfer. For instance, Figure 5.7(b) displays the structure of a white light-emitting dye, **W1**, composed of two ESIPT units covalently linked by a diphenylether cross-linking group: the blue-emissive **HPI** ($\lambda_{\text{max}} = 470 \text{ nm}$) and the orange-emissive **HPNI** ($\lambda_{\text{max}} = 570 \text{ nm}$); both absorbing in the UV region (between 320-350 nm)³⁷. Since there is no overlap between **HPI** emission and **HPNI** absorption due to the bathochromic shift induced by the ESIPT process, any possible energy transfer between the two moieties is completely blocked. Consequently, **W1** presents a broad emission spectrum that corresponds to the superposition of the spectra observed for each individual emitting centre, and, upon 365 nm

irradiation, the system emits white light both, in solution and in solid state (Figure 5.7(c), CIE coordinates: $x = 0.33$, $y = 0.37$).

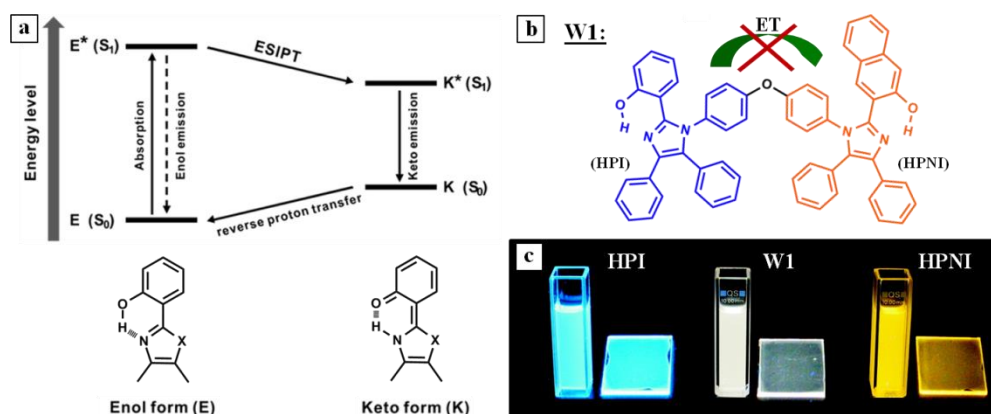


Figure 5.6 (a) Schematic representation of the ESIPT photocycle²⁵. Upon photoexcitation the enol form (E) undergo tautomerisation into keto form ($E^* \rightarrow K^*$) via an extremely fast and irreversible excited-state intramolecular proton transfer (ESIPT). Subsequently, the excited keto form (K^*) decays radiatively to the intermediate ground state (K), which immediately tautomerizes by reverse proton transfer to the original enol form ($K \rightarrow E$). Because K^* exists only transiently, its potential as energy acceptor is negligible and, consequently, the absorption from E and the emission from K^* predominate. The latter results on a large Stokes shift and prevents self-absorption²⁵. (b) Structure of a white-emitting dye **W1** composed of two ESIPT units: the blue-emissive 2-(1,4,5-triphenyl-1H-imidazol-2-yl)phenol (**HPI**, $\lambda_{\text{max}} = 470$ nm), and the orange-emissive 3-(1,4,5-triphenyl-1H-imidazol-2-yl)naphthalen-2-ol (**HPNI**, $\lambda_{\text{max}} = 570$ nm); both absorbing in the UV region (between 320–350 nm). Due to the Stokes shift induced by the ESIPT process there is no overlap between **HPI** emission and **HPNI** absorption and therefore any energy transfer process between the two moieties is frustrated. Adapted from reference 37. (c) Pictures of the photoluminescence of **HPI**, **W1**, and **HPNI** molecules, in solution and dispersed in thin-films, upon irradiation with 365 nm UV light. Adapted from reference 37.

In this work the preparation of organic white-light emitting materials that are not affected by energy transfer process is also pursued, thus aiming at simplifying the design of the final system. However, our approach does not rely on the use of ESIPT dyes but on a different strategy, as will be discussed below.

5.1.2.2 Colour tunability in white-light emitting materials

Aside from energy transfer-free white-light emission, the materials to be developed herein should also display colour tunability. Actually, colour tunability is claimed in many of the approaches described in the bibliography for white-light emitting systems. However, in most of the cases this term is related to the capacity of modifying the colour emitted by varying certain parameters during synthesis or production, such as the concentration ratio of the different luminescent sites in the material^{9,30,39}. Therefore, it often does not refer to the concept pursued in this work – namely, the capability to tune the colour arisen from a given white-light emitting material upon application of an external stimulus. Such objective has been much more seldom accomplished in the literature.

Mostly, colour changes induced on final white-light emitting materials have been demonstrated in solution⁶ through variations of temperature^{26,40,41}, pH^{21,42,43}, solvent polarity^{38,44,45} or by ion additions^{11,46}. In solid state, colour tunability is less common and has only been attained changing the energy of the exciting source. Thus, the emission of some electroluminescent-based designs, specially stacked layer architectures, has been found to be voltage dependent^{18,47}, as in shown in Figure 5.7(a) that gathers the electroluminescent spectra of the WOLED represented in Figure 5.3(b) at different applied voltages. This system is composed of two stacked layers, physically separated, that emit independently and simultaneously blue (**FIrpic**-containing layer) and orange (**IrL₃**-containing layer) light. As voltage increases, the higher energy input and the improvement in charge mobility enhance blue light contribution; and, consequently, the colour of the light emitted varies (white light is attained at 10 V, CIE coordinates: $x = 0.31$, $y = 0.41$). Similarly, for photoluminescence systems colour change has been achieved modifying the relative intensities of the emitters with the excitation wavelength^{37,48,49}. This is the case of the example given in Figure 5.7(b) where the photoluminescent spectrum of co-doped silica particles containing fluorescein isothiocyanate (green emitter) and Ru(phen)₃²⁺ complex (red emitter), is modified varying the excitation wavelength between 365 and 470 nm. The characteristic feature of these dyes is the large spectral overlap in their absorbance that allows their concurrent excitation over a broad range of wavelengths. Since dye molar absorptivity depends on the excitation wavelength, the relative emission intensities of the two dyes change with the energy of the irradiation applied and, therefore, the colour of the light emitted by the particles varies.

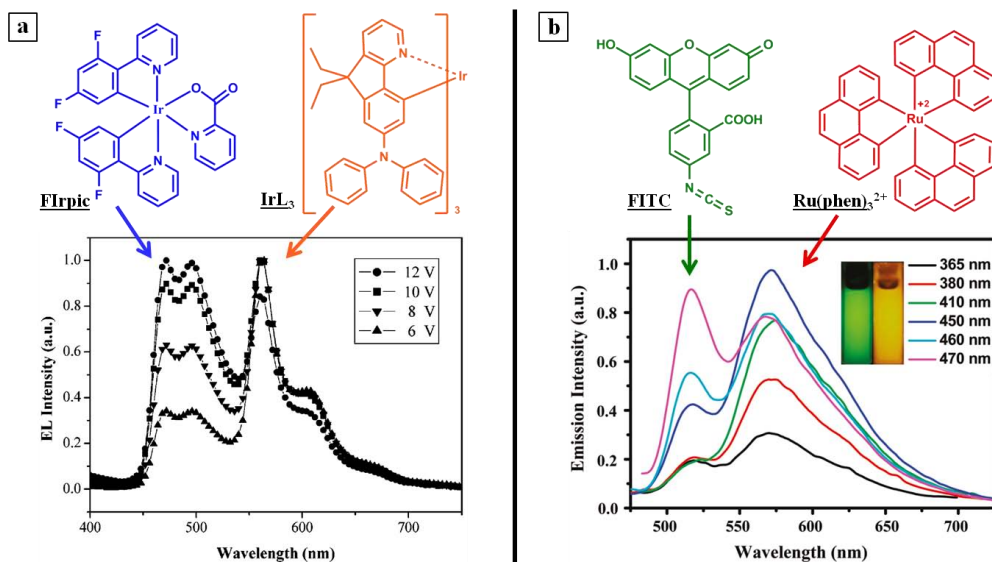


Figure 5.7 (a) Voltage dependence of the electroluminescent spectrum of the WOLED described in Figure 5.3(b): two stacked layers, physically separated and emitting independently and simultaneously blue (**FIrpic**-containing layer, $\lambda_{\text{max}} = 472$ and 496 nm) and orange (**IrL₃**-containing layer, $\lambda_{\text{max}} = 560$ nm) light. As voltage is increased, blue light contribution is enhanced and the resulting emission spectra is modified. Adapted from reference 18. (b) Dependence of the emission spectrum of co-doped silica particles on the excitation wavelength. Two dyes are incorporated in the silica matrix: the green-emissive fluorescein isothiocyanate (**FITC**, λ_{max} in solution = 525 nm) and red-emissive **Ru(phen)₃²⁺** complex (λ_{max} in solution = 585 nm). Varying the excitation wavelength, the relative emission intensities of the two dyes are modified and, consequently, particle emission spectrum changes. The inset shows the different colour emitted by a dispersion of the said nanoparticles upon 365 nm (left) and 450 nm (right) irradiation. Adapted from reference 48.

As a matter of fact, colour tunability combined with white-light emission in solid state is rather scarce. In this work we propose to attain this goal by means of thermal changes, a type of external stimulus suitable for implementation into functional devices.

5.1.2.3 Micro- and nanostructured white-light emitting materials

In view of future applications, additional efforts are currently underway to miniaturise white-light emitting materials down to the micro- and nanoscale.⁶ In fact, different white-light emitting micro/nanostructures based on purely organic emitters or organic/inorganic hybrids, specially doped silica, have been prepared during the last years: particles^{28,50,51}, rods⁵², fibers⁵³ or tubes⁵⁴. In these systems RGB luminescence is obtained through different

strategies, such as energy transfer processes between host matrices and dopants or among dopants^{39,52}, and between excimers (or aggregates) and monomer-like species⁵¹. In addition, distinct approaches are used to incorporate the active dyes within the micro- and nanostructures, ranging from simple dispersion into the host system^{39,52}, covalent or supramolecular tethering to the matrix framework^{50,51}, attachment to their surfaces^{55,56} and encapsulation inside vesicles and micelles^{43,57–59}. Figure 5.8 shows an illustrative example of the latter case, which consists in the encapsulation of a pH-sensitive bispyrene dye (**bPyr**) into the aqueous core of vesicles containing a red-emitting perylendiimide chromophore (**PDI**) in their shell. Varying the conformation of the flexible spacer between the two pyrene units in **bPyr** upon acid-base addition, the concentration ratio of monomeric, blue-emitting, and excimeric, green-emitting, species inside the capsule could be rationally tuned. In combination with selective energy transfer from pyrene excimers to the **PDI** dyes, this allowed both for white-light emission (CIE coordinates: $x = 0.32$, $y = 0.31$, at $\text{pH} = 9$) and colour tunability upon pH variation.

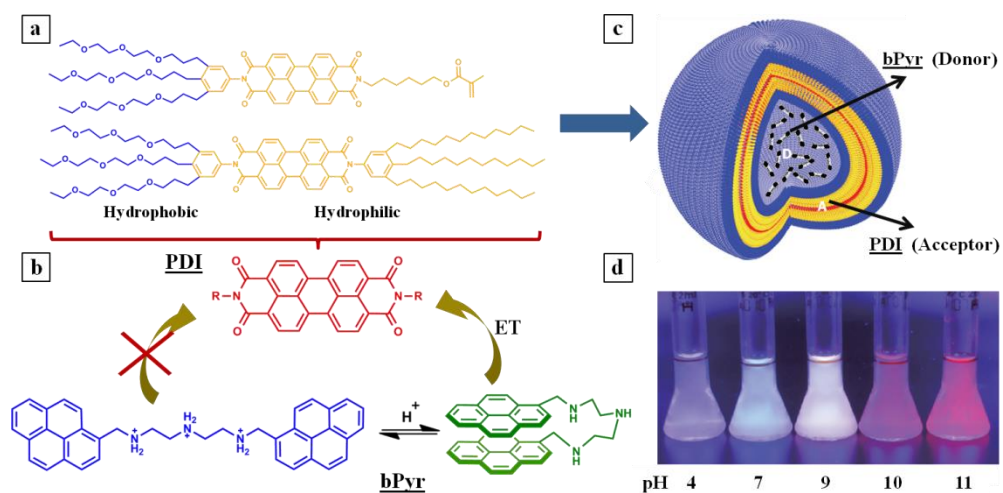


Figure 5.8 (a-d) Schematic illustration of white-light emitting and colour tunable vesicles ((c) made of an amphiphilic perylendiimide dyes (**PDI**, hydrophilic chains in blue and hydrophobic parts in orange, (a) and loaded with a bispyrene-based chromophore (**bPyr**) that can display pH-tunable monomeric (blue) and excimeric (green) emission ((b)). While blue emission is predominant in acid and neutral media where the amino groups of the flexible tether of **bPyr** are protonated, green emission and subsequent energy transfer to the red-emitting **PDI** molecules is favoured upon basification (b), which eventually results in white-light emission at $\text{pH} = 9$ (d), vesicle emission in aqueous solution upon 366 nm irradiation). Adapted from reference 43.

In this work a similar approach based on liquid-filled capsules has been explored for the preparation of solid microstructured materials displaying white-light emission and thermally-induced colour tunability.

5.1.3 Liquid-filled capsules for the design of white-light emitting and colour tunable materials

Based on the experience gained along the previous chapters of this thesis, we decided to exploit liquid-filled polymeric capsules as the vehicle for the preparation of white-light emitting and colour-tunable materials. Our novel approach relied on the following aspects:

(i) *The encapsulation of two different dyes emitting complementary colours within the liquid core of the capsules.* This should provide us with a solid, microstructured white-light emitting material suitable for further processing in the solid state owing to the intrinsic advantages of liquid-filled capsules, such as enhanced dye loadings and prevented aggregation and phase-separation due to dye-matrix incompatibility. In addition, the liquid nature of their core should enormously facilitate achieving white-light emission in the final material by allowing direct transfer into the solid state of the luminescent behaviour of well defined mixtures of the dyes in solution. Actually, such solution-to-solid state transition is often one of the bottlenecks in the preparation of white-light emitting materials as a result of the changes in (supra)molecular organization derived from solvent drying, which can critically affect chromophore interaction and, therefore, colour emission in the final system⁶⁰.

(ii) *The use of low concentrations of dyes within the capsules, which should be both directly excitable with the same irradiation source.* Together with their liquid interior and the short fluorescent lifetimes of the organic chromophores used (\sim ns), this should allow the energy transfer processes arising from intermolecular interactions between the emitting moieties to be prevented. This further simplifies the design and development of the target material, since the optimal dye concentration ratio required to accomplish white-light emission could be directly inferred from the separate spectral properties of the chromophores selected²⁵.

(iii) *The choice of a temperature-responsive fluorophore as one of the two complementary dyes in the interior of the liquid-filled capsules.* As such, the additive combination of the

concurrent emission stemming from both types of chromophores could be thermally changed, thus allowing for (i) fine tuning of white-light emission, and (ii) colour variation on demand using an external stimulus. In particular, an orange-emitting thermally-responsive dye developed in our group (**ZW5**, Figure 5.9) has been used for this purpose⁶¹, whose properties are discussed in detail in the next section. To complement the emission spectrum of this chromophore on our route to white-light emission, a turquoise-emitting dye was selected: 9,10-bis(phenylethynyl)anthracene (**BPEA**, Figure 5.9). **BPEA** is a commercial fluorophore known for its good solubility in a variety of solvents, chemical and thermal stability, and its remarkably high emission efficiency with a fluorescence quantum yield (Φ_f) higher than 0.9. Accordingly, it has been widely used in chemiluminescent formulations or as molecular probe, and it has been studied for application in OLED devices^{62,63}.



Figure 5.9 Chemical structures of **ZW5** and **BPEA**, the dyes of choice in this chapter for the preparation of colour-tunable white-light emitting materials.

5.1.3.1 **ZW5: a thermally-responsive fluorophore**

ZW5 belongs to the family of fluorescent molecular switches based on spirocyclic cyclohexadiene derivatives^{64,65} that has been developed in the “Electrochemistry, Photochemistry and Organic reactivity” group of the UAB, one of the two research groups hosting this thesis work. In particular, **ZW5** was first prepared by Dr. Gemma Prats along her thesis⁶¹. It is composed of two main functional units: (i) a dinitrocyclohexadiene moiety bearing a trifluoromethyl electro-withdrawing group, which absorbs and emits in the visible region of the spectrum with high efficiency; and (ii) a triazine ring tethered to the dinitrocyclohexadiene unit via a spiranic carbon atom, which contains a guanidinium group. Because of the acid-base activity of this group ($\text{pK}_a \sim 11\text{-}12$ in water), this system presents

two different protonation states (Figure 5.10(a)): (i) the zwitterionic state **ZW5**, which is highly fluorescent ($\lambda_{\text{abs}} = 564 \text{ nm}$, $\lambda_{\text{em}} = 595 \text{ nm}$, and $\Phi_f = 0.76$ in acetonitrile, Figure 5.10(b)); and (ii) the anionic state **MC4**, which is not fluorescent due to emission quenching via photoinduced electron transfer (PET) between the deprotonated guanidine group and the cyclohexadiene fluorophore.

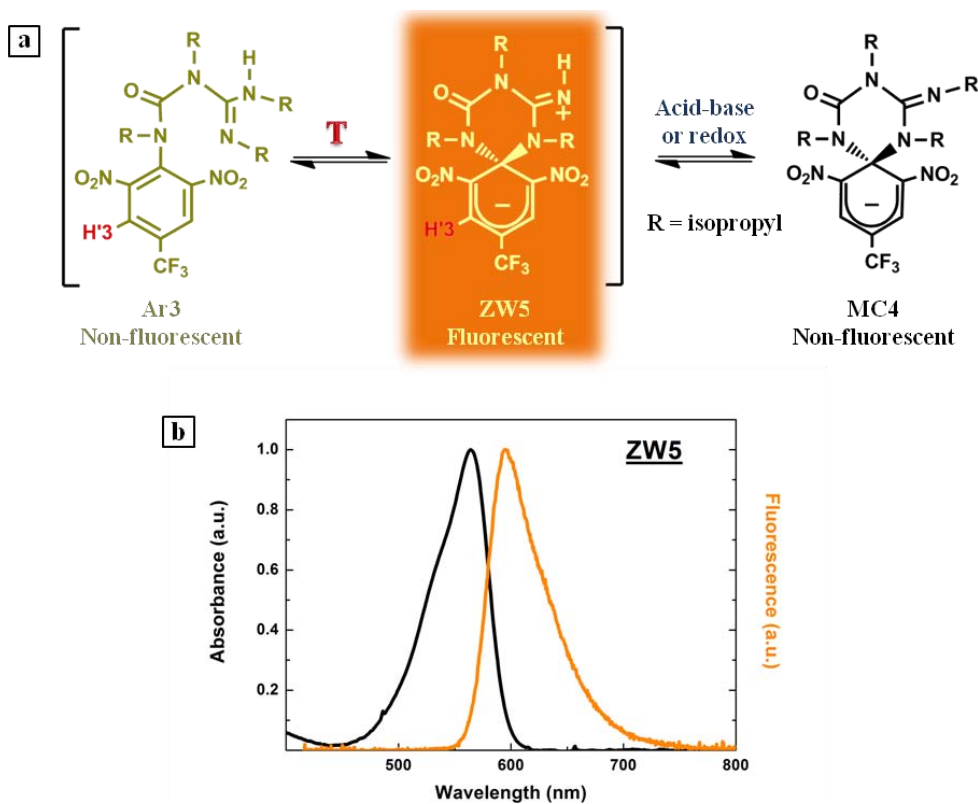


Figure 5.10 (a) Structure and interconversion processes of molecular switch **ZW5**, which can interconvert thermally with the aromatic, non-spirocyclic tautomer **Ar3** and (electro)chemically with the deprotonated state **MC4**. (b) Absorbance and fluorescence spectra of **ZW5** in acetonitrile solution.

As a result, the **ZW5-MC4** system behaves as a molecular switch displaying “on”-“off” fluorescence emission upon chemically- and redox-induced protonation-deprotonation. This switching behaviour is however not to be exploited herein in the development of thermally-responsive white-light emitting materials and the system will remain in its protonated state throughout our study.

On the other hand, the trifluoromethyl moiety in the cyclohexadiene unit of **ZW5** decreases the stability of the spirocyclic structure of the zwitterionic state of the compound with respect to analogous trinitrocyclohexadiene derivatives and, consequently, it can spontaneously evolve to form the non-spirocyclic aromatic isomer **Ar3**. In fact, the protonated state of the switch actually consists of an equilibrium mixture of **ZW5** and **Ar3** tautomers, which are continuously interconverting between each other. Noticeably, the aromatic isomer **Ar3** was found to neither absorb nor emit in the visible region of the spectrum. Thus, the intensity of the orange emission arising from the protonated state of the system (i.e. from the **ZW5-Ar3** mixture) depends on the molar fraction of **ZW5** molecules (i.e. on the equilibrium constant of the tautomerisation process ($K_{\text{ZW5-Ar3}}$)).

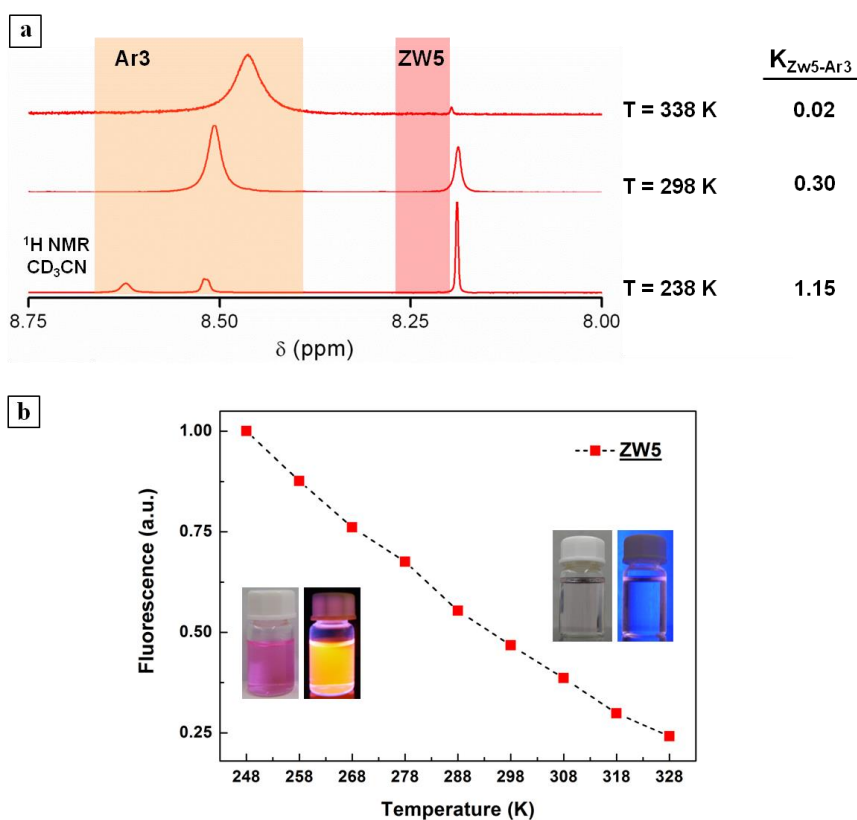


Figure 5.11 (a) Variation of the $^1\text{H NMR}$ signals for H3' in **ZW5** and **Ar3** with temperature. From the integrals of these signals, the equilibrium constants of the **Ar3** \leftrightarrow **ZW5** tautomerisation process at different temperatures were determined⁶¹. (b) Fluorescence intensity at $\lambda_{\text{em}} = 595$ nm of an acetonitrile solution of **ZW5** ($5 \cdot 10^{-6}$ M) upon temperature variation from 248 to 328 K⁶¹. The insets show pictures of the colour change and the emission variation of **ZW5** in acetonitrile solution with temperature.

This equilibrium constant is temperature dependent, thus allowing to thermally control the fluorescence intensity arising from the **ZW5** dye (or, more exactly, from the **ZW5-Ar3** mixture). In particular, the equilibrium concentration ratio $[\text{ZW5}]:[\text{Ar3}]$ decreases with temperature, and so it does the emission intensity of the protonated state of the system (Figure 5.11). In this work, this behaviour is intended to be used to thermally tune the colour emitted by a mixture of complementary dyes such as **ZW5** and **BPEA**.

5.1.4 Objectives

As discussed above, the main goal of this chapter is the synthesis of fluorescent liquid-filled capsules loaded with mixtures of the **ZW5** and **BPEA** dyes to produce *microstructured solid materials* displaying *white-light emission at room temperature* as well as *thermally-induced colour tunability* (figure 5.8). In particular, owing to the spectral and temperature-dependent properties of these fluorophores, white light should switch to orange or turquoise emission upon cooling down or heating the material, respectively.

To achieve this objective, different studies were conducted in a step-wise manner aiming at: (i) selecting the optimal conditions (polymer shell and solvent) for the preparation of the liquid-filled capsules; (ii) finding the proper dye concentration ratio to achieve energy transfer-free white-light emission around room temperature; and (iii) synthesising and optically characterising the target material.

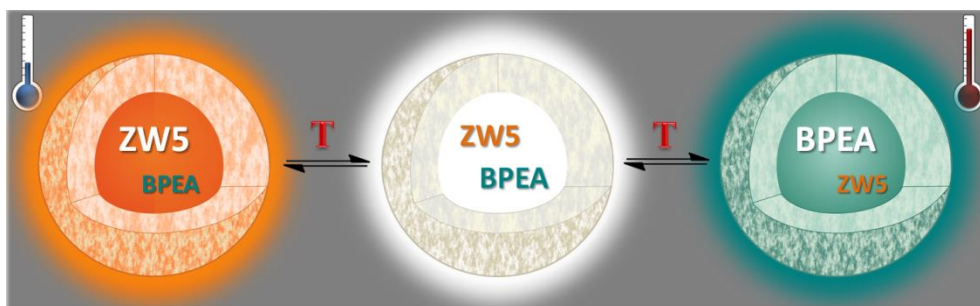


Figure 5.12 Schematic representation of the approach proposed in this work for the preparation of microstructured white-light emitting materials displaying thermally-induced colour tunability.

5.2 Results and discussion

5.2.1 Selection of the capsules nature

Prior to the synthesis of the target dye-loaded liquid-filled capsules, we first needed to establish the conditions that would lead to white emission in these materials while allowing large colour changes through temperature variations. Hence the importance of selecting capsules nature, since their shell should assure the stability of the system and their liquid core guarantee dye fluorescent properties and tunability along the whole range of temperatures selected.

5.2.1.1 Capsules liquid interior

Considering the good results obtained for photochromic and thermochromic capsules in previous chapters, miglyol was the first solvent tested as liquid core for the development of white-light emitting colour-tunable capsules. However, even though **ZW5** and **BPEA** fluorescent properties were preserved when dissolved in this oil, two important problems were encountered. First, **ZW5-Ar3** tautomerisation equilibrium in miglyol was found to be strongly shifted towards the non-fluorescent open form. By comparison with acetonitrile solution absorbance⁶¹, we estimated that only about 2% of the total amount of dye molecules existed as the fluorescent **ZW5** isomer in miglyol solution at room temperature. Second, miglyol solidifies at rather high temperatures (clouding point < 273 K⁶⁶), which would strongly limit the thermal range at which the liquid interior of the capsules would be preserved. Since cooling is required to shift the tautomerisation process towards the **ZW5** isomer, this would ultimately imply that the intensity of the orange emission from this species could only be minorly varied, thus preventing efficient colour tunability in the final material.

In view of this, toluene and other common oils used in our group for encapsulation purposes were also checked. Unfortunately, the molar fraction of **ZW5** molecules at room temperature in all of them was found to be relatively small (< 2%). Therefore, to sufficiently increase the content of the fluorescent form of this dye and satisfactorily tune the colour

emitted by the target capsules, a solvent was required that allowed reaching low enough temperatures. This is the case of the oil finally chosen, dioctyl terephthalate (DOTP), a compound commonly used as plasticiser in plastics, paints and varnishes. Importantly, DOTP melts at 225 K (and does not boil up to 673 K)⁶⁷, thus allowing us to widen the low-temperature working range.

Once selected the solvent for the preparation of liquid-filled capsules, the thermal dependence of the optical properties of **ZW5** and **BPEA** in DOPT was investigated (Figure 5.14). In the case of the commercial dye **BPEA**, its absorption spectrum was found to slightly vary with temperature within the 248-358 K range. According to the chemical structure of this fluorophore and the reversibility of the changes observed, we ascribed this result to the thermal variation of the wavelength-dependent absorptivity of **BPEA**. In spite of this, minimal spectral changes were observed around $\lambda = 400\text{-}425$ nm and $\lambda = 450$ nm, where dye absorbance remained nearly constant. For this reason, we chose the latter excitation wavelength to monitor the thermal dependence of the fluorescence spectrum of **BPEA**. As observed in Figure 5.14(c), a small decrease in the emission intensity was measured upon heating. Similar results have been obtained for this dye in other organic solvents, which were attributed to changes in the refractive index of the medium instead of in fluorescence quantum yield due to thermal enhancement of the radiationless deactivation pathways of the chromophore⁶⁸. For **BPEA** in DOPT, this gives rise to a ~25% decrement in emission intensity at $\lambda_{\text{exc}} = 450$ nm when moving from 263 to 348 K. On the other hand, the shape and position of the fluorescence spectrum of this chromophore barely changes within this temperature range (~ 3 nm blue-shift), which indicates that the colour emitted by this dye should be preserved throughout the thermal window of interest.

More dramatic changes were found when analysing the temperature effect on the optical properties of **ZW5** in DOPT. As shown in Figure 5.14(a-b), a large and reversible decrease of the absorption spectrum of this dye was observed upon heating. According to the previous studies in our group⁶¹, this must be due to the thermal variation of the equilibrium constant for the **ZW5-Ar3** tautomerisation process, which should lead to an increase of the molar fraction of the non-spirocyclic isomer **Ar3** with temperature. Since this species does not absorb in the visible spectrum, a pronounced decrement of the absorption signal in this spectral range was consequently measured. Actually, by comparison with the data previously obtained in acetonitrile⁶¹ and assuming temperature-independent absorptivity

coefficients, the molar content of the fluorescent **ZW5** isomer in the **ZW5-Ar3** equilibrium mixture in DOPT was determined to be 0.8, 2 and 4.3% at 248, 300 and 348 K.

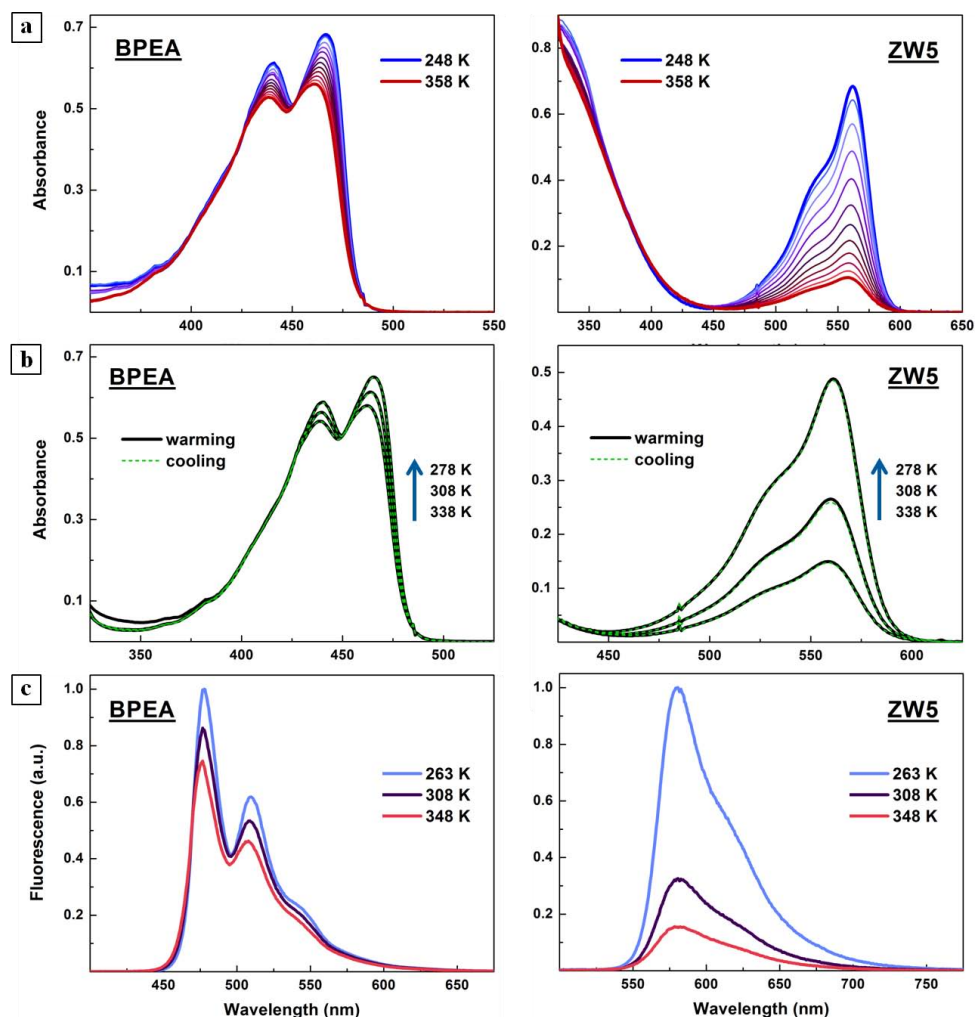


Figure 5.13 (a) **BPEA** (10^{-4} M, 0.2 cm path length cuvette) and **ZW5** ($6 \cdot 10^{-4}$ M, 1 cm path length cuvette) absorption spectra in DOTP recorded by increments of 10 K between 248 and 358 K. (b) **BPEA** and **ZW5** absorption spectra in DOTP at 278, 308 and 338 K, measured during consecutive warming and cooling cycles which demonstrate the reversibility of dye temperature dependence. (c) **BPEA** ($2.7 \cdot 10^{-6}$ M, λ_{exc} : 450 nm) and **ZW5** ($8.4 \cdot 10^{-5}$ M, λ_{exc} : 473 nm) fluorescence spectra at 263, 308 and 348 K.

As expected, the same trend was observed in fluorescence, the **ZW5-to-Ar3** conversion upon heating mainly accounting for the decrease in emission intensity registered. In fact, quantitatively similar changes were observed in absorption and fluorescence spectroscopy for **ZW5** in DOTP, which allows overlooking the contribution of other factors to this result,

such as refractive index effects or temperature-induced reduction of Φ_f . Noticeably, such changes only affected the overall intensity of the emission spectrum, while its shape and position (i.e. the colour of **ZW5** fluorescence) remained nearly invariant along the 263-348 K range scanned (~ 4 nm blue-shift).

Figure 5.14(a) shows the chromaticity coordinates of the emission arising from separated solutions of **BPEA** (0.165, 0.448) and **ZW5** (0.565, 0.434) in DOTP at room temperature. As already commented, these are turquoise- and orange-emitting dyes, respectively. In the absence of any interaction between them, the chromaticity coordinates of the colours that would be emitted by **BPEA-ZW5** mixtures should lie on the straight line drawn in the diagram, which passes next to the (0.333, 0.333) coordinates of pure white colour. In particular, it should be possible to achieve (0.335, 0.442) chromaticity coordinates by properly mixing the complementary fluorescence of **BPEA** and **ZW5**, which correspond to a yellowish white colour (“warm white”).

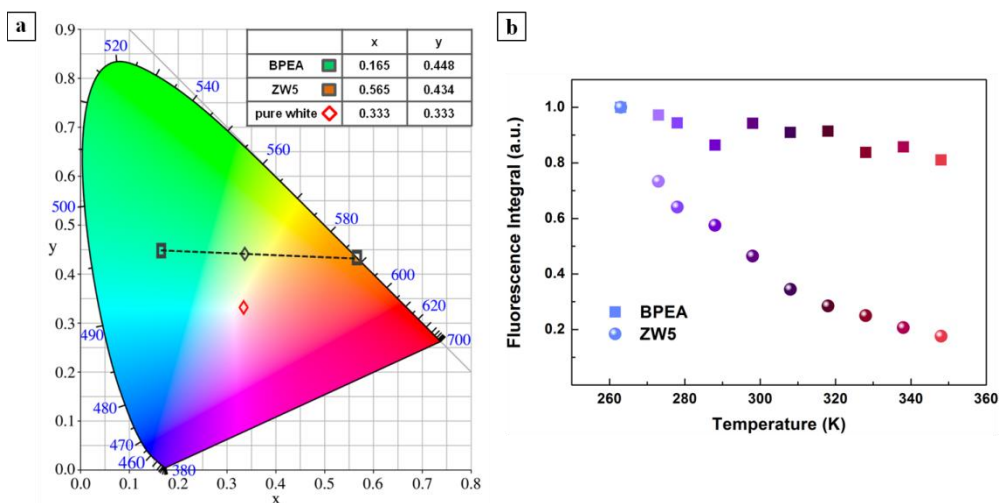


Figure 5.14 (a) CIE chromaticity diagram displaying **BPEA** and **ZW5** chromaticity coordinates in DOTP together with those originated by mixing their emissions in the absence of any interaction between them. The nearest of these coordinates to pure white colour (0.329, 0.420) are also indicated in the diagram. (b) Temperature dependence of the emission integrals arising from separated solutions of **BPEA** ($2.7 \cdot 10^{-6}$ M, $\lambda_{exc} = 450$ nm) and **ZW5** ($8.4 \cdot 10^{-5}$ M, $\lambda_{exc} = 473$ nm) in DOTP.

To achieve this goal and preclude **BPEA-ZW5** energy transfer processes altering the final colour emitted, two additional spectroscopic features of these dyes will be exploited: (i) their high fluorescence quantum yields ($\Phi_f = 1$ and 0.75 for **BPEA** and **ZW5** in DOTP at room

temperature), which would result in large emission intensities even at the highly diluted concentrations required to avoid interchromophoric interactions; (ii) the thermal variation of the fluorescence ratio arising from each of the components of the **BPEA-ZW5** mixture, which should allow fine tuning of the chromaticity coordinates by means of controlled temperature changes. Actually, the latter aspect will not only be used to achieve white emission, but also to scan the emitted colour along the turquoise-orange line in the chromaticity diagram upon application of thermal stimuli. With this aim, we will take advantage of the different temperature dependences of **BPEA** and **ZW5** fluorescence intensities, which are compared in Figure 5.14(b). Clearly, **ZW5** emission decrease in the 263-348 K range is around five-fold larger than for **BPEA**, which should enable rather selective fading of the orange colour arising from **ZW5-BPEA** mixtures upon heating (i.e. upon thermal conversion of the fluorescent **ZW5** species into its non-emitting isomer **Ar3**).

5.2.1.2 Capsules shell

After selecting the oil to be used in the synthesis of the dye-loaded liquid-filled capsules, we then turned our attention to the polymer shell of choice. In a first step, the preparation of polyamide capsules was discarded due to **ZW5** pH-sensitivity (see section 4.2.2.1), which would probably lead to dye instability against terephthaloyl chloride as already observed for the VT compound in chapter 4. Accordingly, we tested dye stability and DOTP entrapment inside polyurea capsules (**PU_DOTP**) as an alternative.



Figure 5.15 Schematic representation of the interfacial polymerisation in oil-in-water emulsions procedure used for the synthesis of polyurea capsules filled with a dye mixture in DOTP.

PU_DOTP capsules were successfully obtained following the same procedure optimised for VT encapsulation in miglyol – namely, via interfacial polymerisation in emulsions created by magnetic or mechanical stirring of a mixture of a DOTP solution of Desmodur® N 3300 and an aqueous solution of DETA (Figure 5.15).

BPEA and **ZW5** solutions were also encapsulated independently in order to check their fluorescence properties after the polymerisation reaction (**BPEA@PU_DOTP** and **ZW5@PU_DOTP**). The capsules obtained were greenish yellow when loaded with **BPEA** and pale pink for **ZW5** (Figure 5.16(a)). Since DOTP possesses nearly the same density as water, no phase separation was observed when stirring was stopped. Therefore, in order to separate the capsules formed from the reaction mother liquor, a sodium sulphate solution was added to induce capsule migration towards the liquid-air interface. After thoroughly washes with water, capsules were lyophilised and collected as a loose powder without traces of oil.

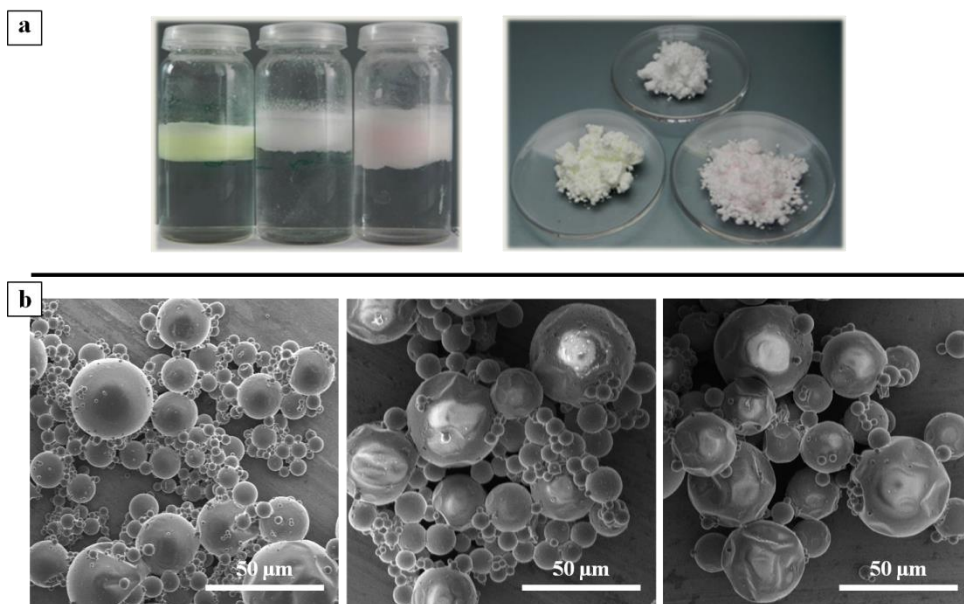


Figure 5.16 (a) Photographs of the capsules prepared before and after lyophilisation: **PU_DOTP** (white, $10 \pm 10 \mu\text{m}$), **BPEA@PU_DOTP** (greenish yellow, $14 \pm 9 \mu\text{m}$) and **ZW5@PU_DOTP** (pink, $11 \pm 10 \mu\text{m}$). **(b)** SEM images of these capsules. In the case of **PU_DOTP**, it was registered for an untreated sample, while they were measured seven months and a half after the drying process for **BPEA@PU_DOTP** and **ZW5@PU_DOTP**.

Capsule morphology was studied by SEM and optical microscopy, as done in the previous chapters (Figure 5.16(b)). The resulting spherical capsules were polydisperse, though

smaller and with smoother surfaces than those obtained at the same reaction conditions using miglyol as oil (e.g. **VT1@PU_mig**, see figure 4.26 in section 4.2.2.3). Negligible changes in size or shape due to dye loading were noticed, and the average diameter of the polyurea capsules prepared was approximately 12 μm ($12 \pm 10 \mu\text{m}$). After lyophilisation, most capsules remained unbroken and only a very small amount of collapsed capsules could be found. Besides, they retained their structure when heated at 358 K (i.e. the maximum temperature to be scanned in our colour tuning experiments), and at least seven months and a half after the drying process.

Capsule fluorescence was first checked with an optical microscope in reflected light fluorescence mode (Figure 5.17). Two different filter sets were used allowing to record emissions at $\lambda > 515 \text{ nm}$ and $\lambda > 590 \text{ nm}$, thus selectively detecting the fluorescence from **BPEA** and **ZW5**, respectively.

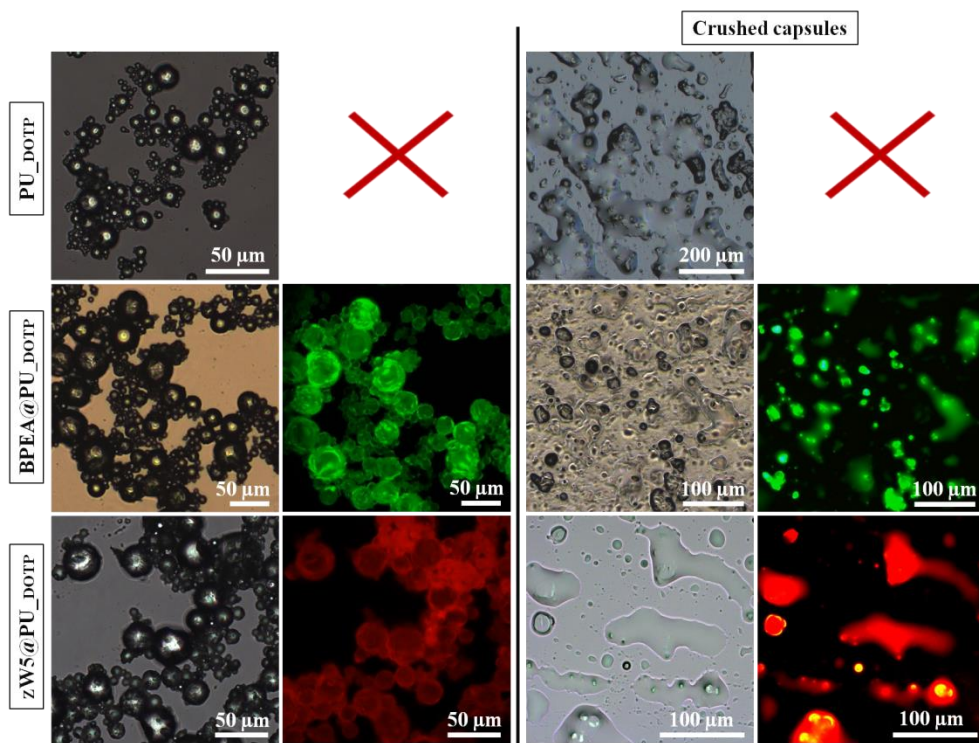


Figure 5.17 Optical micrographs of **PU_DOTP**, **BPEA@PU_DOTP** and **ZW5@PU_DOTP** capsules before and after mechanical crushing. The fluorescence images were taken at $\lambda_{\text{exc}} = 450\text{-}490 \text{ nm}$ and $\lambda_{\text{em}} > 515 \text{ nm}$ for **PU_DOTP** and **BPEA@PU_DOTP**, and at $\lambda_{\text{exc}} = 540\text{-}552 \text{ nm}$ and $\lambda_{\text{em}} > 590 \text{ nm}$ for **ZW5@PU_DOTP**.

Clearly, intense green and red emission was registered for **BPEA@PU_DOTP** and **ZW5@PU_DOTP**, while no fluorescence was measured for dye-free **PU_DOTP** capsules at the same conditions. When crashed, ejection of the liquid interior of the capsules was also confirmed by optical microscopy (Figure 5.17). For **BPEA@PU_DOTP** and **ZW5@PU_DOTP**, this resulted in the formation of fluorescent liquid droplets onto the glass microscopy substrate, thus demonstrating the encapsulation of the dye molecules into the interior of the capsules.

The SEM image of Figure 5.18 shows the wrinkles formed on capsule surface after being smashed, and dye crystallization once the oil was removed. The average shell thickness of the capsules was about 250 nm according to SEM measurements, and the oil content was found to account for around the 88 wt% of capsules total mass. By analysing the absorption spectrum of the liquid ejected, the loading efficiencies estimated for the capsules were 70% for **BPEA** and 80% for **ZW5**, approximately. Taking into account the largest dye concentrations used in the encapsulation process ($\sim 10^{-4}$ M for both dyes), this means that **PU_DOTP** capsules were prepared with payloads ($\text{g}_{\text{dye}} / \text{g}_{\text{capsules}} \%$) as high as 0.002 % and 0.013% in **BPEA** and **ZW5**, respectively. In any case, lower concentrations and payloads were required to achieve energy transfer-free white-light emission, as discussed above.

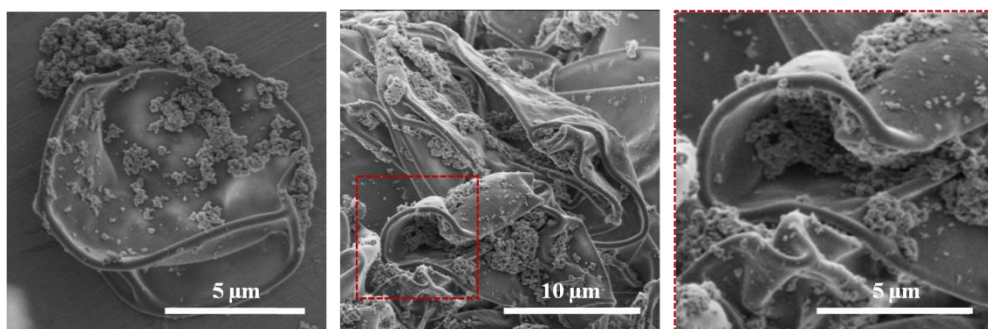


Figure 5.18 SEM images of **ZW5@PU_DOTP** capsules without their liquid core after been smashed.

Finally, we investigated in more detail the maintenance of **BPEA** and **ZW5** fluorescent properties upon encapsulation within **PU_DOTP** capsules. Equivalent emission spectra were measured for **BPEA** and **ZW5** in DOTP solution outside and into the capsules. When monitoring the thermal dependence of **ZW5@PU_DOTP** emission, however, some little differences were found with respect to **ZW5** in free solution. Thus, though both samples behave qualitatively the same, smaller changes in fluorescence intensity were measured

upon temperature variation after encapsulation. For instance, when heating from 273 and 353 K, a 60% emission reduction was registered for **ZW5@PU_DOTP**, while a 80% decrease had been determined before encapsulation. We mainly ascribe this result to inefficient heat diffusion from the temperature-controlled bath surrounding the **ZW5@PU_DOTP** powder sample to the internal core of the capsules where the thermally-sensitive **ZW5** molecules lie. As a consequence, lower temperatures than those externally applied should be achieved in the capsules interior, thus leading to smaller changes in emission intensity than expected.

In spite of this and in view of the overall good properties of the capsules prepared, encapsulation of **BPEA-ZW5** mixtures into **PU_DOTP** was next undertaken to finally attain thermally-tunable white-light emission from microstructured solid materials.

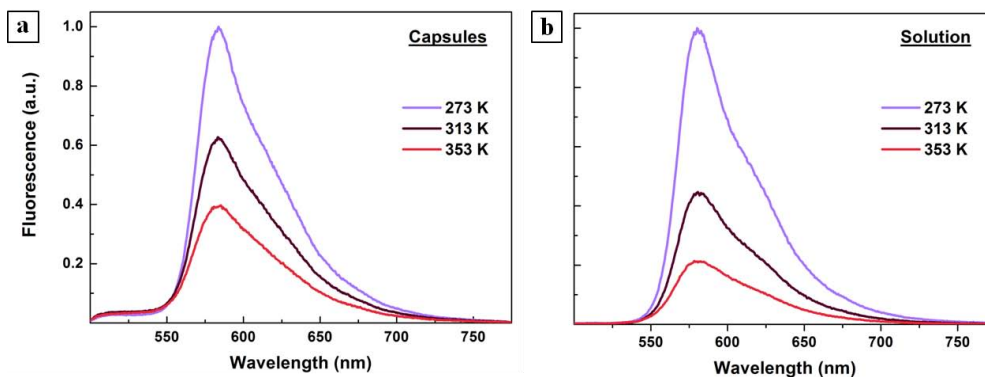


Figure 5.19 Fluorescence spectra of (a) **ZW5@PU_DOTP** capsules and (b) **ZW5** solution in DOTP ($8.4 \cdot 10^{-5}$ M), at 273, 313 and 353 K ($\lambda_{\text{exc}} = 473$ nm).

5.2.2 Selection of dye relative concentration and encapsulation of the optimized solution: preparation of **BPEA-ZW5@PU_DOTP** capsules

To obtain white-light emission from a mixture of **BPEA** and **ZW5** at room temperature, an adequate concentration ratio of both dyes had to be used. To determine this ratio we investigated how the emission colour varied when adding increasing amounts of **ZW5** to a **BPEA** solution in DOTP at room temperature. In these experiments, a low concentration of **BPEA** was considered (10^{-6} M), since this should allow minimising interchromophoric interactions and, therefore, energy transfer processes in the final capsules. Actually,

Dexter/Förster energy transfer can be enhanced by diffusion if the distance diffused during the excited-state lifetime of the donor is comparable or greater than the mean distance between donor and acceptors⁶⁹. The parameter determining the effect of diffusion is given by the following equation:

$$\tau_0/s^2 \quad (5.3)$$

in which D is the sum of the diffusion coefficients of the donor and the acceptor, τ_0 the lifetime of the donor in absence of energy transfer, and s the mean distance between donor and acceptor. Assuming 5-ns fluorescence lifetime for **BPEA** in DOTP⁷⁰, 10^{-6} M concentration for both species and diffusion coefficients⁷¹ around $3 \cdot 10^{-13}$ and $6 \cdot 10^{-13}$ m s⁻¹ for **BPEA** and **ZW5**; we estimated that there would not be any effect of the dye diffusion ($D\tau_0/s^2 \ll 1$), and therefore, energy transfer processes can be discarded at the concentrations of choice. On the other hand, in order to simultaneously excite both dyes, avoid significant thermal variations in **BPEA** fluorescence and reduce the amount of **ZW5** required (i.e. obtain the same emission intensity with a lower concentration of dye), the irradiation wavelength selected for the experiments performed was ~ 428 nm.

Fluorescence changes registered upon **ZW5** successive additions to the diluted **BPEA** solution are shown in Figure 5.21(a). Considering 2.1% content in the fluorescent isomer for **ZW5-Ar3** mixtures in DOTP at room temperature, **ZW5** concentrations added ranged from $5.1 \cdot 10^{-7}$ to $4.2 \cdot 10^{-5}$ M, which correspond to **BPEA:ZW5** ratios of 1:0.4 and 1:37.2, respectively. The chromaticity diagram shown Figure 5.21(b) collects the chromaticity coordinates of the resulting emissions for the **BPEA-ZW5** mixtures analysed. As expected, the colour emitted varied from **BPEA** dark turquoise, when no **ZW5** was added, to yellowish white at the end of the titration (0.333, 0.421; at $4.2 \cdot 10^{-5}$ M).

Note that in contrast to what should be expected in absence of interchromophoric interaction, the chromaticity coordinates did not completely match with those estimated from **BPEA** and **ZW5** individual solutions (0.329, 0.442). Moreover, those determined for **BPEA-ZW5** mixtures did not lie on a perfect straight line in the chromaticity diagram. Based on the changes observed in the shape of the emission spectrum of **BPEA** upon **ZW5** addition, we ascribed this small deviations to **BPEA** fluorescence reabsorption by **ZW5** as the concentration of the latter in the mixture increased (inner-filter effect), which essentially affected the photons emitted in the region of spectral overlap (~ 490 -550 nm).

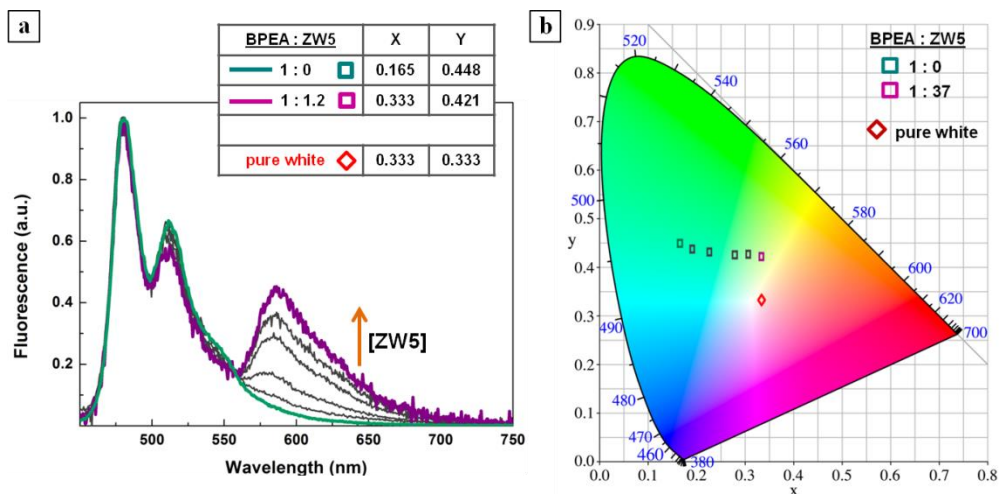


Figure 5.20 (a) Fluorescence spectra (excitation wavelength: 430 nm) acquired by adding increasing concentrations of **ZW5** (from $5.1 \cdot 10^{-7}$ M to $4.2 \cdot 10^{-5}$ M) to a $1.2 \cdot 10^{-6}$ M **BPEA** solution; and table summarizing the colour variation illustrated by the changes on the chromaticity coordinates. (b) Chromaticity diagram collecting the chromaticity coordinates of the spectral variations resulting from the titration showed in (a).

This effect was unavoidable in our solution measurements due to the geometry of our experiments, where a 1-cm optical path cuvette was used and fluorescence was detected in transmission mode and at 90° with respect to the excitation beam. As such, the **BPEA** emitted photons had to travel through approximately 0.5-cm solution of **ZW5** before reaching the detector, thus suffering from reabsorption processes at high enough **ZW5** concentrations. We expect this situation to be prevented upon encapsulation and, eventually, separate detection of micrometer-sized volumes of **BPEA-ZW5** mixtures. Consequently, some discrepancies may be observed between the colours determined in solution and the capsule measurements. In spite of this, we took the results obtained from the titration experiment in solution as a reference for the calculation of the **BPEA:ZW5** ratio to be encapsulated.

To extrapolated the **BPEA:ZW5** ratio required to achieve white-light emission in DOTP solution at room temperature to capsule synthesis, we considered the loading efficiency of each dye and the extent of **ZW5** intensity changes after encapsulation with respect to the free solution situation. In this way, we estimated that 1:64 was the **BPEA:ZW5** ratio needed prior to the encapsulation for a **BPEA** solution of 10^{-6} M. This mixed-dye solution was then encapsulated into polyurea capsules as previously described (Figure 5.15). In this case,

however, an ultra-turrax[®] homogenizer was used to prepare the oil/water emulsion with the purpose of decreasing polydispersity in the final particles.

The resulting capsules (**BPEA+ZW5@PU_DOTP**) were collected as a bright-pink powder after lyophilisation (Figure 5.21(a)). They presented sphere-like morphologies with an average size of $8 \pm 5 \mu\text{m}$ with $177 \pm 74 \text{ nm}$ of shell thickness. The SEM images of Figure 5.21(b-c) display the smoothness of the outer and the inner shell and their hollow interior. Moreover, capsule fluorescence was easily recorded by means of an optical microscope. As shown in the optical images of Figure 5.21(d), simultaneous emission in the **BPEA** and **ZW5** spectral ranges was detected, thus proving the entrapment of both dyes inside the capsules interior.

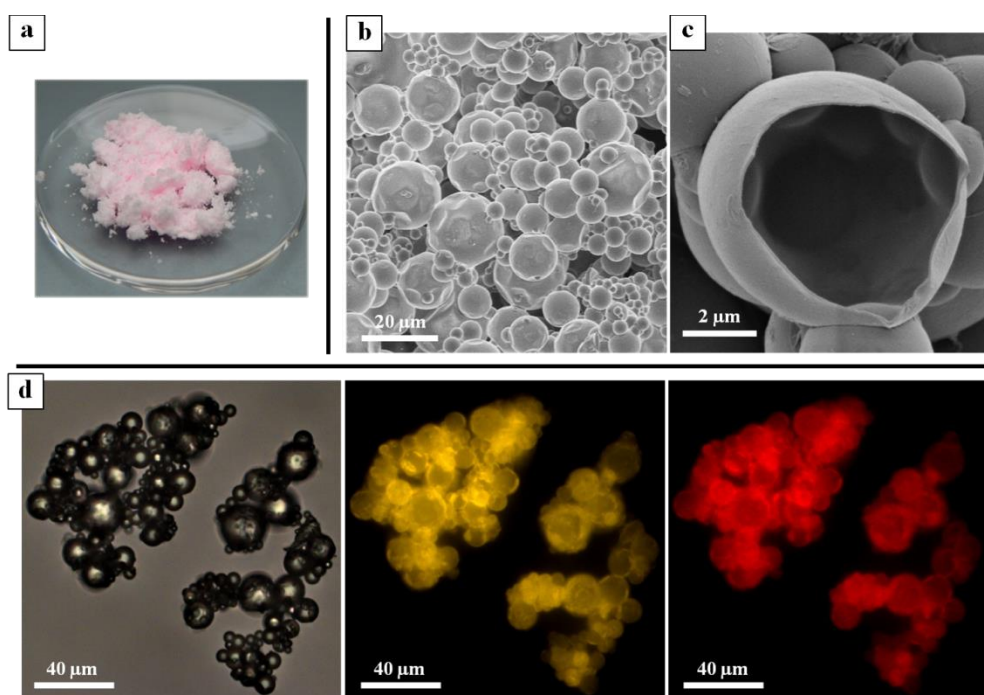


Figure 5.21 BPEA+ZW5@PU_DOTP images. (a) Photograph of the pink powder obtained after capsules synthesis and lyophilisation. (b) SEM image of the sample six months after lyophilisation. (c) SEM image of a broken capsule exhibiting its hollow interior and the shell thickness. (d) Optical micrograph and fluorescence images of the mixed-dye loaded capsules, which were taken at two different conditions: $\lambda_{\text{exc}} = 450\text{-}490 \text{ nm}$ and $\lambda_{\text{em}} > 515 \text{ nm}$ (yellow, mainly **BPEA** fluorescence) and $\lambda_{\text{exc}} = 540\text{-}552 \text{ nm}$ and $\lambda_{\text{em}} > 590 \text{ nm}$ (red, **ZW5** fluorescence).

5.2.3 Colour-tunable white-light emission from liquid-filled capsules

Once prepared, we investigated the white-light emission and colour tunability capabilities of **BPEA+ZW5@PU_DOTP**. With this aim, we acquired the fluorescence spectrum of this solid sample at $\lambda_{\text{exc}} = 428$ nm, in reflection mode and upon temperature variation between 248 K and 358 K (Figure 5.22(a)). These thermal range was selected in order to maximize the extent of the colour variation of the light emitted. The chromaticity diagram of Figure 5.22 depicts the resulting colours emitted at each temperature, while the table inserted in this figure summarizes the most relevant chromaticity coordinates. As can be observed, dyes fluorescence behaviour was not modified when mixed, and capsule emission could be tuned reversibly from bright orange to dark turquoise upon heating.

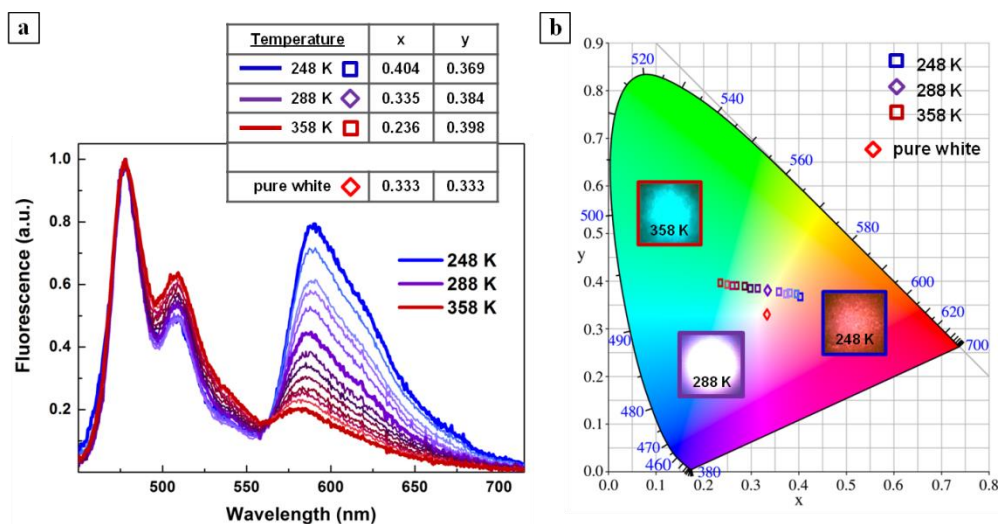


Figure 5.22 (a) **BPEA+ZW5@PU_DOTP** fluorescence spectral changes with temperature and table summarizing the colour variation illustrated by the changes on the chromaticity coordinates. The spectra were acquired at $\lambda_{\text{exc}} = 428$ nm and upon heating from 248 to 358 K by increments of 10 K, including also 273 K. (b) Chromaticity diagram collecting the resulting chromaticity coordinates of the spectra in (a). The insets show pictures of the colour emitted by a cuvette filled with **BPEA+ZW5@PU_DOTP** capsules at 248, 288 and 358 K.

As already discussed, this was achieved by thermally varying the concentration of the orange-emitting **ZW5** dye in the mixture, its conversion into the non-fluorescent **Ar3** isomer being favoured as the temperature increased. Actually, according to our previous measurements, we estimated the **BPEA:ZW5** molar ratio to change from 1:58 (248 K) to 1:9 (358 K) throughout our experiments, thus accounting for the large colour variation

between these two temperatures. Such a variation can be visually observed in the photographs shown in Figure 5.22(b) of the emission stemming from a solid sample of **BPEA+ZW5@PU_DOTP** at 248 and 358 K.

An additional photograph is given in this figure, which corresponds to the temperature (288 K) at which the closest chromaticity coordinates to pure white, (0.335, 0.384), were obtained. This corresponded to a yellowish white light fairly similar to pure white light, and their chromaticity coordinates rather satisfactorily compared with those directly predicted by mixing the separate colours of **BPEA** and **ZW5** emission in DOTP (0.329, 0.420), see Figure 5.14(a). Therefore, this demonstrates that the strategy followed in our work allowed to minimise the energy transfer processes between the fluorophores chosen and, in this way, simplify the experimental work required to find the proper dye concentration ratio for white-light generation. In our case, the small deviation observed with respect to the predicted colour should be attributed to **BPEA** fluorescence reabsorption by **ZW5**, which resulted in a non-negligible decrease of **BPEA** emission in the 490-550 nm region at low temperatures (i.e. at high **ZW5** concentrations, Figure 5.22(a)). In contrast to what was expected, this could not be fully prevented in our solid state fluorescence measurements registered in reflection mode, probably because the excitation beam penetrated deep enough into the sample and the resulting emission had to travel through a significant amount of capsules before reaching the detector. We believe that this effect would be insignificant if instead of acquiring capsule fluorescence in bulk we could perform these measurements over one/few capsules at the microscale, which would allow the real colour arising from the selected **BPEA-ZW5** mixture to be registered. Unfortunately, these experiments could not be performed along this thesis owing to the lack of the proper equipment to vary the temperature of the capsules in situ when monitored under the fluorescence microscope.

A further difference between the final behaviour of the **BPEA+ZW5@PU_DOTP** sample and that predicted according to our preliminary experiments had to do with the temperature required to achieve white-light emission. As already commented, it was experimentally found to take place at 288 K, although the concentration ratio in the dye mixture was designed to produce white light at 298 K. This discrepancy must be ascribed to two different factors: (i) reabsorption processes affecting independent dye emission, as already discussed; (ii) the inaccuracy of the estimates done based on our previous fluorescence measurements in solution and for the capsules loaded with individual dyes (e.g. differences in chromophore loading efficiencies during the preparation of **BPEA+ZW5@PU_DOTP**). Despite all this, a

good agreement was found between the real and predicted temperatures for white emission, thus proving the viability of our approach. Furthermore, this result demonstrates the advantage of introducing thermal colour control into the final material, since it enabled us to fine tuning the optimal emission ratio between the two dyes selected in order to achieve white-light emission. It must be noted that an additional experimental parameter could be used to adjust the colour emitted by **BPEA+ZW5@PU_DOTP** and produce white light at room temperature instead of at 288 K. Although it was not explicitly considered in our work, the difference in absorption spectra between **BPEA** and **ZW5** should allow changes in excitation wavelength to shift the colours obtained to higher (or lower) temperatures, thus accomplishing white-light emission in the desired thermal range. As such, **BPEA+ZW5@PU_DOTP** capsules would behave as white-light emitting solid materials whose colour emission could be tuned by means of two different external stimuli: temperature and frequency of the excitation beam.

5.3 Conclusions

In this chapter we have described a third possible application of liquid-filled capsules for the preparation of stimuli-responsive photoactive materials. Herein, liquid-filled capsules loaded with mixtures of **ZW5** and **BPEA** fluorescent dyes have been employed to produce microstructured solid materials displaying white-light emission at room temperature as well as thermally-induced colour tunability. From the results described above, the following conclusions can be drawn:

- (i) We have demonstrated the synthesis of liquid-filled capsules loaded with diluted solutions of complementary fluorescent dyes, capable to display white-light emission at around room temperature without requiring any energy transfer process.
- (ii) We have also proved that the tunability of the colour emitted in solid state can be obtained by using a temperature-responsive fluorophore as one of the two complementary dyes encapsulated in the interior of the liquid-filled capsules. Since the overall colour emitted arises from the combination of the concurrent emission of the two compounds encapsulated, and the dye ratio in the capsule core varies according to the tautomerisation equilibrium of the thermochromic dye, the final colour emitted can be thermally controlled.

In particular, we have shown the possibility to tune the colour emitted by the capsules prepared from turquoise to orange between 248 and 358 K, attaining white light at 288 K.

(iii) On the other hand, the selection of capsule liquid core is decisive for obtaining the desired chromic behaviour. In addition to preserve the thermochromic interconversion responsible for the colour tunability, it also determines the range of temperatures in which the system can be employed and, therefore, the extent of the colour modulation.

(iv) Importantly, this approach allows almost direct transfer of the solution behaviour of the separate dyes into the final materials, avoiding the repetitive and time-consuming experiments needed to find the optimal settings for white-light emission that are required in several of the strategies reported in the bibliography.

(iii) In spite of this, non-negligible reabsorption processes affect the performance of the solid capsules in bulk, which should be prevented employing just one or few capsules and studying the performance of the system in the microscale. We believe that in this way we would be able to observe the real colour arising from the **BPEA-ZW5** mixture encapsulated.

5.4 References

1. Kamtekar, K. T., Monkman, A. P. & Bryce, M. R. Recent advances in white organic light-emitting materials and devices (WOLEDs). *Adv. Mater.* **22**, 572–582 (2010).
2. D'Andrade, B. W. & Forrest, S. . White organic light-emitting devices for solid-state lighting. *Adv. Mater.* **16**, 1585–1595 (2004).
3. Farinola, G. M. & Ragni, R. Electroluminescent materials for white organic light emitting diodes. *Chem. Soc. Rev.* **40**, 3467–3482 (2011).
4. Wu, H., Ying, L., Yang, W. & Cao, Y. Progress and perspective of polymer white light-emitting devices and materials. *Chem. Soc. Rev.* **38**, 3391–3400 (2009).
5. Xiao, L. *et al.* Recent progresses on materials for electrophosphorescent organic light-emitting devices. *Adv. Mater.* **23**, 926–952 (2011).
6. Mukherjee, S. & Thilagar, P. Organic white-light emitting materials. *Dyes and Pigments* **110**, 2–27 (2014).

7. He, G. *et al.* A color-tunable europium complex emitting three primary colors and white light. *Angew. Chem. Int. Ed.* **48**, 6132–6135 (2009).
8. Chen, J., Zeng, F., Wu, S., Su, J. & Tong, Z. Photoreversible fluorescent modulation of nanoparticles via one-step miniemulsion polymerization. *Small* **5**, 970–978 (2009).
9. Chen, J. *et al.* Design and synthesis of FRET-mediated multicolor and photoswitchable fluorescent polymer nanoparticles with tunable emission properties. *J. Phys. Chem. B* **116**, 4354–4362 (2012).
10. Nishiyabu, R., Sugino, Y. & Kubo, Y. White-light emitting boronate microparticles for potential use as reusable bright chemosensors in water. *Chem. Commun.* **49**, 9869–9871 (2013).
11. Shiraishi, Y., Ichimura, C., Sumiya, S. & Hirai, T. Multicolor fluorescence of a styrylquinoline dye tuned by metal cations. *Chem. Eur. J* **17**, 8324–8332 (2011).
12. Wyman, C., Sloan, P. & Shirley, P. Simple analytic approximations to the CIE XYZ color matching functions. *J. Comput. Graph. Tech.* **2**, 1–11 (2013).
13. Snyder, L. S., Ed: Helander, M. G., Landauer, T. K. & Prabhu, P. V. *Image Quality (in Handbook of Human-Computer Interaction)*. (Elsevier, 1997).
14. Ohno, Y. CIE Fundamentals for Color Measurement. *IS&T NIP16 Conf.* (2000). at <<http://wenku.baidu.com/view/18a92173f242336c1eb95e84.html>>
15. CIE - INTERNATIONAL COMMISSION ON ILLUMINATION. at <<http://www.cie.co.at/>>
16. Interactive 1931 CIE Chromaticity Diagram. at <<http://www.biyee.net/color-science/cie-chromaticity-diagram/>>
17. Schubert, E. F. *Light-Emitting Diodes*. (Cambridge University Press, 2006). at <<http://www.cambridge.org/us/academic/subjects/engineering/electronic-optoelectronic-devices-and-nanotechnology/light-emitting-diodes-2nd-edition>>
18. Yu, X. *et al.* High-efficiency white organic light-emitting devices based on a highly amorphous iridium (III) orange phosphor. *Chem. Mater.* **18**, 5097–5103 (2006).
19. Bairi, P., Roy, B., Chakraborty, P. & Nandi, A. K. Co-assembled white-light-emitting hydrogel of melamine. *ACS Appl. Mater. Interfaces* **5**, 5478–5485 (2013).
20. Yang, Q.-Y. & Lehn, J.-M. Bright white-light emission from a single organic compound in the solid state. *Angew. Chem.* **126**, 4660–4665 (2014).

21. Liu, D., Zhang, Z., Zhang, H. & Wang, Y. A novel approach towards white photoluminescence and electroluminescence by controlled protonation of a blue fluorophore. *Chem. Commun.* **49**, 10001–10003 (2013).
22. Coppo, P., Duati, M., Kozhevnikov, V. N., Hofstraat, J. W. & De Cola, L. White-light emission from an assembly comprising luminescent iridium and europium complexes. *Angew. Chem. Int. Ed.* **44**, 1806–1810 (2005).
23. Gilbert, A. & Baggot, J. *Essentials of Molecular Photochemistry*. (Blackwell Scientific Publications, 1991).
24. Lackowicz, J. R. *Principles of Fluorescence Spectroscopy*. (Springer, 2006).
25. Kwon, J. E., Park, S. & Park, S. Y. Realizing molecular pixel system for full-color fluorescence reproduction: RGB-emitting molecular mixture free from energy transfer crosstalk. *J. Am. Chem. Soc.* **135**, 11239–11246 (2013).
26. Varghese, R. & Wagenknecht, H.-A. White-light-emitting DNA (WED). *Chem. Eur. J* **15**, 9307–9310 (2009).
27. Maiti, D. K. & Banerjee, A. A peptide based two component white light emitting system. *Chem. Commun.* **49**, 6909–6911 (2013).
28. Balan, B., Vijayakumar, C., Ogi, S. & Takeuchi, M. Oligofluorene-based nanoparticles in aqueous medium: hydrogen bond assisted modulation of functional properties and color tunable FRET emission. *J. Mater. Chem.* **22**, 11224–11234 (2012).
29. Tseng, K.-P. *et al.* Spontaneous generation of highly emissive RGB organic nanospheres. *Angew. Chem. Int. Ed.* **50**, 7032–7036 (2011).
30. Giansante, C., Schäfer, C., Raffy, G. & Del Guerzo, A. Exploiting direct and cascade energy transfer for color-tunable and white-light emission in three-component self-assembled nanofibers. *J. Phys. Chem. C* **116**, 21706–21716 (2012).
31. Praveen, V. K., Ranjith, C. & Armaroli, N. White-light-emitting supramolecular gels. *Angew. Chem. Int. Ed.* **53**, 365–368 (2014).
32. Abbel, R. *et al.* Multicolour self-assembled fluorene co-oligomers: from molecules to the solid state via white-light-emitting organogels. *Chem. Eur. J.* **15**, 9737–9746 (2009).
33. Yang, X., Zhou, G. & Wong, W.-Y. Recent design tactics for high performance white polymer light-emitting diodes. *J. Mater. Chem. C* **2**, 1760–1778 (2014).
34. Hendler, N., Belgorodsky, B., Mentovich, E. D., Gozin, M. & Richter, S. Efficient separation of dyes by mucin: toward bioinspired white-luminescent devices. *Adv. Mater.* **23**, 4261–4264 (2011).

35. Kim, S., Seo, J., Jung, H. K., Kim, J.-J. & Park, S. Y. White luminescence from polymer thin films containing excited-state intramolecular proton-transfer dyes. *Adv. Mater.* **17**, 2077–2082 (2005).
36. Gao, H. *et al.* Site isolation of emitters within cross-linked polymer nanoparticles for white electroluminescence. *Nano Lett.* **10**, 1440–1444 (2010).
37. Park, S. *et al.* A White-Light-Emitting Molecule: Rustrated Energy Transfer between Constituent Emitting Centers. 14043–14049 (2009).
38. Sun, W. *et al.* Understanding solvent effects on luminescent properties of a triple fluorescent ES IPT compound and application for white light emission. *J. Phys. Chem. A* **113**, 5888–5895 (2009).
39. Peng, a.-D., Xiao, D.-B., Ma, Y., Yang, W.-S. & Yao, J.-N. Tunable Emission from Doped 1,3,5-Triphenyl-2-pyrazoline Organic Nanoparticles. *Adv. Mater.* **17**, 2070–2073 (2005).
40. Ajayaghosh, A., Praveen, V. K., Vijayakumar, C. & George, S. J. Molecular wire encapsulated into pi organogels: efficient supramolecular light-harvesting antennae with color-tunable emission. *Angew. Chem. Int. Ed.* **46**, 6260–6265 (2007).
41. Samanta, S. K. & Bhattacharya, S. Aggregation induced emission switching and electrical properties of chain length dependent π -gels derived from phenylenedivinylene bis-pyridinium salts in alcohol–water mixtures. *J. Mater. Chem.* **22**, 25277–25287 (2012).
42. Huynh, H. V, He, X. & Baumgartner, T. Halochromic generation of white light emission using a single dithienophosphole luminophore. *Chem. Commun.* **49**, 4899–4901 (2013).
43. Zhang, X., Rehm, S., Safont-Sempere, M. M. & Würthner, F. Vesicular perylene dye nanocapsules as supramolecular fluorescent pH sensor systems. *Nature Chem.* **1**, 623–629 (2009).
44. Molla, M. R. & Ghosh, S. Hydrogen-bonding-mediated J-aggregation and white-light emission from a remarkably simple, single-component, naphthalenediimide chromophore. *Chem. Eur. J* **18**, 1290–1294 (2012).
45. Karpiuk, J., Karolak, E. & Nowacki, J. Tuneable white fluorescence from intramolecular exciplexes. *Phys. Chem. Chem. Phys.* **12**, 8804–8809 (2010).
46. Bhattacharya, S. & Samanta, S. K. Unusual salt-induced color modulation through aggregation-induced emission switching of a bis-cationic phenylenedivinylene-based π hydrogelator. *Chem. Eur. J* **18**, 16632–16641 (2012).

47. Alam, M. M. & Jenekhe, S. A. Binary blends of polymer semiconductors: nanocrystalline morphology retards energy transfer and facilitates efficient white electroluminescence. *Macromol. Rapid Commun.* **27**, 2053–2059 (2006).
48. Xu, J., Liang, J., Li, J. & Yang, W. Multicolor dye-doped silica nanoparticles independent of FRET. *Langmuir* **26**, 15722–15725 (2010).
49. Yang, X. *et al.* Carbazole-based organogel as a scaffold to construct energy transfer arrays with controllable fluorescence emission. *Langmuir* **24**, 13730–13735 (2008).
50. Melucci, M. *et al.* Facile tuning from blue to white emission in silica nanoparticles doped with oligothiophene fluorophores. *J. Mater. Chem.* **20**, 9903–9909 (2010).
51. Malinge, J., Allain, C., Brosseau, A. & Audebert, P. White fluorescence from core-shell silica nanoparticles. *Angew. Chem. Int. Ed.* **51**, 8534–8537 (2012).
52. Lei, Y., Liao, Q., Fu, H. & Yao, J. Orange-blue-orange triblock one-dimensional heterostructures of organic microrods for white-light emission. *J. Am. Chem. Soc.* **132**, 1742–1743 (2010).
53. Hetero-epitaxy, O. À. O. *et al.* Color tuning of nanofibers by periodic organic-organic hetero-epitaxy. *ACS Nano* **6**, 4629–4638 (2012).
54. Lei, Y.-L. *et al.* White-light emitting microtubes of mixed organic charge-transfer complexes. *Adv. Mater.* **24**, 5345–5351 (2012).
55. Wang, X., Yan, J., Zhou, Y. & Pei, J. Surface modification of self-assembled one-dimensional organic structures: white-light emission and beyond. *J. Am. Chem. Soc.* **132**, 15872–4 (2010).
56. Nishiyabu, R., Sugino, Y. & Kubo, Y. White-light emitting boronate microparticles for potential use as reusable bright chemosensors in water. *Chem. Commun.* **49**, 9869–9871 (2013).
57. Zhang, X., Görl, D. & Würthner, F. White-light emitting dye micelles in aqueous solution. *Chem. Commun.* **49**, 8178–81780 (2013).
58. Wang, R., Peng, J., Qiu, F. & Yang, Y. Enhanced white-light emission from multiple fluorophores encapsulated in a single layer of diblock copolymer micelles. *Chem. Commun.* **47**, 2787–2789 (2011).
59. Wang, R., Peng, J., Qiu, F., Yang, Y. & Xie, Z. Simultaneous blue, green, and red emission from diblock copolymer micellar films: a new approach to white-light emission. *Chem. Commun.* 6723–6725 (2009).
60. Rao, K. V., Datta, K. K. R., Eswaramoorthy, M. & George, S. J. Highly pure solid-state white-light emission from solution-processable soft-hybrids. *Adv. Mater.* **25**, 1713–1718 (2013).

61. Prats, G. (UAB). Activación electroquímica de interruptores moleculares en sistemas fotocromicos y ácido-base. *Ph.D Thesis* (2012).
62. Gime, R., Pin, M. & Serrano, L. Luminescent liquid crystals derived from 9,10-bis(phenylethynyl)anthracene. *Chem. Mater.* **16**, 1377–1383 (2004).
63. Levitus, M. & Garcia-garibay, M. A. Polarized electronic spectroscopy and photophysical properties of 9,10-bis(phenylethynyl)anthracene. *J. Phys. Chem. A* **104**, 8632–8637 (2000).
64. Al-Kaysi, R. O., Guirado, G. & Valente, E. J. Synthesis and characterization of a new fluorescent zwitterionic spirocyclic Meisenheimer complex of 1,3,5-trinitrobenzene. *Eur. J. Org. Chem.* **2004**, 3408–3411 (2004).
65. Gallardo, I. & Guirado, G. Electrochemical mechanism of spiro and zwitterionic Meisenheimer compounds: A potential fluorescence molecular switching system. *Electrochem. Commun.* **9**, 173–179 (2007).
66. Miglyol® 812 - Safety data sheet. *Cremer (Oleo Division)*
67. Dioctyl terephthalate (Properties). *Sigma-Aldrich Catalogue*
68. Demeter, A. First steps in photophysics. I. Fluorescence yield and radiative rate coefficient of 9,10-Bis(phenylethynyl)anthracene in paraffins. *J. Phys. Chem. A* **118**, 9985–9993 (2014).
69. Stryer, L., Thomas, D. D. & Meares, C. F. Diffusion enhanced fluorescence energy transfer. *Annu. Rev. Biophys. Bioeng.* **11**, 203–222 (1982).
70. Overestimation of actual dye lifetimes, since BPEA's lifetime in organic solvents lies between 3-4 ns.
71. Diffusion coefficients estimated using the Stokes-Einstein equation considering DOTP viscosity at 298 K and the molecular radius obtained by geometry minimisation calculations with ChemDraw.

Chapter 6

General Conclusions

6.1 General conclusions

In the present doctoral thesis we have demonstrated the fabrication of different types of photofunctional materials based on the encapsulation of photochromic and thermochromic compounds inside liquid-filled polymeric capsules. The encapsulation of solutions of these compounds in the hollow interior of polymeric capsules has not only allowed to retain the enhanced chromic properties that they present in solution, but also to easily tune their stimuli-responsive behaviour. In particular:

(i) *Fast-responsive photochromic materials* were successfully prepared through the encapsulation of photochromic solutions into liquid-filled microcapsules and their subsequent incorporation in polymeric rigid matrices. We have proven that these materials present solution-like colour fading kinetics about one order of magnitude faster than those measured upon direct dispersion of the photosensitive molecules into rigid polymer thin films and solid particles, independently of the nature of the photochromic compound or the encapsulating matrix used. Moreover, the rapid decolouration rates obtained for capsule-containing polymer films and test lens matrices matches the best results reported so far in the bibliography.

(ii) *Robust structures presenting solution-like valence tautomerism in the solid state* were obtained by the encapsulation of thermochromic VT complexes into solid polymeric particles and liquid-filled polymeric capsules. We have proved that the solid polymeric particles prepared retain the thermochromic behaviour of the compounds encapsulated, although in a restricted range of concentrations, polymers and temperatures. On the other hand, liquid-filled polymeric capsules containing VT compounds, have demonstrated to (i) be capable of nicely reproduce the valence tautomerism observed in solution, (ii) allow the fine tuning of the T_c that characterises the thermochromic behaviour just by simply modifying the solvent confined into their core (without the need of synthetic modification of the complex of choice), and (iii) fully retain the reversibility of the VT interconversion when the appropriate liquid core is selected.

(iii) We have also managed to prepared *microstructured solid materials displaying white-light emission at room temperature as well as thermally-induced colour tunability* without requiring any energy transfer process. These systems are based on the synthesis liquid-filled capsules loaded with diluted mixtures of two complementary fluorescent dyes one of which

consist of a temperature-responsive fluorophore. Since the overall colour emitted arises from the combination of the concurrent emission of the two compounds encapsulated, and the dye ratio in the capsule core varies according to the tautomerization equilibrium of the thermochromic dye, we can thermally control the final colour emitted. In particular, we demonstrated colour modulation from turquoise to orange between 248 and 358 K, attaining white light at 288 K.

The versatility and universality as well as the simplicity of the encapsulation methods required for the liquid-filled capsule strategy introduced in this work, make this approach ideal for the direct transfer of the photochromic and thermochromic behaviour of organic dyes, from solution to the solid state, which is needed for the development of enhanced photofunctional materials.

Chapter 7

Experimental Section

7.1 General procedures

7.1.1 Materials

The dyes employed were purchased from Sigma-Aldrich except complex **VT1** and **ZW5** that were synthesised as previously reported in references 1 and 2, respectively. Miglyol[®] 812 (miglyol) was acquired from Oxy-Med Express S.A., Desmodur[®] N 100 and Desmodur[®] N 3300 from Bayer, PVA 86%-89% hydrolyzed (medium molecular weight) from Alfa-Aesar and the rest of reagents from Sigma Aldrich. All of them were used as received without further purification excepting styrene which, prior to use, was washed four times with an aqueous solution of sodium hydroxide (0.1 M) and then four times with water, to remove the inhibitors. Toluene anhydrous was also acquired from Sigma Aldrich, and the other solvents used (HPLC or spectroscopy quality) were obtained from Teknokroma or Scharlab. Distilled water was employed except when indicated.

7.1.2 Microscopy imaging techniques

Optical microscopy images were obtained using a Zeiss Axio Observer Z1m inverted optical/fluorescence microscope with: motorized XY stage, a halogen lamp (Philips 7724) for transmission and reflection modes, Hg lamp excitation source (HBO 103 W/2) for fluorescence images, AxioCam HRc digital camera and standard filters. The two filter sets employed in this thesis are Zeiss filter set 09 (BP 450-490, FT 510, LP 515) and Zeiss filter set 15 (BP 546/12, FT 580, LP 590). Images of crushed capsules and liquid ejection were obtained by smashing capsules between two cover glass slides. Optical microscopy images obtained with polarized light were acquired with a Leica DMRB microscope and Leica MZ FLIII stereomicroscope (samples were treated with oil to enhance the performance of the equipment).

Scanning electron microscopy (SEM) images were collected on Hitachi S-570, Zeiss Merlin (FE-SEM), FEI Quanta 650F (ESEM) and FEI Magellan 400L XHR microscopes at acceleration voltages between 1.2 and 20 kV. Samples were mounted on SEM metal stubs covered with aluminium tape and coated, when needed, with a thin layer of gold (5-40 nm, depending on the sputtering time). Microcapsules were directly deposited on the aluminium

surface if lyophilized, or by drop casting if dispersed in solution, allowing solvent evaporation in air at room temperature.

Transmission electron microscopy (TEM) images were acquired with Hitachi H-7000, Jeol JEM 1400 and Jeol JEM 2011 microscopes at acceleration voltages between 75 and 200 kV. **Scanning transmission electron microscopy (STEM)** images were obtained with FEI Magellan 400L at 20 kV. In both cases, samples were deposited onto holey carbon grids by drop-casting and dried in air at room temperature.

SEM, TEM and STEM images were processed with Gatan DigitalMicrograph and ImageJ programs for measuring particle sizes and shell thicknesses. For measuring particle diameter, three straight lines with the same length were drawn on each image, and the particles analysed were those beneath them. At least 3 images of each sample and no less than 60 particles were analyzed.

Zeiss Axio Observer Z1m, FEI Quanta 650F and FEI Magellan 400L XHR microscopes are located at the ICN2; and Leica DMRB, Leica MZ FLIII, Hitachi S-570, Zeiss Merlin, Hitachi H-7000, Jeol JEM 1400 and Jeol JEM 2011 microscopes at the Servei de Microscòpia of the UAB.

7.1.3 Optical characterization

Steady-state absorption measurements in solution were performed in a HP 8453 spectrophotometer or Varian Cary 4000 spectrometer. Temperature-dependent spectra were registered using a refrigerated circulator bath (Huber MPC-K6) coupled to the sample holder. Thin-films absorption spectra at different temperatures were recorded on a Perkin Elmer Lambda 35 spectrophotometer equipped with a thermostatic cell holder using PMMA as reference.

Time-dependent absorption measurements were performed using two different instruments: (i) short-timescale measurements ($t = 0\text{-}60$ s) were carried out with a ns laser flash-photolysis system (LKII, Applied Photophysics) equipped with a Nd:YAG laser (Brilliant, Quantel) as pump source, a Xe lamp or a He:Ne laser as probe source and a photomultiplier tube (PMT, R928, Hamamatsu) coupled to a spectrograph as detector; (ii)

long-timescale measurements ($t > 60$ s) were registered in a HP 8453 spectrophotometer. Photoexcitation of **PhI**- and **PhIII**-containing materials was carried out at 355 nm using the third harmonic of the Nd:YAG laser. Capsules with **DR13** molecules were irradiated at 532 nm using the second harmonic of the Nd:YAG laser. For all photochromic solid materials, their thermal back-isomerization was monitored in the dark and at room temperature after reaching their photostationary state.

Reflectance measurements were performed in a Varian Cary 4000 spectrometer with an integrating sphere. Temperature-dependent spectra were registered using a refrigerated circulator bath (Huber MPC-K6) coupled to the sample holder which was mounted against the sphere port. Data was acquired relative to a reference sample consisting on capsules synthesised with the same procedure of those to be measured but without dye. Reflectance values were obtained as percentages (the reference is taken to be 100%) and transformed to the Kubelka-Munk (K-M) function^{3,4}, $F(R_{\infty})$.

Fluorescence emission spectra were acquired using a custom-made spectrofluorometer, where a pulsed or a cw laser is used as excitation source and the emitted photons are detected in an Andor ICCD camera coupled to a spectrograph. Temperature-dependent spectra were registered using a refrigerated circulator bath (Huber MPC-K6) connected to the sample holder. Samples were excited at 428 and 450 nm using the Nd:YAG pulsed laser (Brilliant, Quantel) and at 473 nm with the diode cw laser (SDL-BS-300, company).

Quartz cuvettes were used when required.

7.1.4 Other

Proton nuclear magnetic resonance (¹H-NMR) spectra were recorded in CDCl₃ using Bruker DPX250 (250 MHz for ¹H NMR) and Bruker DPX360 (360 MHz for ¹H NMR) spectrometers located at the Servei de Resonància Magnètica Nuclear of the UAB. Proton chemical shifts are given in δ (ppm) and the abbreviations used to describe the signal multiplicities are s (singlet) and m (multiplet).

X-ray diffraction data was recorded at room temperature on PANalytical 'Pert P O MRD diffractometer working in reflection mode with a Co α radiation source, located at

the ICN2. Samples were placed in an amorphous silicon oxide flat plate and measured directly.

Magnetization measurements. Direct current (dc) magnetic susceptibility measurements were carried out on a Quantum Design MPMS SQUID susceptometer with a 55 kG magnet, located at the ICN2. Data was acquired in a field of 10 kG and, for background correction, measurements were also performed on reference samples (PMMA particles without the VT complex obtained under exactly the same experimental conditions). Diamagnetic corrections estimated from the Pascal contents were applied to all the data recorded for the determination of the molar paramagnetic susceptibilities of the compounds.

Most of the procedures employed for the synthesis of capsules and particles required previous **emulsification** of the dye solutions (dispersed phase) in an aqueous solution (continuous phase) containing emulsion stabilizers and/or surfactants (emulsifiers). The oil-in-water emulsions were prepared using normal magnetic stirrers (agitation rates up to 1600 rpm), a mechanical stirrer (IKA RW20; speed range between 60 to 2000 rpm) or a high-shear homogenizer (IKA ULTRA-TURRAX[®] T18 or T25; 3000-25000 rpm).

Lyophilization was sometimes carried out, for which we employed a TELSTAR CRYODOS -50 freeze dryer with one single stage compressor, giving a refrigerating power of 450 W and a final temperature of 223 K; combined with an Edwards RV12 vacuum pump for a final vacuum pressure of $2 \cdot 10^{-3}$ mbar.

7.2 Synthesis of liquid-filled polymeric capsules

7.2.1 Photochromic capsules

The encapsulation of photochromes **PhI**, **PhIII** and **DR13** was done following the methodologies and procedures described next.

Synthesis of toluene melamine-formaldehyde capsules (MF_tol)

In an attempt to synthesise photochromic melamine-formaldehyde capsules we tried to adapt the procedure described in reference 4. In a 100 mL flat-bottom vial, a toluene solution of

the photochromic dye (15 mg of dye in 2.5 mL of toluene) was emulsified with 35 mL of the emulsifier aqueous solution through magnetic or mechanical stirring (1600 or 2000 rpm). Then, 15 mL of a water solution containing formaldehyde (540 μL) and melamine (0.3 g) monomers was slowly added to the emulsion. The pH was adjusted to 4-5 with phosphoric acid and, after 15 min of agitation, ammonium sulphate (0.66 g) was introduced in the mixture. Subsequently, the temperature was increased to 328 K and the agitation rate was reduced to 700 rpm. The reaction proceeds at these conditions during 2 hours after which microcapsules were formed in the mother liquor. Although stable in solution, the capsules broke and collapsed when filtrated or dried. Therefore, in order to increase the shell resistance we modified the nature and/or the amounts of the emulsifier (5 wt% of Arabic gum; 1 %wt of PVA or Tween[®] 20; from 1 to 20 wt% of PVP (polyvinylpyrrolidone, $M_w \sim 40000$) or SDS), the toluene/water ratio (between 20:1 and 2:1), the amount of monomers added (increasing up to ten times) or the addition order of the reactants (the synthesis of melamine-formaldehyde precondensate was also tested^{6,7}); without any success.

Synthesis of toluene polyamide capsules (PA_tol)

Toluene-filled polyamide capsules (**PA_tol**) were prepared using a synthetic experimental procedure adapted from reference 7. In a typical experiment, 3 mL of a water solution containing the stabilizing agent (0.4 wt% for PVA or 20 wt% for PVP) were vigorously stirred (1700 rpm, mechanical stirring) at room temperature in a 30 mL flat-bottom vial. At the same time, terephthaloyl chloride (45 mg) was dissolved in toluene (1 g) upon sonication for 5 minutes. The photochrome of interest (15-25 mg) was then dissolved in the toluene solution, which was subsequently added to the stirred water solution. The vigorous stirring was kept for 2 more minutes, during which an oil-in-water emulsion was formed. Next, an aqueous solution of DETA (650 μL of DETA in 1 mL H_2O) was slowly added to the emulsified system. After the addition of the amine, the stirring was slowed down to 300 rpm for 3 minutes and then stopped. The solution was left standing overnight to complete the polymerization process, observing the formation of particles that lay on the top of the water suspension. The latter was diluted with 100 mL of distilled water and filtered with a nylon filter of 0.22 μm pore size. The solid obtained was repetitively washed with water until no coloured filtrates were observed, and dried in vacuum.

Synthesis of miglyol polyamide capsules (PA_mig)

A similar procedure to that described for **PA_tol** was used to prepare polyamide capsules filled with miglyol (**PA_mig**). In a 30 mL glass vial, a miglyol solution (1 mL of oil) containing terephthaloyl chloride (45 mg) and the photochromic dye (5-10 mg) was added to 3 mL of PVP in water (13 wt%) that had been previously stirred at 1700 rpm (mechanical stirring). Stirring was maintained until the stabilization of the emulsion formed (5 min). Then, DETA (650 μ L in 1 mL H₂O) was added dropwise, after which the stirring was slowed down to 300 rpm for 2 minutes and finally stopped. The resulting mixture was left standing overnight, observing the formation of particles that moved to the top of the water suspension. The mixture was then diluted with 100 mL of distilled water and filtered with a nylon filter of 0.22 μ m pore size. The solid isolated was washed with water until colourless filtrates were observed, and subsequently dried in vacuum.

Attempts to synthesise of polystyrene nanocapsules

PS nanoparticles prepared for the synthesis of hollow polystyrene nanocapsules with a hole in the shell, were synthesised according to reference 8. A three-necked, 250-mL round-bottom flask equipped with reflux condenser, nitrogen inlet, addition funnel and a magnetic stirrer; was charged with deionized water (150 mL), NaSS (20 mg) and NaHCO₃ (0.125 g). Subsequently, the system was immersed into a silicon bath and heated at 343 K while degassed and stirred at 600 rpm. Once temperature was stabilized, styrene (75 g) was introduced through the addition funnel and the mixture was homogenized at 700 rpm for one hour. Then, a preheated KPS solution (0.125 g of KPS in 25 mL H₂O at 343 K) was added dropwise into the mixture starting styrene polymerization. Agitation rate was set at 800 rpm and the polymerization was allowed to proceed for 18 hours. Finally, the white suspension obtained was washed with water in four successive filtrations with a nylon filter of 0.22 μ m pore size, and the powder isolated was air-dried.

Polystyrene hollow capsules with a hole in their shell were synthesise according to the procedure reported by Xia's group⁹⁻¹¹. In a 10 mL glass vial, PS-Nps (32 mg; obtained as described in section **Error! Reference source not found.**) were suspended in deionized water (4.5 mL) using a sonication bath. Then, 200 μ L of toluene were added and particle swelling proceeded under magnetic stirring (900 rpm) during 30 minutes. The resulting suspension of swollen particles was poured dropwise into liquid nitrogen and placed in a

freezer at 255 K (19 h 30 min). Afterwards, the frozen droplets were introduced in a 100 mL shlenck immersed in a cooling bath and vacuum was applied (6 h) to induce the hole formation in the particle surface. Note that during vacuum, temperature was maintained above the melting point of toluene but below that of water to enable solvent evaporation while the hollow structure of the particle was preserved. The defrost sample was centrifuged for 15 min at 4.000 rpm to separate “opened” particles from solid ones (the former float whereas the latter precipitate), and the final hollow capsules were collected by filtration. Alternatively, in order to form the hole in the shell, the frozen suspension droplets were lyophilized until water was completely evaporated, obtaining the hollow particles as a dry powder.

Dye loading was carried out in a 5 mL glass vial by dispersing the as-prepared open capsules in an ethanol solution of **PhI** (4.3 mg of **PhI** in 1 mL EtOH) upon sonication. Afterwards, in order to seal the hole on the capsules surface, the suspension was heated at 343 K in a water bath for 2 hours while it was magnetically stirred at 900 rpm. Finally, three successive filtrations were performed redispersing the final latex in abundant ethanol to remove the non-encapsulated photochrome from the surface of the capsules. Although we obtained hollow capsules through this process, these capsules were always accompanied by a large amount of solid particles and the solvent encapsulated quickly evaporated from the capsule core. To improve the closing treatment we modified the temperature, the time or the solvent employed (isopropanol, dioxane, toluene, hexane, hexadecane or miglyol) without success. Therefore, this methodology was discarded.

7.2.2 Thermochromic capsules

Encapsulation of **VT1** into liquid-filled capsules was done following the methodologies and procedures described below.

Attempts to synthesise of polyamide capsules

We tried to synthesise liquid-filled polyamide capsules containing complex **VT1** by the interfacial polymerization procedure described in section 7.2.1. However, the VT complex decomposed when dissolved in the oil phase containing the terephthaloyl chloride used for the polymerization reaction, due to the formation of hydrochloric acid upon the chloride

hydrolysis. Replacement of the terephthaloyl chloride by other acyl chlorides did not prevent **VT1** degradation, thus this methodology was abandoned.

Attempts to synthesise of liquid-filled capsules by solvent evaporation

We also tested the solvent evaporation method reported in reference 11. The procedure consisted on the preparation of a solution containing 0.25 g of polymer (PMMA, $M_w \sim 120000$ or $M_w \sim 350000$; or PS, $M_w \sim 350000$) and 0.25 g of oil (hexadecane or Miglyol[®] 812) in 5 mL of a volatile solvent (chloroform or dichloromethane). 3:1 and 2:1 polymer/oil ratios were also employed. The resulting solution was added to a 25 mL vial charged with 10 mL of an emulsifier aqueous solution. Different emulsifier contents were used: 0.1 or 1 wt% of SDS, and 1 or 3 wt% of PVA). Then, the mixture was emulsified using magnetic stirring or high shear homogenization (1600rpm, 5000 rpm or 20000 rpm) and the volatile solvent was evaporated at room temperature or heating at 313 K under magnetic stirring. The resulting particles were collected upon centrifugation and washed with water. Different structures were obtained; however, even though we did observe some core-shell architectures, no liquid was ejected after physical crushing and most of the particles presented solid structures. Interestingly, employing 1:1 PMMA/hexane chloroform solution ($M_w \sim 350000$) and SDS as surfactant resulted on non spherical solid particles: half-sphere, oval or coin-like shapes were produced using 1 wt% SDS solutions and 20000 rpm emulsification rates, 1 wt% SDS and 5000 rpm, and 0.1 wt% SDS and 5000 rpm, respectively.

Synthesis of toluene polyurea capsules (PU_tol)

Toluene-filled polyurea capsules (PU_tol) were prepared using a synthetic experimental procedure adapted from reference 12. Desmodur[®] N 100 (1 g) was dissolved in 5.32 g of a toluene solution containing **VT1** complex (0.51 mg/mL). The resulting solution was added to a 50 mL beaker (tall form) containing 20 mL of PVA in water (2 wt%), and was emulsified for 5 minutes using magnetic stirring (1500 rpm) or high shear homogenization (5.000 rpm) according to the desired capsule size. Then, an aqueous solution of DETA (189 μ L of DETA in 3.54 mL H₂O) was added dropwise and the emulsification rate was kept for 5 minutes more. Afterwards, the beaker was introduced in an oil bath heated at 333 K and the reaction was allowed to proceed for 2 hours under magnetic stirring (1500 rpm). Alternatively, smaller capsules were also obtained performing the polymerization at room

temperature overnight. Once the stirring was stopped the capsules moved towards the top of the water suspension. The mother liqueur was then removed (centrifugation was employed if needed: 5 min 6000 rpm), and capsules were washed repetitively with water (x3) and lyophilized.

Synthesis of miglyol polyurea capsules (PU_mig)

A similar procedure to that described for **PU_tol** was used to prepare polyurea capsules filled with miglyol (**PU_mig**). Desmodur[®] N 3300 (1 g) was dissolved in 10.64 g of a miglyol solution containing VT complex (0.04 mg/mL). The resulting solution was added to a 50 mL beaker (tall form) containing 20 mL of SDS in water (2 wt%), and was emulsified for 5 minutes using magnetic stirring (1500 rpm) or high shear homogenization (5.000 or 20000 rpm) according to the desired capsule size. Then, an aqueous solution of DETA (189 μ L of DETA in 3.54 mL H₂O) was added dropwise and the emulsification rate was kept for 5 more minutes. Note that for the highest emulsification rate, bigger beakers were needed during emulsification (250 mL). Afterwards, the beaker was introduced in an oil bath heated at 333 K and the polymerization reaction was allowed to proceed for 2 hours under magnetic stirring (1500 rpm). Once the stirring was stopped, the capsules moved towards the liquid-air interface although due to the similarity between water and miglyol densities ($\rho_{\text{miglyol}} = 0.9438 \text{ g/mL}$) this process was slower than the one observed for **PU_tol**. The mother liqueur was then removed, the suspension was washed repetitively with water upon centrifugation (x3: 5 min, 6000 rpm) and the final capsules were lyophilized.

7.2.3 White-light emitting capsules

Synthesis of miglyol polyurea capsules (PU_DOTP)

Polyurea capsules filled with DOTP (**PU_DOTP**) were synthesised following the procedure optimized for **PU_mig**. First, DOPT solutions containing the corresponding amount of dye were prepared (see section 5.2.2). Dyes (**ZW5** or **BPEA**) were dissolved in the minimum volume of chloroform and the resulting solutions were added to the appropriate amount of DOTP. For dye mixtures, the convenient volumes of each solution were mixed to attain the desired concentrations. Desmodur[®] N 3300 (0.29 g) was dissolved in 3.04 g of dye-DOTP

solution. At the same time, 5.7 mL of SDS in water (2 wt%) were introduced in a 25 mL beaker (tall form) and vigorously stirred by magnetic stirring (1500 rpm) or high shear homogenization (5.000 rpm). The DOPT solution was added dropwise to the stirred aqueous solution an emulsification was performed for 10 minutes. The beaker was then introduced in an oil bath heated at 333 K and the emulsion was stirred at 1500 rpm. Subsequently, an aqueous solution of DETA (47 μL of DETA in 885 μL H_2O) was slowly added to the emulsion (200 $\mu\text{L}/\text{min}$) with a syringe pump (NE-1000, New Era Pump Systems, Inc) and the polymerization was allowed to proceed for 2 hours. Once the reaction was finished, in order to induce the creaming process ($\rho_{\text{DOTP}} = 0.984 \text{ g/mL}$), 60 mL of Na_2SO_4 aqueous solution (1 M) were added to the resulting suspension. The mother liquor was then removed, the suspension was washed repetitively with water upon centrifugation ($\times 4$: 4 min, 6000 rpm) and the final capsules were lyophilized.

7.3 Synthesis of solid polymeric particles

7.3.1 Photochromic solid particles

Synthesis of photochromic polystyrene nanoparticles (**PhI@PS Nps**)

PhI@PS NPs were synthesised by a two stage shot-growth copolymerization adapted from reference 13, in which sodium styrene sulphonate (NaSS) and acetone were used to reduce particle size and increase surface charge. In a typical experiment, a three-necked, 250-mL round-bottomed flask equipped with reflux condenser, nitrogen inlet, addition funnel and a magnetic stirrer, was charged with 7.9 mL of acetone and heated to 343 K in an oil bath. Then 7.04 mL of a **PhI** solution in styrene (4.7 g/mL) were added, and once completely homogenized, 40 mL of deionized water were introduced in the mixture. After 20 min of nitrogen flushing, an aqueous solution (10 mL) containing NaSS (55 mg), potassium persulphate (KPS, 43 mg) and sodium bicarbonate (NaHCO_3 , 27 mg) was added dropwise and magnetic stirring was set at 700 rpm. Once polymerization began, the temperature of the reaction mixture rose to 346 K. An hour after, a second batch of monomer was introduced in the reaction (1.41 mL of **PhI**/styrene solution, 1.58 mL acetone and 7 mL H_2O), which was followed by the addition of a 3 mL aqueous solution of NaSS (0.21 g), KPS (9 mg) and NaHCO_3 (1 mg) 20 min later. Polymerization proceeded during 6 hours and the resulting

particles were collected from the mother liquor by centrifugation (10.000 rpm). Finally, after repeated washing with EtOH and centrifugation (x3), the pellet was purified and the latex particles obtained were allowed to air-dry.

7.3.2 Thermochromic solid particles

Attempts to synthesise VT1@PMMA particles by emulsion polymerization

We first tried to synthesise PMMA-based VT particles upon methyl methacrylate (MMA) polymerization, adapting the methodology described in reference 14. A two-necked, 20-mL round-bottom flask equipped with reflux condenser, nitrogen inlet and a magnetic stirrer; was charged with a KPS aqueous solution (11 mg of KPS in 7.22 mL H₂O) and a MMA solution containing the VT complex (5 mg of VT1 in 267 μ L MMA). The system was immersed into a silicon bath and heated at 343 K while degassed and stirred at 1500 rpm. The polymerization was carried out for 1 h and the resulting particles were washed with water and collected by centrifugation (x3: 10 min, 15.000 rpm). Unfortunately, as the reaction proceeded the VT compound precipitate on the flask walls and, as consequence, white particles were obtained indicating the poor efficiency of dye encapsulation through this methodology. For this reason the used of this methodology for the encapsulation of VT1 was discarded.

Synthesis of VT1@PMMA particles by solvent evaporation

Two similar procedure based on solvent evaporation were followed for the synthesis of thermochromic poly(methyl methacrylate) particles.

(i) For the synthesis of VT1@PMMA microparticles, an homogenous dichloromethane solution (15.5 g) of PMMA (0.56 g, $M_w \sim 350000$) and complex VT1 (11 mg), was added drop by drop to a beaker containing 100 mL of SDS/PVP aqueous solution (4 wt% and 9 wt% respectively), while the latter was emulsified using IKA ULTRA-TURRAX[®] at 10.000 rpm. The emulsion generated was then poured into a 250 mL round bottomed flask and dichloromethane was subsequently evaporated overnight by heating the uncovered flask at 323 K under magnetic stirring (500 rpm). The resulting particles were collected by filtration and washed thoroughly with water. Filters with different pore sizes were used to enhance

monodispersity. Millimetre-sized particles were obtained with the same methodology but changing the conditions: 10 mL of dichloromethane solution (1.5 g of PMMA and 30 mg of **VT1**); 40 mL of SDS/PVP aqueous solution (1 wt% and 2 wt%, respectively), emulsification performed with magnetic stirring at 1000 rpm, and evaporation in a 100 mL round bottomed flask.

(i) **VT1@PMMA** nanoparticles were prepared adapting the procedure described in reference 15. In a typical experiment, 4 mL of a dichloromethane solution containing PMMA (100 mg, $M_w \sim 350000$) and the VT complex (2 mg) were added to a 25 mL beaker (tall form) charged with 10 mL of a PVA aqueous solution (1 wt%). The mixture was emulsified using IKA ULTRA-TURRAX at 24.000 rpm in an ice bath (bigger beakers were needed during emulsification), and dichloromethane was subsequently removed from the emulsion by evaporation at room temperature under magnetic stirring (300 rpm, 1.5 h). The resulting particles were collected by centrifugation and washed by redispersion in distilled water (x3: 5 min, 15.000 rpm).

Synthesis of solid polyurea particles containing VT1 complex (VT1@PU)

Solid polyurea particles (**VT1@PU**) were synthesised using a similar procedure to that described for **PU_tol**. A 50 mL beaker containing 20 mL of PVA in water (2 wt%, PVA) was placed in an oil bath and the solution was magnetically stirred at 1500 rpm. Then, a toluene solution of complex **VT1** (1.8 mg in 1 mL toluene) was added to 1 g of Desmodur[®] N 100 and the resulting mixture was introduced to the stirred aqueous solution. Subsequently, DETA (189 μ L of DETA in 3.54 mL H₂O) was added dropwise and the oil bath was heated up to 333 K. The polymerization reaction proceeded for 2 hours and, once the reaction was finished and the stirring was stopped, the resulting polymer particles precipitated. The mother liquor was removed and particles were washed with abundant water and lyophilized.

7.4 Preparation of polymeric films

7.4.1 Photochromic polymeric films

Polymeric thin films loaded with free PhI

Chloroform solutions containing **PhI** (1.2 mg/mL) and the polymer of interest (25 mg/mL of PMMA, $M_w \sim 350000$; PS, $M_w \sim 350000$; or PC, $M_w \sim 64.000$) were deposited by drop casting onto freshly cleaned glass slides. After evaporation of the solvent at room temperature, polymer films were formed of approximately 200 μm in thickness and 5 wt% in photochrome content.

Polystyrene films loaded with PhI@PA_mig capsules (PhI@PA_mig@PS)

24 mg of **PhI@PA_mig** capsules and 100 μL of Span[®] 85 were added to 5 mL of a chloroform solution of PS (7.5 mg/mL, $M_w \sim 350000$). The resulting suspension was sonicated for 30 seconds to ensure capsule dispersion and dropcasted onto a clean glass slide. Span[®] 85 was used to prevent aggregation of the microcapsules during the solvent evaporation and the formation of the polymer film (4 - 5 h). In this way, uniform films with thickness of approximately 200 μm and 6 wt% of capsule content (i.e. photochrome loadings of 0.08 %) were prepared.

Preparation of test lens matrices loaded with PhI@PA_mig capsules (PhI@PA_mig@lens)

Test lens polymeric matrices were prepared by cross-linking of poly(ethylene glycol) dimethacrylate (PEGDMA, $M_n = 750$) and ethoxylated bisphenol A diacrylate (EBPDA, $M_n = 680$), following the procedure described in reference 16. In a typical experiment, 0.135 g of **PhI@PA_mig** capsules were dispersed in 1.5 g of EBPDA by sonication and magnetic stirring. Then, 0.375 g of PEGDMA were added and the mixture was stirred for 5 min. 2,2'-azobis(2- methylpropionitrile) (AIBN) was subsequently poured (0.1 g) and once homogeneously dispersed, the mixture was casted into a mold and cured at 353 K for 24 h. In this way, cross-linked polymer films of approximately 0.85 mm in thickness and 6 wt% of capsules (i.e. photochrome loadings of 0.08 %) were obtained.

7.4.2 Thermochromic polymeric films

Polymeric thin films loaded with VT1

Dichloromethane solutions containing 15 wt% of polymer (PMMA, $M_w \sim 350000$; PC, $M_w \sim 64.000$; or PVAc, $M_w \sim 100000$) and 2, 4 or 8 wt% of complex **VT1** were prepared by vigorous stirring, and let to stand at least for 10 minutes. Then solutions were then casted onto a glass substrate in a closed chamber with anhydrous sodium sulphate to control the initial evaporation of the solvent and avoid humidity.

7.5 References

1. Larsen, S. K. & Pierpont, C. G. Cobalt and manganese complexes of a schiff-base biquinone radical ligand. *J. Am. Chem. Soc.* **110**, 1827–1832 (1988).
2. Prats, G. (UAB). Activación electroquímica de interruptores moleculares en sistemas fotocromicos y ácido-base. (2012).
3. Džimbeg-Malčić, V., Barbarić-Mikočević, Ž. & Itrić, . u belka-Munk theory in describing optical properties of paper (I). *Tech. Gaz.* **18**, 117–124 (2011).
4. Dahm, D. J. & Dahm, K. D. *Interpreting Diffuse Reflectance and Transmittance: A Theoretical Introduction to Absorption Spectroscopy of Scattering Materials*. (IM Publications, 2007).
5. Misawa, H., Kitamura, N. & Masuhara, H. Laser manipulation and ablation of a single microcapsule in water. *J. Am. Chem. Soc.* **113**, 7859–7863 (1991).
6. Hong, K. & Park, S. Melamine resin microcapsules containing fragrant oil: synthesis and characterization. *Mater. Chem. Phys.* **58**, 128–131 (1999).
7. Zhang, X. X., Fan, Y. F., Tao, X. M. & Yick, K. L. Fabrication and properties of microcapsules and nanocapsules containing n-octadecane. *Mater. Chem. Phys.* **88**, 300–307 (2004).
8. Pastine, S. J., Okawa, D., Zettl, A. & Fréchet, J. M. J. Chemicals on demand with phototriggerable microcapsules. *J. Am. Chem. Soc.* **131**, 13586–13587 (2009).
9. Im, S. H., Jeong, U. & Xia, Y. Polymer hollow particles with controllable holes in their surfaces. *Nat. Mater.* **4**, 671–675 (2005).

10. Jeong, U., Im, S. H., Camargo, P. H. C., Kim, J. H. & Xia, Y. Microscale fish bowls: a new class of latex particles with hollow interiors and engineered porous structures in their surfaces. *Langmuir* **23**, 10968–10975 (2007).
11. Bai, M.-Y. *et al.* A facile and general method for the encapsulation of different types of imaging contrast agents within micrometer-sized polymer beads. *Adv. Funct. Mater.* **22**, 764–770 (2012).
12. Zhao, Y., Fickert, J., Landfester, K. & Crespy, D. Encapsulation of self-healing agents in polymer nanocapsules. *Small* **8**, 2954–2958 (2012).
13. Chao, H. Microencapsulated adhesive. US6375872 B1 (2002).
14. Zeng, F. *et al.* Preparation of highly charged, monodisperse nanospheres. *Macromol. Chem. Phys.* **203**, 673–677 (2002).
15. Wang, X., Xu, S. & Xu, W. Luminescent properties of dye-PMMA composite nanospheres. *Phys. Chem. Chem. Phys.* **13**, 1560–1567 (2011).
16. Feczko, T., Varga, O., Kovacs, M., Vidoczy, T. & Voncina, B. Preparation and characterization of photochromic poly(methyl methacrylate) and ethyl cellulose nanocapsules containing a spirooxazine dye. *J. Photochem. Photobiol. A-Chemistry* **222**, 293–298 (2011).
17. Ercole, F., Malic, N., Harrisson, S., Davis, T. P. & Evans, R. A. Photochromic polymer conjugates: the importance of macromolecular architecture in controlling switching speed within a polymer matrix. *Macromolecules* **43**, 249–261 (2010).

